(9)

ONR Grant No. N00014-90-J-4077

Relaxor Ferroelectrics for Electrostrictive Transducers

FINAL REPORT

Period September 30, 1990 - September 30, 1992

Sponsored by

Office of Naval Research (ONR)

Submitted to:

Dr. Robert Ting
Navy Research Laboratory
Underwater Sound Ref. Division
Box 8336
Orlando, FL 32856

Submitted by:

Thomas R. Shrout

Mr. Norman Meeks

Sei-Joo Jang

Dr. Wallace Smith

Materials Research Laboratory
Penn State University
University Park, PA 16802

OUTLINE

PAGE

EXECUTIVE SUMMARY

The higher order electro-mechanical coupling "electrostriction" was proposed as an alternative to the piezoelectric phenomena commonly employed for sonar-type transducers. In contrast to piezoelectric ceramics (e.g. PZTs) electrostrictors offer enhanced strain-energy density, without the detrimental effects such as aging, hysteresis, or "walk-off", associated with macro--domains. Although all insulating materials exhibit electric field induced strains, only those in which large polarizations can be induced are of present interest. As such, four types of electrostrictor-type families were proposed based upon their polarization change mechanisms, including:

Type I.	Relaxor ferroelectrics, general formula $Pb(B_1B_2)O_3$
Type II	Relaxors, PLZTs, general formula $Pb_{1-y}La_y(Zr_{1-x},Ti_x)O_3$
Type III	"Pinched" ferroelectric, e.g. $Ba(Ti_{1-x}Sn_x)O_3$
Type IV	Normal ferroelectric, e.g. Ba_{1-x},Sr_xTiO_3

In relation to the Navy sonar-transducer requirements below:

- Large E-field induced strains $\geq 0.03\%$
- Operating temperature range 0-30°C
- Minimal strain E-field hysteresis
- Low loss/heating

the performance of the four types of strictors have been summarized in the following table.

For comparison, two types of PZTs--I, III or "hard" ferroelectrics, are also given. Based on the results from this work, it is clear that the Type I $Pb(B_1B_2)O_3$ strictors offer overall superior performance and warrant further investigation in prototype form.

Performance Summary of Electrostrictors for Sonar Transducers

Material Type	Example	Strain Level	Temp. Range	*Hysteresis	*Freq Dependency	*Heating/ Dielectric Loss	Elastic s_{ij}	Microstructural Dependency
Normal IV	$(Ba,Sr)TiO_3$	-	-	0	0,+	?	+ +	-
Type III	$Ba(Ti,Sn)O_3$	0	+	+	?	?	-	-
Relaxor II	PLZT	+ +	+ +	0	0,-	-	+	0
Relaxor I	$Pb(B_1B_2)O_3$	+	+	+ +	+	+	+	+
Piezo Type I,III	PZT-4,8	+	+ + +	-	+	0	-	0

*Subjective in relation to T_m.

+	-	Best
0	-	Moderate
-	-	Worst

RELAXOR FERROELECTRICS FOR ELECTROSTRICTIVE TRANSDUCERS

I. INTRODUCTION

Objectives

The principal objective of this program was to investigate the potential of electrostrictive actuator materials for use in NAVY-type sonar. The anticipated performance requirements for such materials are summarized in the following:

Electrical

- Operating temperature range 0-30°C
- High sensitivity; i.e. large E-field induced strain (≥0.03%)
- Minimal strain E-field hysteresis
- Low dielectric loss, i.e. no heating

} 1 kHz

Physical

- Elastically stiff (low compliance), i.e. generate large forces
- Mechanically robust; Note: a prestress of ~3000 psi (20 MPa) is usually required.

An additional objective of the program was to categorize or classify families of electrostrictors, analogous to "hard" and "soft" piezoelectrics (PZTs) or NAVY Type I and II, respectively.

Background

Electrostrictive ceramics are used in many applications where effective and reliable electromechanical actuation is important. The primary electrostrictive materials are those ferroelectrics in which a large reversible dielectric polarization can be induced with an appropriate electric field. Applications of the electrostrictive effect continue to grow as new families and ferroelectric compositions are explored. For actuation purposes, the strong basic electrostrictive coupling can be used for very high precision positioning control. Present applications involve ultrasonic transducers (Shrout and Fielding, 1990), pressure valves (Uchinio et al., 1980), and actuator stacks for adaptive optics (Ealey and Wheeler, 1989; Ealey, 1990). In addition to sonar transducers, other areas of possible exploration include "smart" materials with tunable vibration/strain sensing and combined actuation functions (Mamboodri and Wheeler, 1992), higher

frequency medical ultrasound (Takeuchi et al., 1989), and nonlinear transducers for fiber optic electric-field sensors (Vohra et al., 1991).

Advantages offered by electrostrictors over piezoelectrics and other technologies for application in sonar transducers include the following:

1. Electrostrictors operate with reduced hysteresis of the strain-electric field response for micropositioning without "walk-off" or remanent strain.

2. Reduced aging and creep effects due to the lack of macro-domain interaction.

3. High response speed ($\lesssim$10 μs) with accurate control and strain values (>.03%) achievable at reasonable field levels leading to high sensitivity and a displacement range of several tens of microns with (± .01 μm) reproducibility.

II. ELECTROSTRICTIVE CLASSIFICATION OF FERROELECTRIC CERAMICS

Electrostriction occurs to some extent in all materials of any symmetry class unlike piezoelectric materials which must be non-centrosymmetric (possessing a permanent electric dipole) as in PZT ceramics which must undergo a poling process in order to be piezoelectrically active. The relations between strain x_{ij}, electric field E_k, dielectric polarization P_k, and crystal symmetry can be summarized as in Table I for both piezoelectricity and electrostriction.

Table I. Relationships between strain x_{ij}, electric field E, dielectric polarization P_k, and crystal symmetry for piezoelectric and electrostrictive materials.

Relations	Piezoelectricity	Electrostriction
• Strain-Electric Field	$x_{ij} = d_{ijk}E_k$	$x_{ij} = M_{ijkl}E_kE_l$
• Strain-Polarization	$x_{ij} = g_{ijk}P_k$	$x_{ij} = Q_{ijkl}P_kP_l$
• Crystal Classes	Non-centrosymmetric (permanent electric dipole)	All families (E-field induced dipoles)
Polycrystalline Ceramics	Ferroelectric (Hysteresis/P-E)	All ceramics (No hysteresis)

The piezoelectric constants d_{ijk} and g_{ijk} relate the electroelastically induced strain to the applied electric field and concomitant material polarization, respectively. The M_{ijkl} and Q_{ijkl} coefficients relate the electrostrictive strain to the same quantities. Piezoelectricity may be viewed as a polarization biased electrostrictive effect with the magnitude of this effective piezoelectric coefficient given for material polarization P_3 and in reduced notation

$$d_{33} = 2\,\varepsilon_0 Q_{11} K_3 P_3; \text{ or } d_{induced} = 2\,\varepsilon_0 Q_{11} K P_{induced} \quad [1]$$

where ε_0 is the permittivity of free space (8.854×10^{-12} F/m), K_3 the dielectric constant and P_3 the induced polarization. Since the relationship between induced polarization and applied field is given as follows:

$$P_{induced} = \varepsilon_0 K E_{applied} \quad [2]$$

$$d_{induced} = 2\,\varepsilon_0^2 Q_{11} K^2\, E_{applied} \quad [3]$$

$$\rightarrow x_{induced} = 2\,\varepsilon_0^2 Q_{11} K^2 E_{applied}^2 \quad [4]$$

it can be observed that for large induced strains the material should possess a large dielectric constant K; and/or be able to have a large polarization induced, since $x_{induced} \propto K^2$. This observation points out the utility of what are known as relaxor ferroelectrics (Jang, 1979) which exhibit a broad frequency-dispersive dielectric constant, peak temperature T_m, and a spontaneous polarization P_s which disappears at a temperature T_d well below T_m as presented in Figure 1. Large effective field induced piezoelectric coefficients can thus be achieved by relaxor ferroelectrics (Pan et al., 1989).

As shown in Figure 1(a), an effort has been made to ascertain the delineating borders between the various regimes of electromechanical behavior for relaxor ferroelectric perovskite ceramics:

- **Regime III. Piezoelectric ($T < T_d$)**
- **Regime II. Micro-Macrodomain ($T_d < T < T_m$)**
- **Regime I. Electrostrictive ($T \gtrsim T_m$)**

Typical P-E behavior for representative materials in the three aforementioned regimes are presented in Figure 1(b). Note the lack of hysteresis and remanent P for Regime I, the low hysteresis without remanence for Regime II (due to micro-macro domain reorientation), and traditional ferroelectric behavior in Regime III.

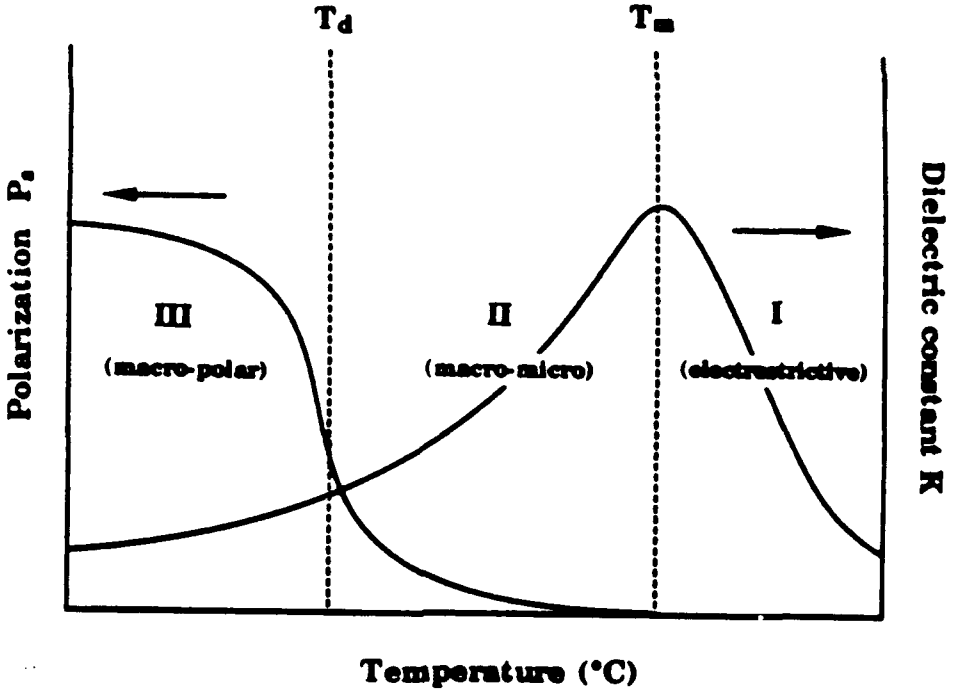

(b)

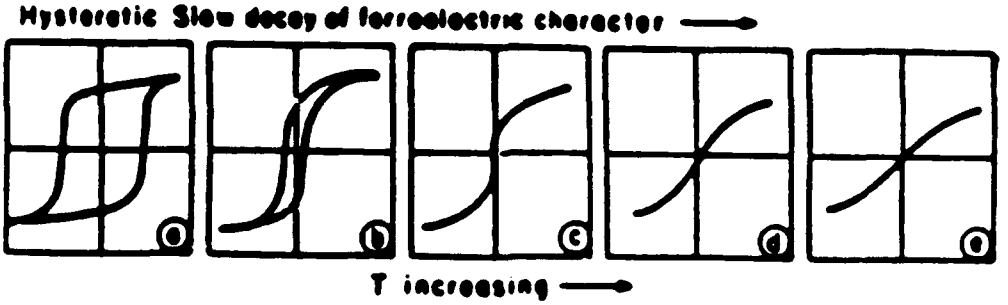

Figure 1 (a) Polarization and dielectric temperature behavior for a relaxor ferroelectric. Three behavior regimes are defined. (b) Typical polarization versus electric field behavior as function of temperature for a relaxor ferroelectric.

Regime III materials have a stable remanent polarization (P_r) and large associated strain levels which display "butterfly" strain-E field loops (see Figure 2a). The increase of remanent polarization, however, leads to increased hysteresis and "walk off", reducing the difference between the maximum induced strain and the initial position, as a result of the remanent strain offset.

Regime II materials are those relaxor materials which are located in a temperature region where nanometer-scale or "micro" domains greatly influence the polarization/electromechanical properties. The polarization fluctuations arising from thermal motions around and just below the broad ferroelectric phase transition are a critical parameter. Their size is linked with chemical inhomogeneity, cation ordering, and the electric dipolar field interactions between themselves and the polarizable crystal lattice. In this regime, the micro polar regions couple strongly with each other but not the nonpolar lattice, thus their polarizability is effectively large under electric field, leading to large electric permittivities and large electrostrictive strains from micro-macrodomain reorientation (see Figure 2b).

Regime I electrostrictive materials are those normal and relaxor ferroelectrics which operate above the dielectric constant maximum temperature (T_m) and are characterized by non-hysteretic strain (x-E) (Figure 2c) and polarization (P-E) field loops. The strain electric field response is primarily nonlinear and quadratic. The absence of macroscale domains implies reduced aging, lack of remanent strain, improved reproducibility(low hysteresis), and low power consumption (low loss). Hence a broad transition, with high Curie constant materials are desirable to allow a wide temperature usage range for electrostrictors.

III. MATERIALS SELECTION

Based upon the expressions [1] through [4] given above in relation to the four principal requirements for electrostrictors for sonar transducers, i.e. (1) large induced strains, (2) operating temperature range 0-30°C, (3) minimal hysteresis, and (4) low dielectric loss (minimal heating), criteria for selecting various classes of electrostrictor materials can be summarized in Table II.

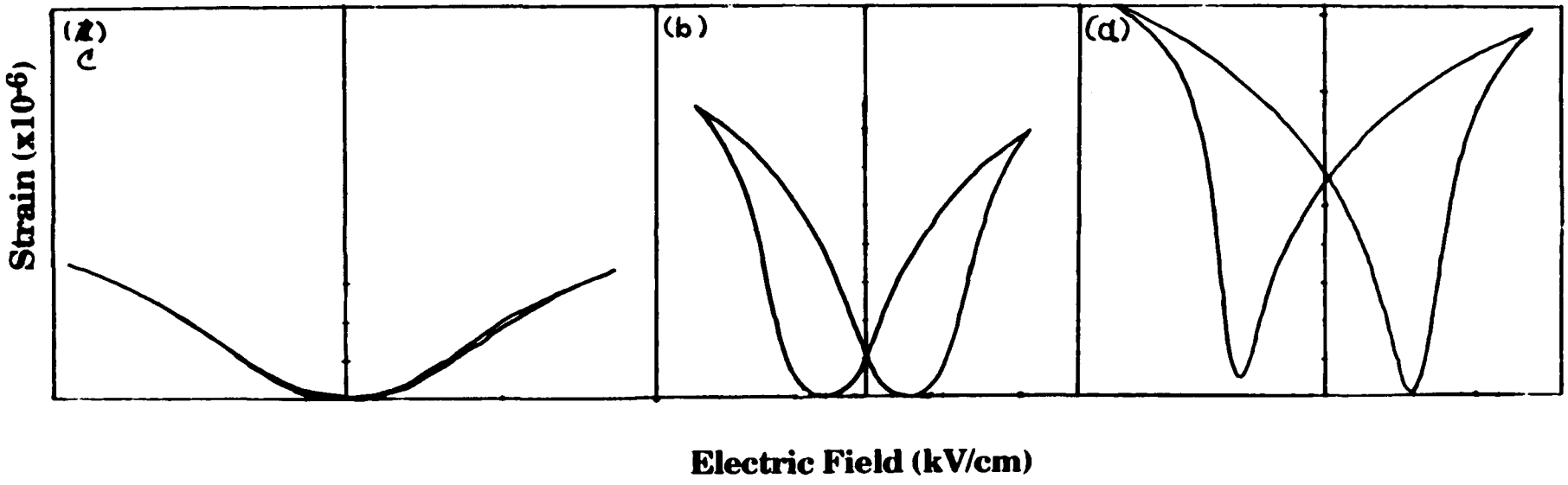

Figure 2. Typical strain-field behavior for Type II relaxor (PLZT 9/65/35) in a) Regime III ($T < T_d$), b) Regime II ($T_d < T < T_m$), and c) Regime III ($T > T_m$).

Table II. Selection Criteria - Electrostrictor Materials for Sonar

Criteria:		
• Large induced piezo, d_{ind}	→	Large induced polarization, P_{ind} (1) large K (2) phase change, e.g. micro→macro (3) K vs. E-field stability (P/E)
• Operating temp. range 0°-30°C	→	(1) broad dielectric transition, (2) large $\Delta T = T_{max}-T_d$ (micro-macro)
• Minimal hysteresis (no remanent polarization, P_r)	→	(1) paraelectric region (Regime I) (2) micro-domains only (Regime I & II)
• Low loss/heating	→	Regime I - paraelectric-no domains

As is found in the case of the large family of piezoelectric materials, based principally on $Pb(Zr,Ti)O_3$-PZT (e.g. Navy Type I, II, III, or "hard" and "soft"), the numerous families of perovskite electrostrictors in which large polarizations can be induced requires some type of classification. The criteria for the different perovskite electrostrictors classified by this scheme arises from a phenomenological basis and from the intrinsic polarization change mechanism applicable for each family. Many of the relevant criteria for material selection of suitable compositions and the temperature behavior in which they can operate effectively are presented in Table III.

As presented, four compositional families based on the perovskite crystal structure ABO_3 were selected for this program. Representing the four electrostrictive classifications, advantages and disadvantages relevant to sonar transducers (Table II) are summarized in the following paragraphs and associated figures and tables.

Table III Classification of Electrostrictive-based Perovskites*

Family	Behavior Type	T_{max}/T_d	Polarization/Structure Relationships
Type I $Pb(B_1B_2)O_3$ e.g. $Pb(Mg_{1/3}Nb_{2/3})O_3$	Relaxor	$T_m>T_d$	• $T>Tm$ $\sqrt{P^2} \neq 0$ • Micro-polar regions • B-site nanoscale ordering • Little grain size dependency
Type II e.g. $Pb_{1-y}La_y(Zr_xTi_{1-x})O_3$ PLZTs - $y \geq 0.7$ $x \geq 0.65$	Relaxor	$T_m>>T_d$	• $T>Tm$ $\sqrt{P^2} \neq 0$ • Lattice vacancy/softening-decoupling • Micro-polar regions • Moderate grain size dependency
Type III e.g. $Ba(Ti_{1-x}Sn_x)O_3$ $x = 0.1$	"Pinched" Ferroelectric	$T_m=T_d$ (diffuse†)	• Spontaneous strain develops $P_s<T_c$ • $P_s = 0$ at $T>T_C$ • "Pinching" of phase transition R, O, T, C (rhombo, ortho, tetra, cubic) • Prominent grain size dependency
Type IV e.g. ††$(Ba_{(1-x)}Sr_{(x)})TiO_3$	Normal Ferroelectric	$T_m=T_d$ (diffuse†)	• Spontaneous strain develops $P_s<T_C$: $P_s = 0$ at $T>T_C$ • Paraelectric $x > 0.3$ • Macro-heterogeneity → diffuse

* L.E. Cross, "Piezoelectric and Electrostrictive Sensors and Actuators for Adaptive Structures and Smart Materials," Proc. AME 110th Annual Meeting, San Francisco, CA (Dec. 1989).

† Diffuse or broadening of phase transition due to macro heterogeneity.

†† Note: (x) depends on operational temperature, e.g. room temperature paraelectric $x > 0.3$.

Type I. $Pb(B_1B_2)O_3$ - Relaxors

The well known perovskite ferroelectric $Pb(Mg_{1/3}Nb_{2/3})O_3$ [PMN] typifies the Type I electrostrictor. Representative dielectric and polarization behavior for this type is given in Figure 3 for a PMN composition modified with the normal ferroelectric $PbTiO_3$, allowing the transition to be shifted from T_m ~-10°C to that near room temperature. From this figure the advantages and disadvantages of this material become apparent.

Further advantages not readily apparent include low dielectric loss (Regime I), low E-field/K dependency, and low thermal expansion. In addition, a wide range of compositional modifications are possible (A- & B-site); however, their role on the nano-scale ordering and subsequent polar/dielectric behavior are not well understood.

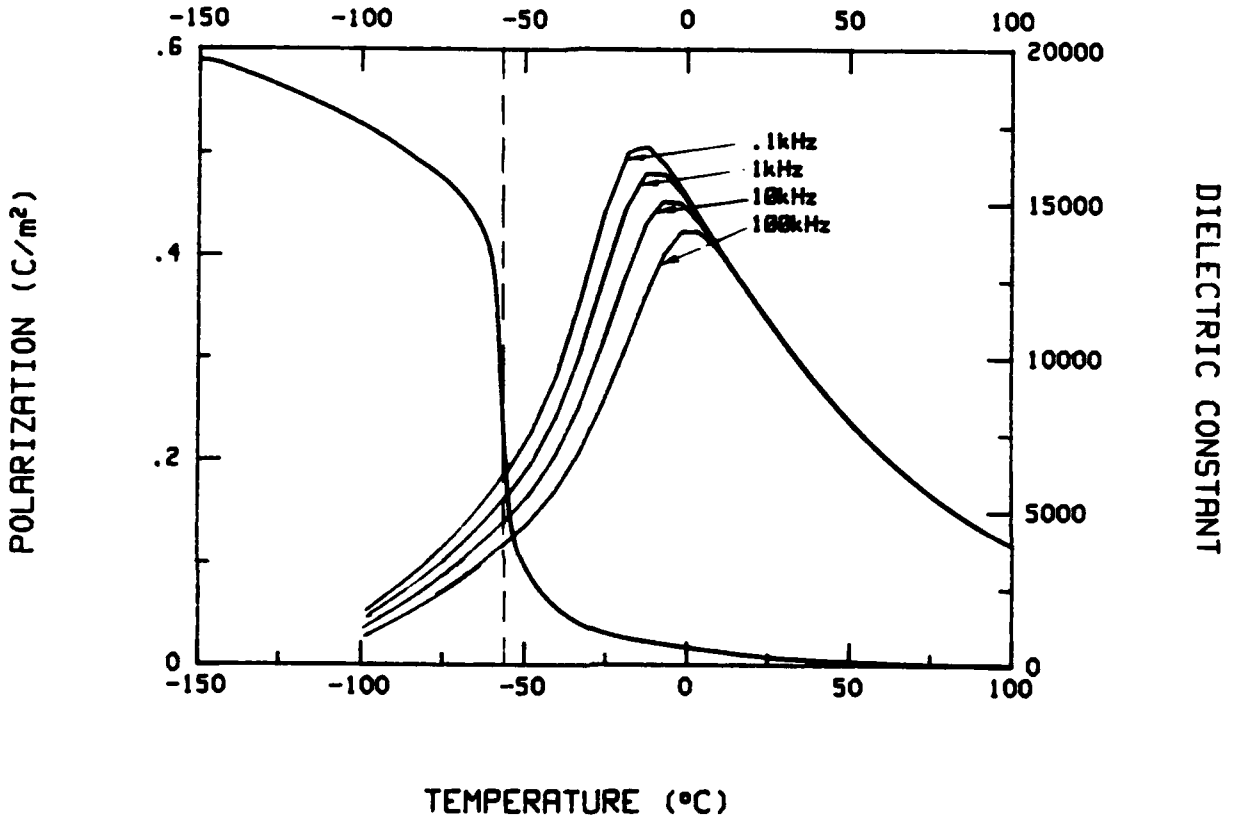

Advantages

- **Very high K's (>25,000)**
- **Diffuse phase transition**
- **No remanent polarization ($T > T_d$)**
- **Moderate $\Delta T = T_m - T_D$**

Disadvantages

- **Frequency dependence**

Figure 3 **Dielectric and polarization temperature behavior of Type I electrostrictor. Example PMN:PT. Dashed line indicates depolarization temperature (T_d).**

Type II. Relaxors "PLZTs"

The well known PLZT phase diagram and corresponding P/E behavior are given in Figure 4. As shown, only a narrow compositional range offers relaxor and/or "slim-loop" ferroelectric behavior. Figure 5 depicts the dielectric and polarization temperature behavior for a relaxor PLZT composition and the corresponding polar regimes. Similar to the Type I relaxors, PLZTs offer a very diffuse phase transition (Meng et al., 1985) and larger ΔT-T_m-T_D Regime II. Unlike the Type I relaxors, the underlying phenomena associated with the diffuseness and dispersive nature of PLZT relaxors is believed to be related to A-site lattice vacancy decoupling of the highly polarizable Pb-cations to the ferroelectric B-site ions. Disadvantages include compositional variability (i.e. compositions to shift T_m to room temperature or below are not possible), hence higher dielectric losses, owing to Regime II operation only. .

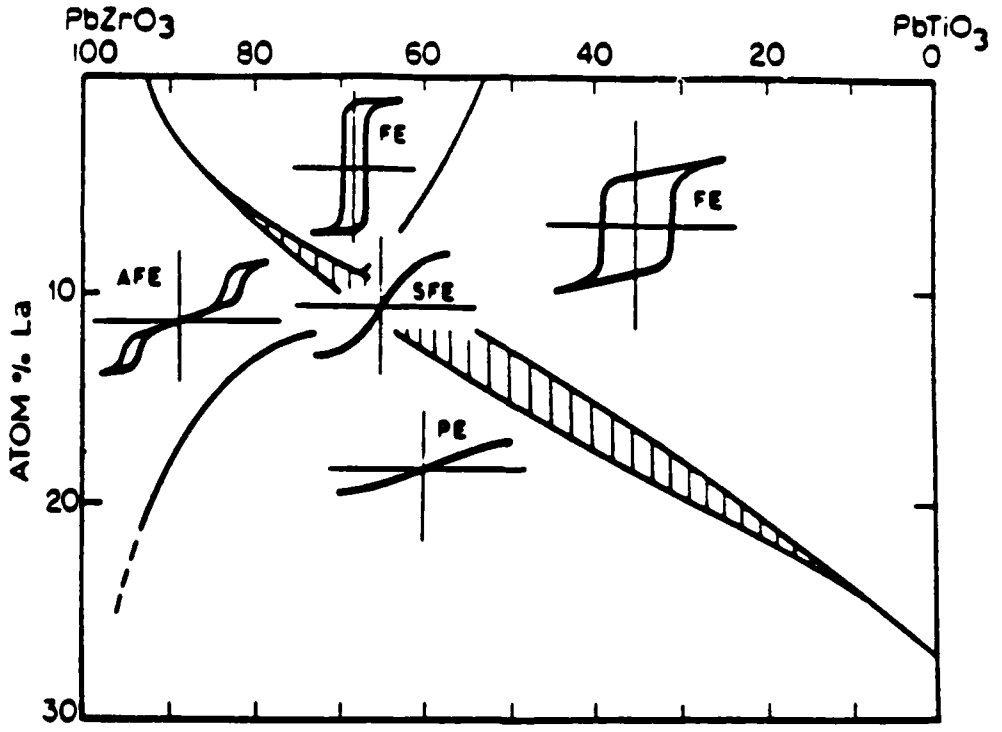

Figure 4. Type II PLZT Relaxor Ferroelectrics. $Pb_{1-x}La_x(Zr_yTi_{1-y})_{1-x/4}O_3$ phase diagram showing polarization/E-field behavior. (After Haertling and Land, 1971).

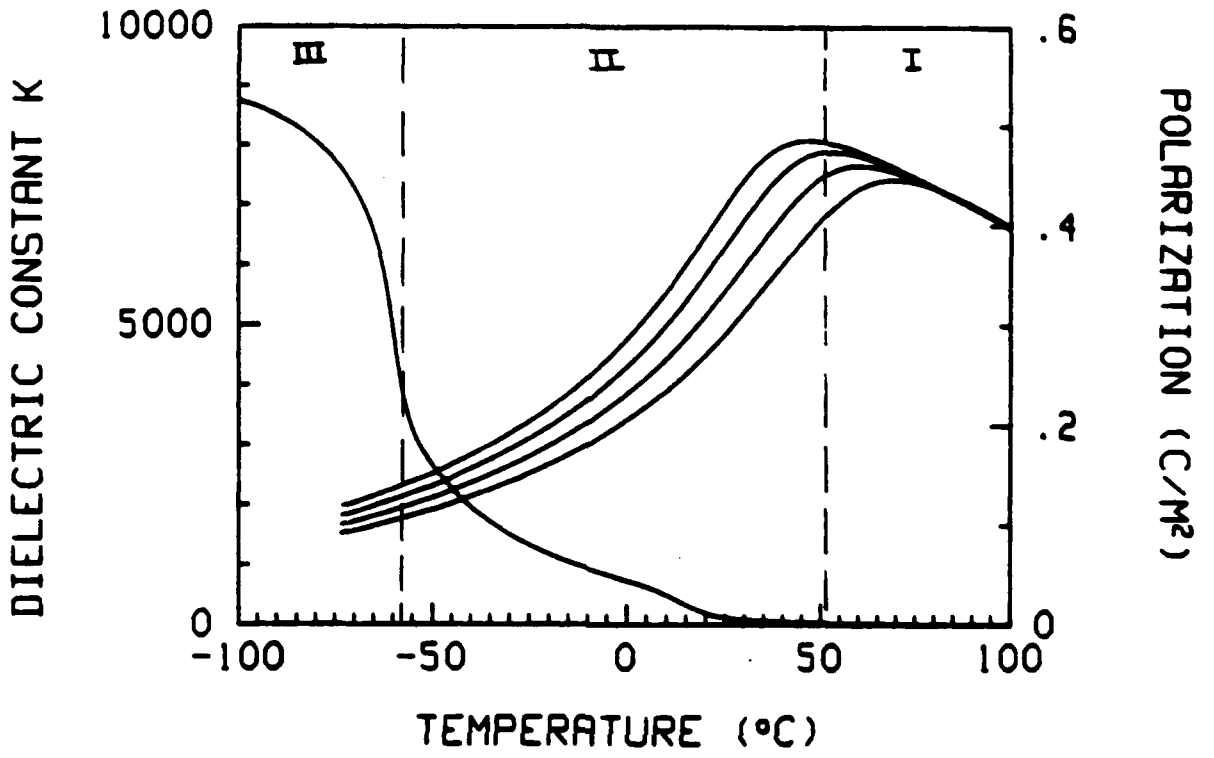

Figure 5. Type II relaxor characteristic dielectric and polarization temperature behavior. Note: Regime I is well above room temperature.

Type III. "Pinched" Ferroelectrics

The phase diagram highlighting the "pinching" of ferroelectric phases for $Ba(Ti_{(1-x)}Sn_x)O_3$ is given in Figure 6(a) with corresponding dielectric temperature curves given in Figure 6(b). As shown, the "pinching" phenomena gives rise to an anomalously high level of polarizability at x = 0.1-0.13, with little frequency dispersion (von Ciemenski et al., 1990). Being a normal ferroelectric, however, the depolarization temperature T_d is expected to be the same as T_m. A level of diffuseness can be engineered through processing, however, leading to a prominent grain size dependency. As with the Type II relaxors, the compositional variability in the Type III family is very limited as to the level of Sn and/or Zr, the latter which, unfortunately, shifts T_m well above room temperature. To date, little is yet known in regards to the structure-polar behavior of these materials.

(a)

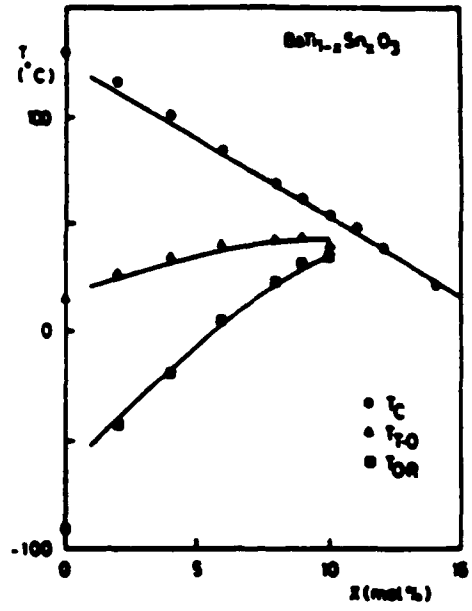

(b)

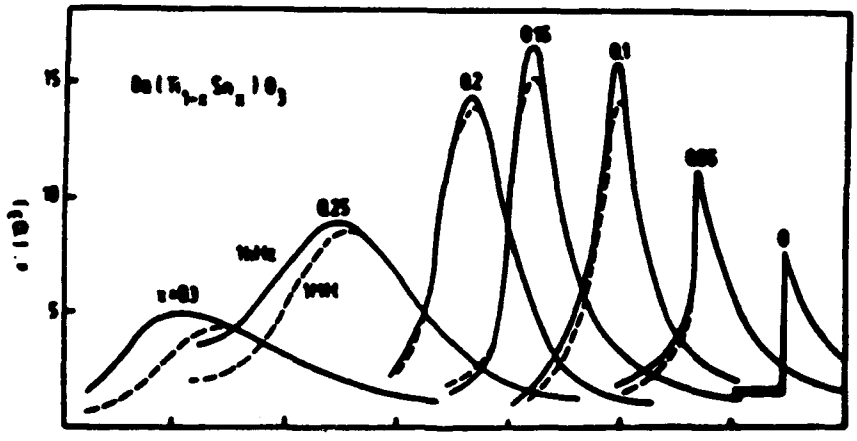

Figure 6 **(a) Phase diagram of the Type III "Pinched" ferroelectric $Ba(Ti_{1-x}Sn_x)O_3$ family (after Toyoda et al., 1989); with corresponding dielectric temperature behavior (b) (after Novosil'tsev and Khodakov, 1956).**

Type IV. ABO_3 Normal Ferroelectrics

The solid solution $Ba_{1-x}Sr_xTiO_3$ exemplifies the family of normal ferroelectrics whose transitions can be adjusted from near 0 Kelvin all the way to 130°C for the end member $BaTiO_3$ (Smolenskii and Isupov, 1954). As shown in Figure 7, high Ks are possible throughout the compositional range. As with the Type III electrostrictors, the transitions are very narrow with the depolarization temperature equal to that for K_m. A level of diffuseness, yet frequency independent, can be achieved through processing techniques creating macro-inhomogeneity.

In summary, each of the four families of electrostrictors presented above offers certain advantages and disadvantages relevant to sonar transducer applications. Such features will become more evident in the sections to follow.

IV. EXPERIMENTAL

This section presents details of the subsequent physical and electrical processing/fabrication and characterization of various electrostrictors in relation to sonar transducers.

Compositional Engineering

Compositional modifications made for the various types of perovskite electrostrictors are presented below.

Compositional Family		Modification	Reason/Property
Type I $Pb(Mg_{1/3}Nb_{2/3})O_3$[PMN]	B-Site	• Ti^{+4}	• Shift T_{max} upward
	A-Site	• Sr^{+2}, Ba^{+2}, Ca^{+2}	• Shift T_{max} downward
			• Effect $\Delta T = T_{max}-T_d$
		La^{+3}	• $\uparrow \Delta T = T_{max}-T_d$
			• Inhibit grain growth
Type II $Pb_{1-y}La_y(Zr_{1-x}Ti_x)O_3$		Increase La↑ y	• Shift T_m downward
			• $\uparrow \Delta T_{m-d}$
Type III $Ba(Ti_{1-x}Sn_x)O_3$ x=0.13		• x=0.1, 0.13 only	• Moderate shift in T_m
Type IV $Ba_{1-x}Sr_xTiO_3$		• Vary x	• Shift T_m

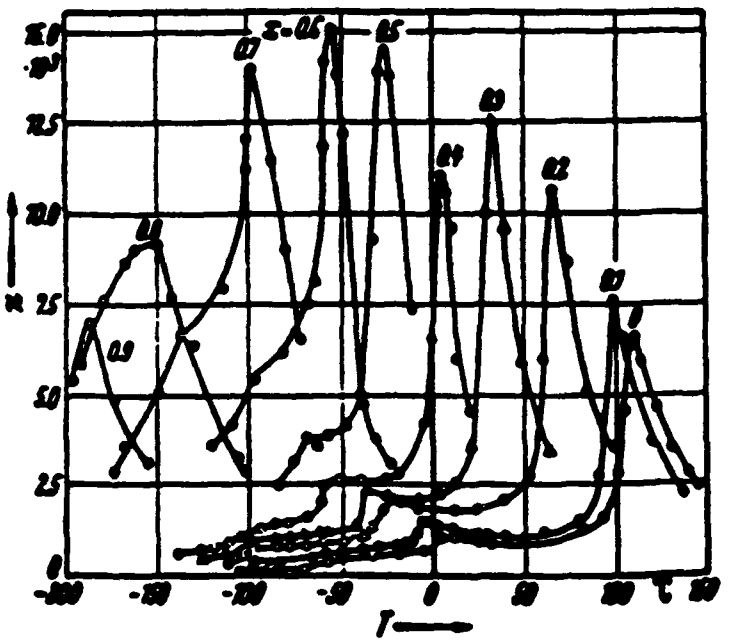

Figure 7. **Dielectric temperature behavior for Type IV $(Ba_{1-x}Sr_x)TiO_3$ normal ferroelectric (after Smolenskii and Rozhachev, 1954).**

Ceramic Processing

The material families presented above were prepared using state-of-the-art mixing/calcination synthesis methods. To insure homogeneity and a high degree of reactivity, high energy milling (vibratory) was used. Details of the raw materials and processing methods used to densify the ceramics are reported elsewhere.(Swartz and Shrout, 1982; Kim, 1990) Specific modifications, however, for the various types of materials included the following:

		Processing Modification	Reason
Type I	PMN-Relaxors	Annealing @900° in O_2	• Minimize Aging
Type II	PLZT Relaxors	Annealing @900° in O_2	• Maximize K
Type III	$Ba(Ti_{1-x}Sn_x)O_3$	Pre-reacted B-site oxides	• Macro-heterogeneity control
			• Maximize K
Type IV	$Ba_{1-x}Sr_xTiO_3$	High purity raw materials	• Compositional homogeneity (macro-heterogeneity control)

The calcined powders and fired disks were characterized by a number of experimental parameters. X-ray powder diffraction was used to insure phase(s) purity e.g. perovskite vs. pyrochlore-Type I. Geometric densities for sintered disks were used to establish the effectiveness of the powder processing/sintering densification. Scanning electron microscopy (SEM) was used to determine grain size and fracture behavior. Prior to electrical characterization, the ceramic disks were prepared by polishing with alumina powder (≤ 600 microns) to achieve parallel surfaces onto which sputtered gold electrodes were applied. An air-dried silver paste was overlayed to improve electrical contact.

Electrical Characterization

Electrical characterization of the materials fabricated included the following:

- K. vs. temperature and frequency (100 Hz, 1 kHz, 10 kHz, and 100 kHz).
- Dielectric Loss (same as above).
- Remanent polarization temperature behavior
- Strain vs. E-field @ 0.1-100 Hz (resistive strain gauge technique) and selected Interferometer measurements (≤1 kHz)

- Polarization (P) vs. E-field (as above) in conjunction with the strain-field loops
- Polarization/strain temperature behavior at given E-fields (10 KV/cm and 20 KV/cm)
- Polarization/depolarization temperature behavior (T_d determination)

Dielectric measurements were made on representative samples using an automated Hewlett-Packard system. The system included an LCR meter[+] and a temperature controlled sample box[++]. The capacitance and dielectric loss were measured pseudo-continuously at various frequencies (10^2, 10^3, 10^4, and 10^5 Hz) as the samples were cooled from high temperature (130°C to -60°C) at a rate of 2 degrees per minute.

The dielectric constant (K) was determined from the measured capacitance (C) of the sample in the following way:

$$K = \frac{(C)(t)}{(A)(\varepsilon_0)} \tag{3}$$

where ε_0 is the permittivity of free space (8.854×10^{-12} F/m) A is the electroded area and t is the thickness between the electrodes of the sample.

To further classify the various types of materials, the Curie-Weiss constants were also determined. Dielectric measurements above the T_{Burns} temperature (>350°C), i.e. onset of polarization fluctuations, were required for both Type I and II relaxors.

Electromechanical testing of the transverse electrostrictive strain (x) and polarization (P) - E-field properties were carried out simultaneously for appropriately prepared ceramic samples. The low-frequency strain/E-field response was measured with a bonded strain gauge technique. Thin (~0.3 mm thick), polished samples, with sputtered gold electrodes of known area, were used. A polyimide foil gauge[♦] was bonded to the sample surface using an adhesive cement.[♦♦] The resistance of the gauge for various temperature and E-field conditions was measured with a dc double-bridge method. The dielectric polarization for the same low frequency (~0.1 Hz) cyclic field drive was concurrently measured by a modified Sawyer-Tower method in conjunction with a digital oscilloscope and X-Y recorder.[**] The temperature range (-10° - 40°C) for this project could be achieved by a temperature controlled oven/cryostat.

+ Model 4274A and 4275A LCR meter, Hewlett-Packard Inc., 1820 Fubarcadero Rd., Palo Alto, CA.

++ Model 2300, Delta Design, Inc., 5775 Kearny Villa Rd., San Diego, CA.

♦ Kyowa KFH-02-C1-11, Kyowa Electronic Instruments Co. Ltd., Japan.

♦♦ Kyowa PC-6

** Tektronix 2430A Digital Oscilloscope, Beaverton OR and Hewlett-Packard, XY Recorder, Palo Alto, CA.

In view of the stated purpose for the application frequency requirement (≤ 1 kHz), higher frequency measurements of the strain (x) and polarization (P) were made on selected samples of Type I and II relaxors. It is important to note that frequencies higher than 1 Hz for the strain gauge technique required optimum bonding of the resistive gauge and extreme care had to be taken to ensure an elastically responsive deformation. As such, only frequencies up to 100 Hz have been made using this technique along with a Sawyer-Tower circuit for dielectric polarization measurements. Higher frequencies (100 - 1 kHz), utilized a Kyowa model 300 Wheatstone Bridge, or alternatively the Mach-Zender strain interferometer as reported elsewhere (Zhang, et al., 1989).

The polarization/depolarization temperature behavior was determined using the Byer and Roundy method. Thin ceramic polished disc specimens (<0.2 mm) were electroded and cooled under E-field, poling from above the temperature of dielectric constant maximum (T_m) to -150°C, well below T_d. After removing the DC field and neutralizing the surface space charges, the poled samples were heated at a constant rate of 2 degrees per minute while recording the pyroelectric current. The pyroelectric coefficient (p_i) = (dPi/dT) was calculated from the pyroelectric current:

$$p = \frac{i}{A(dT/dt)} \left[\frac{C}{m^2\ K}\right] \tag{5}$$

where i is the pyroelectric current, A the electroded area, and dT/dt the heating rate. The polarization was then calculated by integrating the pyroelectric coefficient

$$P_1 = \int p\, dT \quad \left(\frac{C}{m^2}\right) \tag{6}$$

From the P_R temperature data, the depolarization temperature T_d was determined by extrapolation as depicted previously in Figure 3.

Physical Characterization

An additional requirement of the proposed electrostrictors is their performance under an applied stress. In order to evaluate the electromechanical behavior of the materials under significant load, field-induced strains were measured under known stress levels from applied weights using the linear voltage differential transformer (LVDT) method. The deflection of a metal rod with an insulating end tip of known area could be used to find the characteristic stress-strain curves for the ceramic compositions (Type I & II only). The longitudinal strain measurements

were also evaluated by an elastic constant measurement for given initial (deformation) strain and field level. The Poisson's ratio (- s_{11}/s_{12}), relating the longitudinal and transverse compliances, indicates along with the higher induced strain levels for the longitudinal configuration, that it is the appropriate geometry for stress-strain load line behavior for Navy sonar applications under prestress. To estimate the load carrying ability of the various types of relaxors, the elastic compliance (s_{11}^{E}) determined from the resonance techniques in conjunction with strain measurements was used to calculate anticipated loadline performances. In every case there is a trade-off between desired levels of strain induced and the maximum pressure (stress) which can be pushed against for a given electric field.

In relation to mechanical strength and toughness, literature values were obtained for comparison. Preliminary strength and toughness values for Type I and IV materials were also determined using the standard 4-point fracture /indentation method.

V. RESULTS AND DISCUSSION

The results presented are broken down into four sections: (1) Dielectric Behavior, (2) Polarization and Strain Behavior, (3) Physical Characteristics, and (4) Compositional Engineering. The data presented is further sectioned into Electrostriction Classification. A theme of commonality within classes is emphasized as well as engineered differences. At the end of each section, the different types of electrostrictors are contrasted with special reference to sonar transducers. Owing to the large volume of data compiled, only representative dielectric, polarization, and electromechanical behavior will be presented. Specific data for various compositions are given in the attached Appendices.

A. Dielectric Behavior

In this section we present both the low field dielectric (a.c.) and high E-field bias dielectric temperature behavior for the various electrostrictors. Key parameters to note here are T_{max} and K_{max} (@ 1 kHz), dielectric loss above and below Tm and relative temperature coefficients of capacitance, i.e. broadness of transition.

Type I Relaxors - $Pb(B_1B_2)O_3$

Dielectric Temperature Behavior. Figure 8 depicts the phase diagram for the relaxor ferroelectric $Pb(Mg_{1/3}Nb_{2/3})O_3$ and the normal ferroelectric $PbTiO_3$ showing various regions of interest. As shown, the compositions near room temperature (T_m ~20°C @ 1 KHz) are comprised of ~7-10% $PbTiO_3$. It is important to point out that with increasing $PbTiO_3$ the dielectric peak becomes less diffuse and more normal polar-like behavior is observed. Similarly, as T_m is lowered the material exhibits more relaxor-like behavior. These observations are clearly evident in Figure 9, showing dielectric temperature and frequency data for a wide range of $PbTiO_3$ modifications. The consequences of this behavior in relation to the 0-30°C operational temperature range is that lower K_{max}'s are observed and subsequently lower anticipated E-field induced strains, but the broader transitions offer more temperature stability. Hence most of the compositions investigated were (1-x) PMN-(x)PT with $x \leq 0.1$. It is important to note that characteristic of relaxor Type I materials, the dielectric loss maximum occurs at a temperature significantly lower than T_m. Loss values on the order of ~0.1 can occur below T_m (Regime II) while being extremely low <.001 above. The consequences of this loss behavior in Type I relaxors will become evident in the section on high frequency drive.

E-field Bias Behavior. Figure 10 depicts the dielectric D.C. bias behavior at temperatures slightly below T_m, at T_m, and above for a 0.9 PMN-0.1 PT composition . As presented, the level of K_{max} decreased with bias with values saturating at around ~K-5000 for a bias level of 15 KV/cm. Figure 11 shows the actual dielectric temperature-dependent behavior at various bias levels for a similar PMN-PT composition, again showing the dramatic decrease in K, particularly at ~T_m, with the transition shifting upward with increasing bias. The dielectric loss bias behavior shown in Figure 11(b) reveals a dramatic "clamping" effect, as expected. Dielectric temperature plots for numerous relaxor-based compositions are compiled in Appendix A.

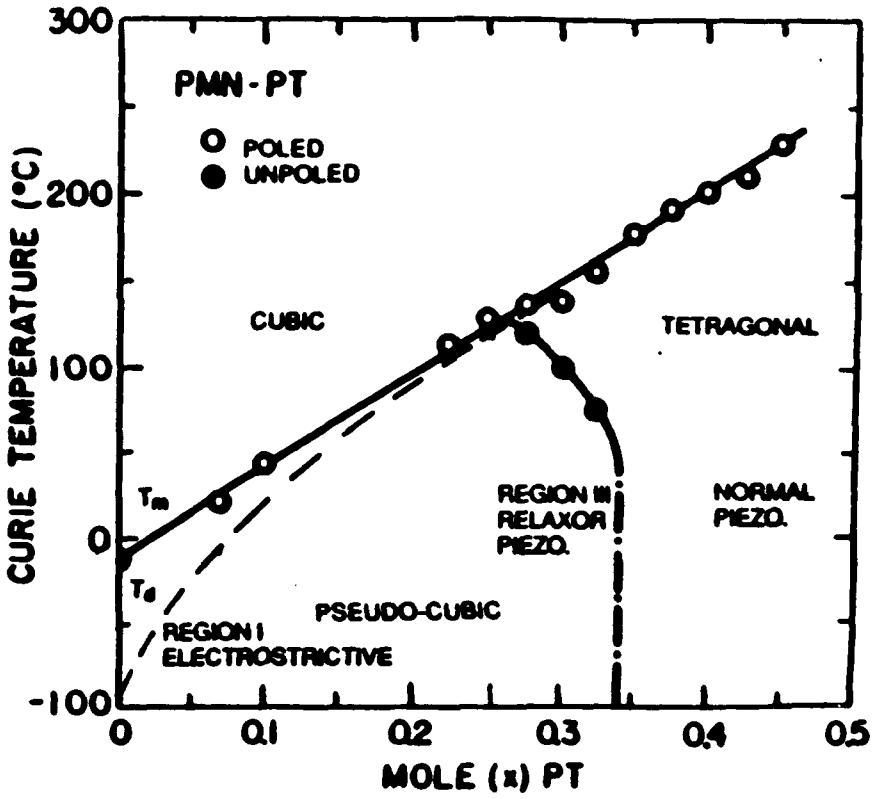

Figure 8. Phase diagram for PMN-PT systems indicating regions of interest, including T_d and morphotropic phase boundary (after Choi et al., 1989).

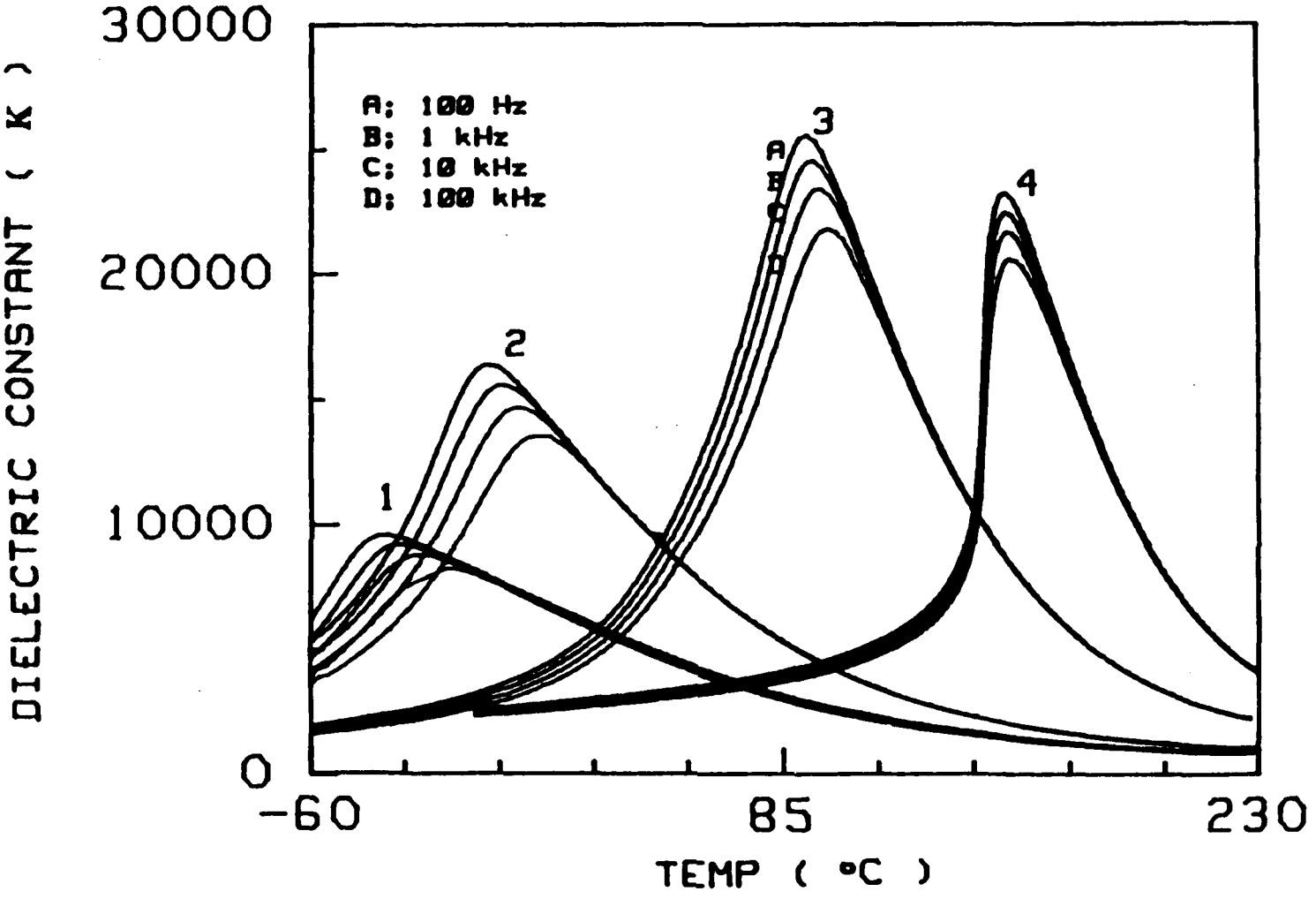

Figure 9. **Dielectric temperature behavior for a range of PMN-PT. 1 mole % La compositions (N. Kim Master's Thesis, Penn State University, p. 78 (1990), (1) 100/0, (2) 93/7, (3) 80/20, (4) 65/35.**

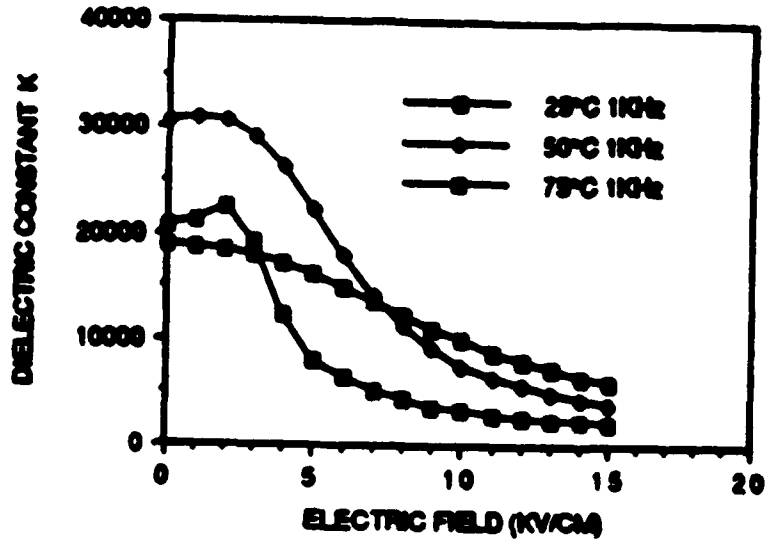

Figure 10. Maximum dielectric constant (K_m) at 1 KHz as a function of applied field for a 0.9 PMN-0.1PT composition at 25, 50, and 75°C. Note: $T_m \approx 40°C$.

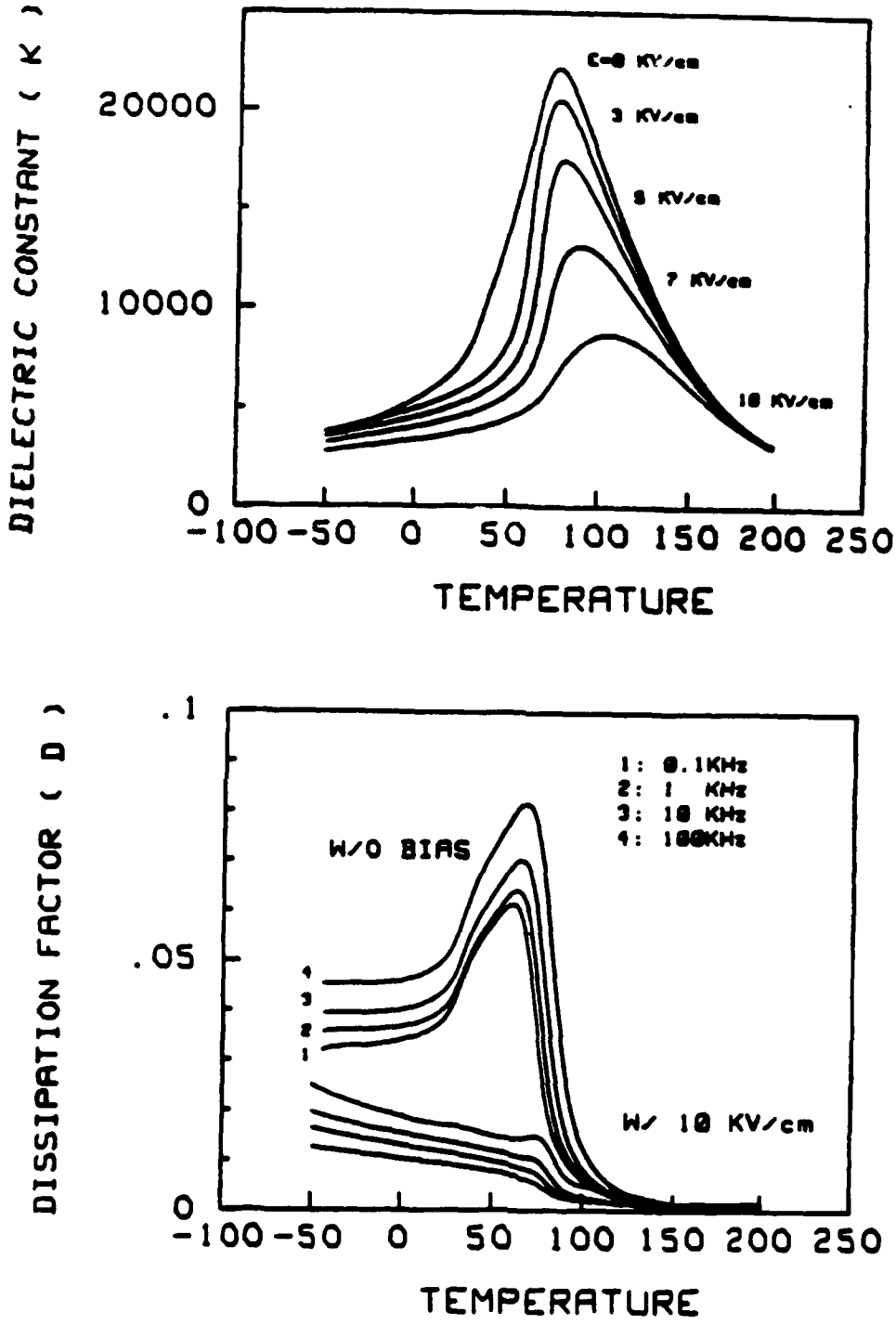

Figure 11. Effect of DC bias field on the dielectric behavior as a function of temperature in a PMN:PT ceramic at 1 KHz. (Top)
Effect of bias (0 vs. 10 KV/cm) on loss as a function of frequency at 0.1 KHz, 1 KHz, 10 kHz and 100 KHz. (Bottom)

Type II Relaxors - PLZT

Dielectric temperature curves for several PLZT compositions are given in Figure 12. As shown, with increasing La modifications, both K_m and T_m decrease while the diffuseness is enhanced. This dramatic effect of La is believed to be the result of a vacancy decoupling of the ferroelectric lattice to the highly polarizable Pb cations. It is further evident from Figure 12 that the level of K for temperatures in the 0-30°C range are relatively small. As such, electrostriction electromechanical functionality is limited to the polar Regime II, which possesses high dielectric loss, see Figure 13.

E-Field Bias Behavior. The dielectric E-field bias behavior for a 9/65/35 PLZT composition is given in Figures 14 and 15. As shown in Figure 15, the level of K increases with E-field even up to 15 KV/cm. This indicates that the level of $P_{induced}$ is far from being saturated and should be greater than that for Type I relaxors. In contrast to the Type I and normal ferroelectrics, Tm decreases with D.C. bias (see Figure 14a), reflecting anti-ferroelectric behavior, though yet to be substantiated. As seen in Figure 14b, the loss at 1 KHz increases with bias up to 9 KV/cm.

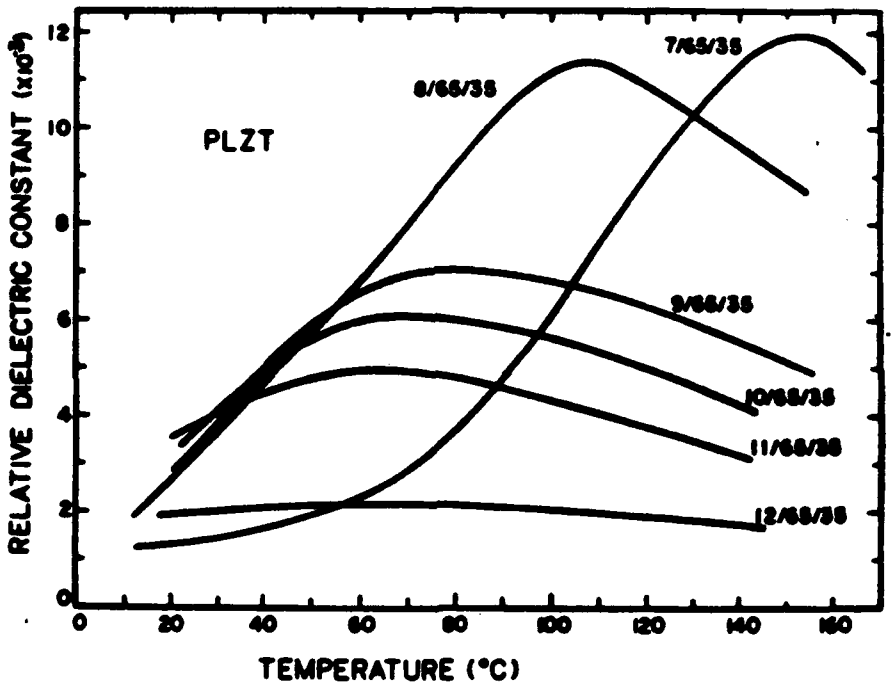

Figure 12. Dielectric temperature behavior for various Type II PLZT relaxor compositions.

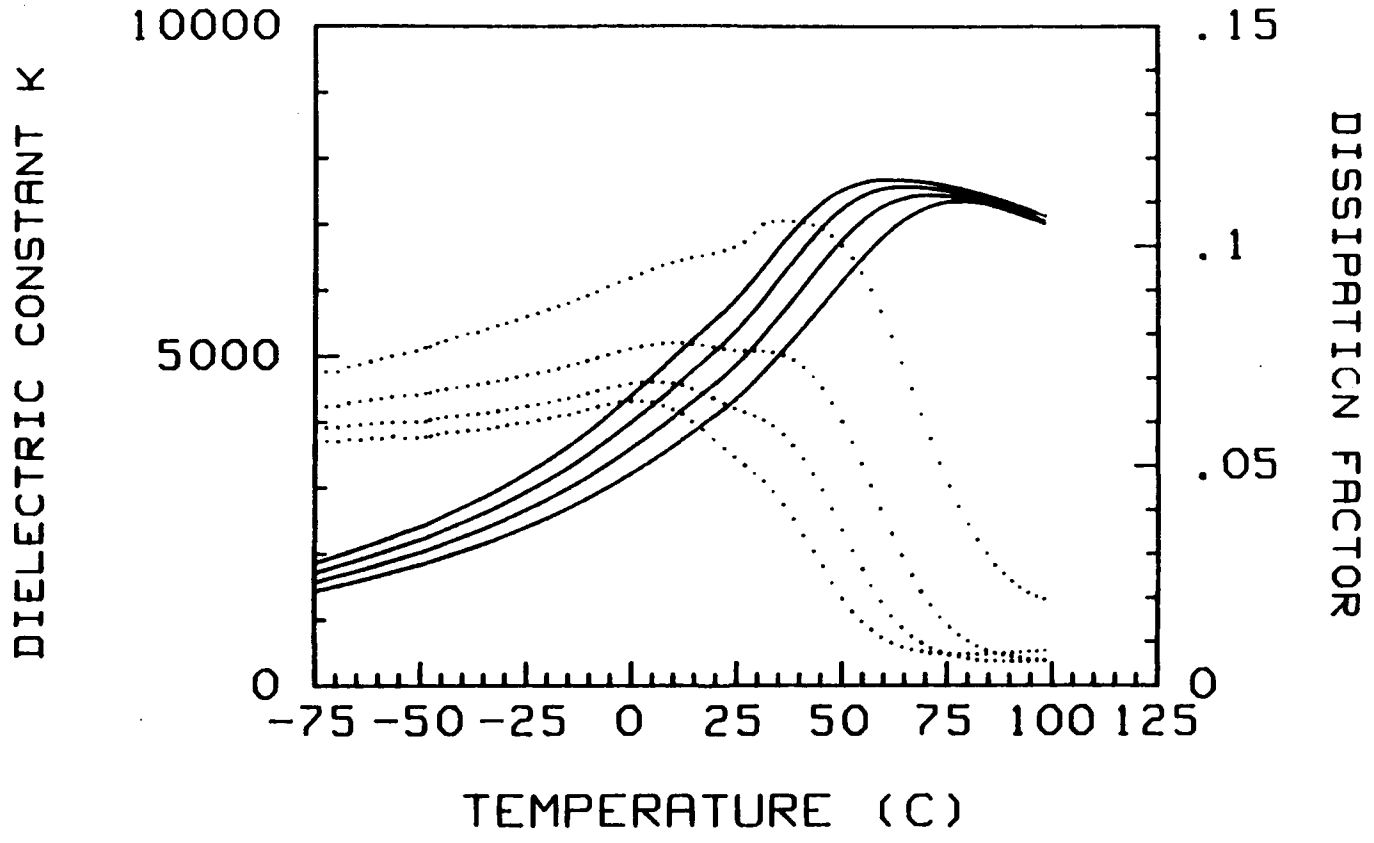

Figure 13. Dielectric constant and loss as a function of frequency for PLZT 9/65/35.

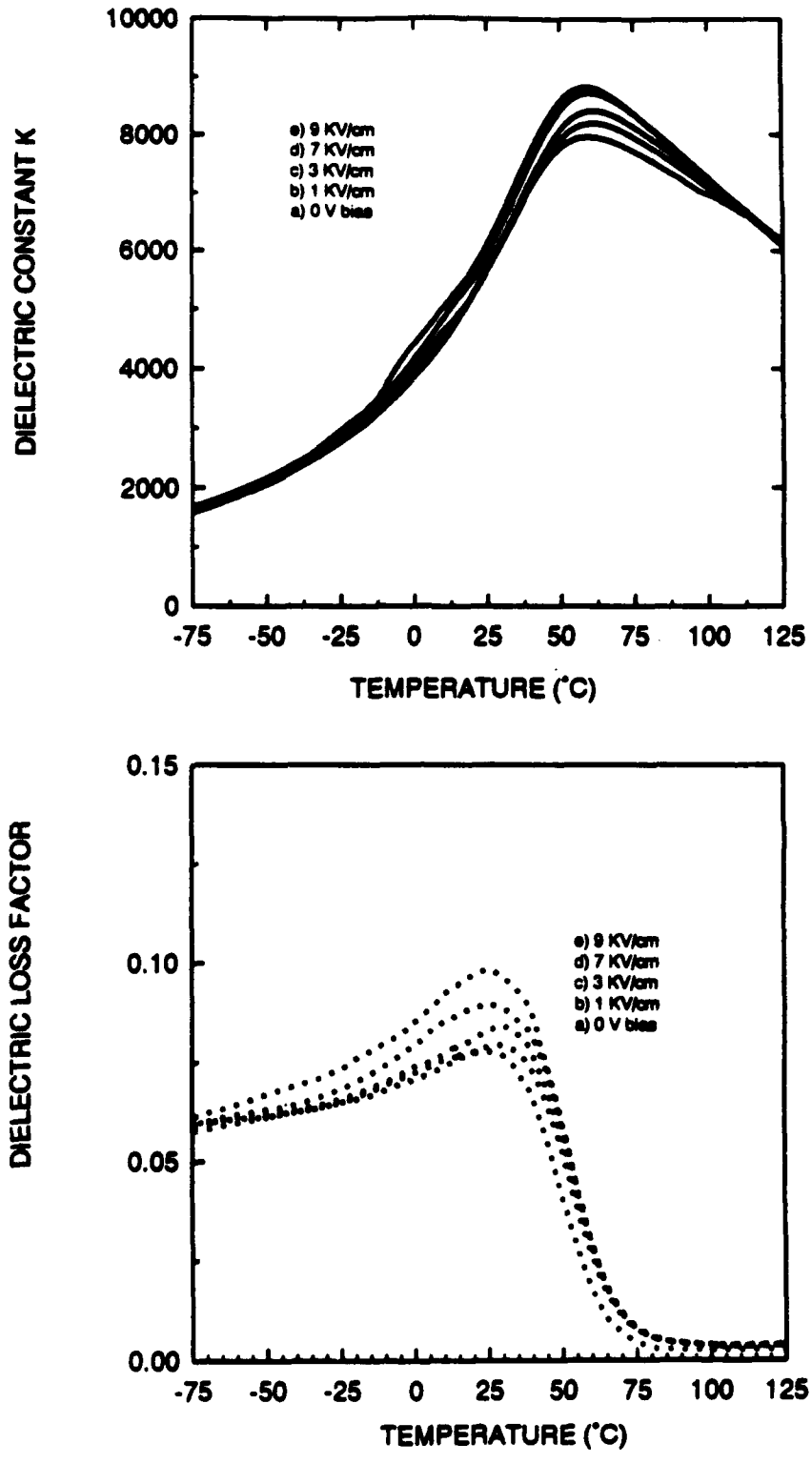

Figure 14. Dielectric constant and loss (@ 1 KHz) as function of temperature and applied field for 9.0/65/35 PLZT composition.

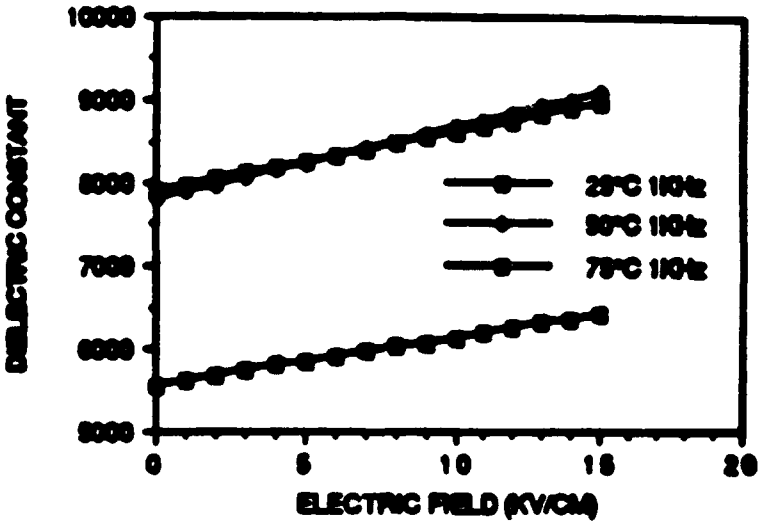

Figure 15. Dielectric constant (@ 1 KHz) as function of applied field for 9/65/35 PLZT composition at 25, 50, and 75°C.

Type III. "Pinched" Ferroelectric $Ba(Ti_{1-x}Sn_x)O_3$

The dielectric temperature behavior for $Ba(Ti_{1-x}Sn_x)O_3$ x=0.13 prepared in this work is presented in Figure 16. As shown, the K_{max} value is extremently high (>35,000) with little frequency dispersion. However, the transition peak behavior is very narrow in contrast to relaxors. It is interesting to point out that significantly higher levels of K_m were achieved as compared to the work by Ciemenski et al. (1990), even for extremely large grain size samples, whereas grain sizes in this work were found to be only on the order of ~3 microns. Also, unlike Type I and II relaxors, the dielectric loss maximum occurs in close proximity to T_m.

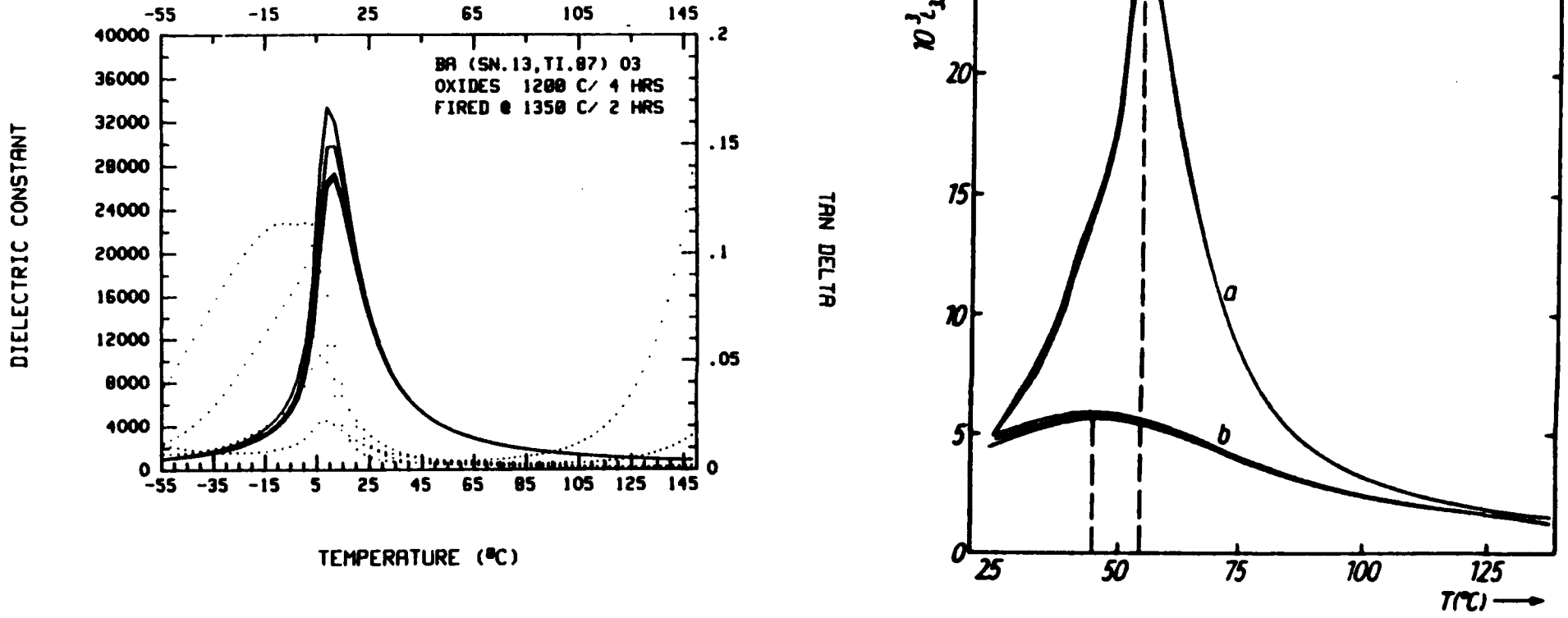

Figure 16. Dielectric temperature behavior for a Type III $Ba(Ti_{1-x}Sn_x)O_3$ material.
(Left--this work; Right--Ciemenski et al, 1990)
Note: Curve (a) is for large-grained sample and curve (b) is for fine-grained (~2 μm).

Type IV. ABO_3 Normal Ferroelectrics

Dielectric temperature curves for several compositions of $Ba_{1-x}Sr_xTiO_3$ (x = 0.50, 0.45, 0.4, and 0.35) are given in Figure 17. As shown, the selected compositions have their T_m near room temperature with K_m values in the range of 15,000-20,000, with little evidence of any compositional dependency. The losses within the temperature usage range (0-30°C) decrease with increasing Sr-modification. The high values of K_m observed in relation to those reported in Figure 7 reflect minimal macro-heterogeneity in composition. As with the Type III materials, the transition is narrow with minimal frequency dispersion (see Figure 18).

E-FieldBias Behavior.

Figure 19 depicts the dielectric-bias behavior for a $Ba(1-x)Sr(x)TiO_3$ (x=0.3) composition with Tm near room temperature. As expected of normal ferroelectrics, the level of K_{max} dramatically falls off with a slight upward shift in T_m. The sharper K/E-field relation signifies lower anticipated levels of induced polarization (P_{ind}). The effect of bias on loss is shown in Figure 19b. As with all ferroelectrics, the loss decreased with bias. As a note, the loss values for both Type III and IV normal ferroelectrics below Tm are significantly lower than that found for relaxors.

Summary of Dielectric Behavior

A summary of the dielectric behavior for the four types of electrostrictors is given in Table IV. As presented, all the material families possess Curie constants on the order of 1.5×10^5/°C reflecting their commonality as "displacive" type ferroelectrics, although the Type I and II relaxors have onsets of polarizations at T_B ~350°C, well above T_m. The broad transitions of the relaxors reflect good temperature stability in contrast to the steep K_{max} curves for the normal ferroelectric materials. The steep bias dielectric behavior for the latter offers low field operation potential, but expectedly low induced polarizations and thus strains. Higher losses are found for the relaxors, below T_m, but can be very low (on the order of <.001) above. As anticipated, AC loss decreases with DC bias for all the ferroelectric families.

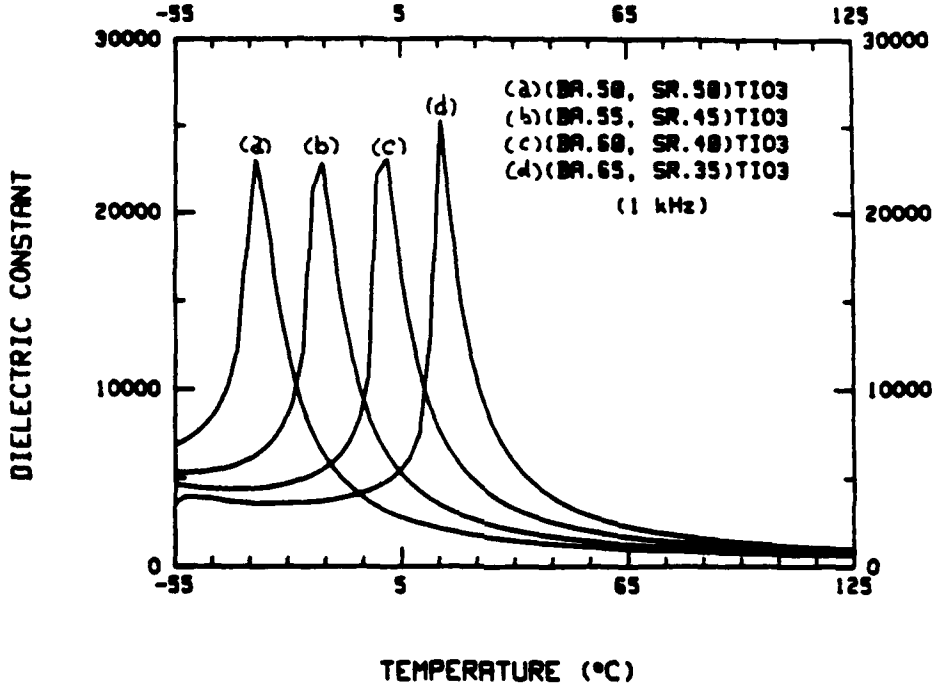

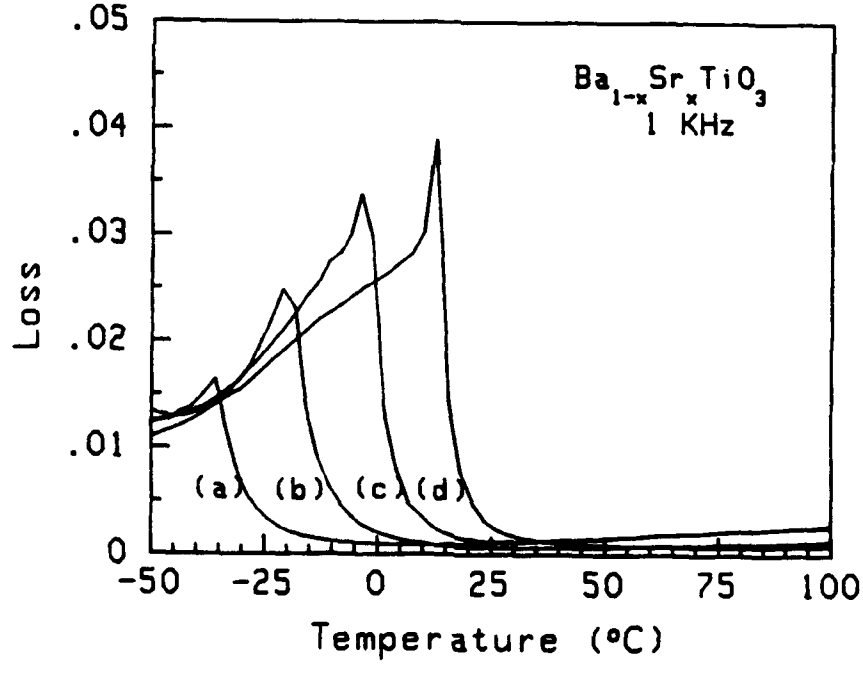

Figure 17. Dielectric constant and loss at 1 KHz as function of temperature for $(Ba_{1-x}Sr_x)TiO_3$ with varying Sr^{2+} content.

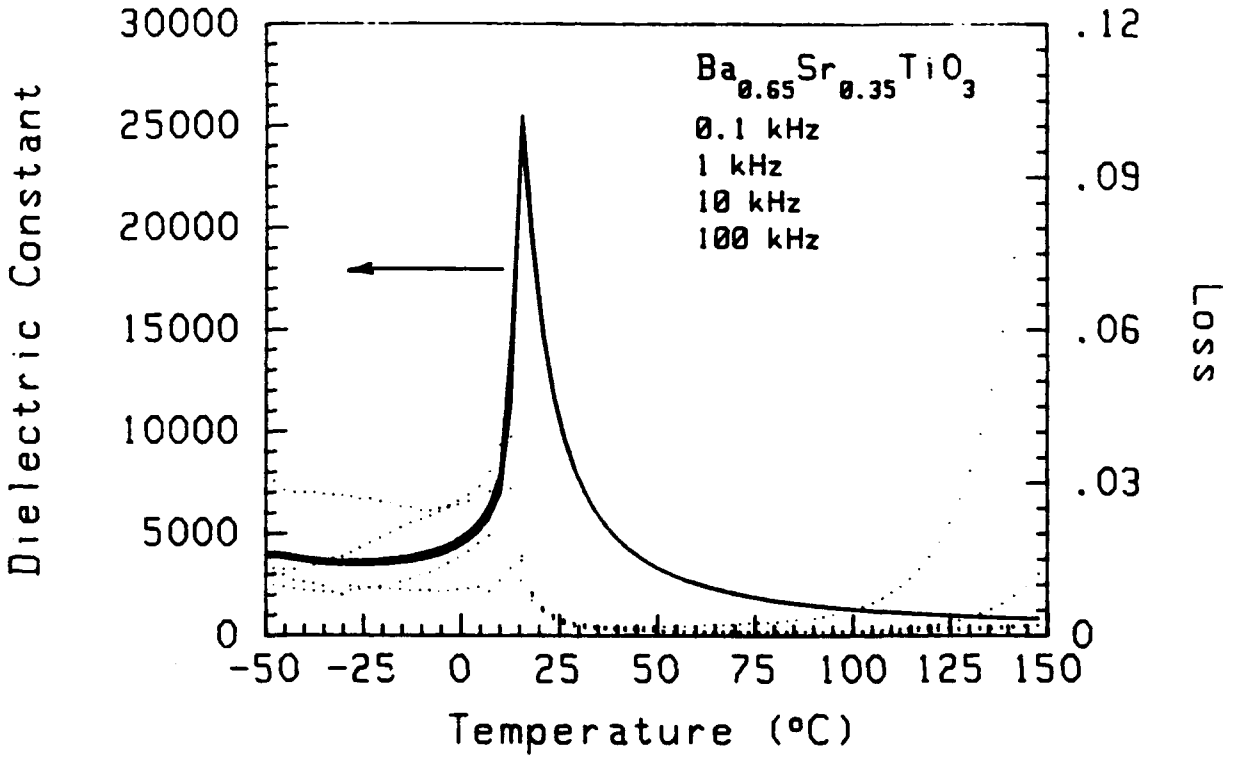

Figure 18. Dielectric temperature behavior for $Ba_{.65}Sr_{.35}TiO_3$.

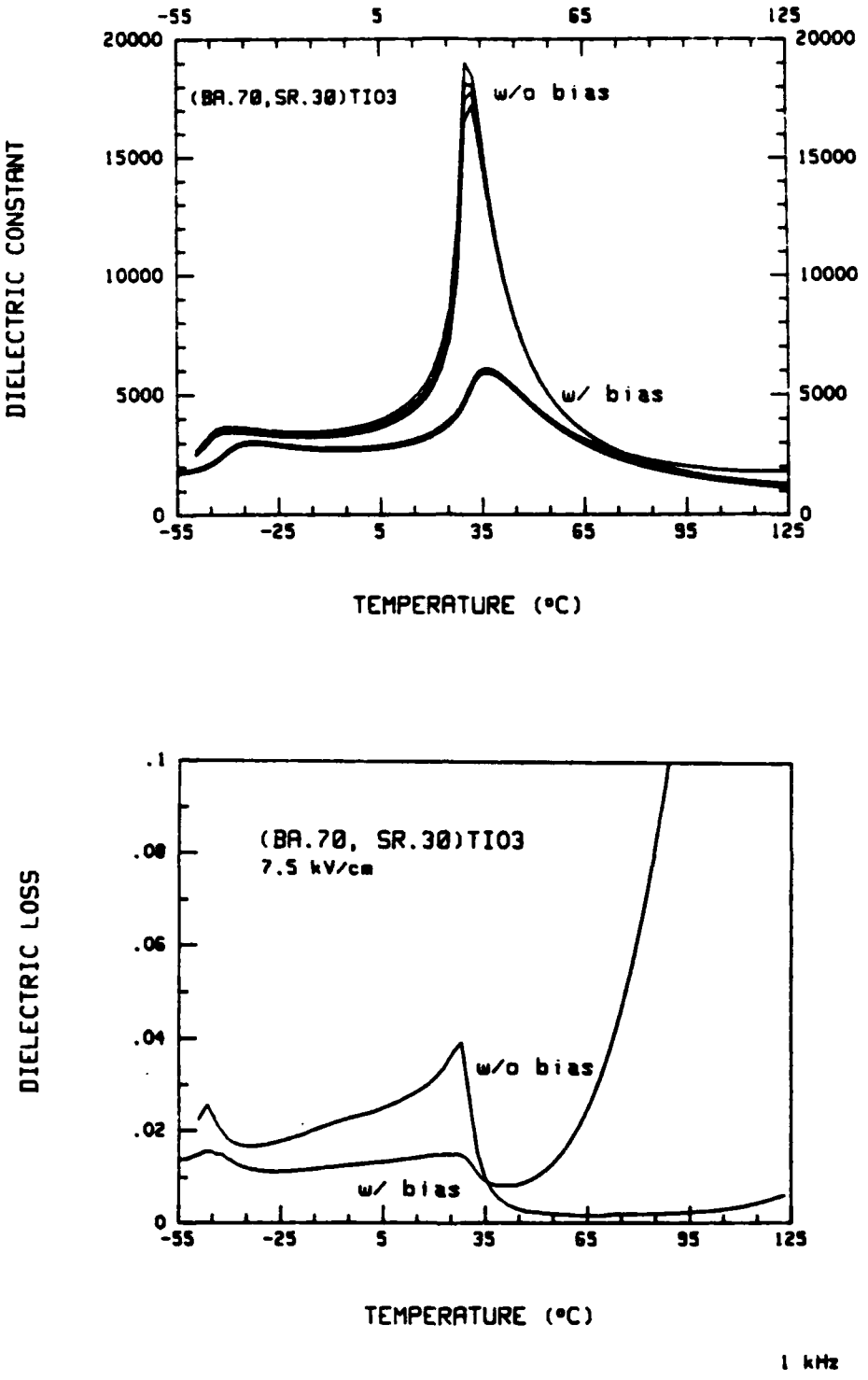

Figure 19 **(a) Dielectric constant and (b) loss as function of applied bias field (0 and 7.5 KV/cm) for a Type IV normal ferroelectric $(Ba_{1-x}Sr_x)TiO_3$ (x=0.30) at 1 KHz..**

Table IV. Summary of Dielectric Properties for the Classes of Electrostrictor Materials

Material Type	Example	K_{max}	Loss $<T_m>$	Transition Behavior	E-field/K Behavior	*Curie Constant C($x10^5$°C)
Type IV Normal	$(Ba,Sr)TiO_3$	15,000-20,000	0.03-<.003	very narrow	steep	1.5
Type III	$Ba(Ti,Sn)O_3$	≤35,000	~0.1-<.003	very narrow	very steep	~1-1.5
Relaxor II	PLZT	~6,000-9,000 (dispersive)	~0.1	very broad	minimal	~1.5
Relaxor I	PMN-PT	≤30,000 (dispersive)	0.08-<.001	broad (dispersive)	moderate	~1.5

*Note: Must be determined above T_B for Type I and II relaxors.

B. Polarization/Strain Behavior

This section presents the experimental results of the polarization temperature behavior and associated coupling to electrostrictive strain. In addition to polarization and E-field strain behavior, the level of hysteresis as defined in Figure 20 is given. As shown, the maximum departure from reversibility is defined. As a special note, most of the strain loops and P/E hysteresis curves were obtained at low frequencies, ≈0.1 Hz. Results of higher frequency measurements for selected materials and behavioral impact in relation to sonar transducers will be discussed.

As for the dielectric data, only representative behavior for the types of electrostrictors will be presented. Additional data for specific compositions is compiled in Appendix B.

Type I. Relaxors - PMN-PT

The remanent polarization temperature behavior for a representative Type I composition 0.95 PMN-.05PT (T_m @ 1 KHz ~15°C) is shown in Figure 21. As presented, the depolarization temperature T_d is well below K_m, being ~ -20°C, or -27°C if one uses the peak pyroelectric temperature value. Thus a ΔT-T_m-T_d value of ~45°C offers electrostrictive coupling (Regimes II and I) for the temperature range of interest, (i.e. 0-30°C).

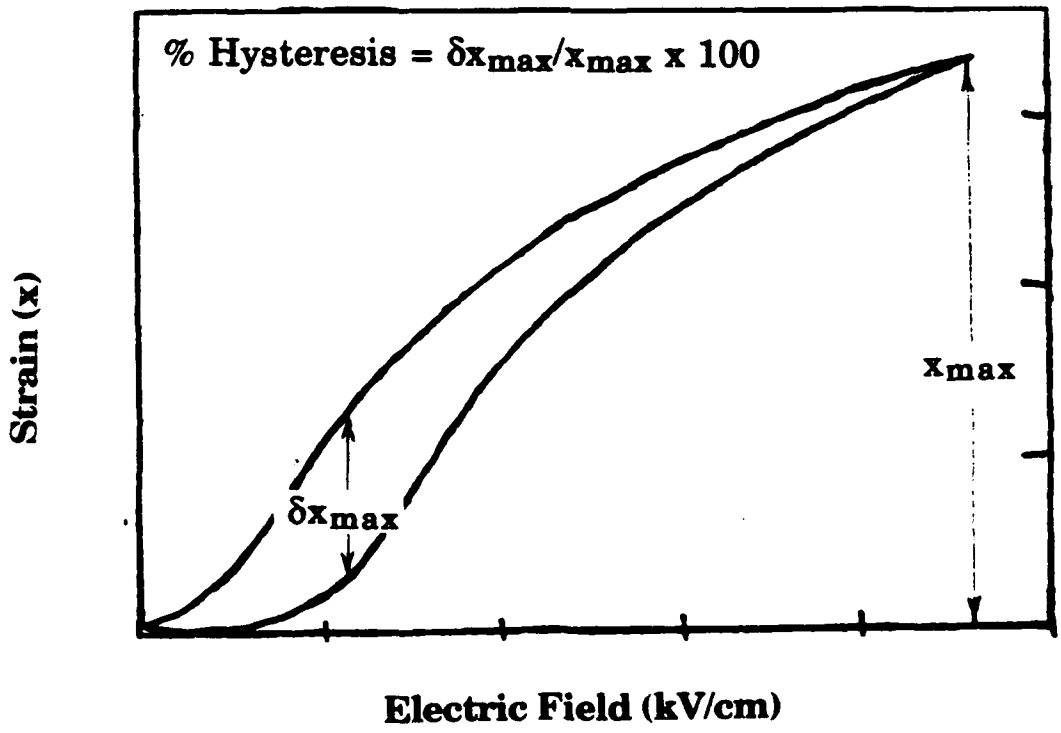

Figure 20. Schematic definition of % strain hysteresis.

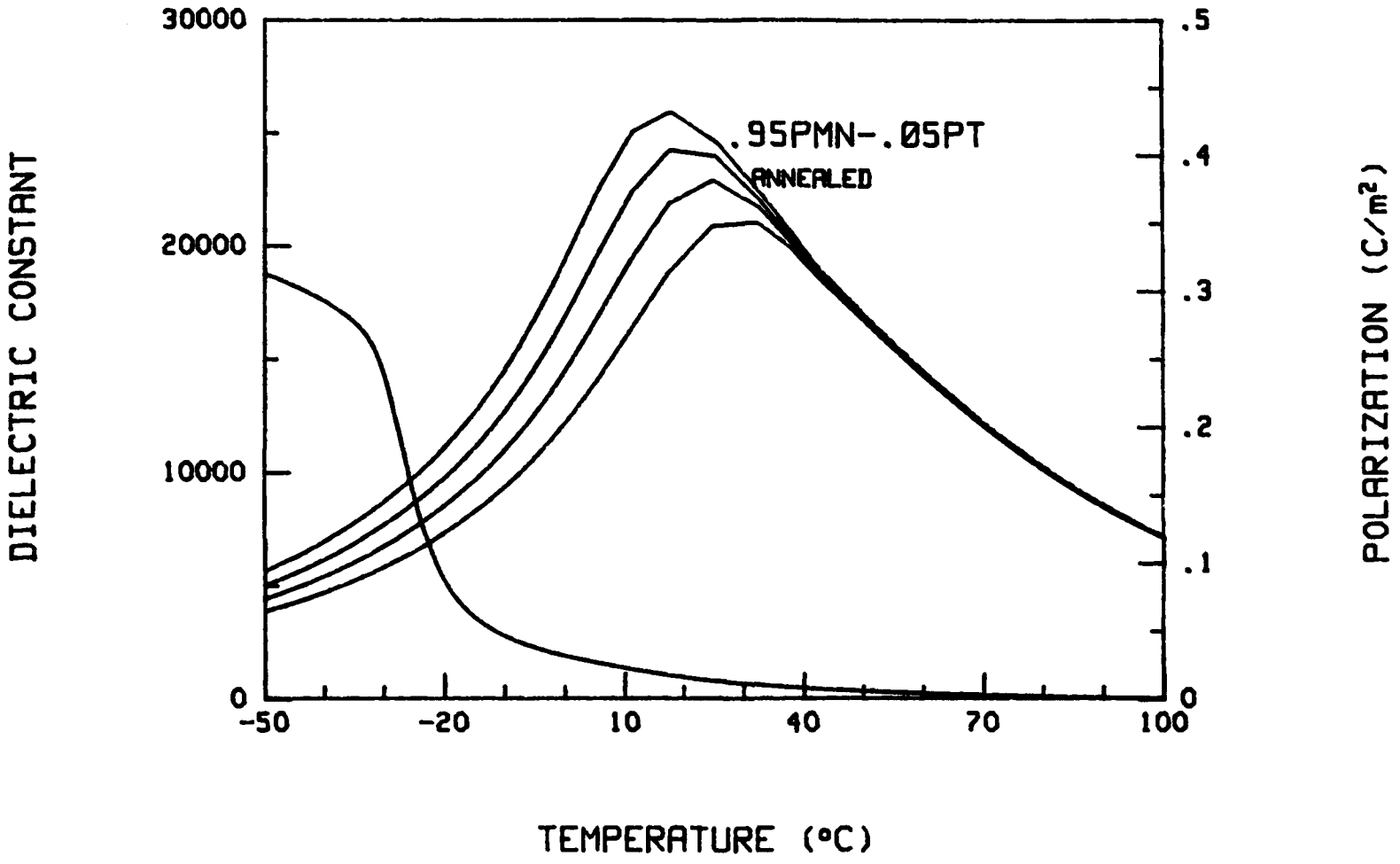

Figure 21. Dielectric and polarization temperature behavior for Type I relaxor 0.95PMN-0.05PT.

Figure 22 shows the level of induced polarization (P_{ind}) and corresponding transverse strain levels @ 20 KV/cm over the temperature range of interest. The strain levels are non-remanent, as expected, since operating in polar Regimes I and II. As shown, the level of induced strain and P_{ind} increase with decreasing temperature as T_d is approached. Since the measurement frequency was low (≤1 Hz), the effective T_m is lower than the ~15°C quoted above. From the actual strain/E-field hysteresis curves, presented in Figure 23, minimal hysteresis is observed in proximity to T_m (or Regime I) while increasing with decreasing temperature, whereupon micro-macrodomain switching occurs (i.e. Regime II). It is not until temperatures approach T_d that significant hysteresis and strain remanence appears.

Room temp polarization-field (P-E) data for 0.95 PMN-0.5PT show characteristic non-linear "slim-loop" behavior (see Figure 24a). The level of P_{ind} @ 20 KV/cm is found to be on the order of 0.3 C/m^2, as collaborated in Figure 22, indicating P-E saturation and/or complete phase switching. Naturally, the field required to obtain such switching decreases as T_d is approached as substantiated in Figure 23 above. Corresponding transverse strain-field (x-E) data are presented in Figure 24b. Note the lack of remanence and minimal hysteresis in the strain data.

Type II. Relaxors - PLZT

The remanent polarization temperature behavior for a representative PLZT composition (11/65/35) with T_m @ 1 KHz shifted close to room temperature is given in Figure 25. As shown, there is a long, continuous remanent polarization tail over a very wide temperature range, reflecting a mixture of stable micro and macro-domains. From this figure it is evident that large polarization (P_{ind}) and corresponding strains can be readily obtained over a wide temperature range. Though difficult to assess from this figure, the $\Delta T=T_m-T_d$ regime is >100°C, offering the potential for a very wide temperature usage range.

Figure 26 exhibits the level of induced polarization and corresponding transverse strains (@ 20 KV/cm) over the temperature range of interest. As presented, little temperature-dependence is observed, owing to the large ΔT_{m-d} regime. Naturally, if T_d is higher (i.e. lower La level PLZTs) more strain and polarization can be induced at room temperature, however, greater hysteresis and temperature dependence are observed. Further discussions are presented in the section on compositional modifications.

The room temp polarization-E-field curve presented in Figure 27 reflects non-linear "slim-loop" behavior as found for Type I materials. In contrast, the induced polarization @ 20 KV/cm is far from being saturated. Again, this reflects a significantly lower T_d (-125 vs. -20°C for Type I).

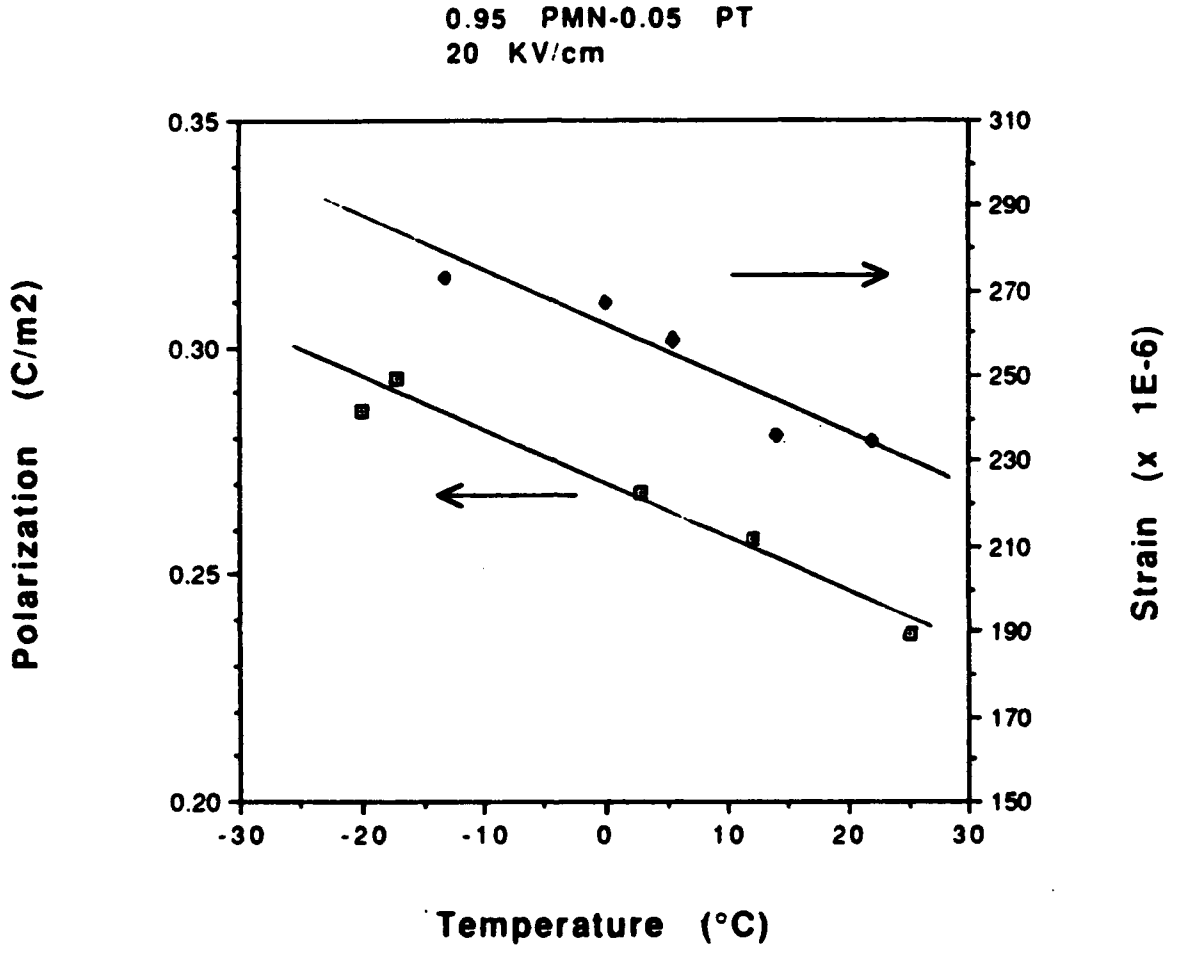

Figure 22. **Induced polarization (P_{ind}) and corresponding transverse strain at 20 KV/cm as a function of temperature for a Type I relaxor. Example: 0.95PMN-.05PT. Note: Transverse strain is negative.**

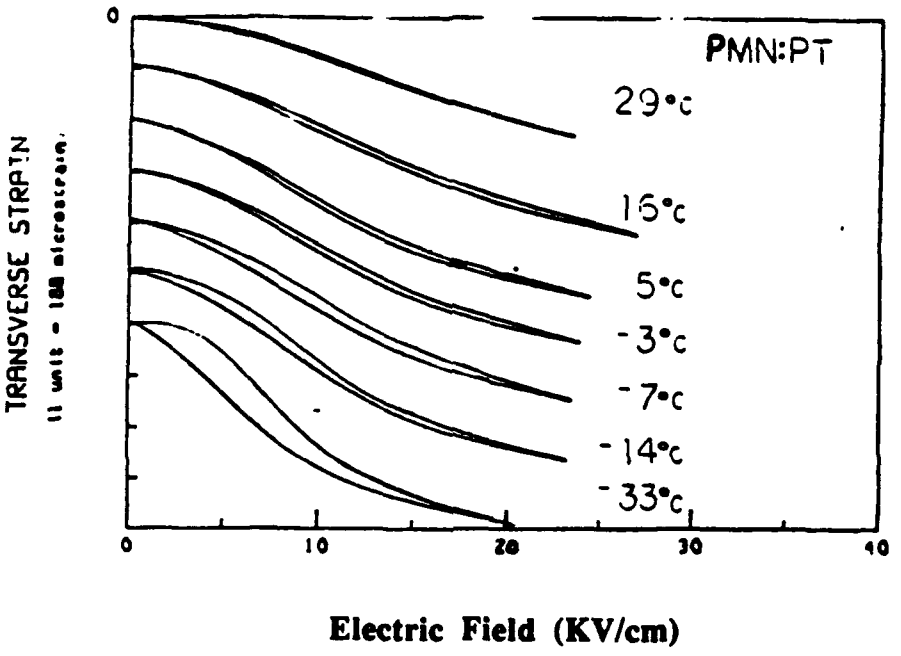

Figure 23. Induced strain vs. electric field behavior and function of temperature for 0.95PMN-0.05PT ($T_m \approx 15°C$, Td ≈ -20°C @ 1 KHz).

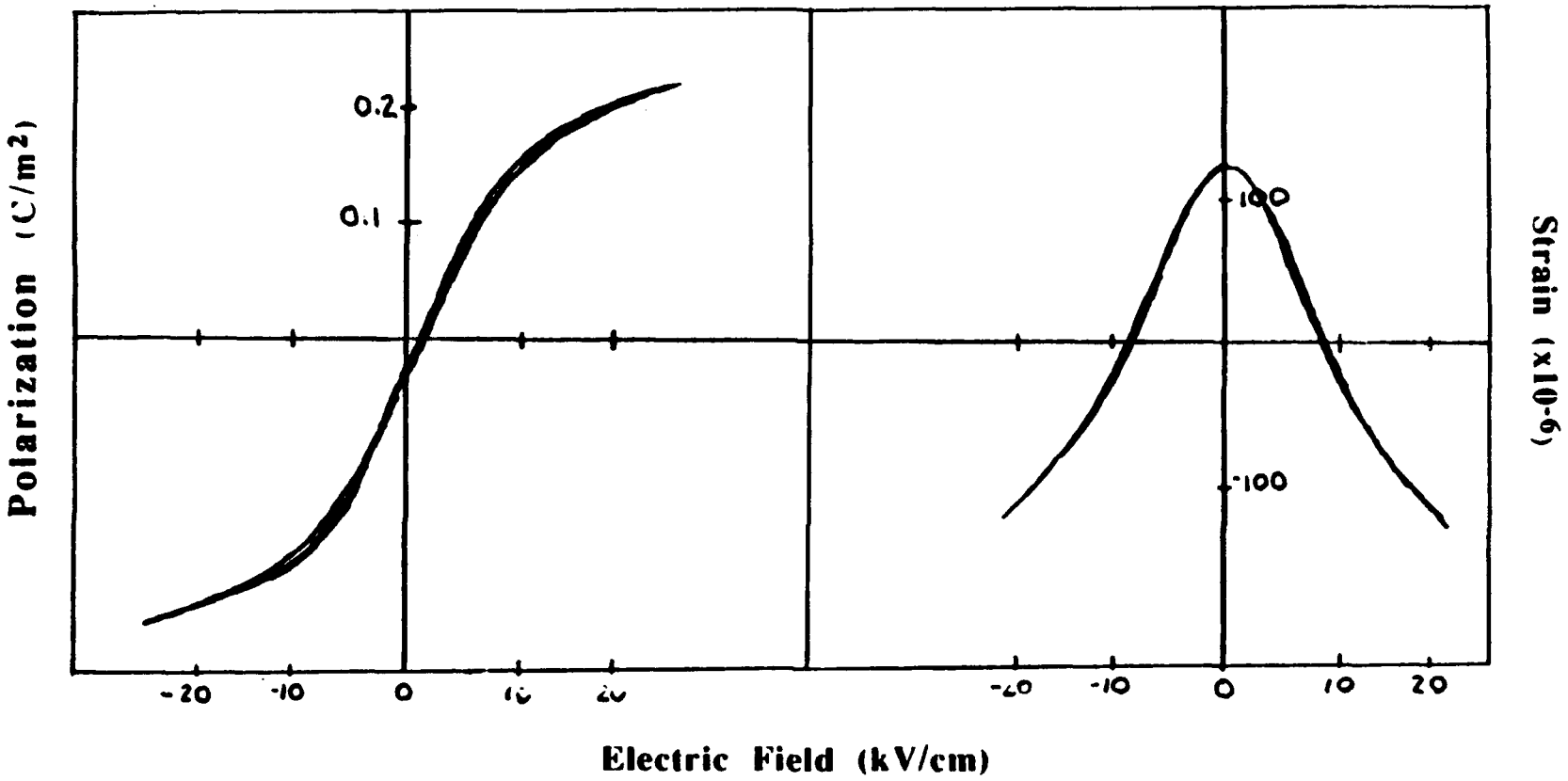

Figure 24. Room temperature a) polarization and b) transverse strain versus electric field for Type I relaxor 0.95 PMN-0.05PT.

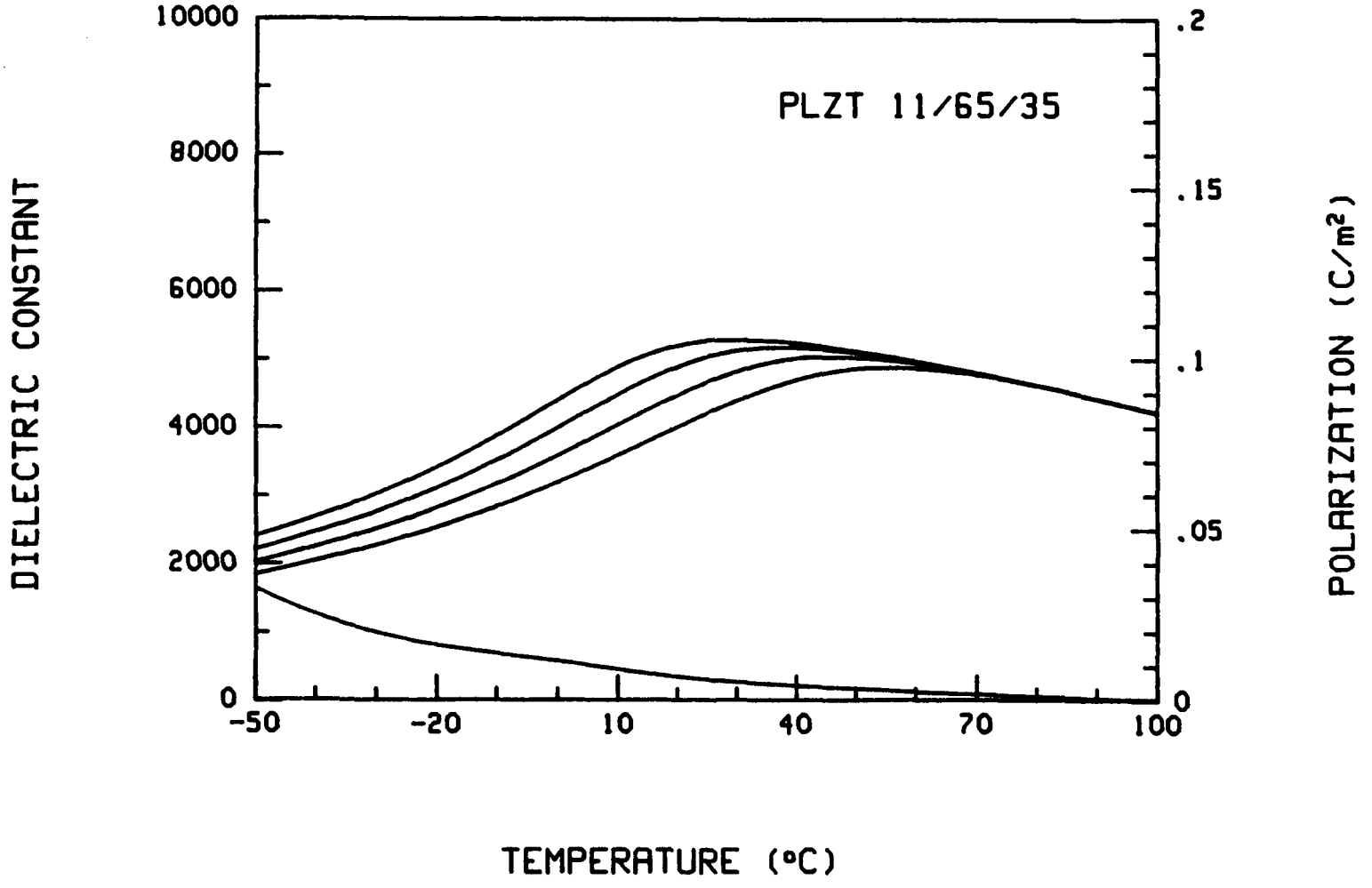

Figure 25. Dielectric and polarization temperature behavior for Type II relaxor PLZT (11/65/35).

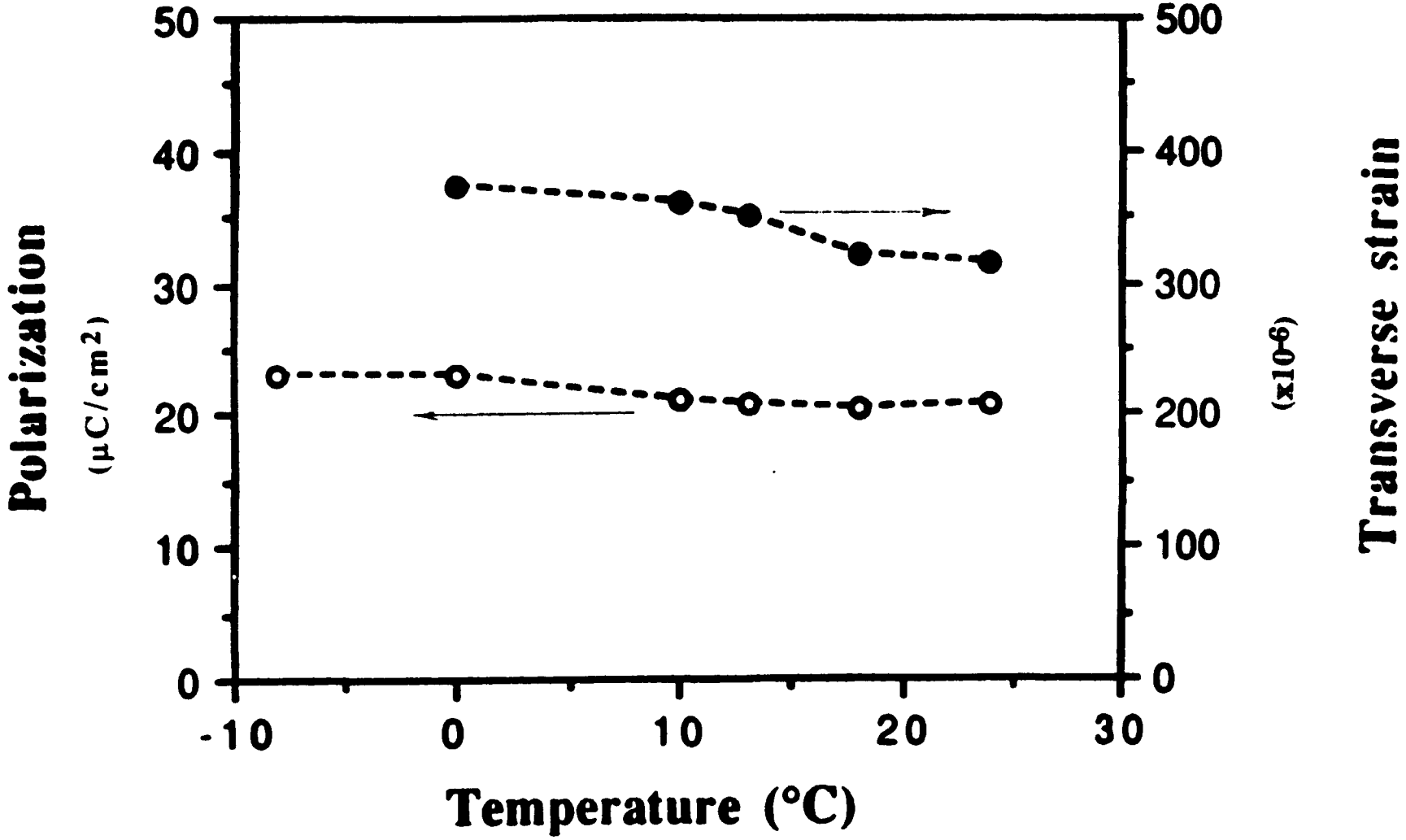

Figure 26. Induced polarization (P_{ind}) and corresponding transverse strain at 20 KV/cm for a Type II relaxor PLZT (11/65/35).

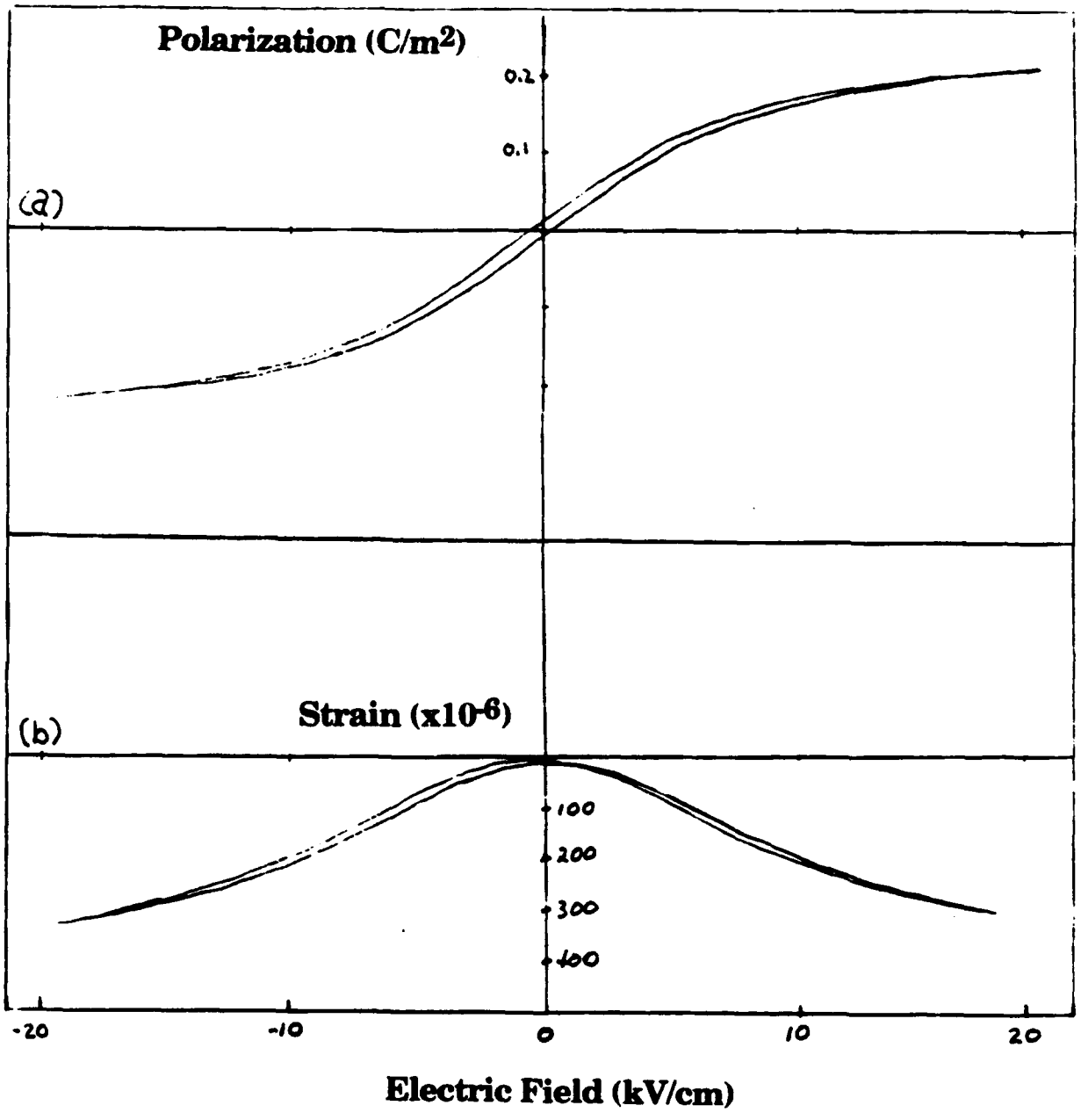

Figure 27. Room temperature a) polarization and b) transverse strain versus applied electric field for Type II relaxor PLZT (11/65/35).

The corresponding transverse strain-field (x-E) loop is presented in Figure 27b. Again, as with the Type I relaxors, there is no remanence and minimal hysteresis. As in Figure 27, the strain @ 20 KV/cm is far below the saturation level. Figure 28 presents the required E-field levels for a transverse strain of ~300 x 10^{-6} as a function of temperature. As expected, lower fields are required with decreasing temperature. The low level of hysteresis shown also reflects a low T_d.

Type III. "Pinched Ferroelectrics" $Ba(Ti_{1-x}Sn_x)O_3$

The polarization and dielectric temperature behavior for $Ba(Ti_{1-x}Sn_x)O_3$ x=0.13 is presented in Figure 29. Interestingly, no depolarization temperature (T_d) was evident as polarization decreased continuously up to ~100°C. A slight change in slope did appear near T_m. This behavior is believed to be the consequence of a "core-shell" structure where a $BaTiO_3$ ferroelectric core is encompassed in a compositionally-modified shell. However, further experiments will have to be performed to confirm this.

Figure 30 shows the level of induced polarization and transverse strain (@ 20 KV/cm) over the temperature range of interest. Compared with the lead-based relaxors, both Types I and II, the level of P_{ind} and strains are considerably smaller. Surprisingly, little temperature dependence is observed. A further surprise arises from the polarization hysteresis loops showing extremely non-linear P-E behavior with substantial dP/dE at low E-fields, indicating large changes in K with bias and low E-field saturization, see Figure 31. Also shown in Figure 31, nearly linear strain (x-E) E-field behavior is observed at low biases followed by a rapid saturization region

Along with minimal temperature dependence, an additional unexpected behavior is the lack of any significant strain-field hysteresis over a wide temperature range, including no remanent "walk off". This observed behavior is again believed to be associated with a core-shell model, whereby macrodomain switching in the ferroelectric core contributes to the strain, but upon E-field reversal, a large compressive stress generated by the shell rapidly reorients the domains back to their original position, resulting in minimal hysteresis.

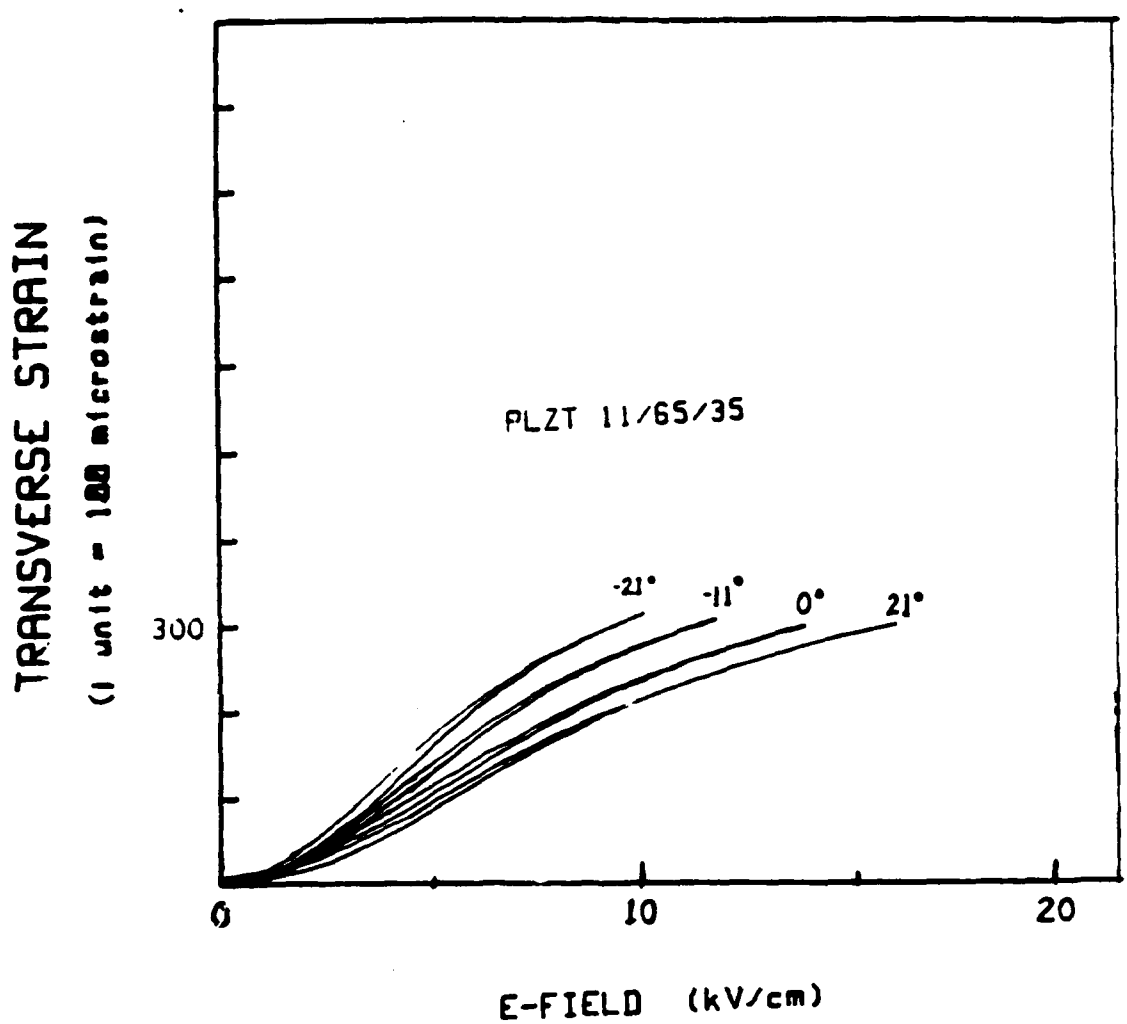

Figure 28. Constant transverse strain-level (300 μ) as function of electric field at various temperatures for PLZT (11/65/35).

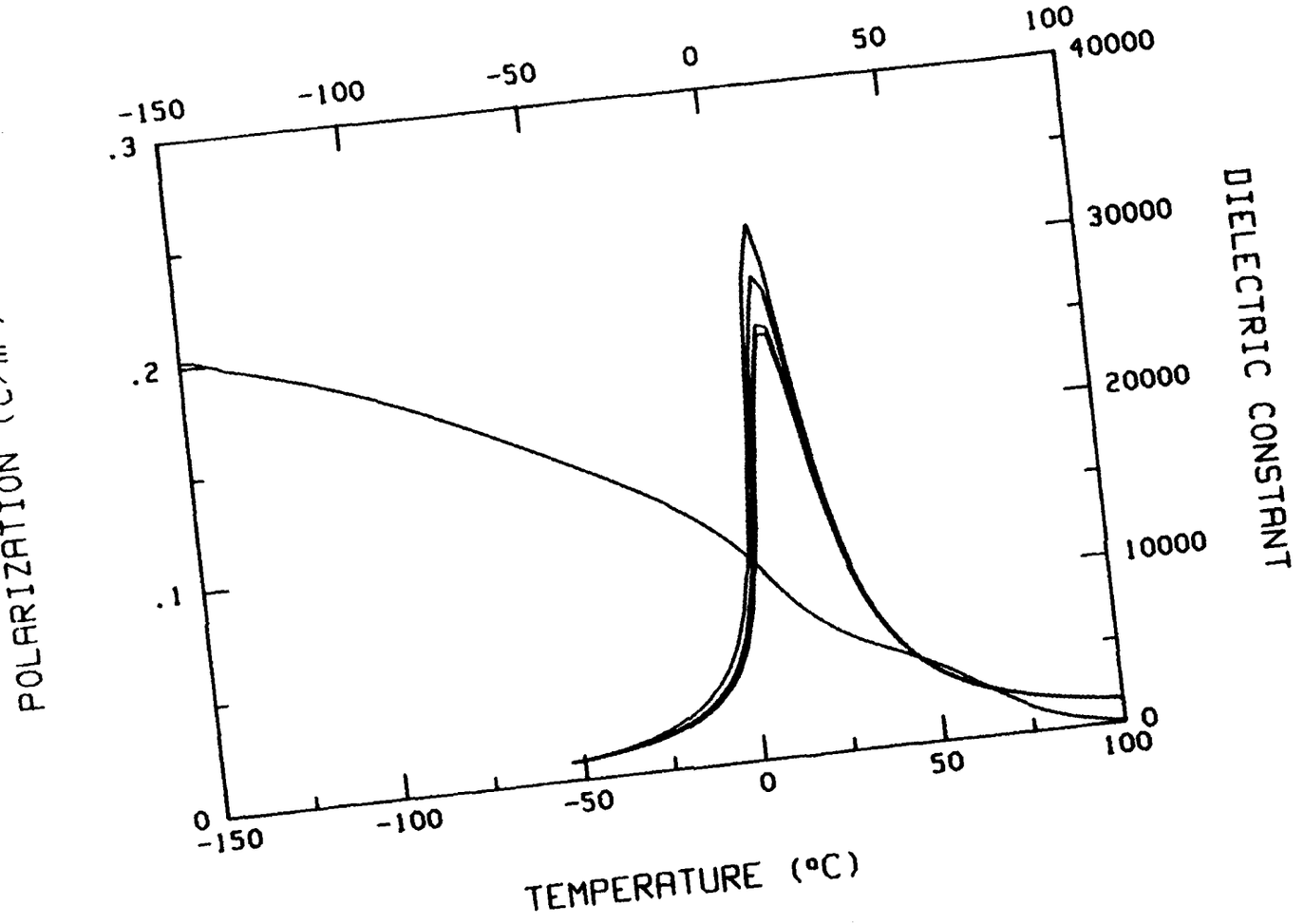

Figure 29. Dielectric and polarization temperature behavior for Type III "Pinched" ferroelectric $Ba(Ti_{1-x}Sn_x)O_3$ (x=0.13).

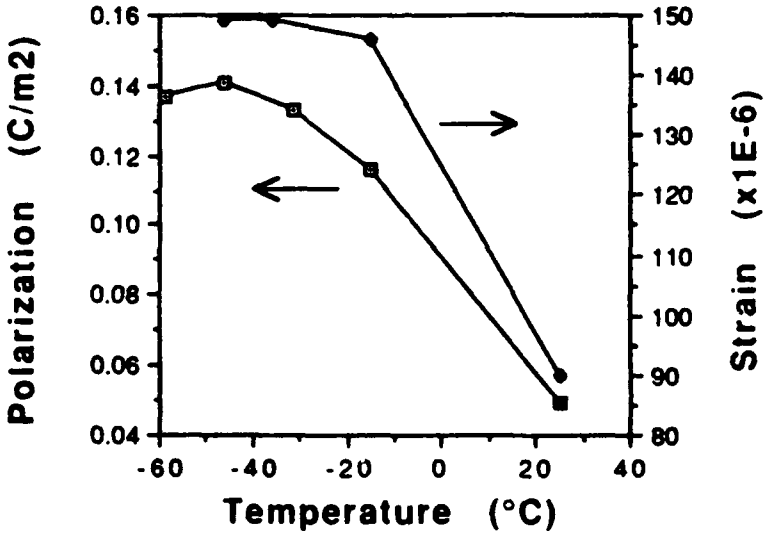

Figure 30. Induced polarization and transverse strain for Type III "pinched" ferroelectric $Ba(Ti_{1-x}Sn_x)O_3$ (x=0.13).

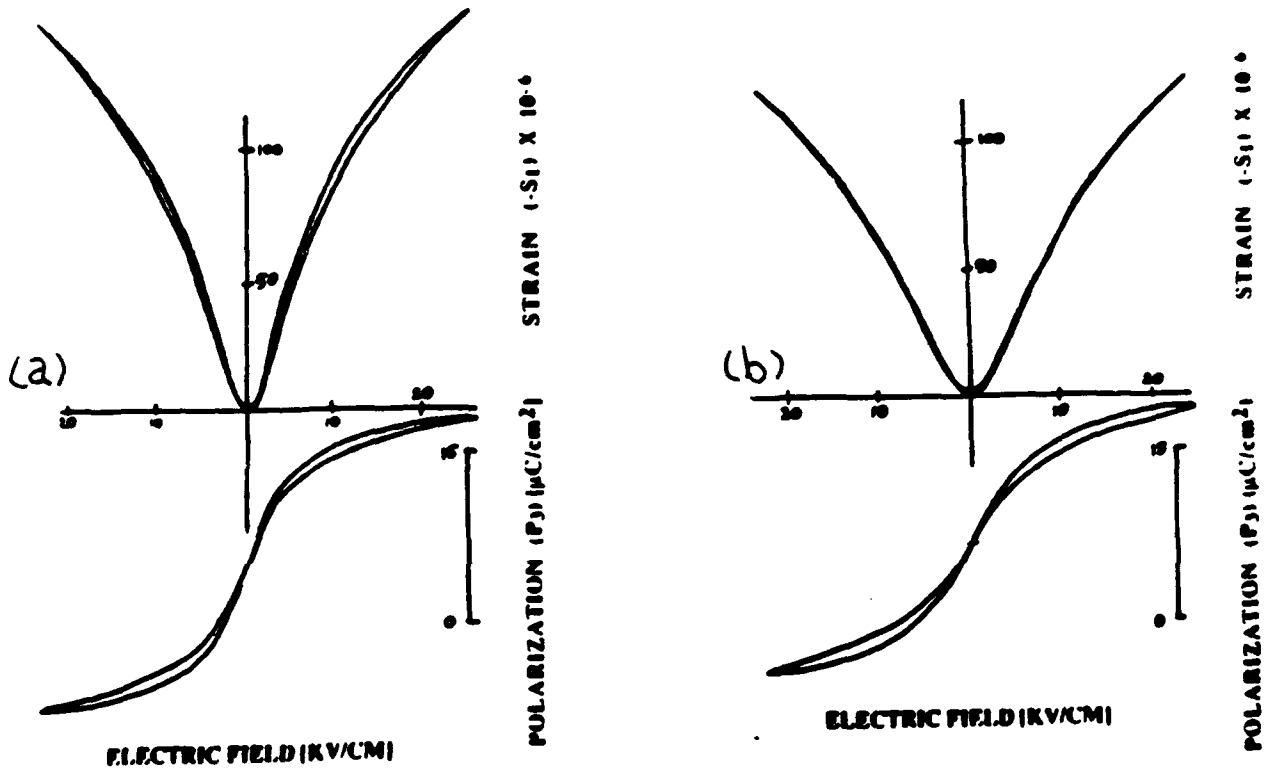

Figure 31. Transverse strain and polarization hysteresis loops as a function of E-field for Type III $Ba(Ti_{0.85}Sn_{.13})O_3$ at temps (a)-13°C, and (b) 2°C.

Type IV. Normal Ferroelectric/Paraelectric $Ba_{1-x}Sr_xTiO_3$

The polarization dielectric temperature behavior for $Ba_{1-x}Sr_xTiO_3$ x=0.35 is presented in Figure 32. As expected for normal ferroelectrics, the depolarization temperature is equivalent to T_m. However, for higher Sr containing compositions, a polarization tail occurs, indicating a core-shell or macro-heterogeneous structure as for the Type III materials (see Figure 33). Also depicted in Figure 33 are additional phase transitions: (1) cubic → tetragonal, tetr → orth, orth → rhombohedral with decreasing temperatures, respectively. These transitions are also evident from the pyroelectric data presented in Figure 34.

Figure 35 gives the level of induced polarization and corresponding transverse strains obtainable at 20 KV/cm over the temperature range of interest. As shown, the strain levels and P_{ind} (Regime I) are very small in contrast to Type I and II relaxors. A significant temperature dependence is observed with a corresponding increase in hysteresis with decreasing temperature (see Figure 36). Similar to the Type III materials, little remanent strain, even at temperatures well below T_m, was observed. This again reflects a possible core-shell or stress related/domain-stress phenomena. As seen in Figure 36, there is a maximum in the induced strain at ~-50°C, although there is relatively little change in induced polarization. Additional studies are required to elucidate the mechanism(s) responsible for the observed behavior.

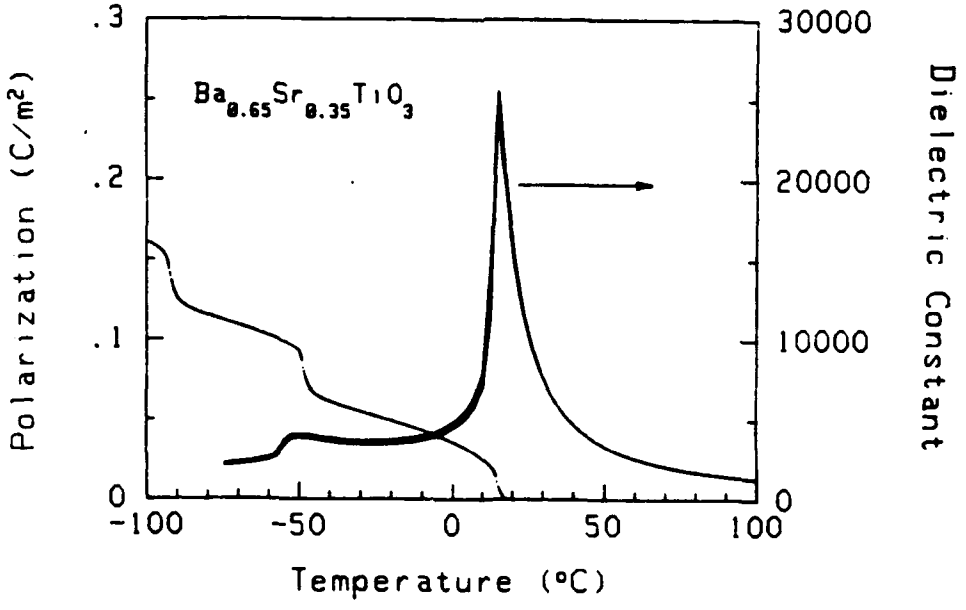

Figure 32. Dielectric and polarization temperature behavior for a Type IV normal ferroelectric $Ba_{1-x}Sr_xTiO_3$ (x=0.35).

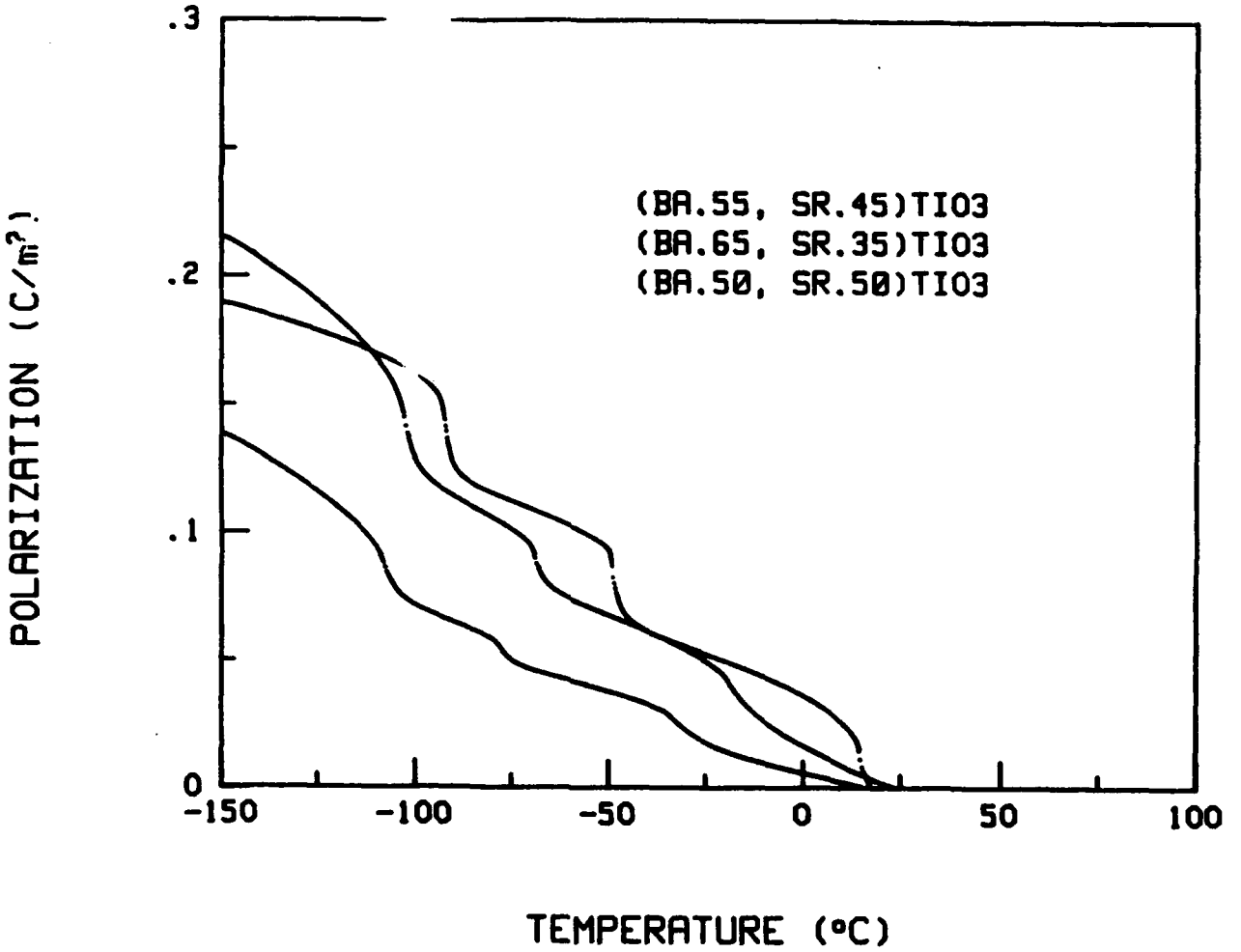

Figure 33. Remanent polarization as function of temperature for Type IV normal ferroelectric $Ba_{1-x}Sr_xTiO_3$.

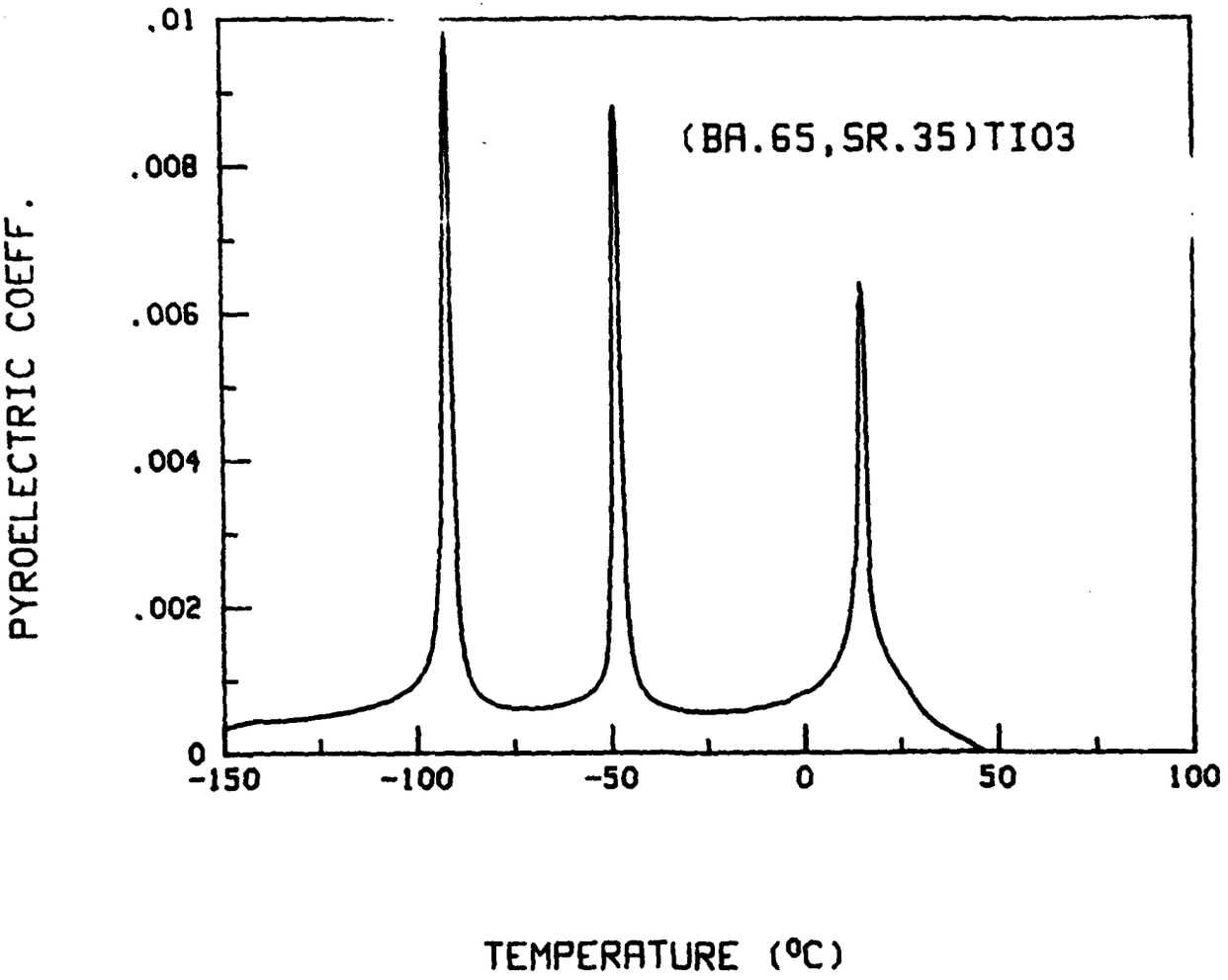

Figure 34. Pyroelectric coefficient as function of temperature for Type IV ferroelectric $Ba_{1-x}Sr_xTiO_3$ with x=0.35.

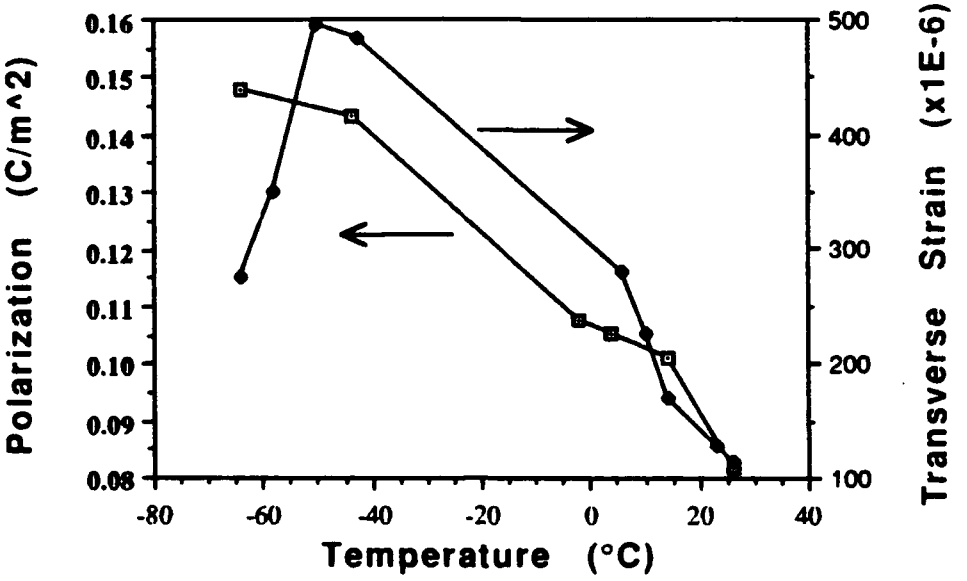

Figure 35. Induced polarization and corresponding transverse strains at 20 KV/cm for a Type IV material $Ba_{1-x}Sr_xTiO_3$ (x=0.35).

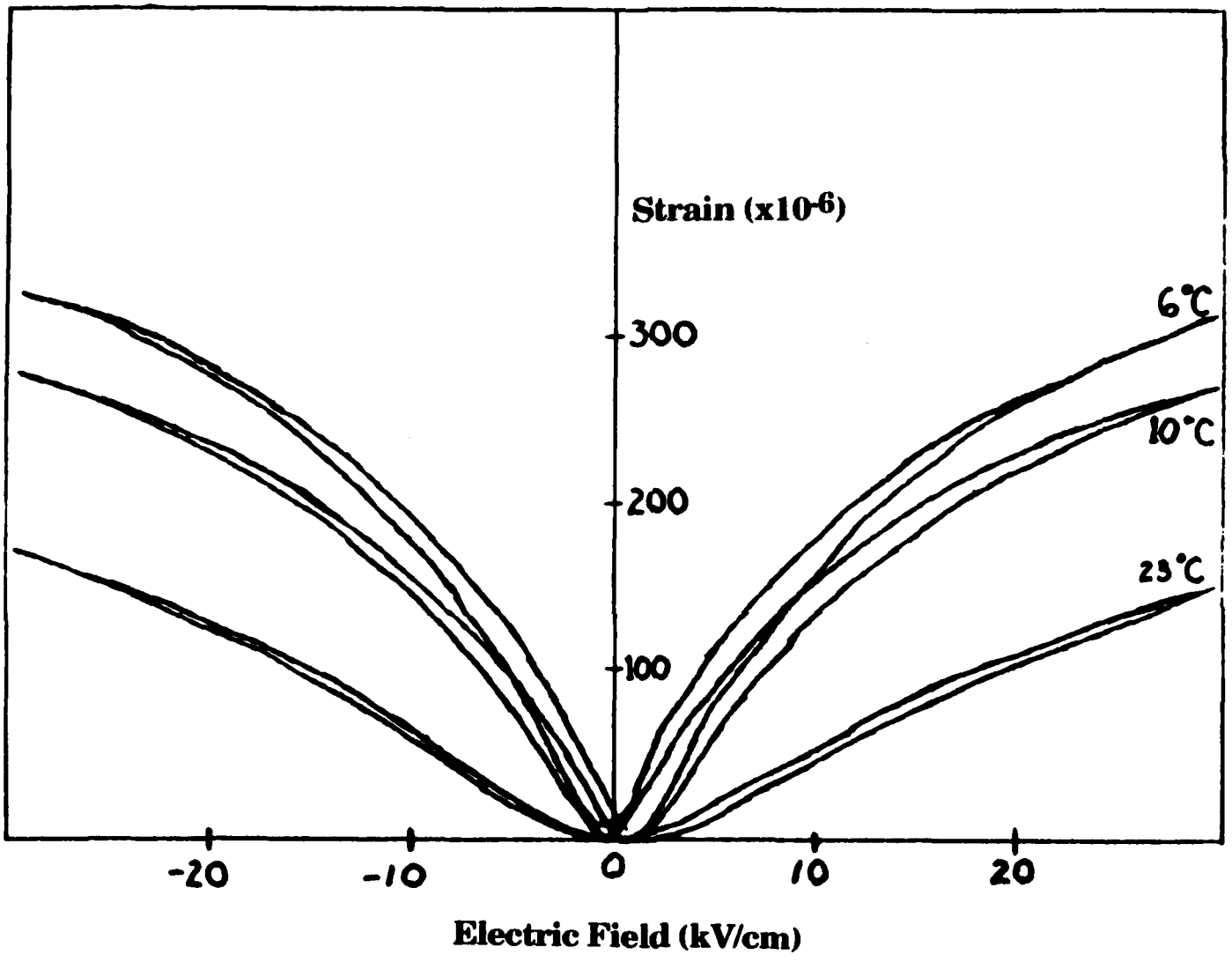

Figure 36. Strain hysteresis loops as function of temperature for $Ba_{1-x}Sr_xTiO_3$ (x = 0.35).

Strain-Hysteresis

Contrast of strain hysteresis behavior for the four types of strictors is made difficult due to their differing intrinsic polarization change mechanisms. In an attempt, Figure 37 gives the level of strain hysteresis as a function of temperature for several compositions. As shown, the relaxor Type I materials offer minimal hysteresis behavior over a wide temperature range, increasing as T_d is approached. Unusual hysteresis temperature behavior is observed for $Ba_{0.65}Sr_{0.35}TiO_3$. As previously reorted in Figure 35, the temperature at which the maximum strain occurs (@ 20 KV/cm) coincides witht he temperature of maximum hysteresis ($\simeq$ 50°C). This temperature corresponds to that for the tetragonal-orthorhombic phase transition for this composition (see Figure 34). Again, there may be a "core-shell" domain/stress-effect responsible for the observed behavior. As presented, all four electrostrictor families show acceptable hysteresis levels (≤10%) within the temperature range of interest (0-30°C). It must be noted that additional contributions to hysteresis may come from inadequate processing, leading to heterogeneity, and also from insufficient bonding of the strain gauges.

The impact of hysteresis becomes more evident at high frequencies, as discussed in the next section.

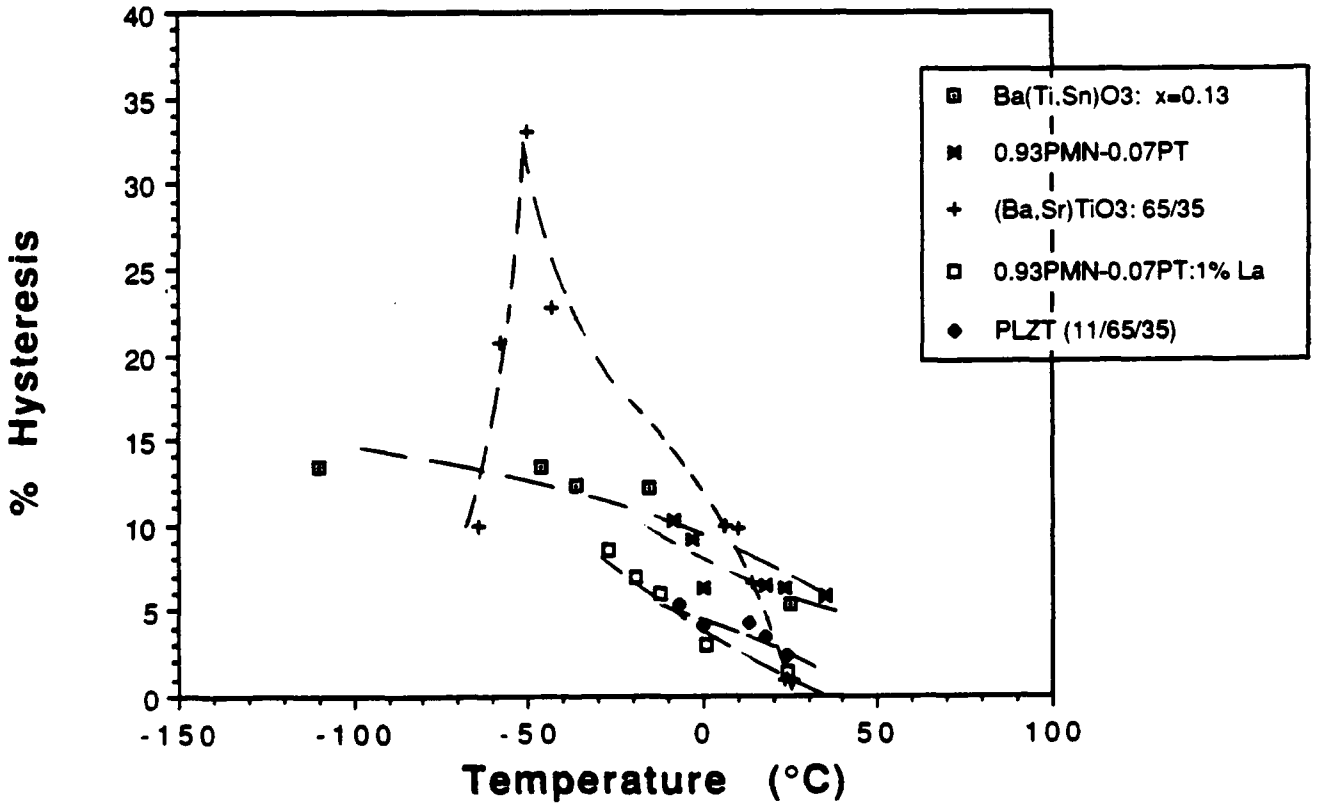

Figure 37. Maximum hysteresis as a function of temperature for the various types of electrostrictors.

Frequency Behavior. The transverse strain frequency dependence for selected electrostrictors, Type I and II relaxors, are given in Figure 38. As shown little frequency dependence is evident up to 100 Hz (strain gauge technique). This behavior is consistent with that reported by W. Pan et al., 1989, for PMN-PT compositions given in Figure 39, where increased dependence does occur near T_m. Strain gauge measurements at higher than 100 Hz were found to be unreliable as a result of inadequate elastic bonding.

Longitudinal strain measurements using the Mach-Zehnder interferometric for the PLZT 9/65/35 composition are presented in Figure 40. The strain dispersion is again similar to that previously reported by Zhang et al., 1989, but less dispersive than the PMN-PT systems, again owing to the latter's operation in Regime II.

It is important to note that the longitudinal strain levels are approximately 2 to 2.5 higher and positive as compared to transverse values.

Heating Effects. The data reported thus far suggests that the Type I and II relaxors best meet the requirements for Navy sonar transducers. However, it will be made evident that high frequency drive electromechanical behavior may limit implementation of such materials, particularly the Type II relaxors.

The effect of high-frequency, high-field drive for a representative Type II relaxor, selected based on its near-ideal strain/polarization behavior within the usage range of 0-30°C, is presented in Figure 41. As shown, the level of induced polarization decreased and the internal temperature increased rapidly ($\leq$ 10°C/min.) upon application of the drive field. The net effect was that the level of induced polarization dropped to half its initial value within 10 minutes. The reason for this decrease is made obvious upon investigation of the dielectric loss data (Figure 41). The pronounced self-heating is a natural consequence of the high loss within the temperature usage range (Regime II).

Conversely, minimal decrease in induced polarization level was observed for a representative Type I relaxor composition during high-frequency, high-field drive within the aforementioned temperature range (see Figure 42). Again, this behavior is easily explained by examination of the dielectric loss data (see Figure 42). Self-heating is drastically reduced due to operation in Regime I only, with associated low loss. Additional studies are required to address such issues as high drive/frequency conditions and subsequent thermal consequences.

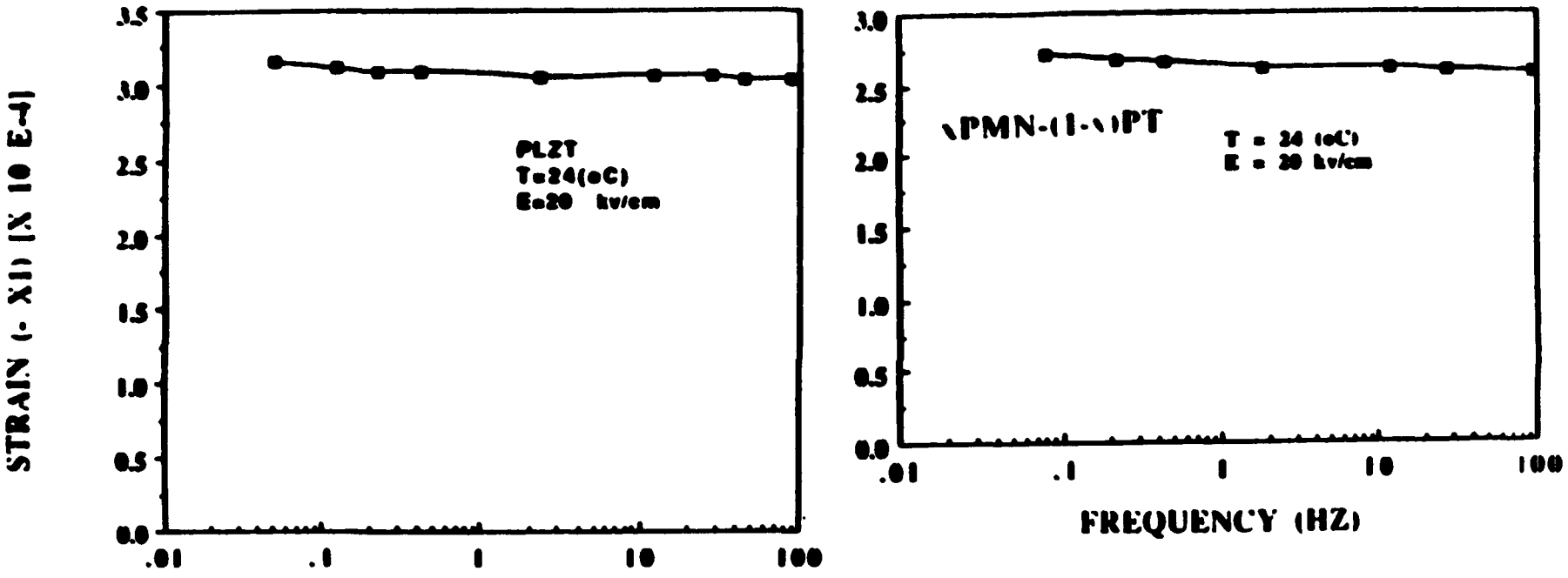

Figure 38. Transverse strain/frequency-dependence for selected Type I and Type II relaxors at room temperature. Note: strain gage techniques.

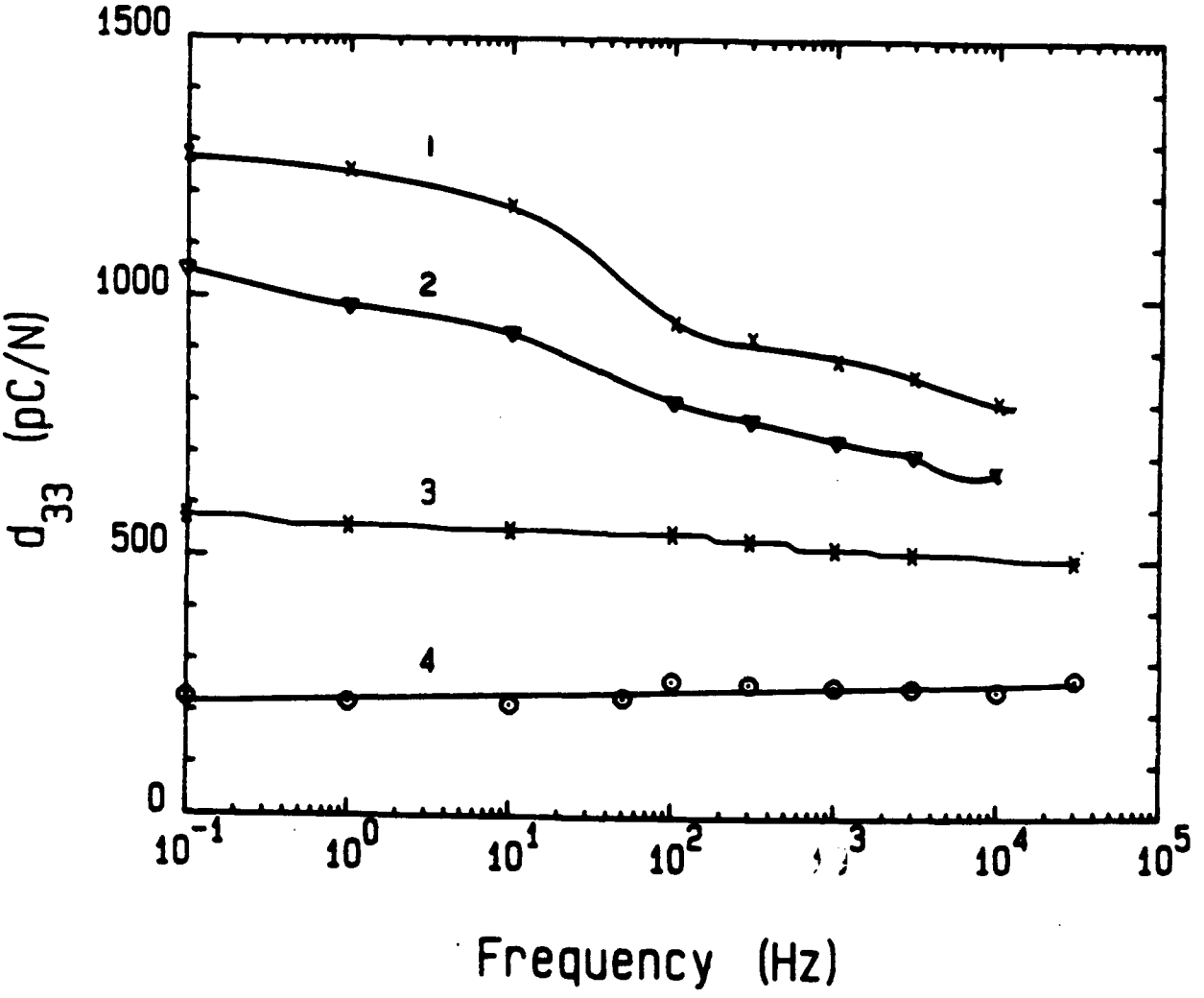

Figure 39. Maximum induced piezoelectric strain coefficient (d_{33}) for various Type I relaxors as function of frequency: (1) 0.93PMN-0.07PT (T_m = 20°C); (2) 0.90 PMN 0.10PT (T_m - 40°C); (3) 0.93PMN 0.07PT + La (T_m = -5°C); (4) PMN (T_m = -10°C) (after Pan et al., 1989).

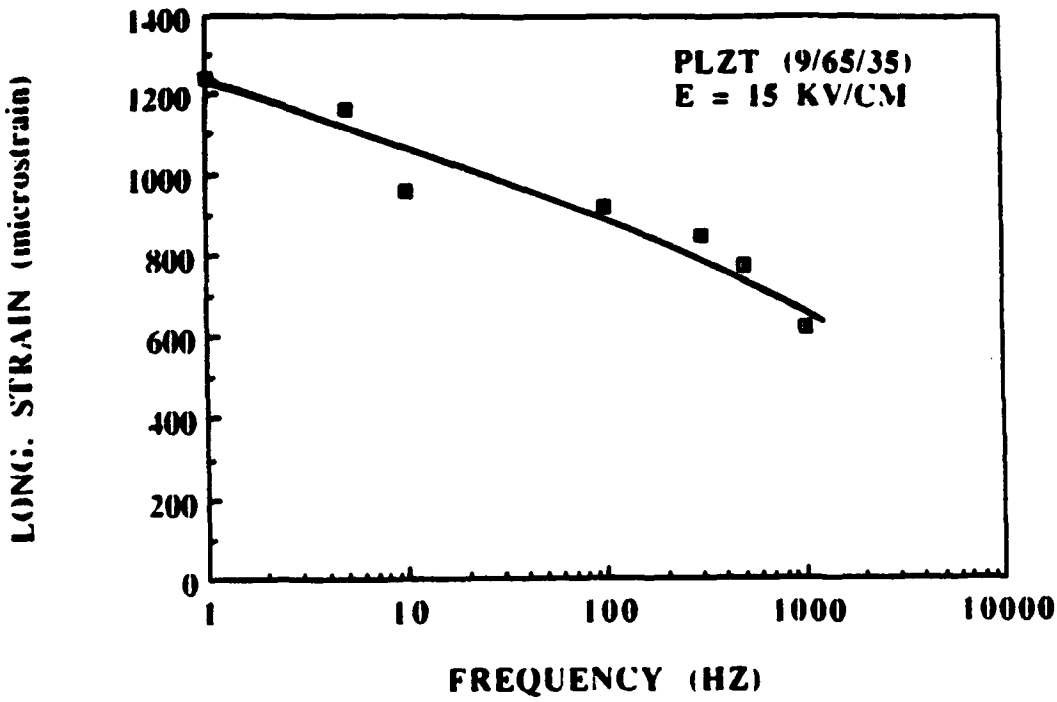

Figure 40. Longitudinal strain as function of frequency for PLZT (9/65/35) at 15 KV/cm as measured by Mach-Zehnder ultradilatometer.

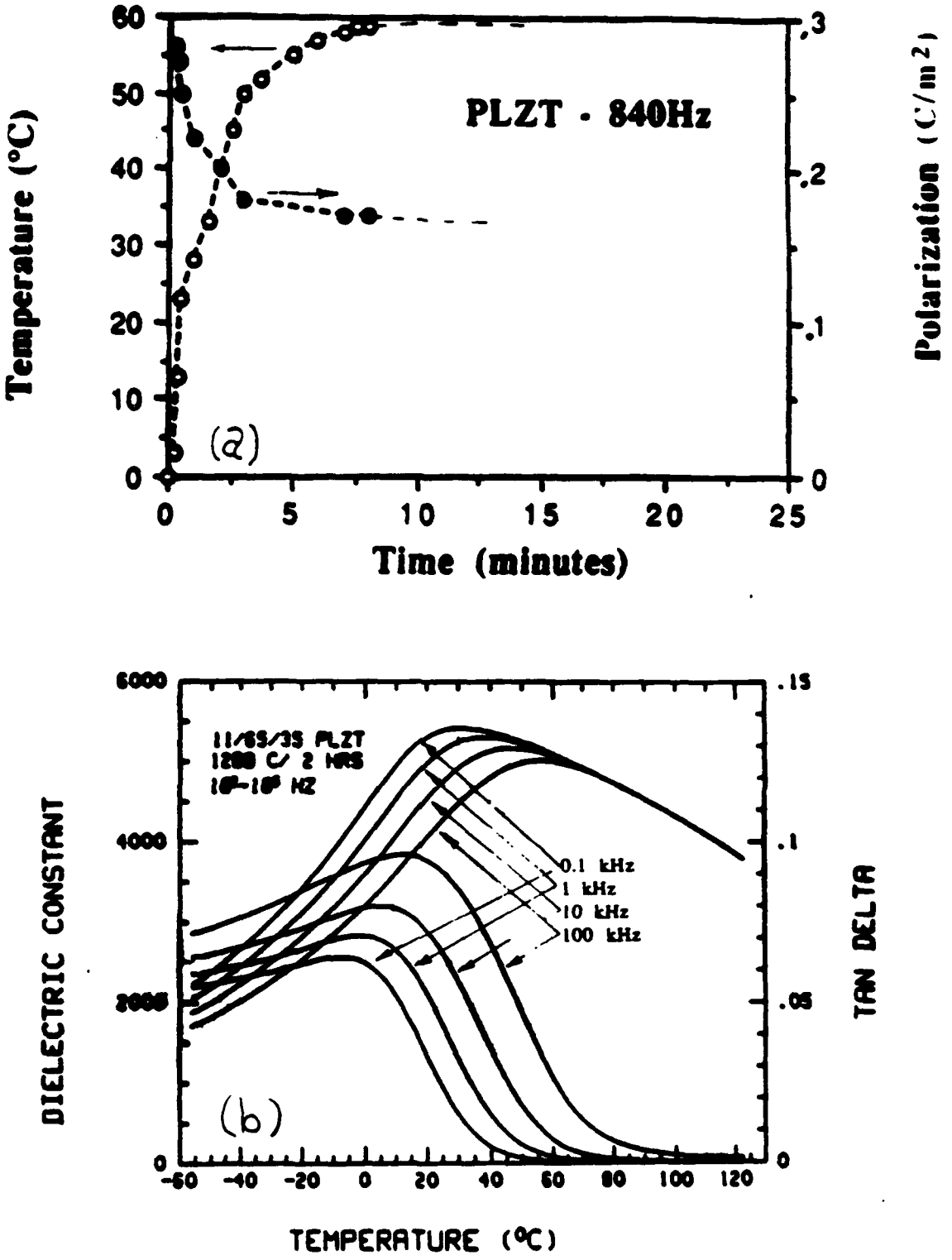

Figure 41. (a) Effects of high-frequency/high field drive on the internal temperature and remanent polarization of a representative Type II relaxor (PLZT 11/65/35) and (b) the associated dielectric temperature behavior data.

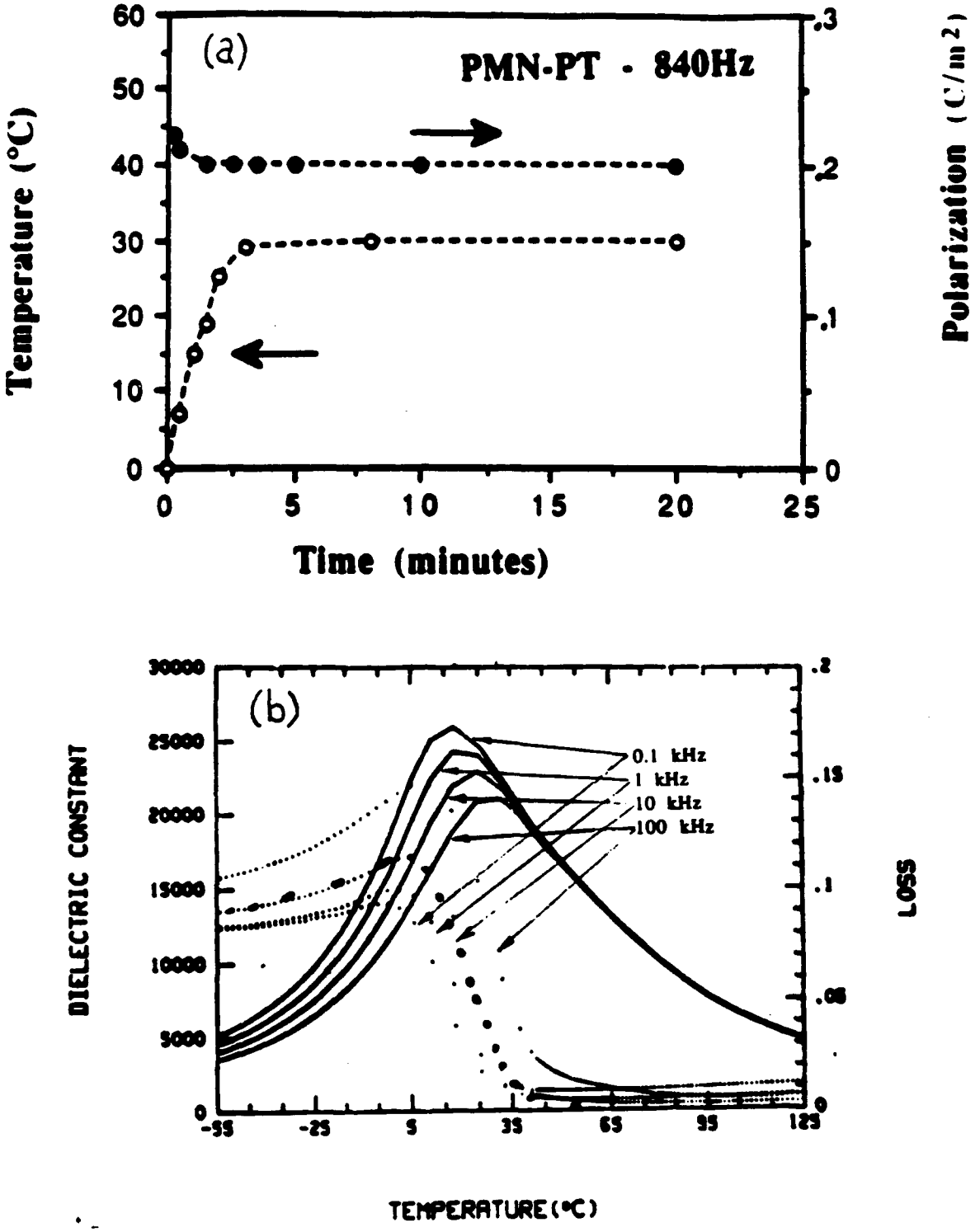

Figure 42. (a) Effects of high-frequency/high/field drive on internal temperature and remanent polarization for a representative Type I relaxor (0.93PMN-0.07PT); and (b) associated dielectric temperature behavior.

Summary of Polarization/Strain Behavior

Table V summarizes relevant information in relation to the polarization/strain behavior for the four types of electrostrictors. As presented, the largest strains and polarizations are possible for the relaxors, even though the electrostrictive Q values are lower. In relation to Navy sonar requirements the electrostrictors are ranked accordingly:

- Large Induced Strain - Type II > Type I > Type III > Type IV
- Operating Temp Range - Type II > Type I > Type III > Type IV
- Minimal Hysteresis - Type I > Type II > Type III > Type IV
- Low Loss/Heating - Type I >> Type II

As summarized above, the relaxor ferroelectrics offer the best potential for application in Navy Sonar Transducers.

Table V. Summary of Polarization Strain Temperature Behavior

Material Type	Example	$\Delta T = T_{max} - T_d$	Depolarization	P_r C/m^2	Pind E=10 KV/cm [20 KV/cm]	% Hysteresis	Strain (Transverse) Micro-strain	Q_{12} m^4/C^2
Type IV	$(Ba,Sr)TiO_3$	0°C	sharp	~0.15	0.002-0.1 [-0.14]	0-10%	10-140 30-240	-.013
Type III	$Ba(Ti,Sn)O_3$	?	continuous	0.2	0.08-0.15 [Saturated]	5-10%	~100 ~200	-.01
Relaxor II	PLZT	~25°C	moderate-broad tail	~0.5	0.15-0.25 [0.2-0.3]	0-10% 30-80%	†100-500 300-700	-.007
Relaxor I	PMN-PT	~120°C	moderate-sharp	~0.4	0.15-0.2 [0.2-0.3]	0-5% 5-10%	100-300 300-500	-.004

†Note: Strains larger than 700μ strain had correspondingly large hysteresis and remanence.

C. Physical Characteristics

In this section stress-strain relationships, including relationships between elasto-electrostrictive behavior and E-field dependence on compliance, mechanical strength and toughness are presented. For the sake of completion, thermal expansion coefficients are also given. The data is compiled and summarized for the various types of strictors and compared to PZT-4 and 8, the two most commonly employed materials for sonar. For a figure of merit, the elasto-energy storage at a give strain level will be used.

Owing to their established potential for sonar transducers, most of the work presented below is for the Type I and II relaxors.

Stress-Strain Behavior

The measured displacement of a ceramic actuator or sonar under loaded (prestressed) conditions can establish the relationship between elastic electrostrictive and compliance behavior. Ferroelectric transducers can generate large strains or large forces, but a trade-off between the two is in effect for any given driving field. The linear relationship at modest loads between the stress and strain (Hooke's Law) implies a generalized elastic constant coefficient

(Strain) = (Electrostrict. Coefficient)(Polarization)^2 + (Elast. Compliance)(Stress).

or specifically in reduced tensor form for perovskite material symmetry.

$$X_3 = Q_{11}P_3^2 + s_{11}X_3 \qquad \text{(longitudinal strain)} \qquad (7)$$

$$X_2 = Q_{12}P_3^2 + s_{11}X_2 \qquad \text{(transverse strain)} \qquad (8)$$

where the prestressing transverse or longitudinal loads are represented by X_2 and X_3, respectively, and the s_{ij} are the elastic compliances. Strain hysteresis loops were undertaken while the electrostrictively induced strains for the sample pushed against the load, thus the measurement only accounts for that component of the total field and load induced deflection. The electromechanical coupling and elastic constants obtained from resonance measurement methods and values of Young's modulus and Poisson ratio were used as a check on the measured elastic compliances of the strain/force loadline slopes by the direct LVDT method.

The longitudinal stress-strain response (Figure 43b) under applied load for a Type II relaxor [PLZT (9/65/35)] was calculated from the measured longitudinal strains by LVDT

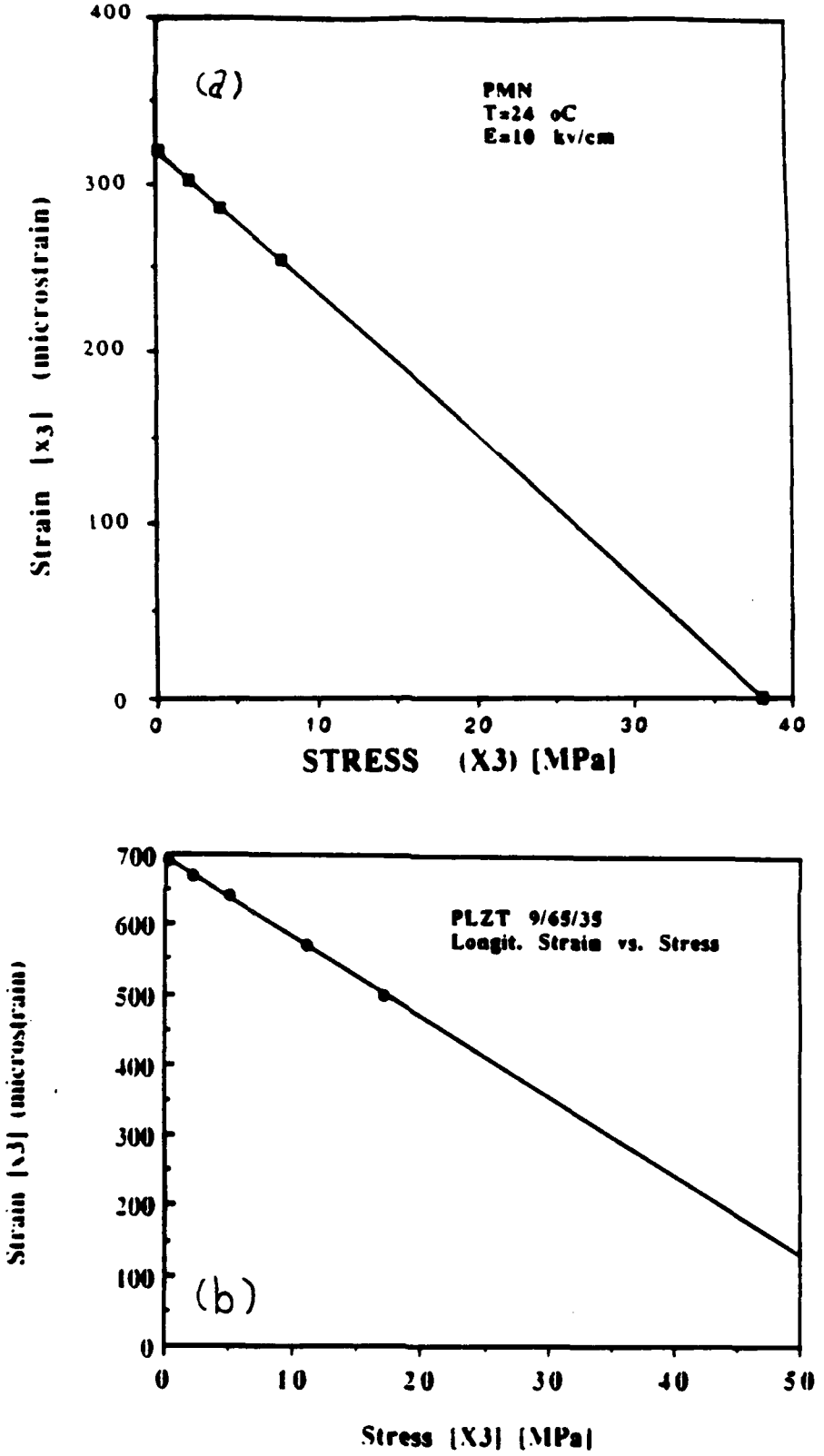

Figure 43. Longitudinal strain versus stress loadlines at 10 kV/cm (calculated from measured elastic compliances and strains) for (a) PMN; and (b) PLZT (9/65/35).

method at lower stress loading and the elastic compliances (s_{11}^E) from the resonance measurements of thin electroded samples. The calculated load line curves indicate that the PLZT compositions have initial high strain levels and can push a considerable load (>20 MPa) and still maintain a reasonable strain level (~175 $\mu\varepsilon$). The effective compliance (from resonance measurements) of $s_{11}^E = 9.95 \times 10^{-12}$ m^2/N was employed in the calculations of the loadlines.

The Type I PMN composition (Figure 43a) has a higher stiffness (response under field and load) than does the elastic response of the PLZT (9/65/35). The PMN elastic constants at an electric field of about 10 KV/cm (by the resonance technique) were $s_{11}^E = 8.4 \times 10^{-11}$ m^2/N. The ceramic Poisson Ratio (σ^E) of 0.299 was measured for this field level.

In actuality, the coupling-E-field behavior for electrostrictors is quite complex, being frequency dependent, T_m proximity dependent, etc. Representative figures of the elastic compliance s_{11}^E for a Type I relaxor PMN-PT first shows a "softening" effect with bias followed by the expected stiffening (Figure 44a). For PLZT, the s_{11}^E softens with bias even for temperatures in proximity to T_m (see Figure 44b). The normal ferroelectrics, however, always stiffen, as shown in Figure 44c, which also reflects a significant temperature dependence, with s_{11} maximized near T_m.

Investigation of the elastic stiffness c_{33} reveals that all four types of strictors stiffen with increasing bias (see Figure 45). Preliminary mechanical fracture data for physical characteristics of the four types of strictors are summarized in Table VI, including preliminary mechanical fracture data. As presented, all the strictors possess superior performance in relation to PZT 4 and 8. In particular, the low thermal expansion behavior for PMN Type I materials allows greater utilization of the electrostrictive strain of which 20% can be associated with thermal fluctuations in normal ferroelectrics. However, though the mechanical toughness of relaxor is comparable to the others, the mechanical fracture strength reflects the need for further processing enhancement and microstructural control.

Based on the data generated thus far, "strain-energy" values for a given strain level rank the strictors as follows:

Type IV		Type I		Type II		Type III	
$Ba,SrTiO_3$	>	PMN	>	PLZT	>>	$Ba(Ti_{1-x}Sn_x)O_3$	Low strain levels <300 μ strain
		and for high strain levels					
Type I	>	Type II	>	>>		PZTs	High strain levels >300 μ strain

with the relaxors capable of higher strain levels far surpassing PZTs (see TableVII).

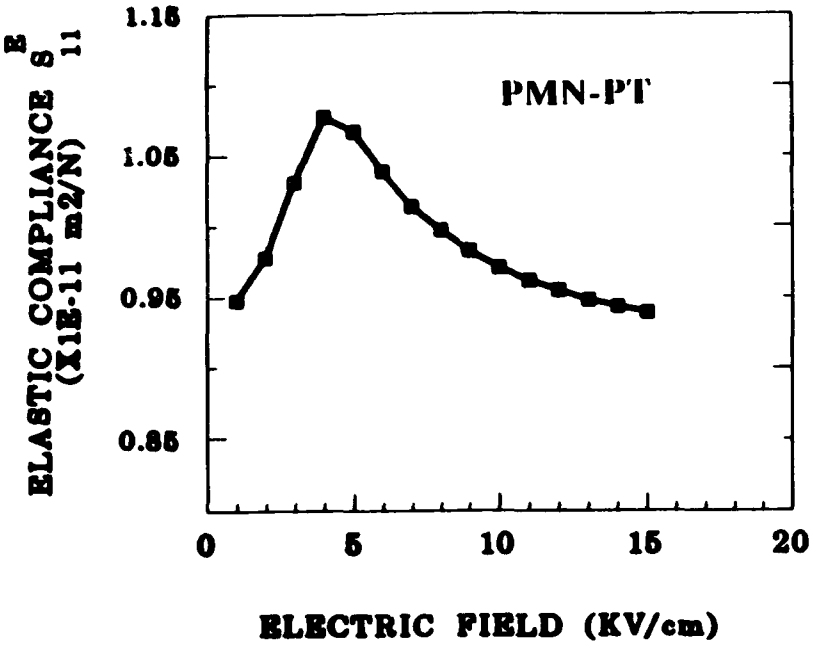

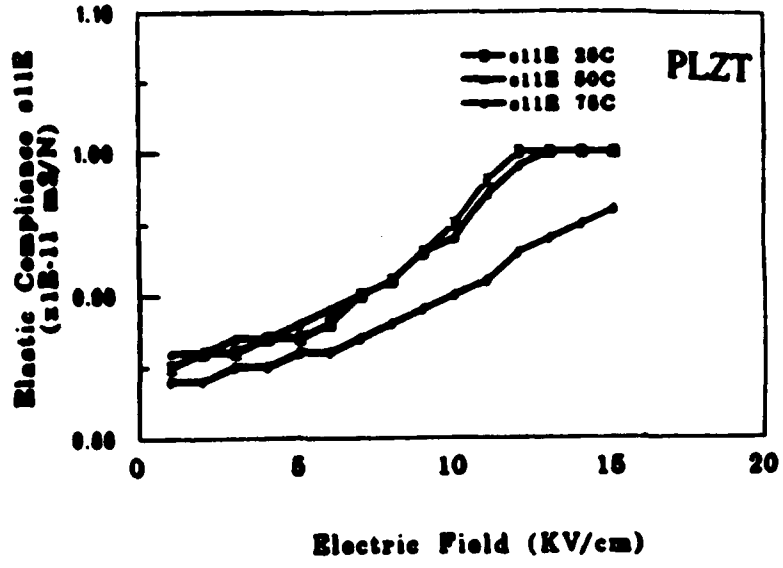

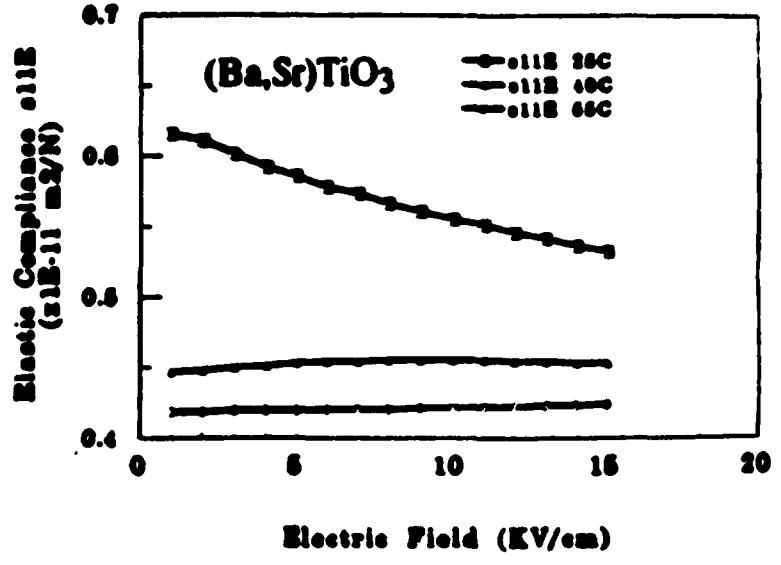

Figure 44. Elastic compliance s_{11}^E as function of applied electric field for (a) PMN-PT; (b) PLZT (9/65/35); and (c) $(Ba_{1-x}Sr_x)TiO_3$ (x=0.35).

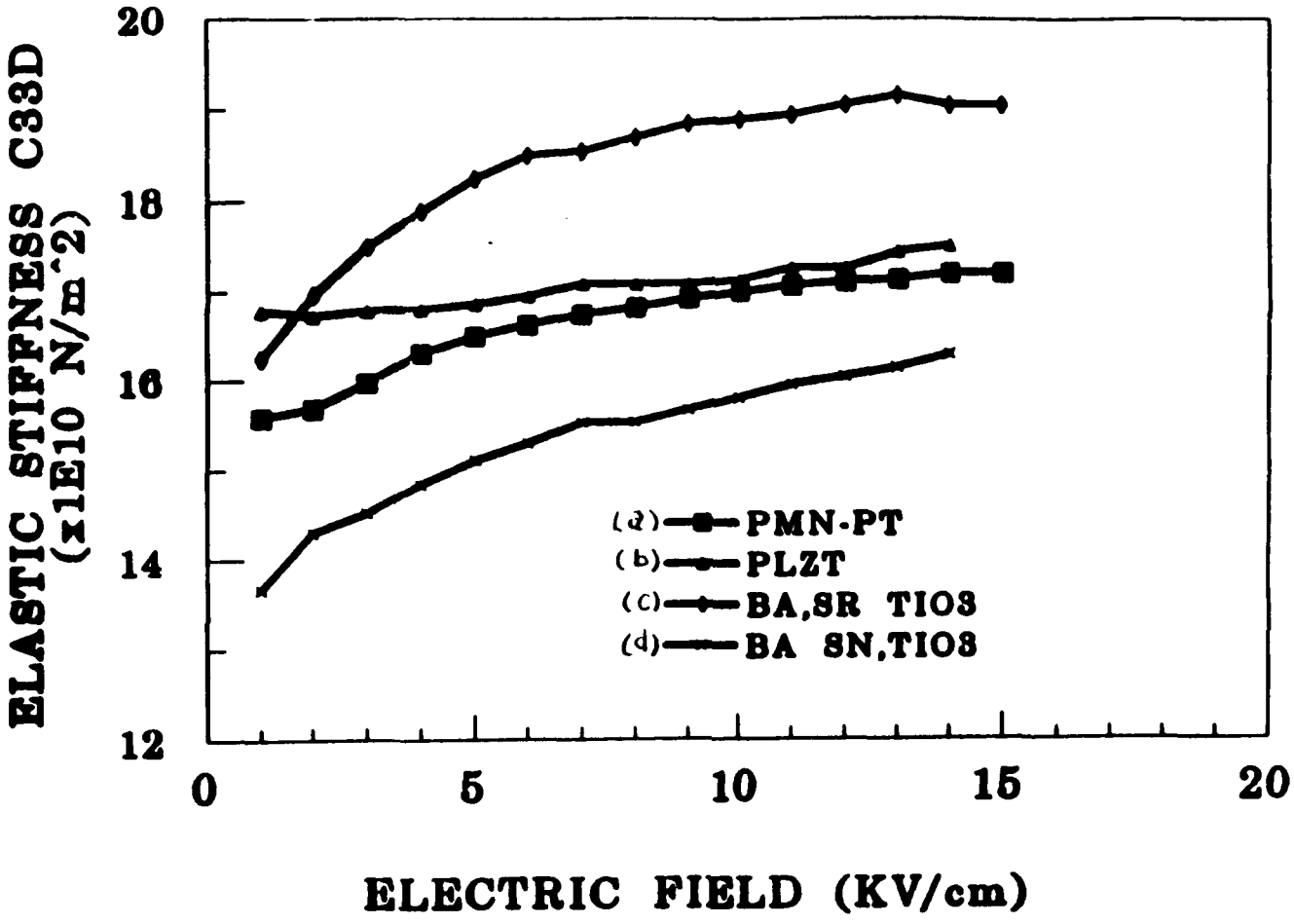

Figure 45. Elastic stiffness c_{33}^{D} as function of applied electric field for the four types of strictors: (a) 0.9PMN-0.1PT; (b) PLZT (9/65/35), (c) $Ba_{1-x}Sr_xTiO_3$ (x=0.35); and (d) $BaTi_{1-x}Sn_xO_3$ (x=0.13). Determined using thickness and remanence at ~5 MHz.

Table VI. Summary of Physical Characteristics

Material Type	Example	Elastic Compliance ††s_{11}^E (x 10^{-11} m^2/N)	E-field Dependence	Mechanical Strength MPa	Toughness MPa $m^{1/2}$	Thermal Expansion (x10^{-6}/°C)
Type IV	$(Ba,Sr)TiO_3$	4-6	stiffens	~100	0.8-1.5	~10
Type III	$Ba(Ti,Sn)O_3$		stiffens	---	---	~10
Relaxor II	PLZT	8-13	†softens	~100	---	~5
Relaxor I	PMN-PT	8-10	†stiffens	30-70	0.8-1.2	≤1
Piezo Type I, III	PZT-4-8	10-12	stiffens	50-100	0.8-1.2	~2-3

*Compositionally, microstructurally and process dependent.

†E-field dependence of compliance and/or stiffness coefficients dependent on relation to T_m and level of bias.

††Highest levels of compliance generally occur near T_m.

Table VII. Summary of Physical and Mechanical Properties

Material Type		E (GPa)	*Sfracture (MPa)	K_{IC}	Hardness (GPa)	†Strain-Energy Density (J/m^3)
Type I	(a)	105	23	1.0	3.1	~1.3×10^4
	(b)	97	37	1.3	3.8	~1.2
	(c)	77	33	1	4.1	~0.9
Type IV		116	39	1.4	3.4	~1.5
PZT-Type IV		66	58	1.6	2.8	~0.8

*4-point Flexure Method

†Constant strain level = 500 μ strain

D. Compositional Engineering

Based on the data thus far, electrostrictors appear to be promising candidates for sonar transducers, particularly Type I and II relaxors. The question to be answered in this section is, "Can further performance enhancement be compositionally engineered?" Performance enhancement goals include the following:

- Shift $T_m \rightarrow$ 0-30°C operating range
- Enhance K_m and $P_{ind} \rightarrow$ increased strain
- Transition broadening/(Regime I) increase temp usage range
- Increase $\Delta T = T_m - T_d$ (Regime II)
- Mechanical/integrity, i.e. grain size $\leq$ 3 microns

T_m and K_m Modifications.

Type II and IV "Pinched" and Normal Ferroelectrics

Figure 46 summarizes the effect of numerous cationic substitutions in the normal ferroelectric $BaTiO_3$. As presented, only Pb^{+2} and Bi^{+3} (not shown) can shift T_m upwards whereas A-site and B-site cations generally cause T_m to shift downward. As for the case of Type III ferroelectrics, the effect of Sn^{+4} and Zr^{+4} on specific transitions is unequal, ultimately leading to a single phase transition or "pinching".

In terms of optimizing K_m, large grain sizes are generally used to minimize low polarizable grain boundary effects and/or macro-heterogeneity. As already presented in this work, see Table IV, the K_m for the Type III and IV materials were quite high, though evidence in Figure 29 suggests a core shell structure for Type III materials. In the case of Type IV $Ba,SrTiO_3$ whereupon the T_m can be readily shifted with varying Sr substitutions, no significant change in P_{ind} levels and/or corresponding strain can be achieved. Data for various Type IV compositions are reported in Appendix A.

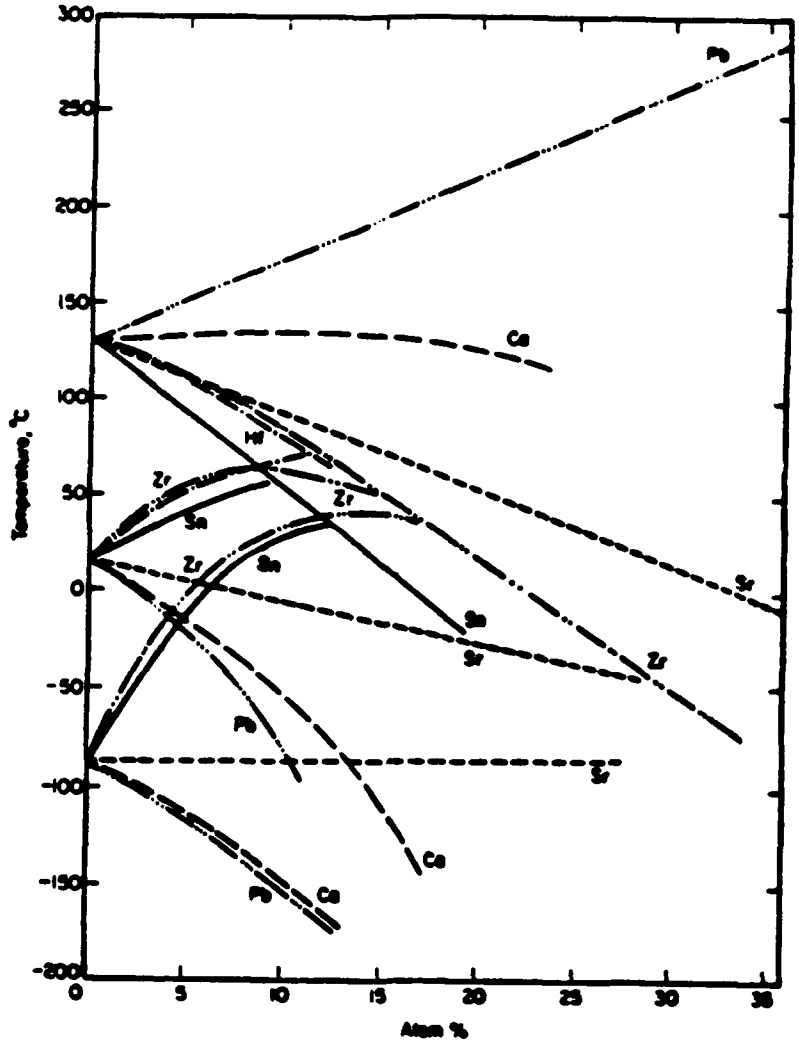

Figure 46. The effects of cationic substitution on the normal ferroelectric $BaTiO_3$ on T_m and the various ferroelectric phase transitions (after Jaffe, Cooke, and Jaffe, "Piezoelectric Ceramics," p. 94 Academic Press, NY (1971).

Only two compositional variations were made with the Type III $Ba(Ti_{1-x}Sn_x)O_3$ material, i.e. x= 0.10,0.13. The latter was to shift T_m downward toward the temperature range of interest (see Figure 47). As presented in Figure 48 and contrasted to $Ba(Ti_{1-x}Sn_x)O_3$ x = 0.13, see Section B, the higher T_m resulted in slightly higher achievable strains but more normal ferroelectric behavior by way of increasing levels of remanent polarization with decreasing temperature and correspondingly remanent strains (see Figure 49).

Type I. Relaxors (PMNs)

K_{max} vs. T_{max}

As discussed earlier in Section A and shown in Figure 8, the most widely used compositional modification made with the relaxor PMN is with the normal ferroelectric $PbTiO_3$. To reiterate its impact, increasing the amount of $PbTiO_3$ does the following:

- T_{max} increases ~ 4°C/mole%
- Diffuseness decreases
- K_{max} increases
- T_d increases → ΔT_{m-d} approach 0°C → "normal ferroelectric"

As with substitution of Ti^{+4}, the effect of various B-site compositional modifications were all found to be similar, as presented in Figure 50. As shown, regardless of the B-site substitution, K_m was found to be dependent on the position of T_m, hence no performance gains in relation to Ti^{+4} substituted compositions was apparent. Hence, compositional modifications focused on A-site substitutions, including isovalent cations of Ba^{+2}, Sr^{+2}, and Ca^{+2}, heterovalent cations of La^{+3}, and Bi^{+3}. Based on preliminary studies, it was found that only modifications in the range of 1-3 mole % were permissable owing to their dramatic effect on T_m, shifting it well below the temperature range of interest.

As previously noted for B-site modifications, the effect of A-site cations on K_{max} in relation to T_{max} was also found to be strongly interrelated as shown in Figure 51. The impact of cation substitutions on the level of K_{max}, revealed, that with increasing A-site modifications, K_{max} decreased. This behavior is explained on the basis of replacing the highly polarizable Pb^{+2} cation with a less polarizable one. From the results given in Figure 52, the decrease in K_m could be correlated/ranked in terms of relative polarizability of the cation. Another explanation may be related to solid solution limits as for bismuth substitution, resulting in a low-polarizable grain boundary phase.

The dielectric compositional behavior in this work was found to be consistent with that of Butcher and Thomas (1991) for Ba modified PMN, whereby a ferroelectric decoupling of the Pb-NbO octahedra model was proposed.

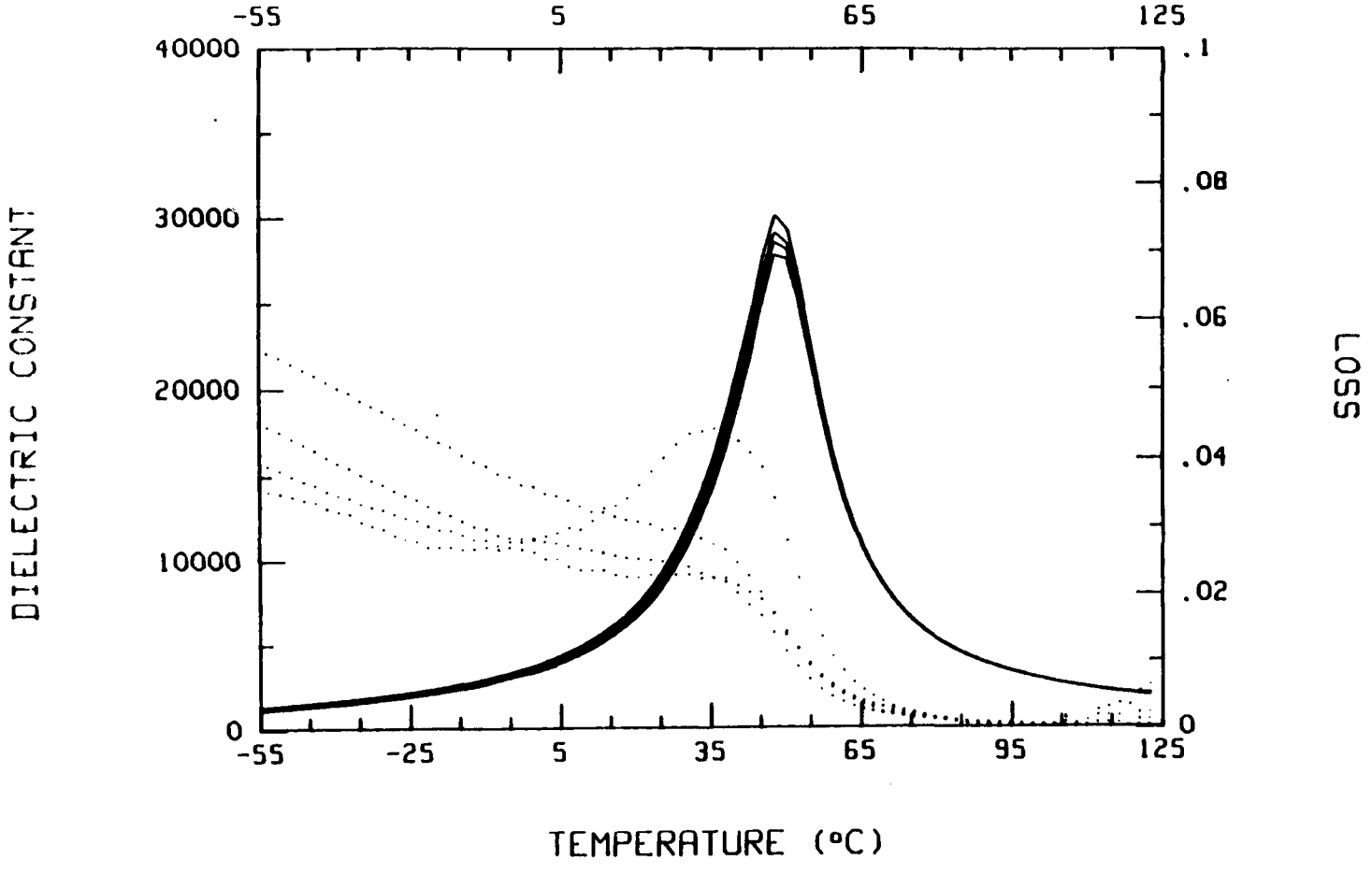

Figure 47. Dielectric temperature behavior for Type IV strictor $BaTi_{1-x}Sn_xO_3$ (x = 0.10).

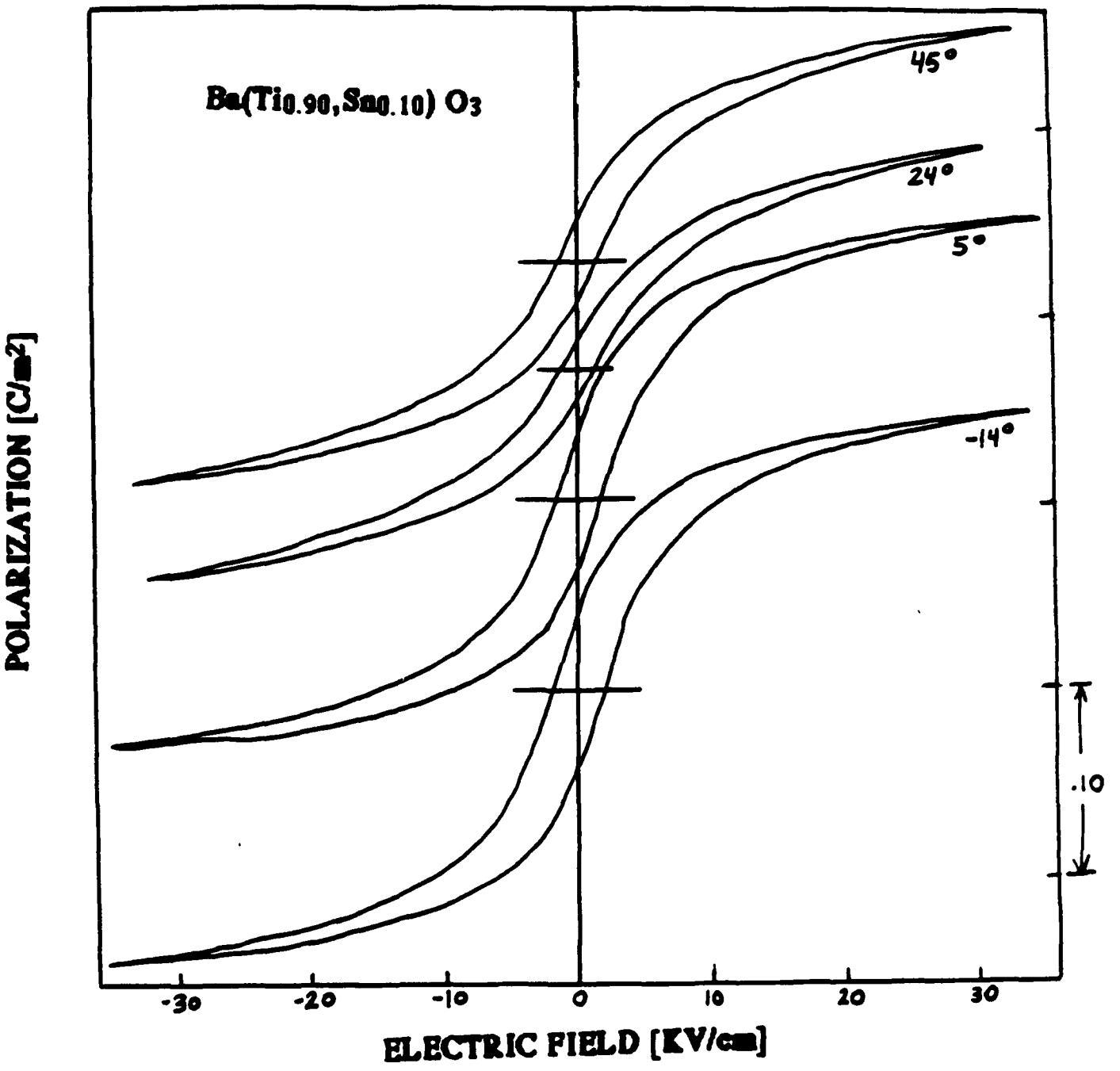

Figure 48. Polarization as function of electric field at several temperatures for $Ba(Ti_{0.9}Sn_{0.1})TiO_3$.

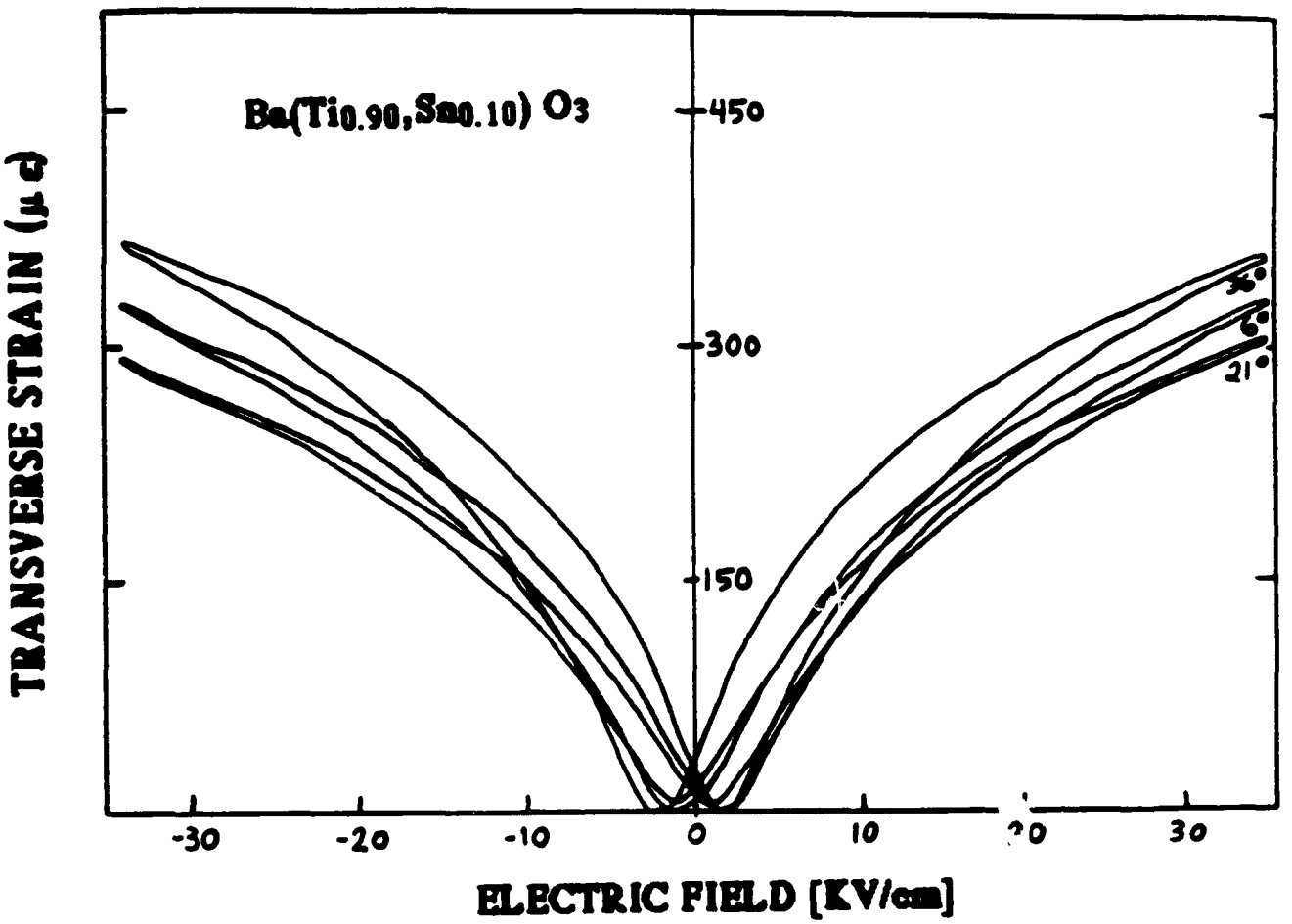

Figure 49. Transverse strain as function of electric field at several temperatures for $Ba(Ti_{0.9}Sn_{0.1})TiO_3$.

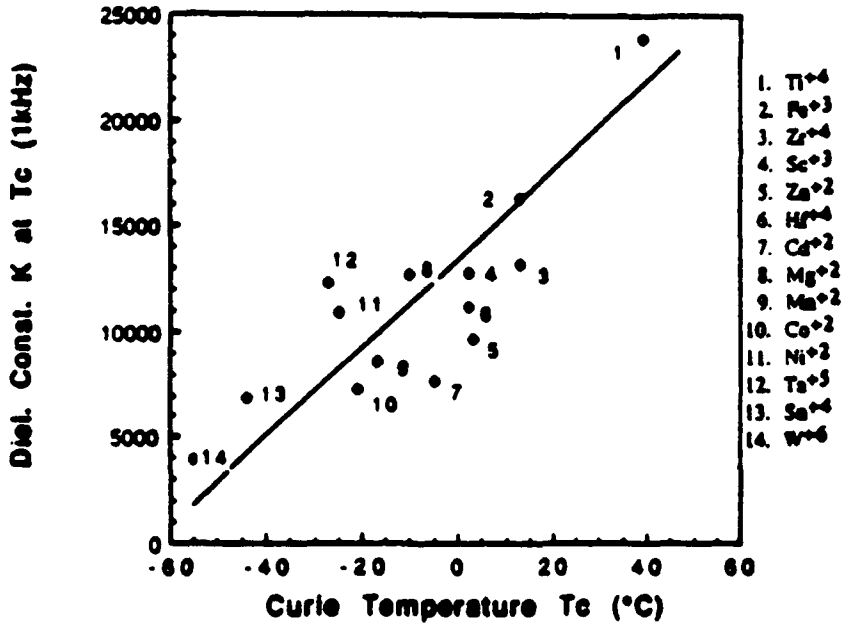

Figure 50. Dielectric constant (K_m) as function of T_m (1 KHz) for B-site compositionally-modified PMN ceramics (after Voss et al., 1983).

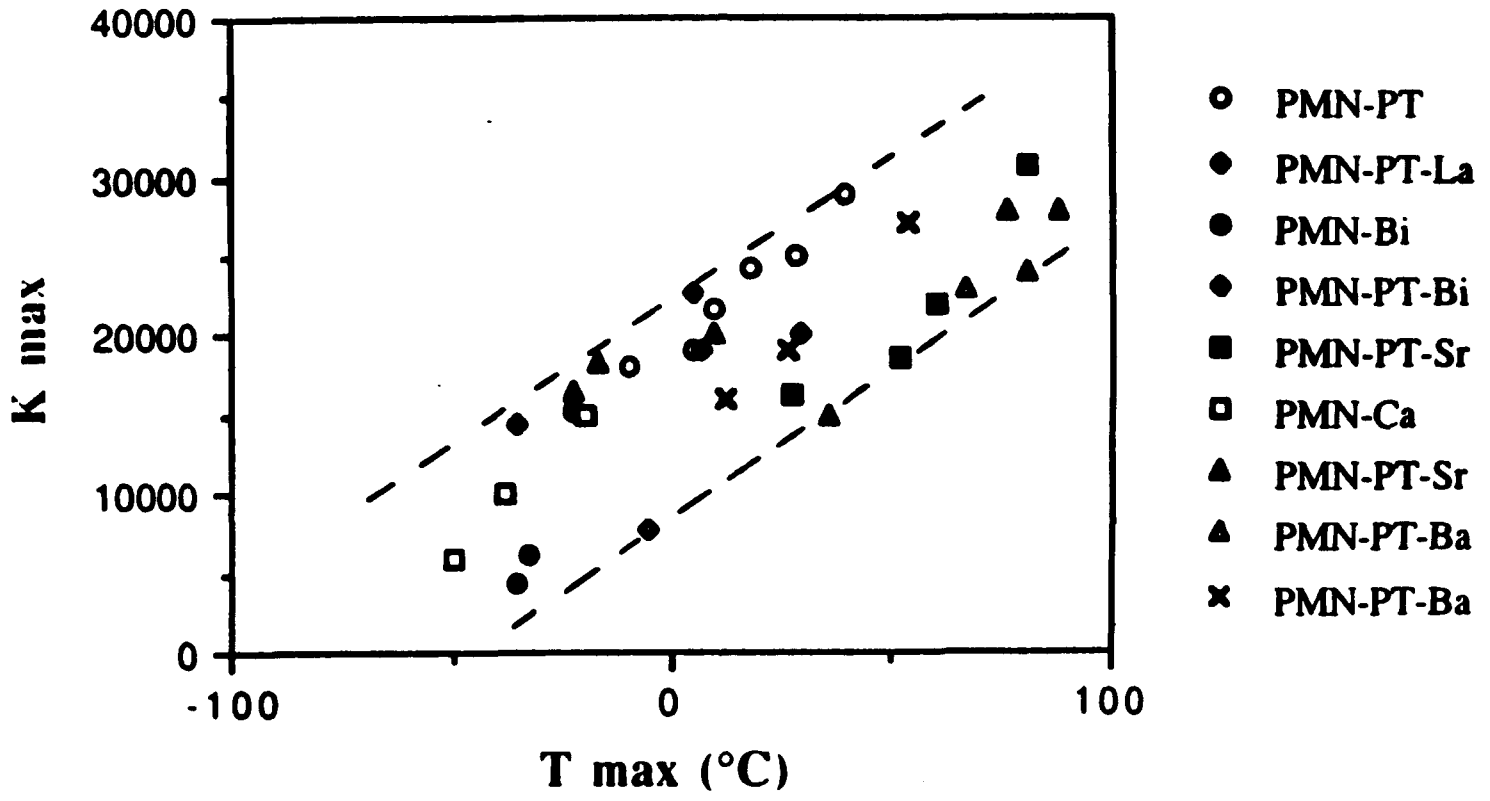

Figure 51. Dielectric constant (K_m) as function of T_m for various A-site and B-site modifications of PMN.

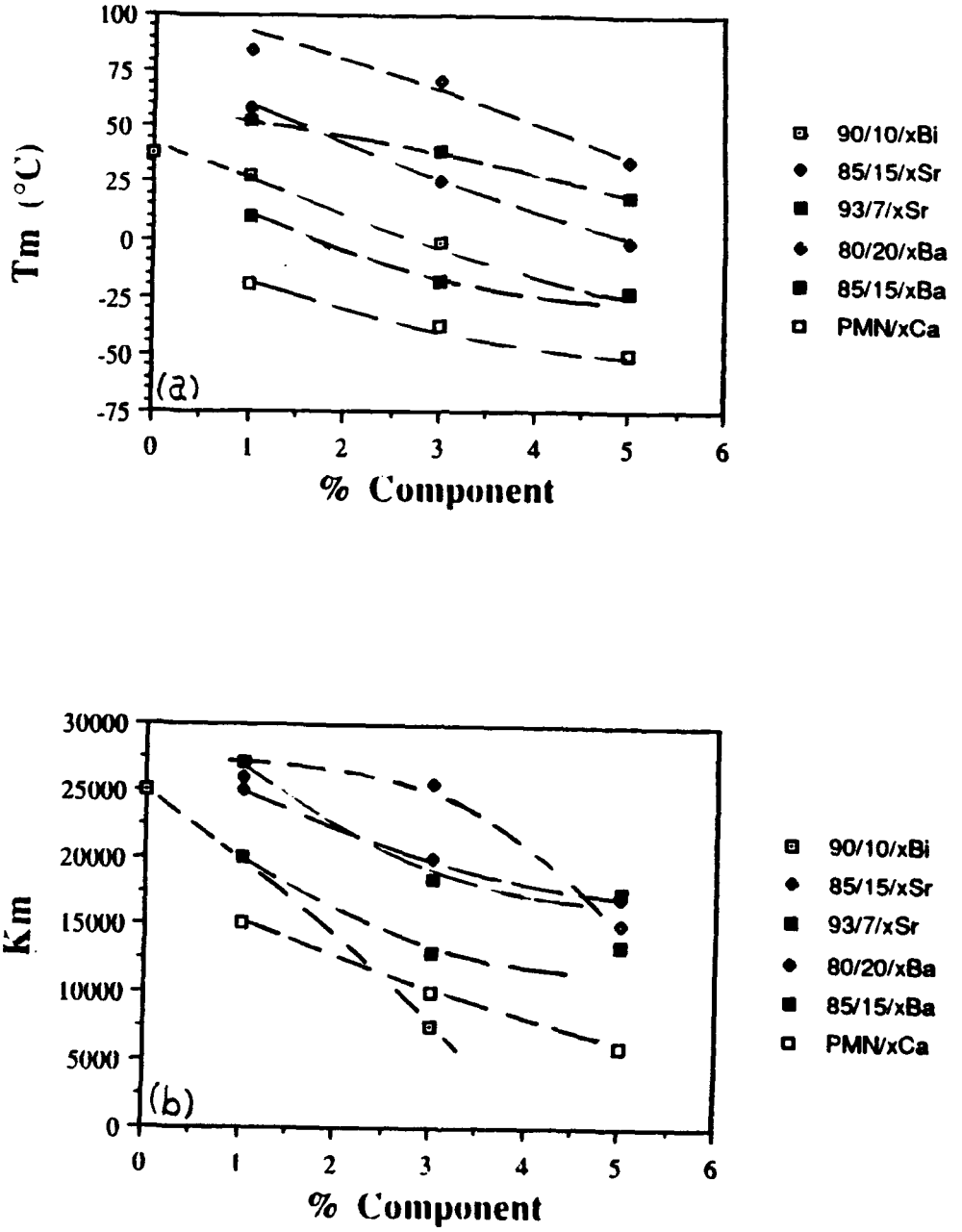

Figure 52. Variation in (a) T_{max} and (b) K_{max} at 1 KHz with A-site cation substitution in PMN and PMN-PT.

Depolarization (T_d) Dependence

Although K_{max} vs T_{max} was found to be nearly compositionally independent for both A-site and B-site modifications; the depolarization behavior was not. As shown in Figure 53 for PMN-PT compositions T_d, and more importantly T_m-T_d, follows a nearly linear relationship with T_m (i.e. T_m-T_d increases as T_m is lowered).

Furthermore, with La modifications on the A-site, a dramatic increase in T_m-T_d for the same T_m was found, without any degradation in polarization levels (see Figure 54). As can be seen from this figure, the net effect of La modificaitons is to broaden T_m-T_d (Regime II), promoting high strain levels, with minimal hysteresis and frequency-related problems.

The effects of other A-site modifications on T_d are presented in Figure 55. As seen in this Figure, T_d decreases with increasing A-site modification and increasing T_m. The net effect is to "broaden" Regime II (see Figure 56); however, T_m-T_d decreases with increasing T_m, and Regime II is shifted downward, out of the temperature range of interest. An important observation from Figures 55 and 56 is the apparent non-linearity of the trend in T_d with composition, suggesting limited solubiity of these A-site modifiers (especially Ca) in the PMN-PT structure.

Induced Polarization/Strain Dependence

One effect of PT modification is to increase T_m. By shifting Tm near room temperature; Km (as previously noted) is increased, and levels of induced polarization and strain are subsequently increased (see Figure 57). As seen in this figure, as T_{max} in increased so, too, are the levels of induced polarization and strain, within the temperature range of interest. Induced polarization/strain as function of temperature are presented in Figure 58. As expected, the trend for all compositions is increasing polarization/strain with decreasing temperature, with induced strain behavior (within the temperature range of interest) increasing with PT modifications, (i.e. room temperature strain increases as T_m increases).

The effects of A-site modifications (i.e. La, Sr, Ca) are less clear, probably due again to limited solubility in the PMN-PT structure. However, La-modified compositions, with their low depolarization temperature, broad polar Regime II, minimal hysteresis, and large induced strain (see Figure 58) are attractive candidates for sonar use. As illustrated in Figure 59, the La-modified PMN-PT compositions offer high-strain levels (>300 x 10^{-6}) at modest fields (20 KV/cm).

The temperature-dependence of induced polarizations and strains at 10 KV/cm and 20 KV/cm for the various A-site modifications are presented in Figure 60. As expected, strain levels increase with decreasing temperature, in accord with polarization data. Induced polarization/strain data are compiled in Appendix B for varous modifications of the four types of electrostrictors studied in this work.

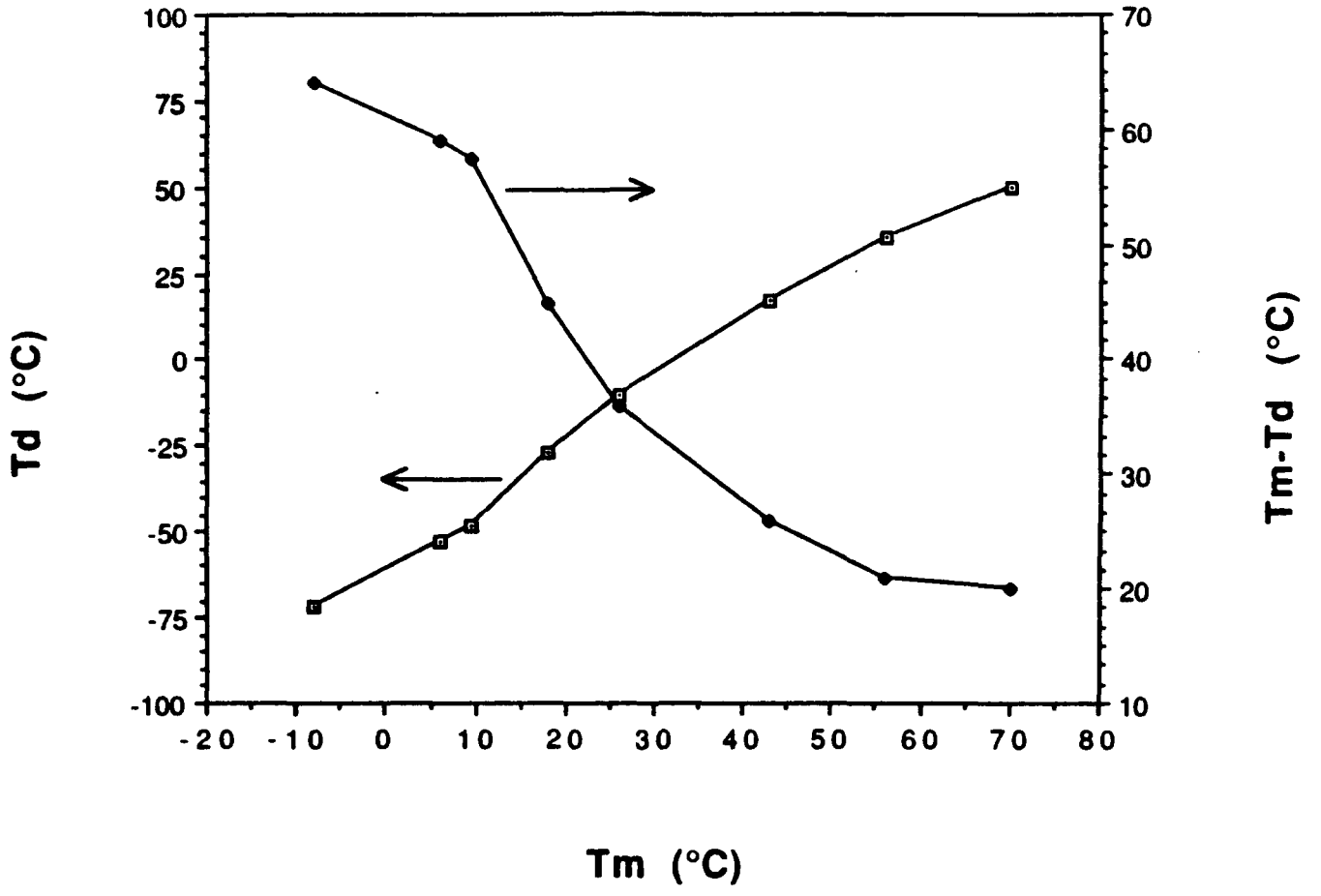

Figure 53. Variation of T_m, T_d, and T_m-T_d with PT content for (1-x) PMN-(x) PT (1 KHz).

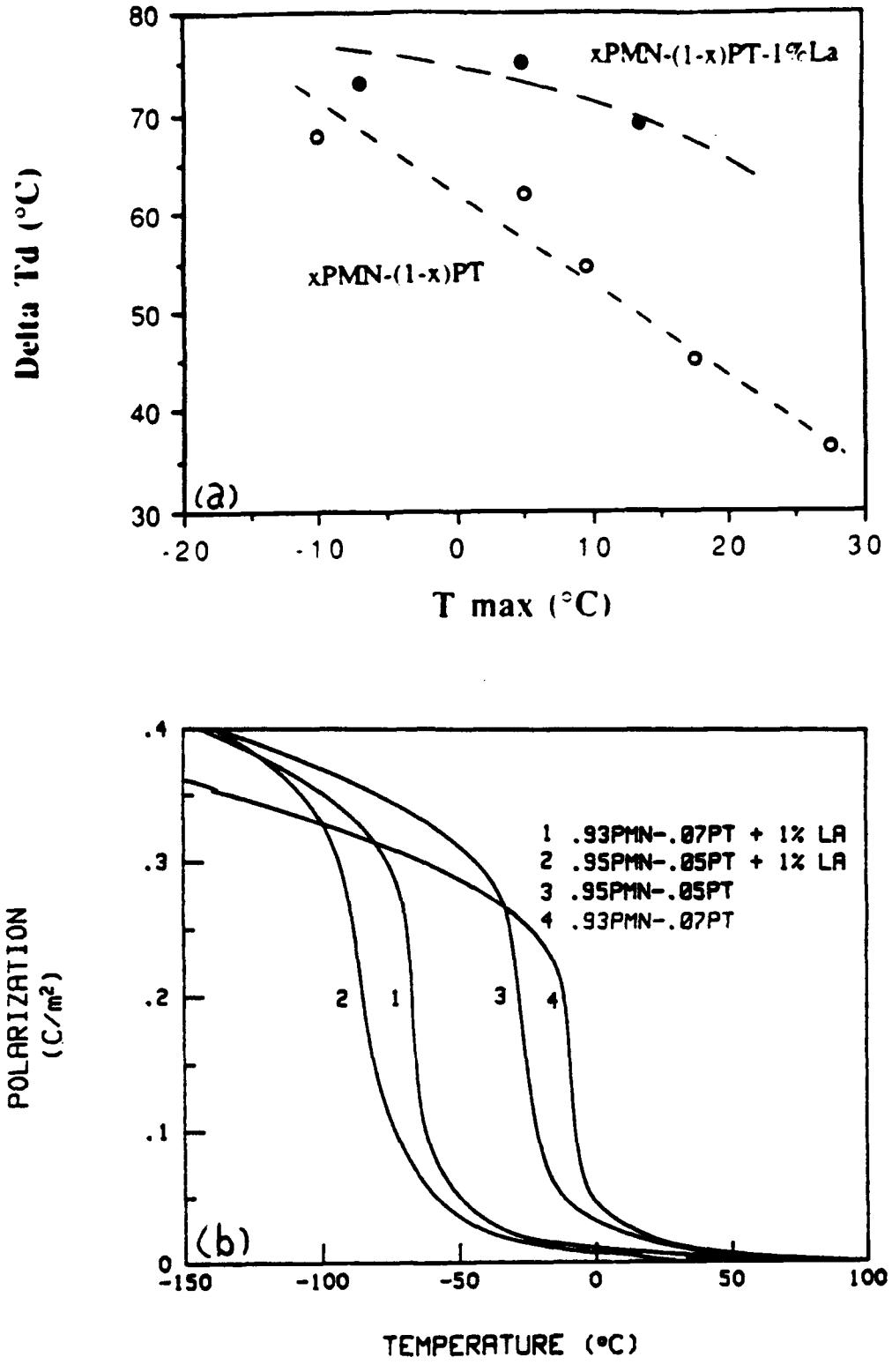

Figure 54. Effect of lanthanum substitution on the polarization temperature behavior of PMN-PT: (a) variation of ΔT (T_m-T_d) with T_m for PMN-PT and PMN-PT La; (b) polarization temperature behavior for undoped and La-doped PMN-PT's (Note: decrease in T_d with La-modification.)

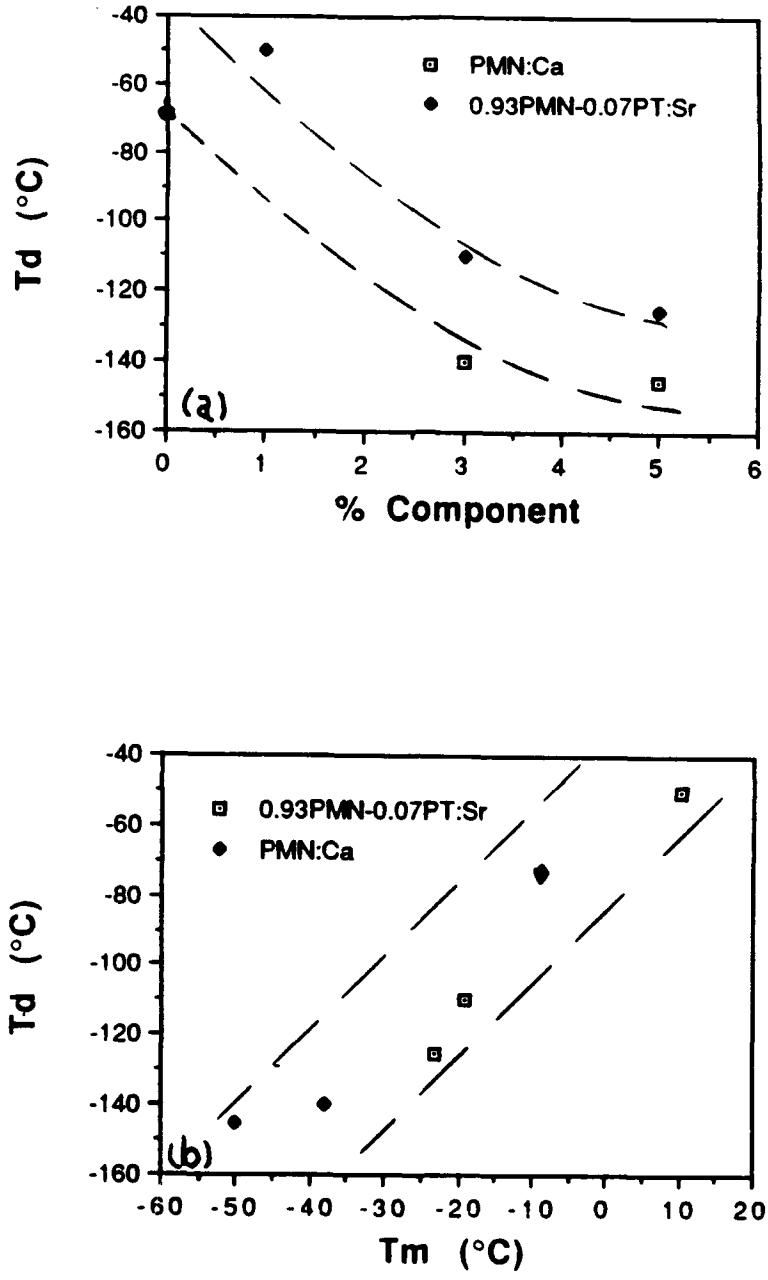

Figure 55. Effects of A-site modification (Ca^{+2}, Sr^{+2}) on (a) depolarization temperature (T_d) of PMN-PT ceramics and (b) variation in T_d with T_m for A-site modified PMN-PT.

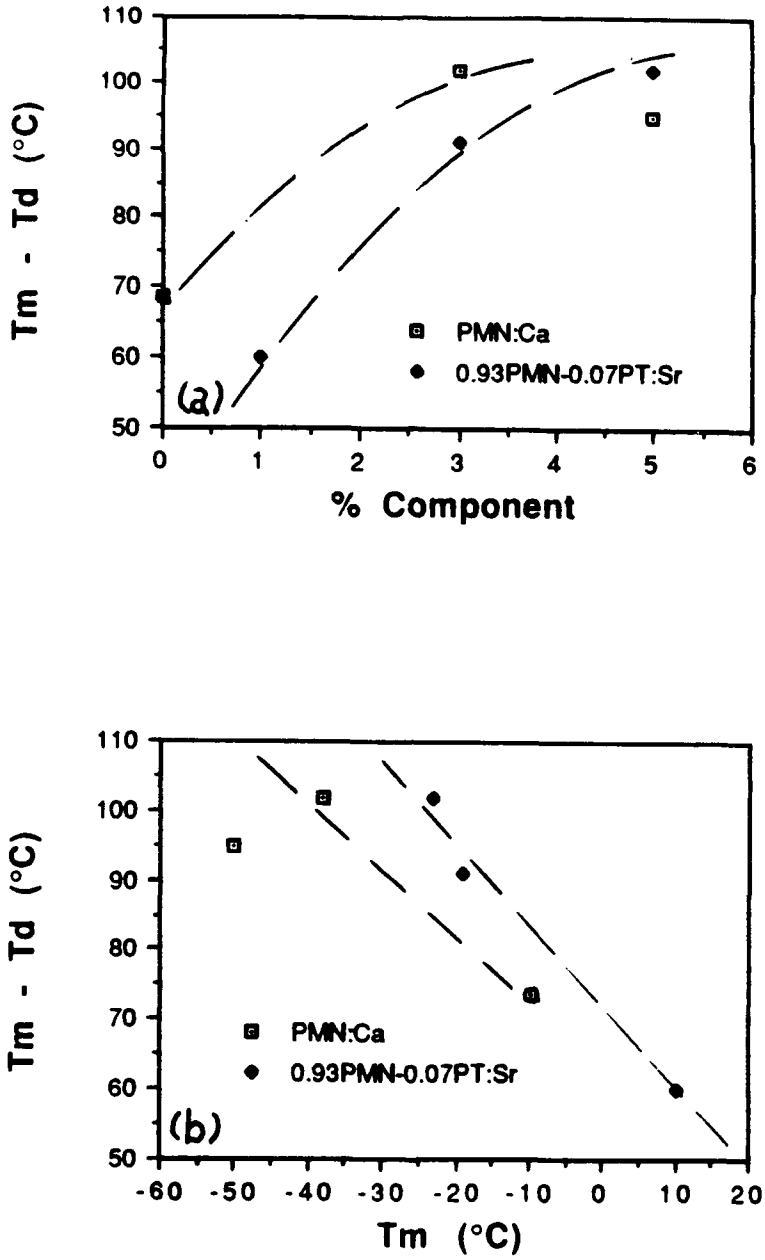

Figure 56. Effects of A-site modification on width of polar Regime II (T_m-T_d) in PMN-PT: (a) T_m-T_d as function of A-site modification; (b) T_m-T_d as function of T_m.

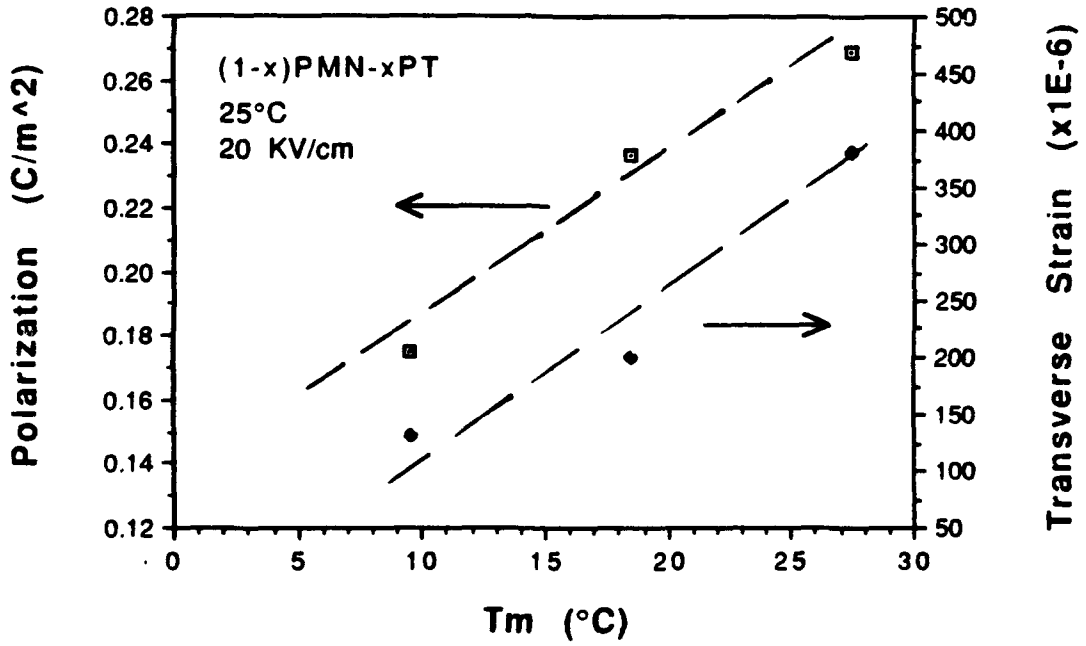

Figure 57. Variation of induced polarization and strain with T_m for (1-x) PMN - (x) PT system with T_m in temperature range of interest.

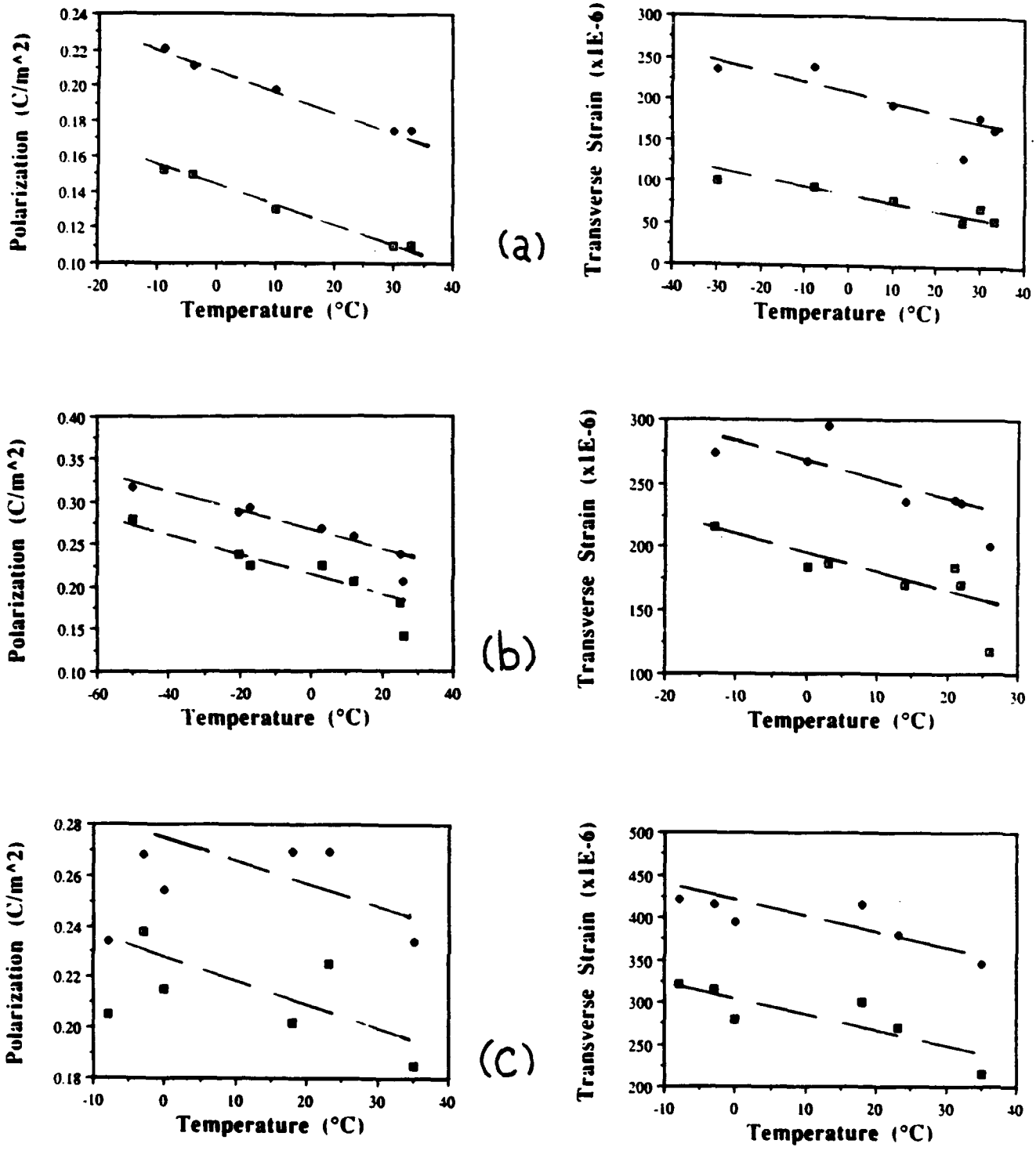

Figure 58. Induced polarization and strains at 10 KV/cm and 20 KV/cm as function of temperature for PT-modified PMN: (a) 0.97 PMN-0.03 PT; (b) 0.95 PMN-0.05; (c) 0.93 PMN-0.07 PT.

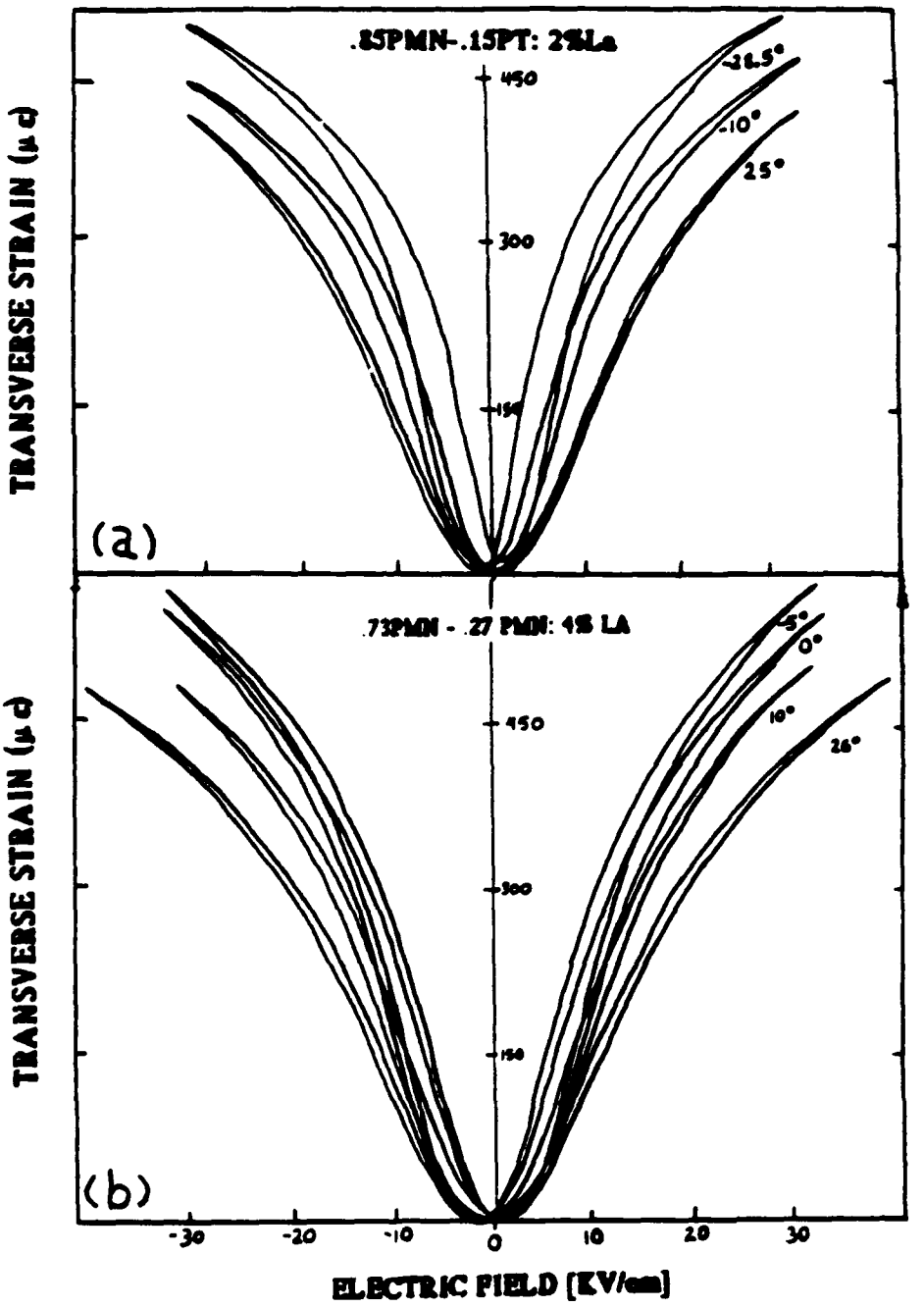

Figure 59. Induced strain as function of applied electric field for La-modified PMN-PT compositions: (a) 0.85 PMN-0.15 PT: 2% La (T_m = 20°C, T_d = -49°C); (b) 0.73 PMN-0.27 PT: 4% La (T_m = 33°C, T_d = -35°C).

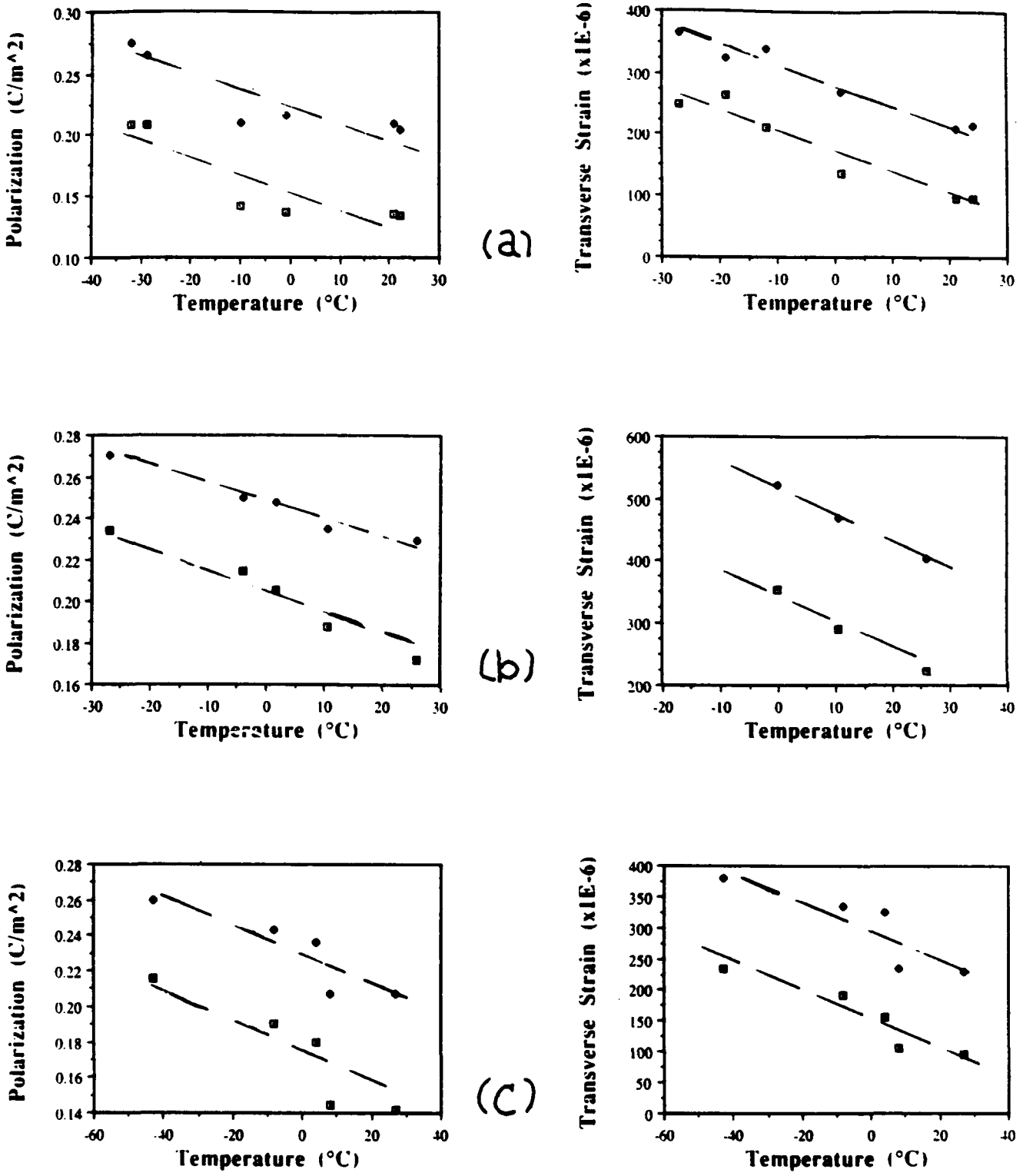

Figure 60. Induced polarization/strain at 10 KV/cm and 20 KV/cm as function of temperature for A-site modified PMN-PT compositions: (a) 0.93 PMN-0.07 PT: 1% La; (b) 0.73 PMN-0.27 PT: 4% La; (c) 0.93 PMN-0.07 PT: 1% Sr.

Type II. Relaxors PLZT

Presented in section I, the PLZT family of relaxors is somewhat compositionally limited in that only PLZTs with a range of La ≥ 0.7% and Zr:Ti ratios ~65:35 exhibit relaxor dielectric behavior.

As with Type I relaxors, a direct correlation between Km and Tm was observed, as presented in Figure 61. As presented, K_m decreased linearly with T_m, even though processing-related variations were observed, i.e. the same composition could give rise to dramatic differences in T_m, owing to La distribution/uniformity.

The observed relationship is also believed to be the result of a de-coupling of the ferroelectric octahedra, in similar fashion to the Type I relaxors, but due to Pb or A-site vacancies. The polarization dependence also reflects this model, as presented in Figure 62, showing decreasing levels of P_r and decreasing depolarization temperatured T_d with increasing La-modification. Also note the significantly larger ΔT values (>100°C) as compared to that for Type I , suggesting a different "de-coupling" phenomenon.

The induced polarization/strain behaviors of the studied PLZT compositions are summarized in Figure 63. Again, as with the Type I relaxors, both the levels of induced polarization and strain increased with decreasing temperature. All compositions exhibit large strains (>300 x 10^{-6}) at low field levels (<20 KV/cm), within the sonar usage temperature range; however, hysteresis levels for PLZT 9/65/35 are too high for this application (i.e. >> 10%) (see Figure 64).

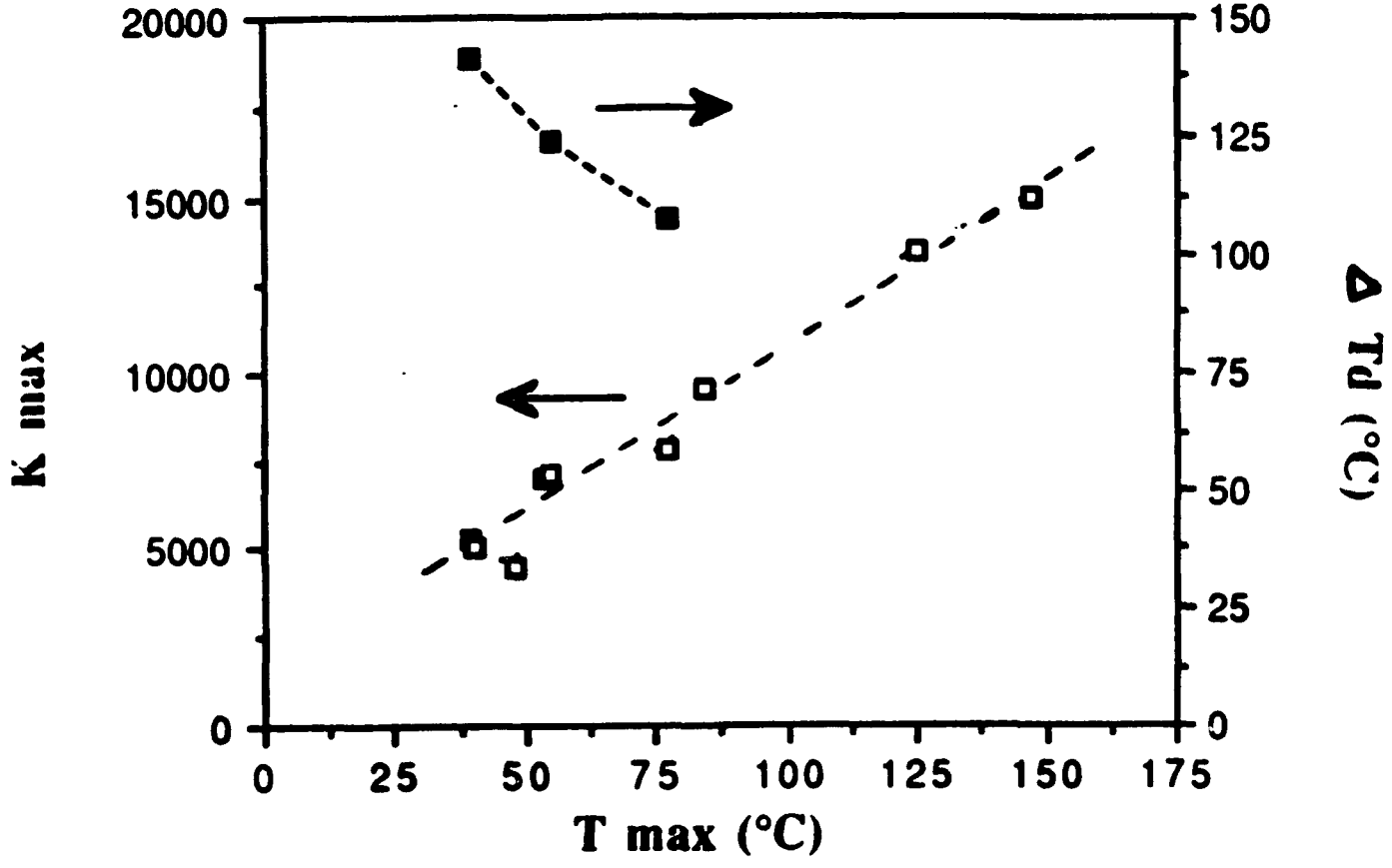

Figure 61. Dielectric constant and ΔT (T_m-T_d) versus T_{max} for various Type II relaxor PLZT compositions.

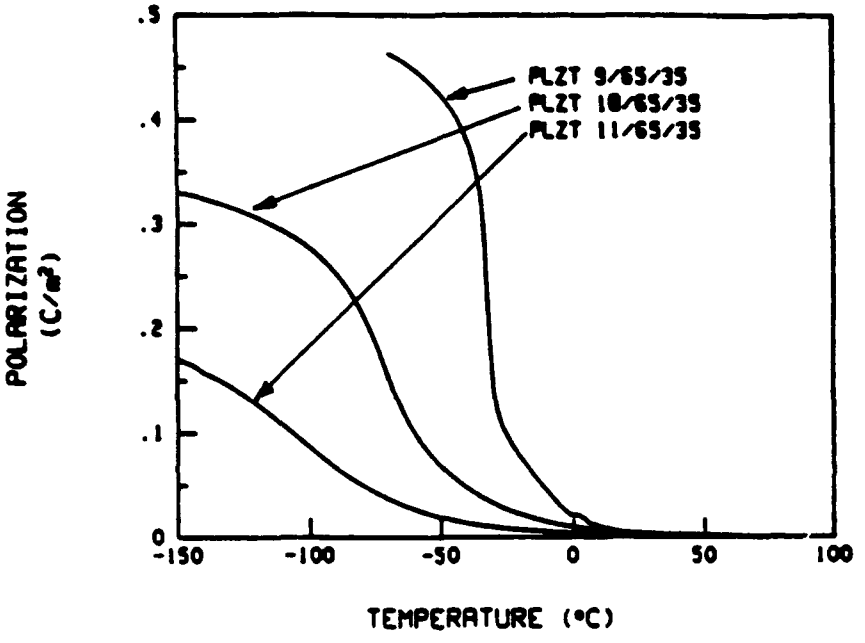

Figure 62. Polarization temperature behavior for Type II relaxor PLZT compositions illustrating effects of La-modifications on depolarization behavior.

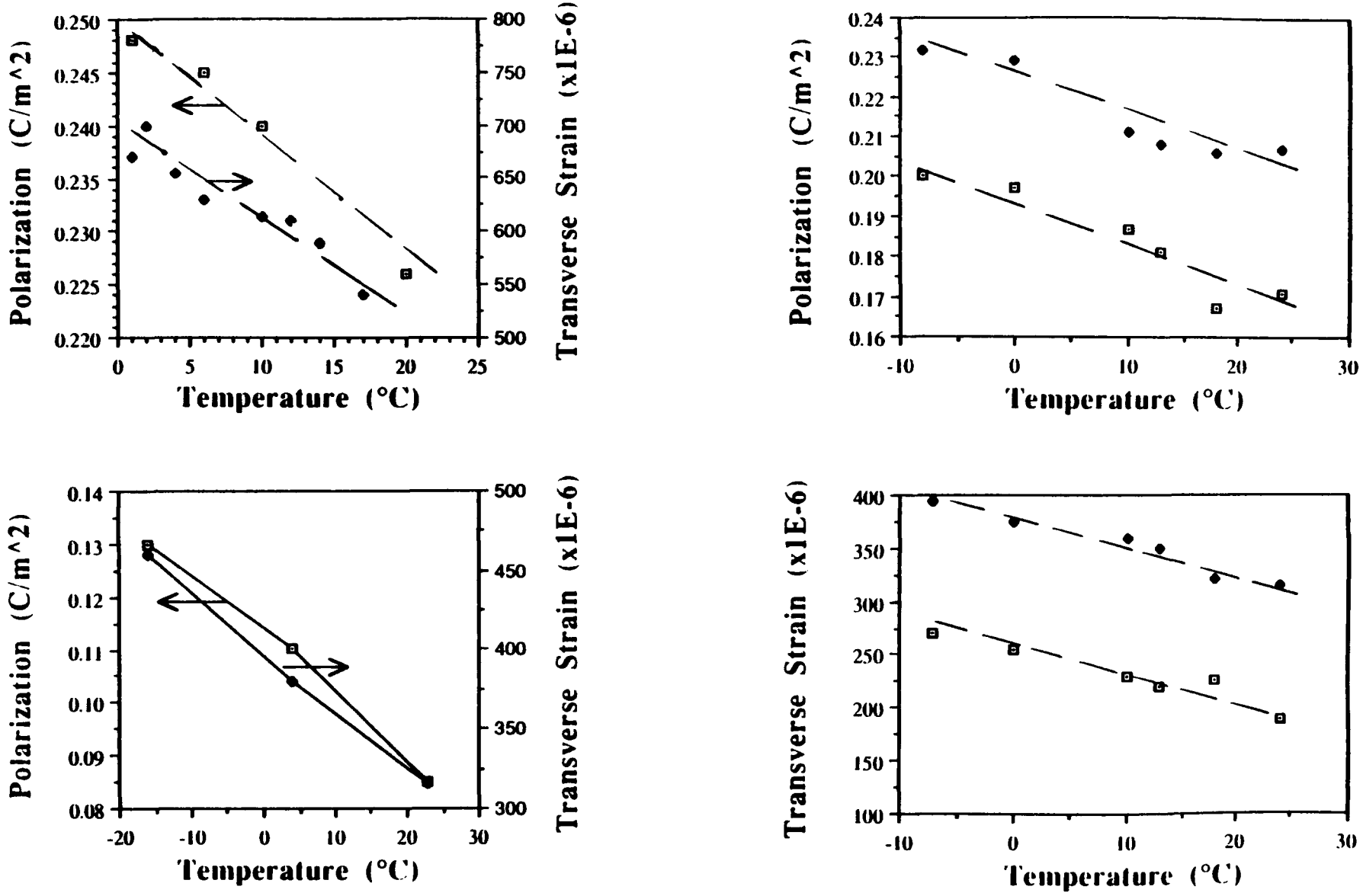

Figure 63. Induced polarization/strain, temperature behavior for Type II relaxor PLZT compositions: (a) PLZT (9/65/35) (10 KV/cm data); (b) PLZT (10/65/35) (10 KV/cm data); (c) PLZT 11/65/35 (10 KV/cm and 20 KV/cm date).

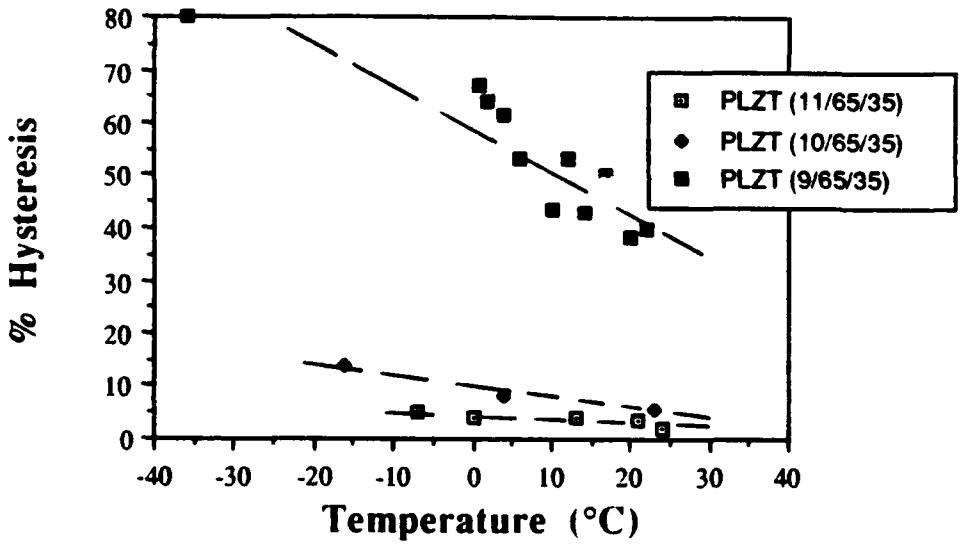

Figure 64. Hysteresis as function of temperature for Type II relaxor compositions.

SUMMARY

The results presented discuss the potential of electrostrictor-based actuators for Navy-type sonar transducers. Analogous to piezoelectric ceramics, e.g. Navy Type I - PZT-4, electrostrictors have been classified into four Types, based on their associated polarization change mechanisms. In relation to the following requirements for Navy Sonar Transducers:

- Large E-field induced strains ≥ 0.03%
- Operating temperature range 0-30°C
- Minimal strain E-field hysteresis
- Low dielectric loss
- High strain energy density

the performance of the four types of strictors have been summarized Table VIII. For comparison, Navy Type I and III-PZTs were included.

From the results presented, it is clearly evident that the Type I $Pb(B_1B_2)O_3$ relaxors offer overall superior performance.

Table VIII. Performance Summary of Electrostrictors for Sonar Transducers

Material Type	Example	Strain Level	Temp. Range	*Hysteresis	*Freq Dependency	*Heating/ Dielectric Loss	Elastic s_{ij}	Microstructural Dependency
Normal IV	$(Ba,Sr)TiO_3$	-	-	0	0,+	?	+ +	-
Type III	$Ba(Ti,Sn)O_3$	0	+	+	?	?	-	-
Relaxor II	PLZT	+ +	+ +	0	0,-	-	+	0
Relaxor I	$Pb(B_1B_2)O_3$	+	+	+ +	+	+	+	+
Piezo Type I,III	PZT-4,8	+	+ + +	-	+	0	-	0

*Subjective in relation to T_m.

+ - Best
0 - Moderate
- - Worst

ONGOING AND FUTURE WORK

Though it is clear that the Type I relaxors offer superior performance for sonar-transducers, it is not yet clear how such materials will function under pre-stress and high frequency drive conditions. In other words, what are the micro-mechanical limitations and ultimate reliability of these materials? Specific areas of development to be investigated include the following:

- Materials Synthesis
  - — grain growth control for enhanced mechanical integrity

- Proto-type MultilayerTransducers
  - —examine load effects and overall "elastic energy" behavior under high drive conditions.

- Fatigue Testing
  - — examine life of actuators based on fatigue and degradation studies, while incorporating NDE for critical flaw characterization.

REFERENCES

T.R. Shrout and Joseph Fielding, Jr., "Relaxor Ferroelectric Materials," Proc. IEEE Ultrasonics Sympos., (1990).

K. Uchino, S. Nomura, L.E. Cross, and R.E.Newnham, "Electrostriction in Perovskite Crystals and its Application to Transducers," J.Phys. Soc. Jpn. [49], p. 45-48, Supp. B (1980).

M.Ealey and C. Wheeler, "A Standardized Electrodisplacive Transducer," SPIE Symp. of Aerospace Sensing, Orlando, FL March (1989).

M. Ealey, "Adaptive Optics," Optical Engineering Vol. **25**, p. 112, (1990).

C.G. Mamboodri and C.A. Wheeler, "Tunable Vibration/Strain Sensing with Electrostrictive Materials," Symp. on Adaptive Structures and Smart Materials, Blacksburg, VA, p. 285 (1992).

H. Takeuchi, H. Masuzawa, C. Nakaya, and Y. Ito, "Medical Ultrasonic Probe Using Electrostrictive Ceramics/Polymer Composites," IEEE Ultrasonics Symposium, p. 705,(1989).

S.T. Vohra, F. Bucholtz, and A.D. Kersey, "Fiber-optic dc and low frequency electric field sensor," Optics Letters **16** (18) p. 1445 (1991).

W.Y.Pan, W.Y. Gu, D.J. Taylor, and L.E. Cross, "Large Piezoelectric Effect Induced by Direct Current Bias in PMN:PT Relaxor Ferroelectric Ceramics, Jpn. JAP **28**, (4) p. 653 (1989).

S.J. Jang, "Electrostrictive Ceramics for Actuator Applications," Ph.D. Thesis, The Pennsylvania State University (1979).

N. Kim, "The Role of Lanthanum Modification on the Fabrication and Properties of Lead Magnesium Niobate-Lead Titanate Ceramics," M.S. Thesis, The Pennsylvania State University (1990).

Z.Y. Meng, U. Kumar, and L.E. Cross, "Electrostriction in Lead Lanthanum Zirconate-Titanate Ceramics," J. Am. Ceram. Soc. **68**, [8], p. 459-62 (1985).

G.A. Smolenskii and V.A. Isupov, Zh. Tekh. Fiz. **24**, p. 1375 (1954).

J. Von Cieminski, H. Th. Langhammer, H.-P Abicht, "Peculiar Electromechanical Properties of Some $Ba(Ti,Sn)O_3$ Ceramics," Phys. Stat. Sol. (a) **120**, p. 185 (1990).

J. Von Cieminski and H. Beige, "High Signal Electrostriction in Ferroelectric Materials," J. Phys. D: Appl. Phys. **24**, p. 1182 (1991).

J. Von Cieminski, "Modeling of High-Signal Electrostriction. I-II," Z. Naturforsch. **45a**, p. 1090 (1990).

L.E. Cross, "Piezoelectric and Electrostrictive Sensors and Actuators for Adaptive Structures and Smart Materials," Proc. AME 110th Annual Meeting, San Francisco, CA (Dec. 1989).

B. Jaffe, W.R. Cook, and H. Jaffe, "Piezoelectric Ceramics," p. 94, Academic Press, NY (1971).

S.J. Butcher and N.W. Thomas, "Ferroelectricity in the system Pb1-xBax $(Mg_{1/3}Nb_{2/3})O_3$," J. Phys. Chem. Solids, **52** [4], 595 (1991).

N.S. Novosil'tsev and A.L. Khodakov, Zh. Tech. Fiz, **26**, 310 91956).

G.A. Smolenskii and K.I. Rozhacher, Zh. Tech. Fiz, **24**, 1751, (1954).

Q.M. Zhang, S.J. Jang, and L.E. Cross, J. Appl. Phys., **65** [7] 2807 (1989).

S. Choi et al., Ferroelectrics, **100**, 29 (1989).

G.H. Haertling and C.E. Land, J. Am. Cer. Soc., **54**, 1 (1971).

D.J. Voss, S.L.Swartz, and T.R. Shrout, "The Effects of Various B-Site Modifications on the Dielectric and Electrostrictive Properties of Lead Magnesium Niobate Ceramics," Ferroelectrics, **50**, 203 (1983).

S.L. Swartz and T.R. Shrout, "Fabrication of Perovskite Lead Magnesium Niobate," Mat. Res. Bull., **17**, 1245 (1982).

K. Toyoda et al., "Re-Examination of the Phase Transitions in Solid Solutions of Perovskite-Type Oxides," Ferroelectrics, **93**, 335 (1989).

LIST OF TABLES

LIST OF FIGURES

PAGE

Appendix A. Dielectric Data.

Table A1. Dielectric data for modified Type I relaxor PMN compositions.

Composition	T_{max} (1 kHz)(°C)	T_d (°C)	$T_{max} - T_d$ (°C)	K_{max} (1 kHz)	tan δ_{max} (1 kHz)
PMN-PT					
PMN	-10	-78	68	18.0×10^3	0.1 @ -24°C
0.98PMN-0.02PT	5	-58	63	19	0.095 @ 11°C
0.97PMN-0.03PT	9.5	-45	54.5	21.5	0.09 @ 2°C
0.95PMN-0.05PT	17.5	-27	44.5	24.3	0.10 @ 12°C
0.93PMN-0.07PT	27.5	-9	36.5	25.0	0.095 @ 19.8
La/PMN/PT					
1/100/0	-35	--	--	14.4	0.11 @ -47°C
1/95/5	-7	-80	73	19.0	0.09 @ -15°C
1/93/7	5	-69	74	22.7	0.11 @ -9°C
7/65/35	13.5	-55	68.5	13.7	0.05 @ 7°C
4/73/27	34	-20	55	19.0	0.09 @ 20°C
3/79/21	25.5	-48	73.5	19.0	0.09 @ 14°C
2/85/15	17.5	-49.5	67	20.5	0.10 @ 5°C
1/91/9	12	-48	60	22.5	0.12 @ 0°C
Ca/PMN/PT					
1/100/0	-20	--	--	15.2	--
3/100/0	-38	--	--	10.3	--
5/100/0	-52	--	--	7.2	--
Sr/PMN/PT					
1/93/7	9	-50.5	59.5	20.2	0.10 @ -5°C
3/93/7	-16.5	-115	98.5	18.4	0.12 @ -38°C
5/93/7	-23	-135	112	16.5	0.12 @ 44°C
Ba/PMN/PT					
1/85/15	59.5	23	36.5	22.9	--
3/85/15	39	29	10	18.4	--
5/85/15	19	--	--	17.5	--
Bi/PMN/PT					
1/100/0	-23	--	--	15.3	0.15 @ -35°C
3/100/0	-35	--	--	6.1	0.15 @ -50°C
5/100/0	-35	--	--	4.5	0.15 @ -55°C

Table A2. Dielectric data for Type II relaxor PLZT compositions.

Composition	T_{max} (1 kHz)(°C)	T_d (°C)	$T_{max} - T_d$ (°C)	K_{max} (1 kHz)	tan δ_{max} (1 kHz)
PLZT					
9/65/35	77	-31	108	7.8×10^3	0.06 @ 36°C
10/65/35	55	-69	124	7.12	0.08 @ 19°C
11/65/35	39	-102	141	5.31	0.08 @ 1°C

Table A3. Dielectric data for Type III "pinched" ferroelectrics $Ba(Ti_{1-x}Sn_x)O_3$.

Composition	T_{max} (1 kHz)(°C)	T_d (°C)*	$T_{max} - T_d$ (°C)	K_{max} (1 kHz)	tan δ_{max} (1 kHz)
$Ba(Ti_{1-x}Sn_x)O_3$					
x = 0.10	48	--	--	29.0×10^3	0.055 @ -55°C
x = 0.13	8	1,63	7,-55	32.5	0.09 @ 3°C

* Note: "Pinched" ferroelectric; multiple phase transitions in vicinity of T_{max}.

Table A4. Dielectric data for Type IV normal ferroelectric $(Ba_{1-x}Sr_x)TiO_3$.

Composition	T_{max} (1 kHz)(°C)	T_d (°C)	$T_{max} - T_d$ (°C)	K_{max} (1 kHz)	tan δ_{max} (1 kHz)
$Ba_{1-x}Sr_xTiO_3$					
x = 0.35	~~25~~ 17	~~25~~ 17	0	26.0×10^3	--
x = 0.40	1	1	0	23.5	--
x = 0.45	-15	-15	0	23.5	--
x = 0.50	-31.5	-31.5	0	23.5	--

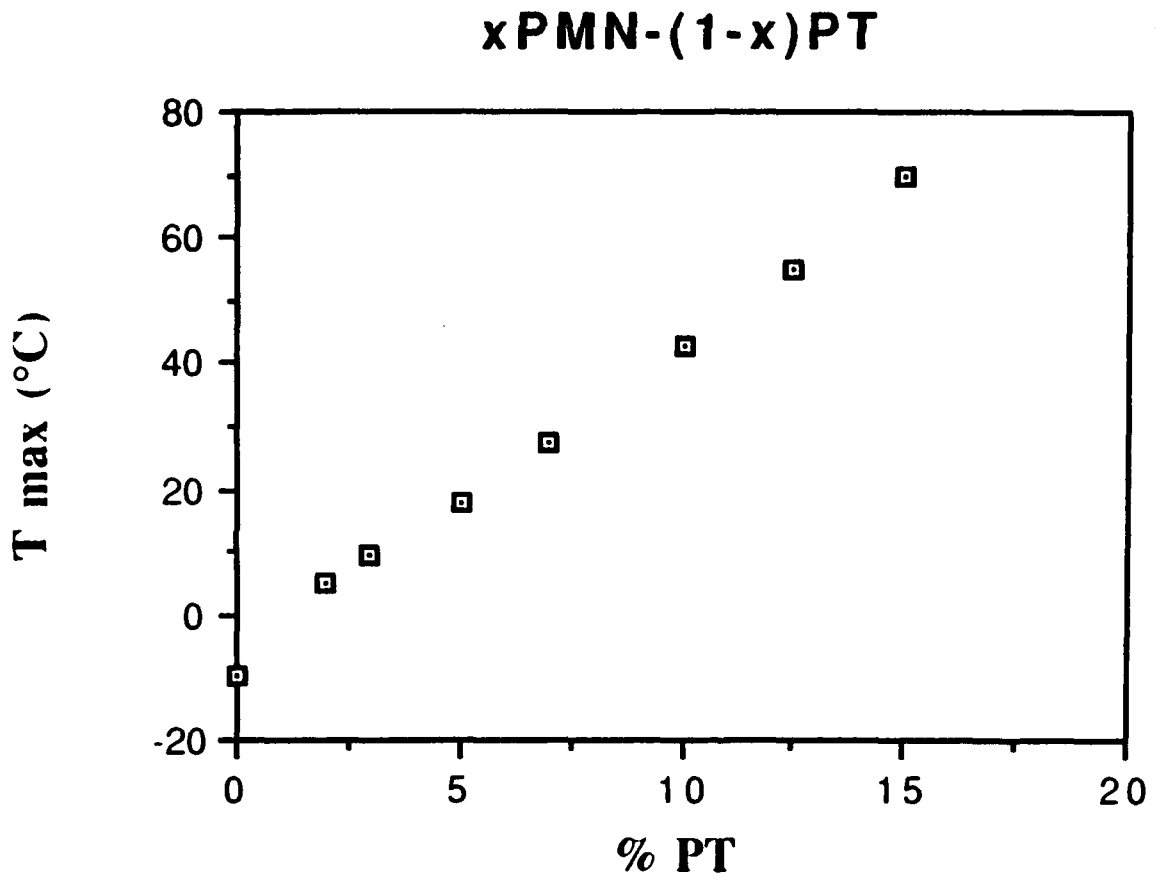
xPMN-(1-x)PT
T max (°C)
80
60
40
20
0
-20
0
5
10
15
20
% PT

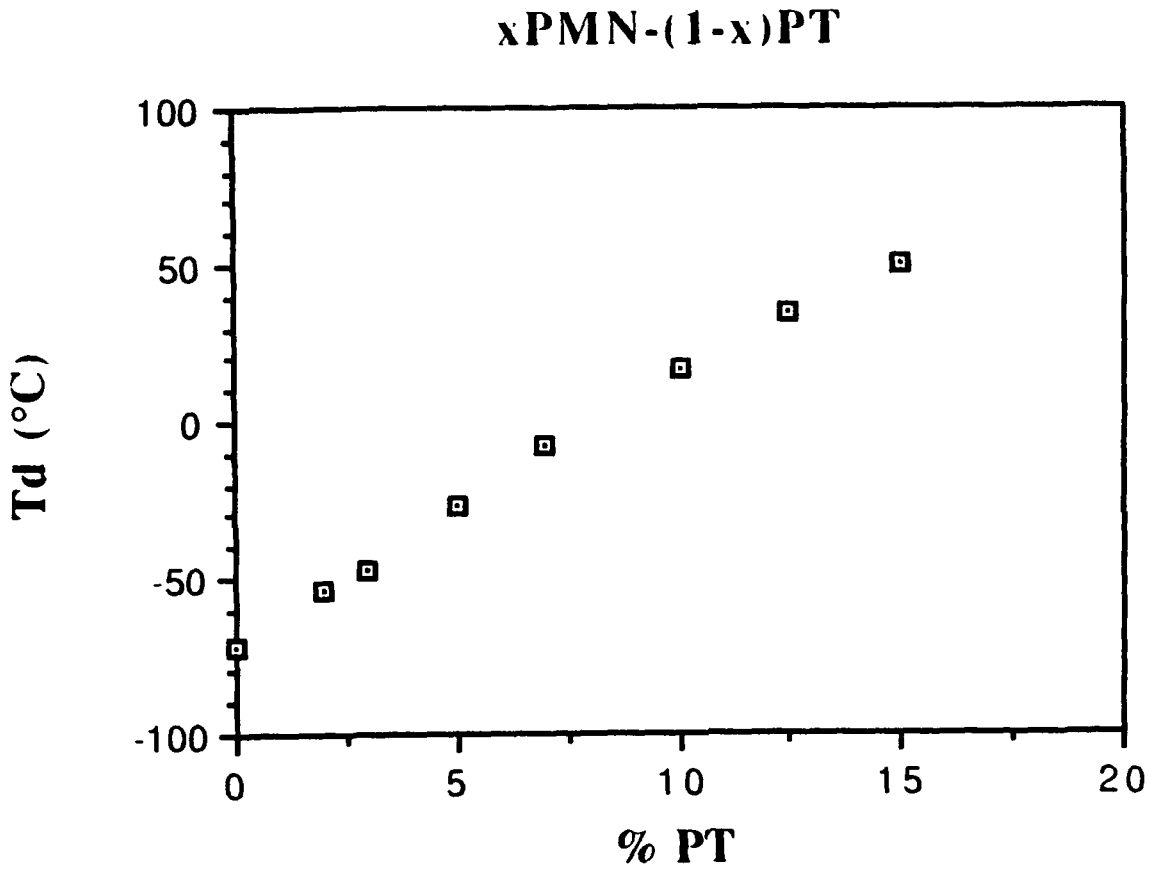
xPMN-(1-x)PT
100
50
0
-50
-100
Td (°C)
0
5
10
15
20
% PT

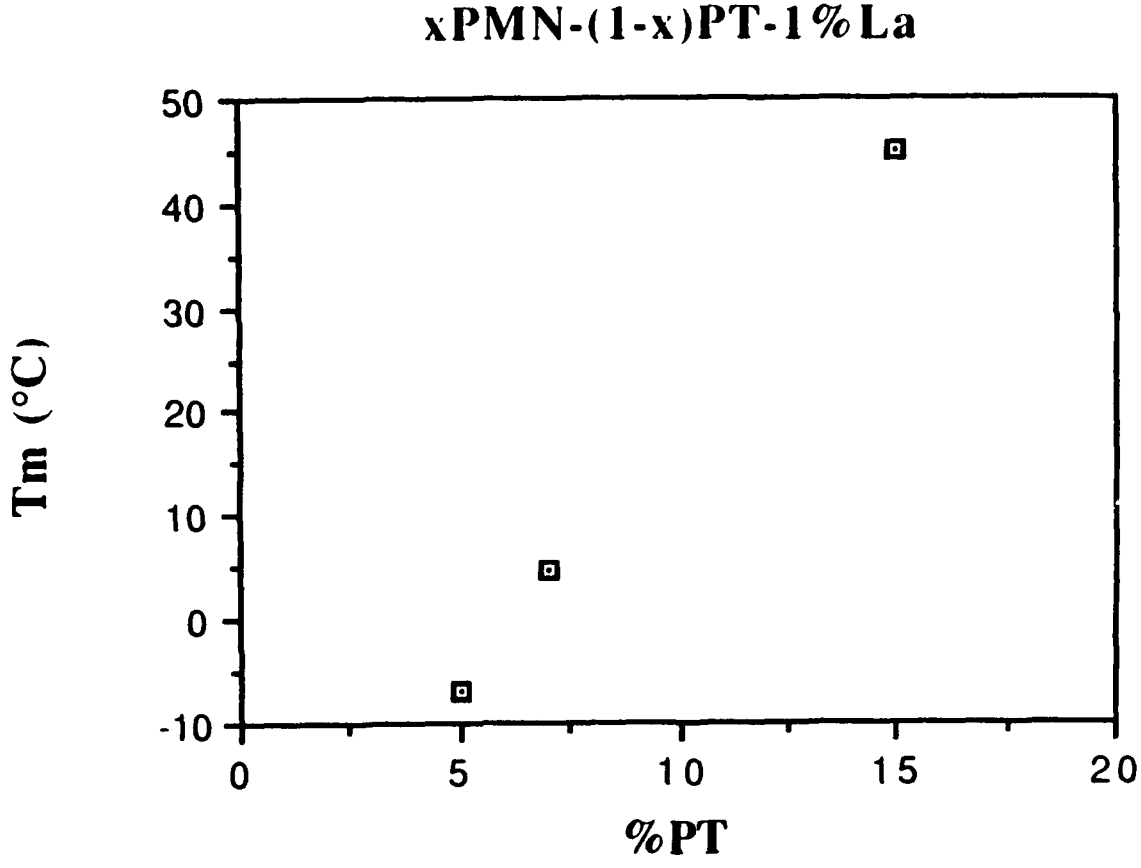
xPMN-(1-x)PT-1%La
Tm (°C)
50
40
30
20
10
0
-10
0
5
10
15
20
%PT

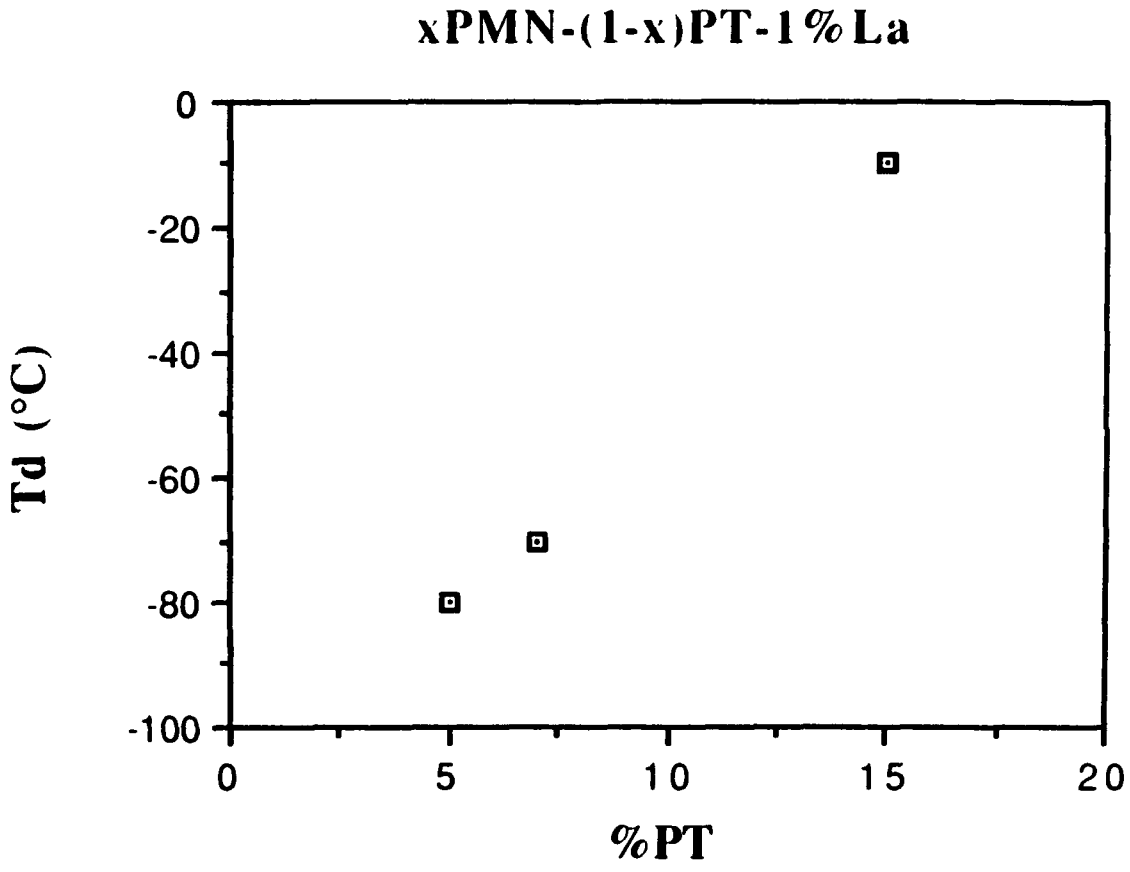
xPMN-(1-x)PT-1%La
Td (°C)
0
-20
-40
-60
-80
-100
0
5
10
15
20
%PT

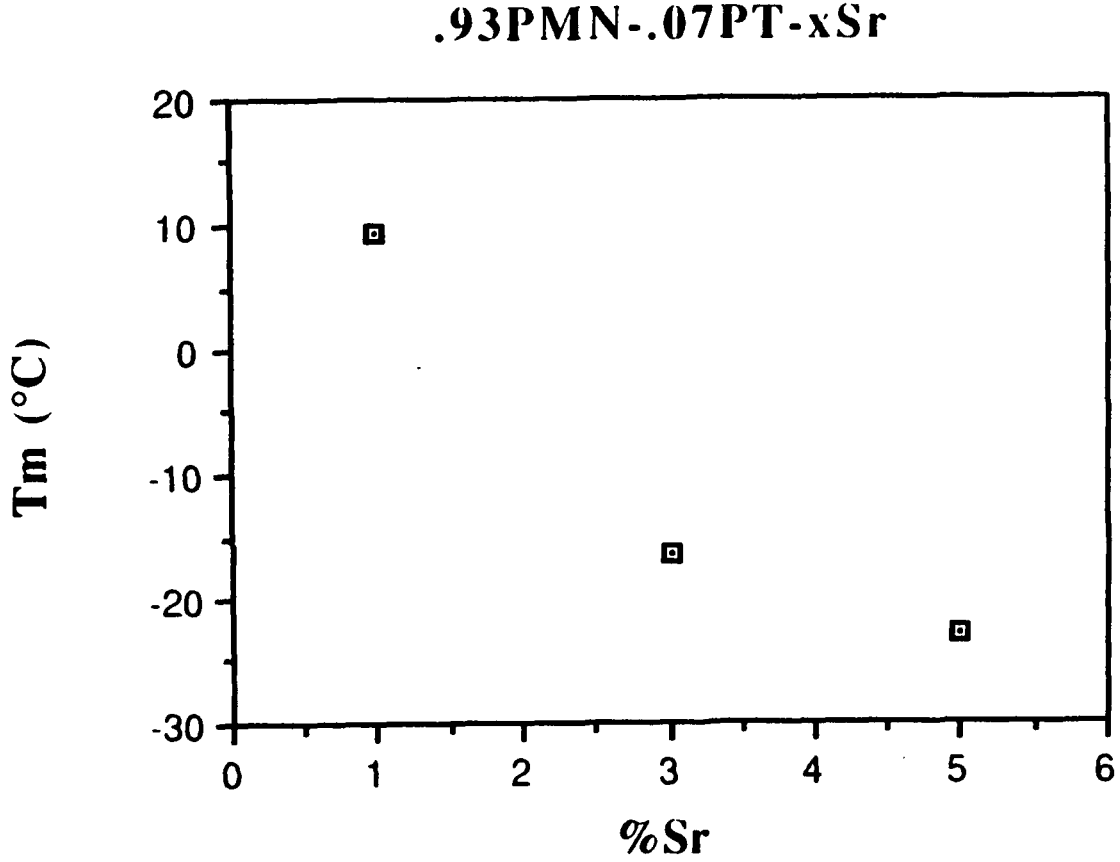
.93PMN-.07PT-xSr
Tm (°C)
20
10
0
-10
-20
-30
0
1
2
3
4
5
6
%Sr

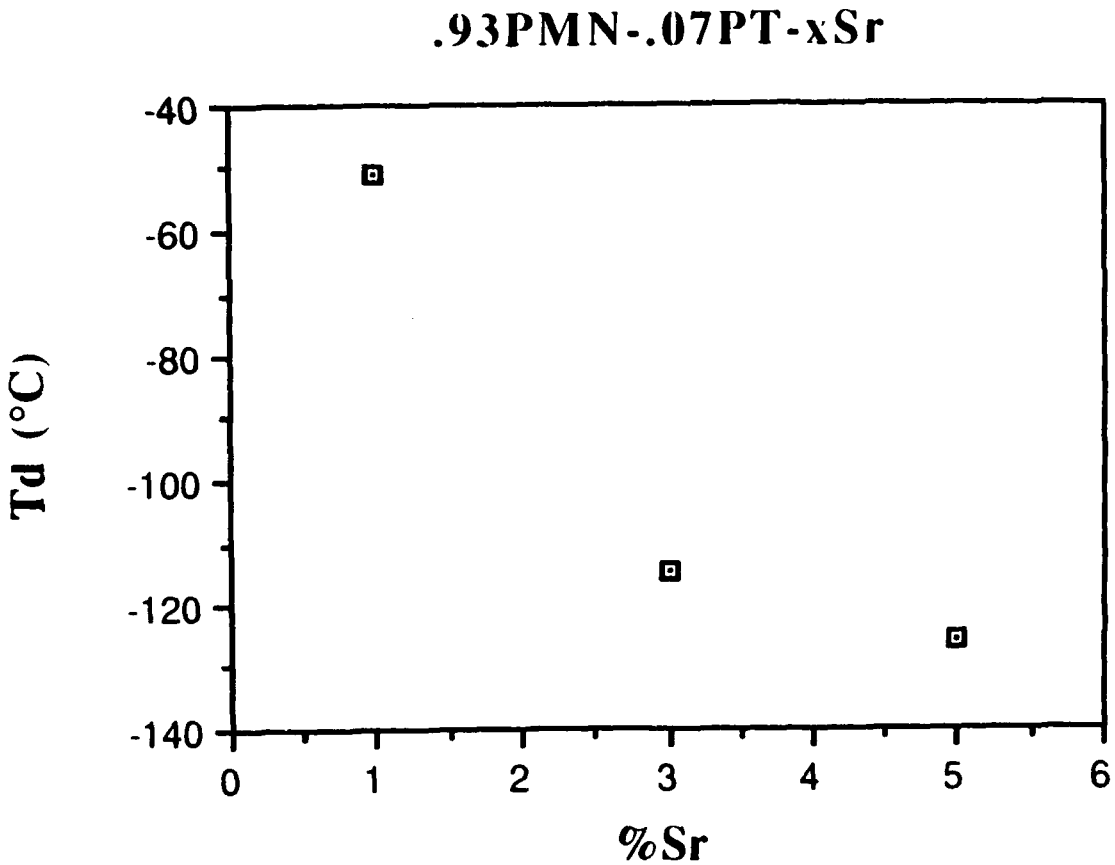
.93PMN-.07PT-xSr
Td (°C)
-40
-60
-80
-100
-120
-140
0
1
2
3
4
5
6
%Sr

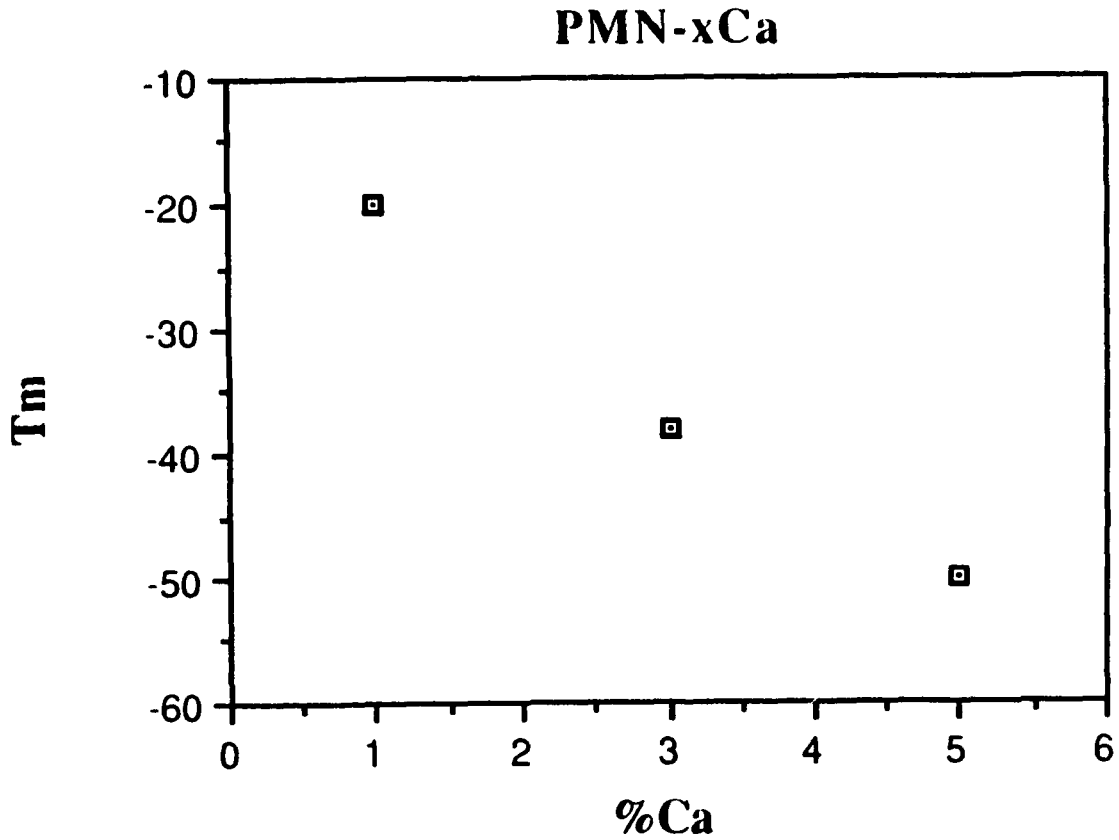
PMN-xCa
-10
-20
-30
-40
-50
-60
Tm
0
1
2
3
4
5
6
%Ca

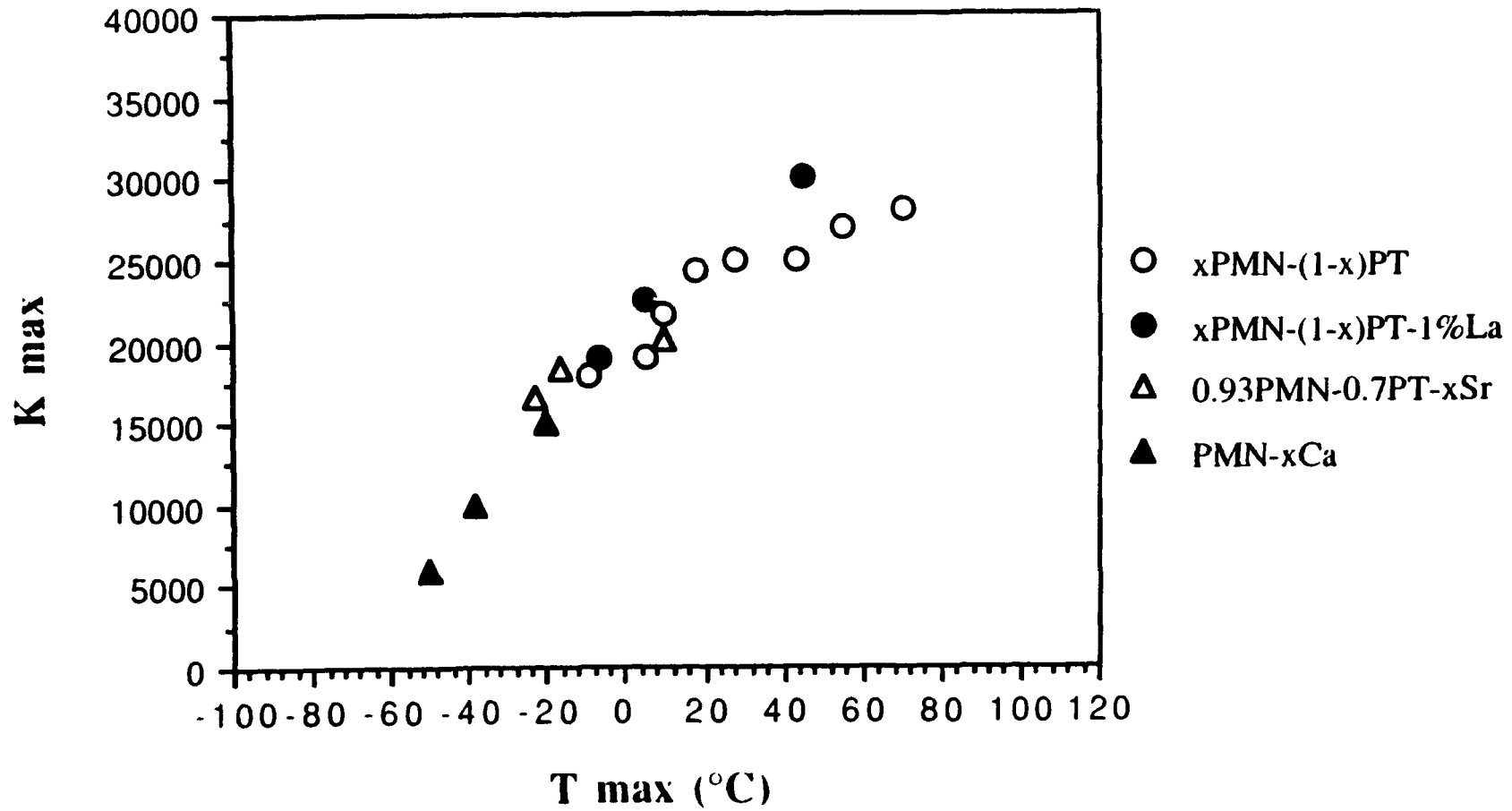
40000
35000
30000
25000
20000
15000
10000
5000
0
K max
-100 -80 -60 -40 -20 0 20 40 60 80 100 120
T max (°C)
xPMN-(1-x)PT
xPMN-(1-x)PT-1%La
0.93PMN-0.7PT-xSr
PMN-xCa

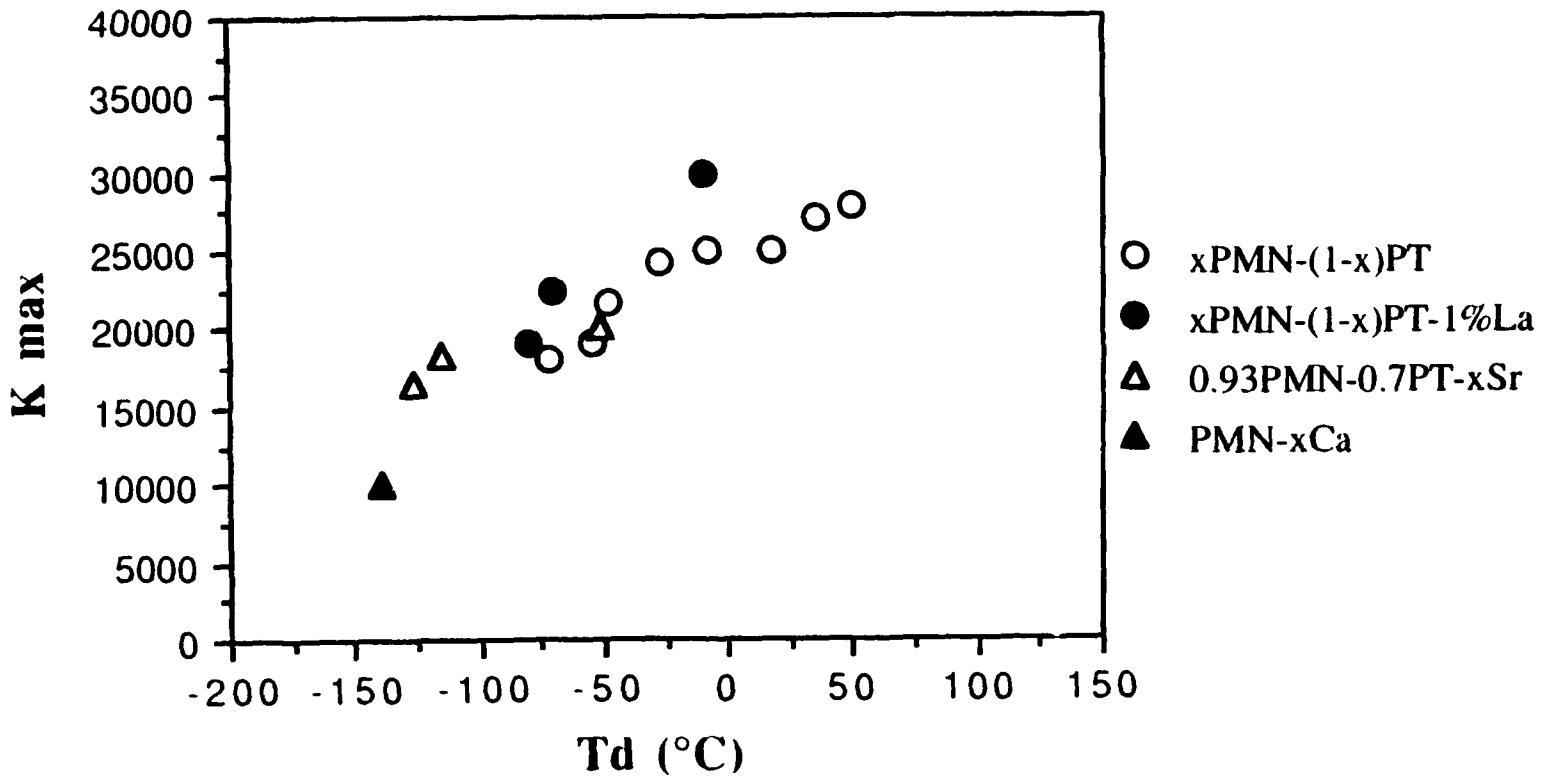
40000
35000
30000
25000
20000
15000
10000
5000
0
K max
-200
-150
-100
-50
0
50
100
150
Td (°C)
xPMN-(1-x)PT
xPMN-(1-x)PT-1%La
0.93PMN-0.7PT-xSr
PMN-xCa

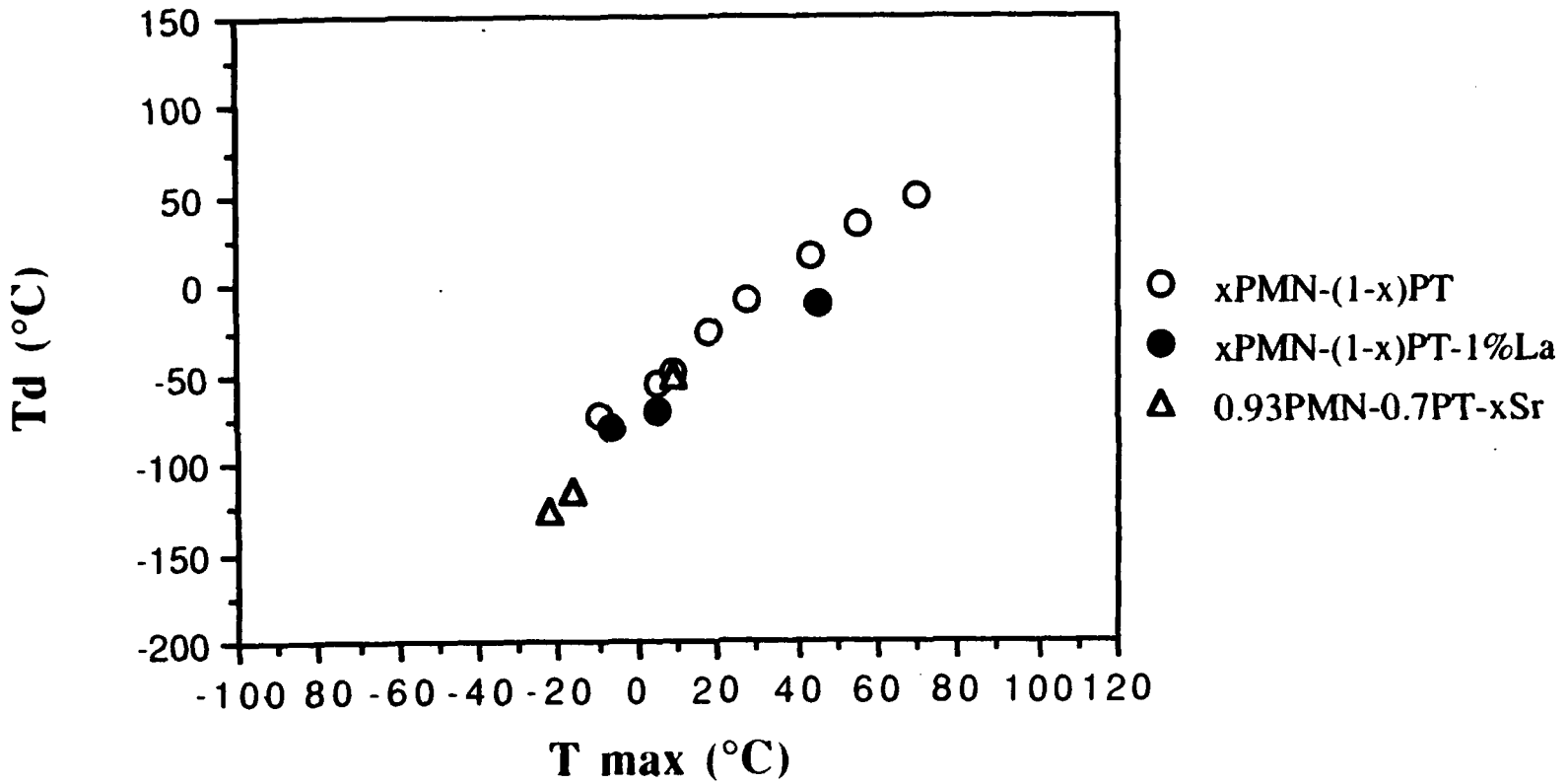
150
100
50
0
-50
-100
-150
-200
-100 80 -60 -40 -20 0 20 40 60 80 100120
Td (°C)
T max (°C)
xPMN-(1-x)PT
xPMN-(1-x)PT-1%La
0.93PMN-0.7PT-xSr

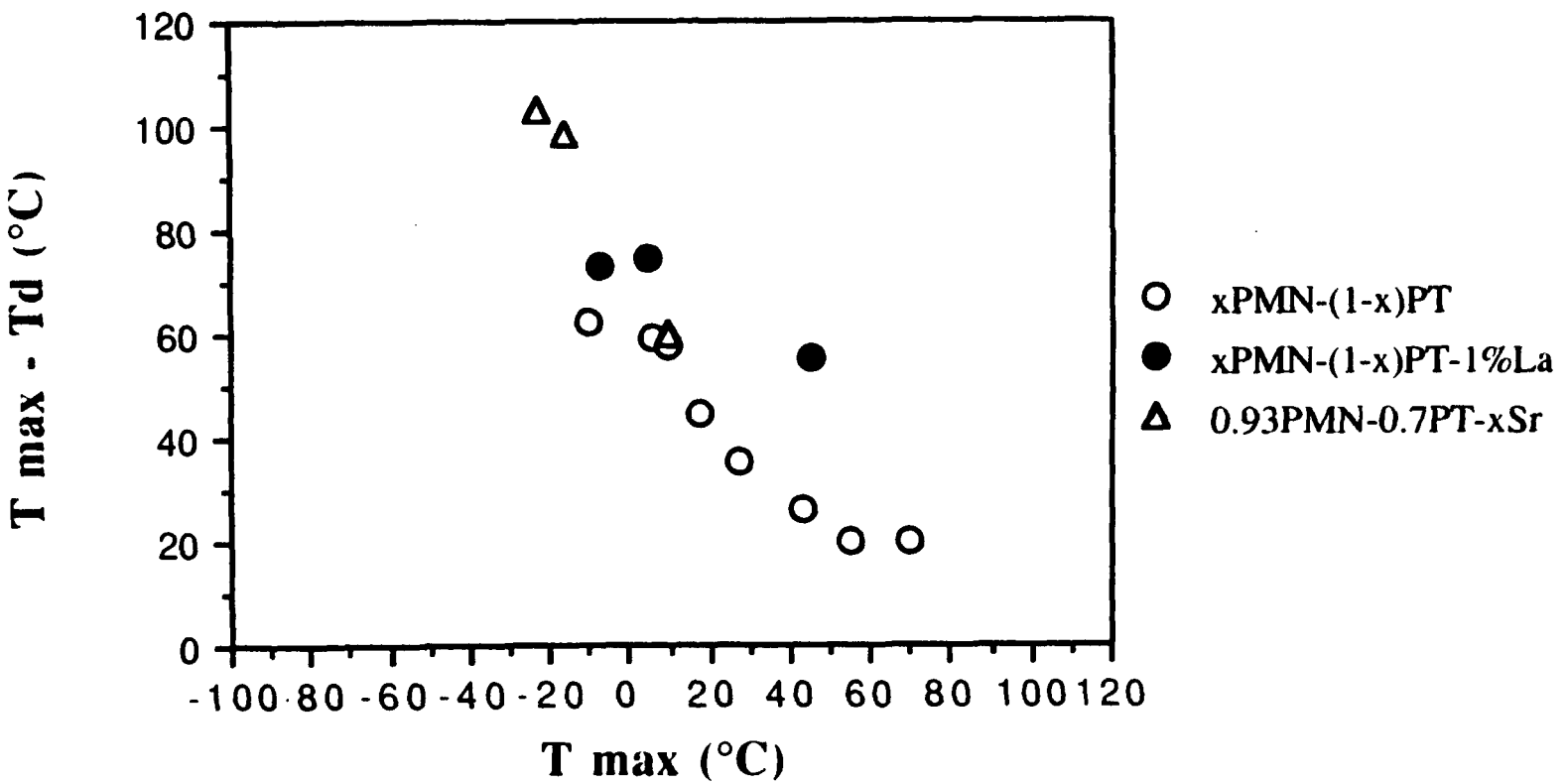

Add PLMN from data source

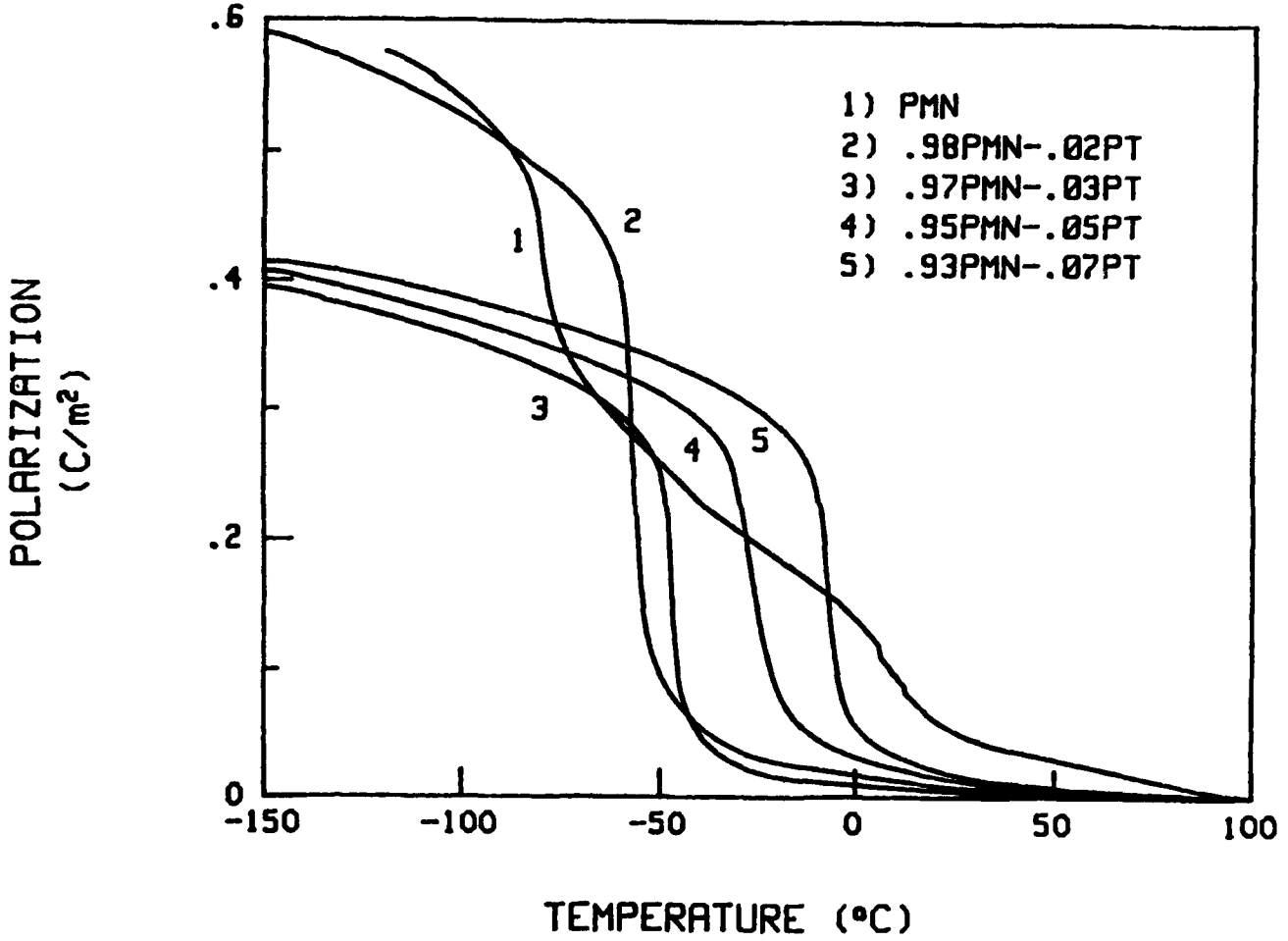
.6
.4
.2
0
-150
-100
-50
0
50
100
POLARIZATION (C/m²)
TEMPERATURE (°C)
1) PMN
2) .98PMN-.02PT
3) .97PMN-.03PT
4) .95PMN-.05PT
5) .93PMN-.07PT
1
2
3
4
5

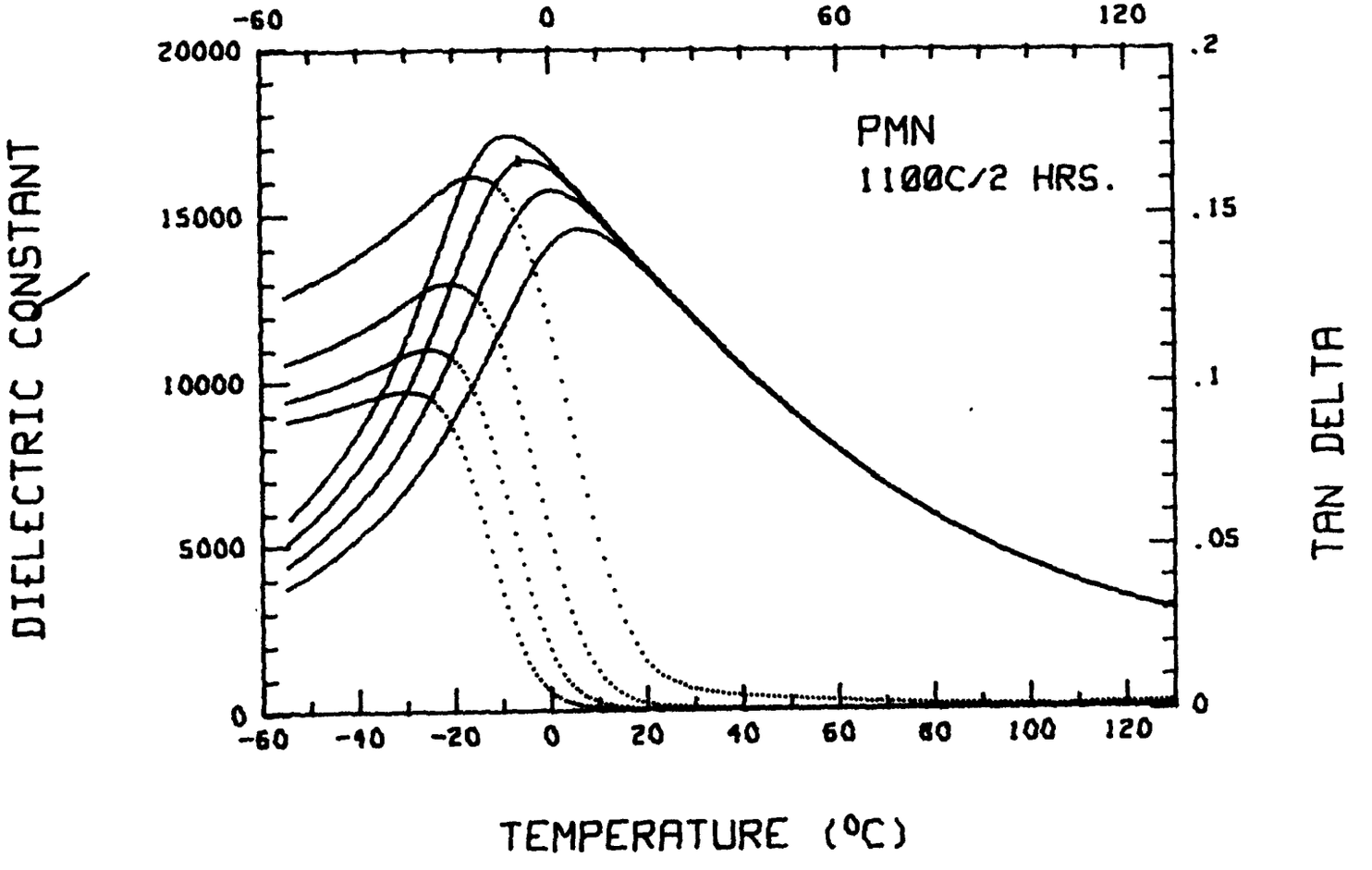
PMN
1100C/2 HRS.
DIELECTRIC CONSTANT
TAN DELTA
TEMPERATURE (°C)
-60
0
60
120
20000
15000
10000
5000
0
.2
.15
.1
.05
0
-60
-40
-20
0
20
40
60
80
100
120

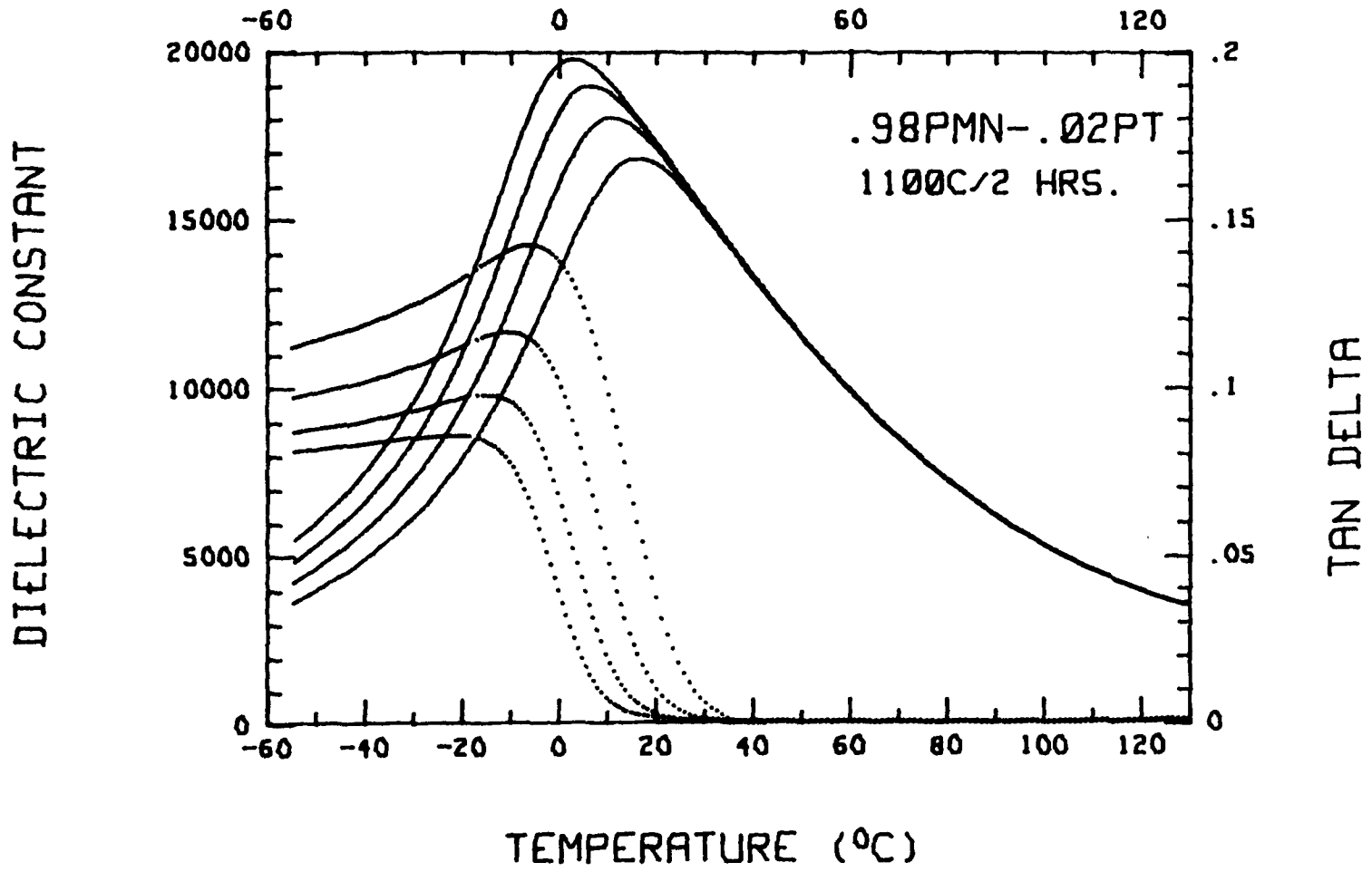
.98PMN-.02PT
1100C/2 HRS.
DIELECTRIC CONSTANT
TAN DELTA
TEMPERATURE (°C)
-60
0
60
120
20000
15000
10000
5000
0
.2
.15
.1
.05
0
-60
-40
-20
0
20
40
60
80
100
120

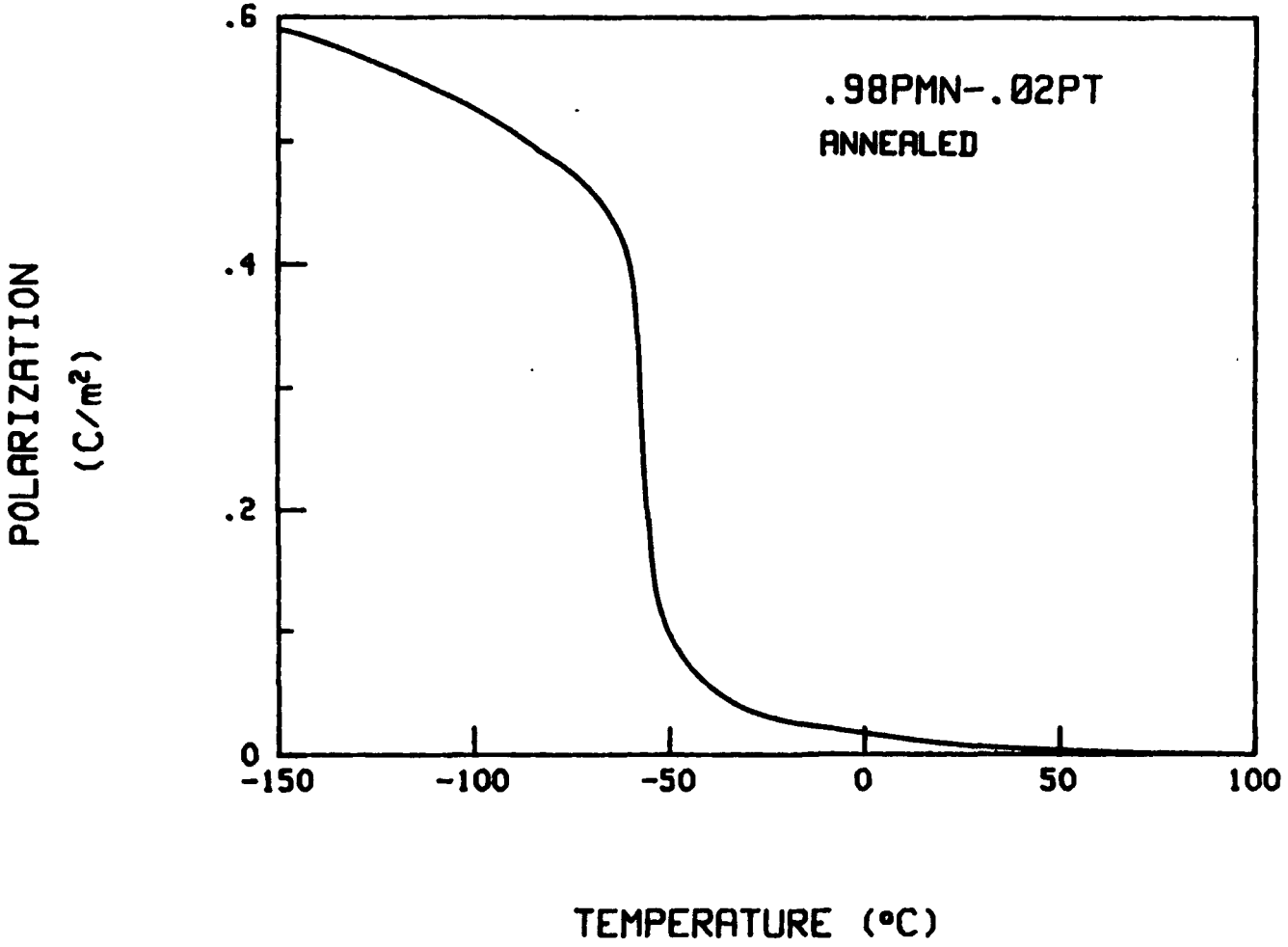
.98PMN-.02PT
ANNEALED
.6
.4
.2
0
-150
-100
-50
0
50
100
POLARIZATION
(C/m²)
TEMPERATURE (°C)

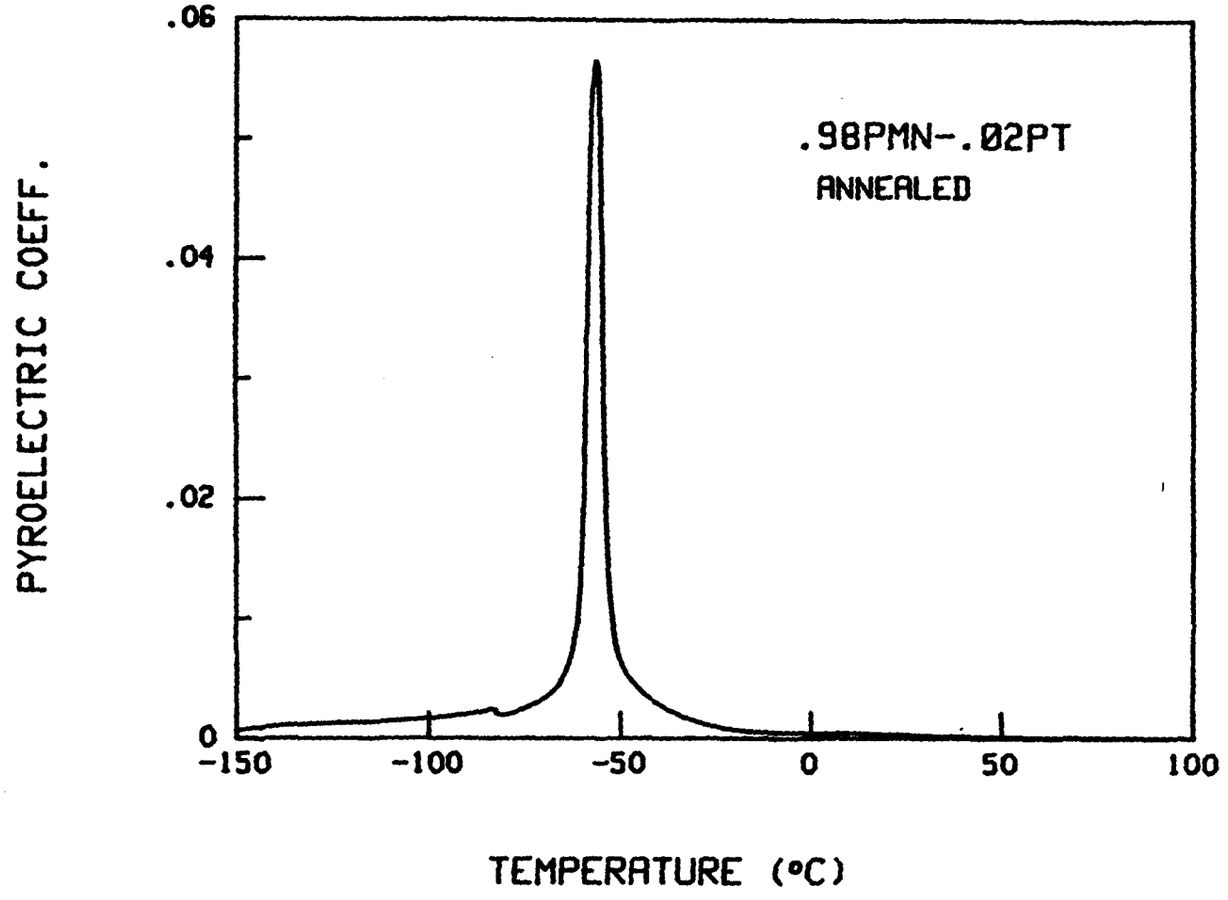
.06
.04
.02
0
PYROELECTRIC COEFF.
.98PMN-.02PT
ANNEALED
-150
-100
-50
0
50
100
TEMPERATURE (°C)

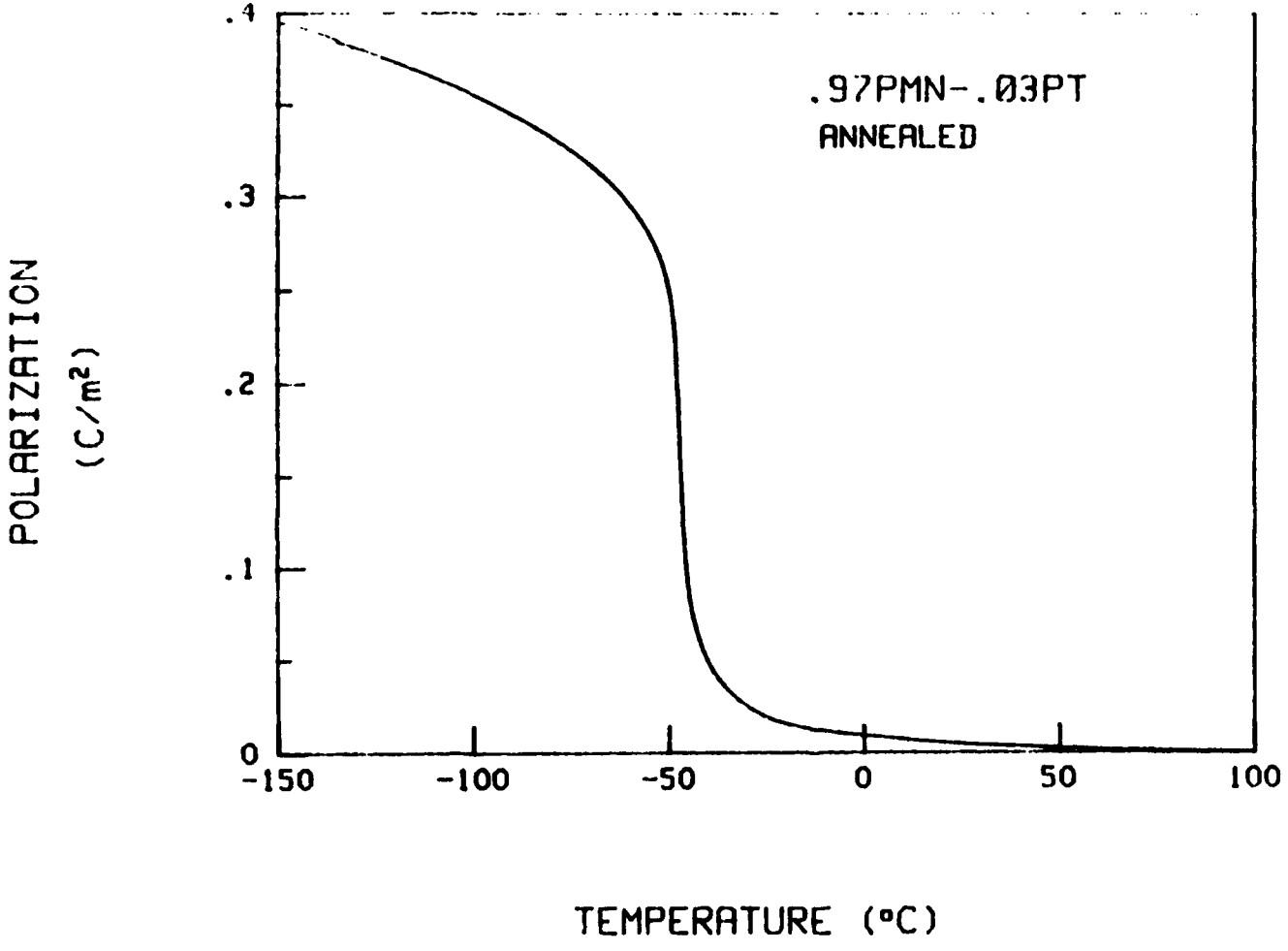
.97PMN-.03PT
ANNEALED
POLARIZATION
(C/m²)
.4
.3
.2
.1
0
-150
-100
-50
0
50
100
TEMPERATURE (°C)

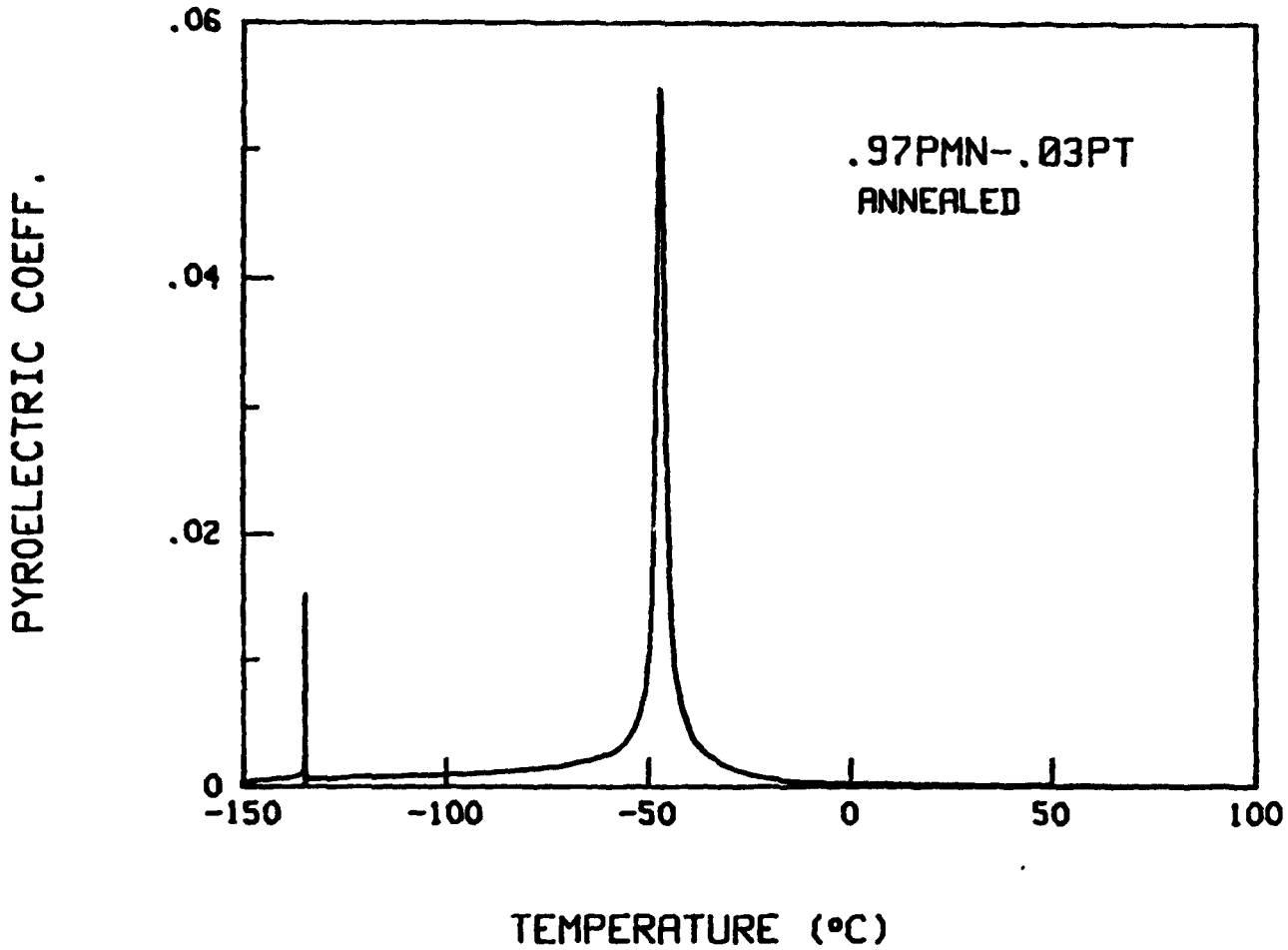
.06
.04
.02
0
PYROELECTRIC COEFF.
.97PMN-.03PT
ANNEALED
-150
-100
-50
0
50
100
TEMPERATURE (°C)

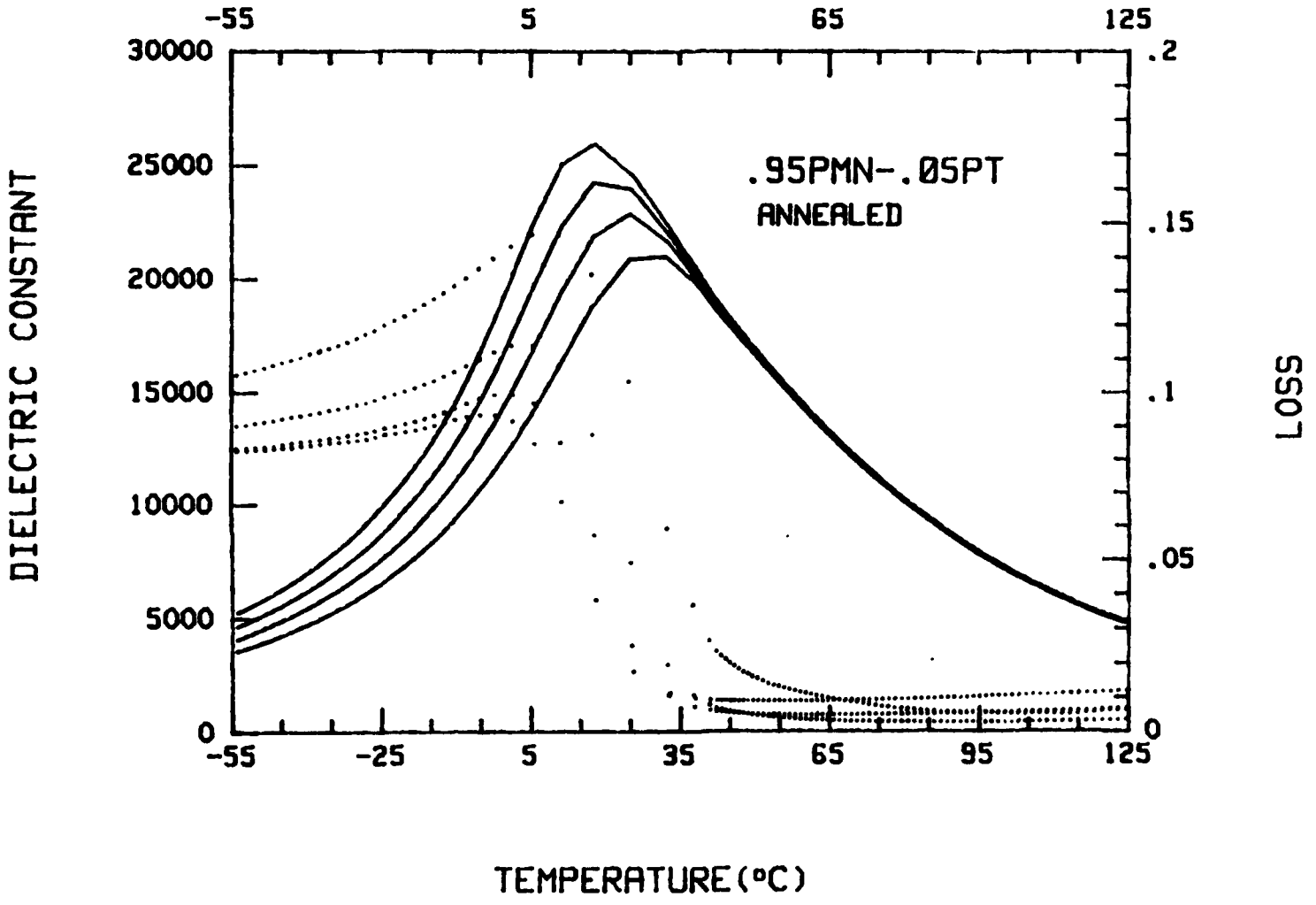
-55
5
65
125
30000
25000
20000
15000
10000
5000
0
.2
.15
.1
.05
0
.95PMN-.05PT
ANNEALED
DIELECTRIC CONSTANT
LOSS
-55
-25
5
35
65
95
125
TEMPERATURE(°C)

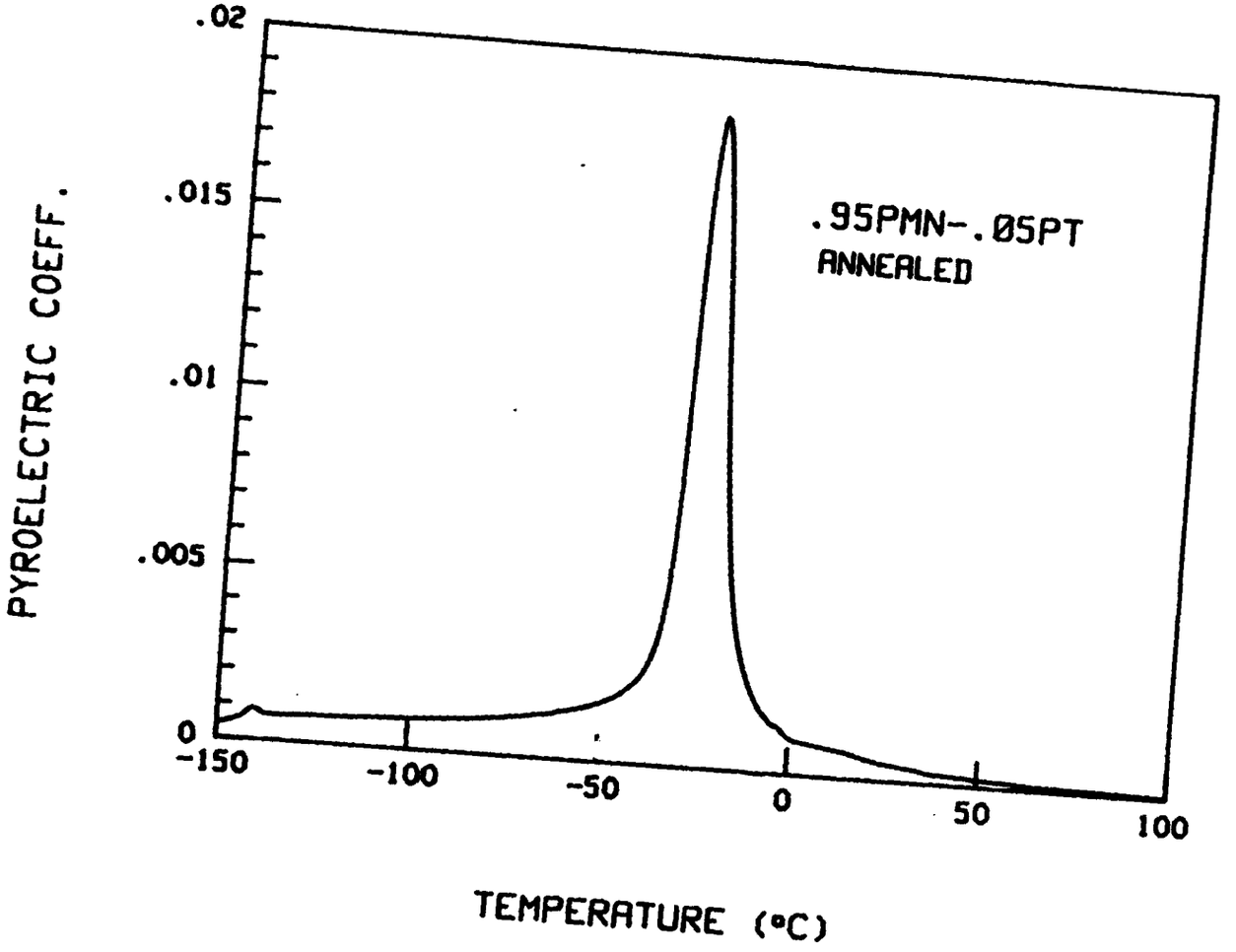
.02
.015
.01
.005
0
PYROELECTRIC COEFF.
.95PMN-.05PT
ANNEALED
-150
-100
-50
0
50
100
TEMPERATURE (°C)

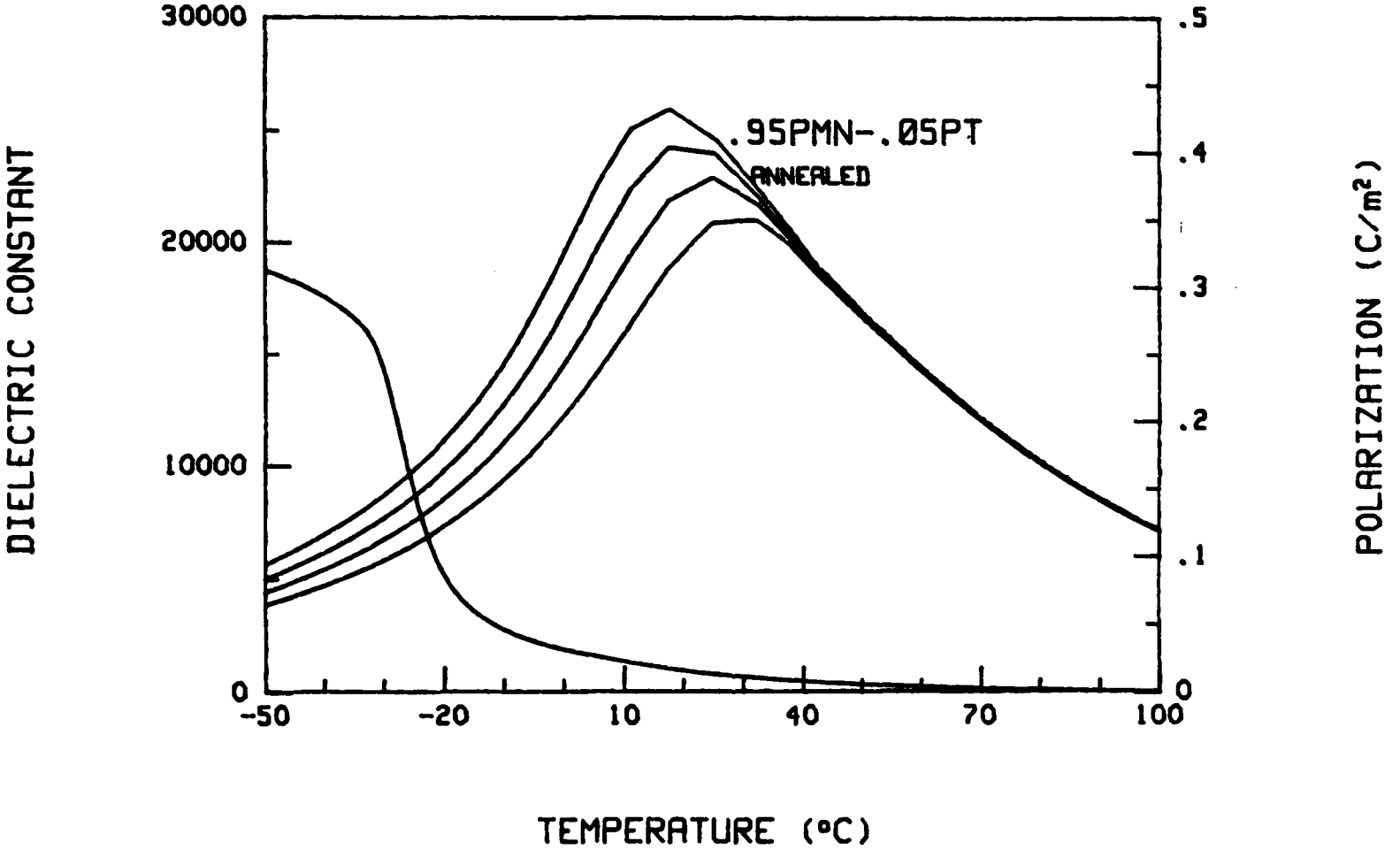
30000
20000
10000
0
.5
.4
.3
.2
.1
0
-50
-20
10
40
70
100
.95PMN-.05PT
ANNEALED
DIELECTRIC CONSTANT
POLARIZATION (C/m²)
TEMPERATURE (°C)

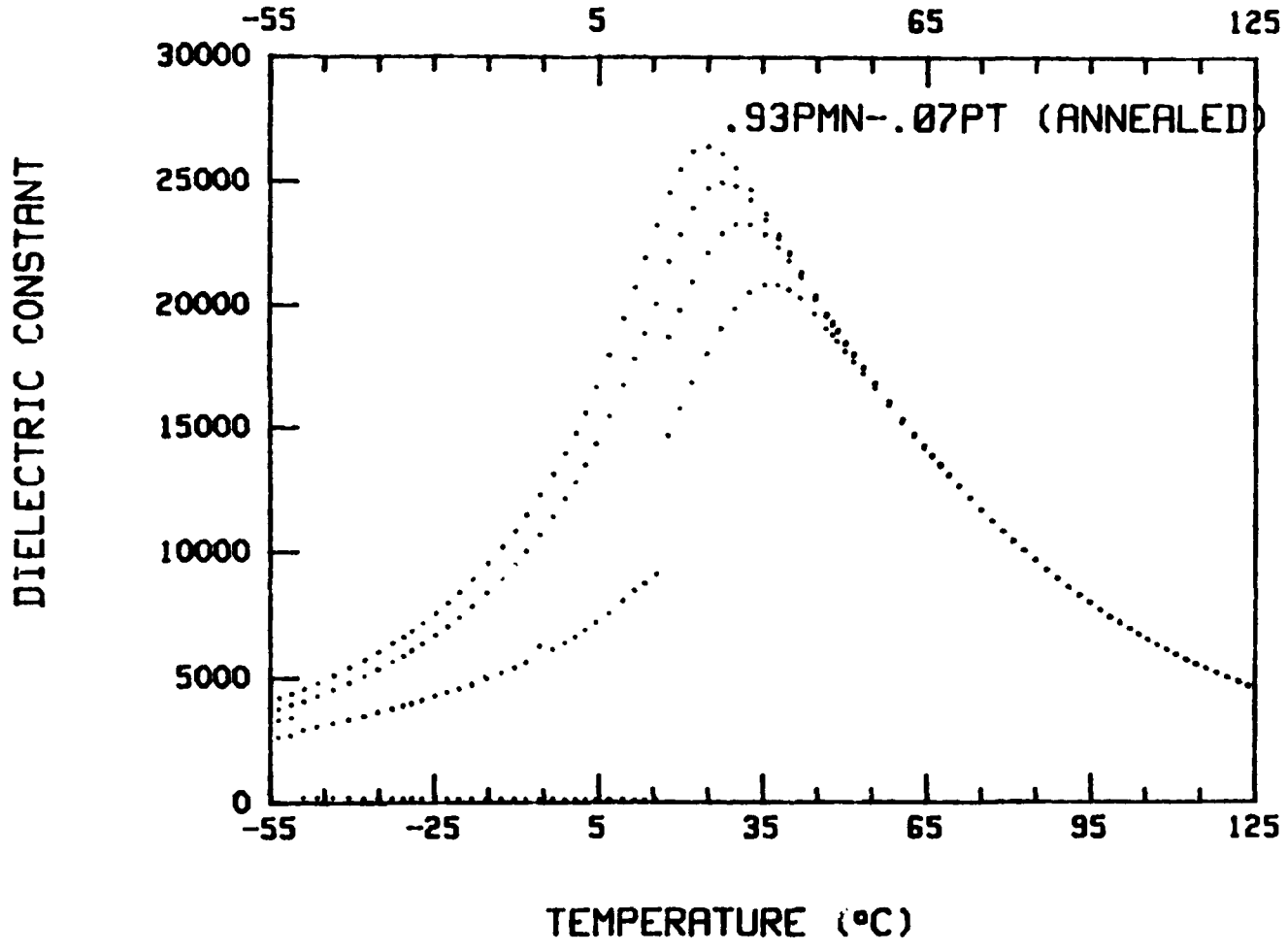
-55
5
65
125
30000
25000
20000
15000
10000
5000
0
.93PMN-.07PT (ANNEALED)
DIELECTRIC CONSTANT
-55
-25
5
35
65
95
125
TEMPERATURE (°C)

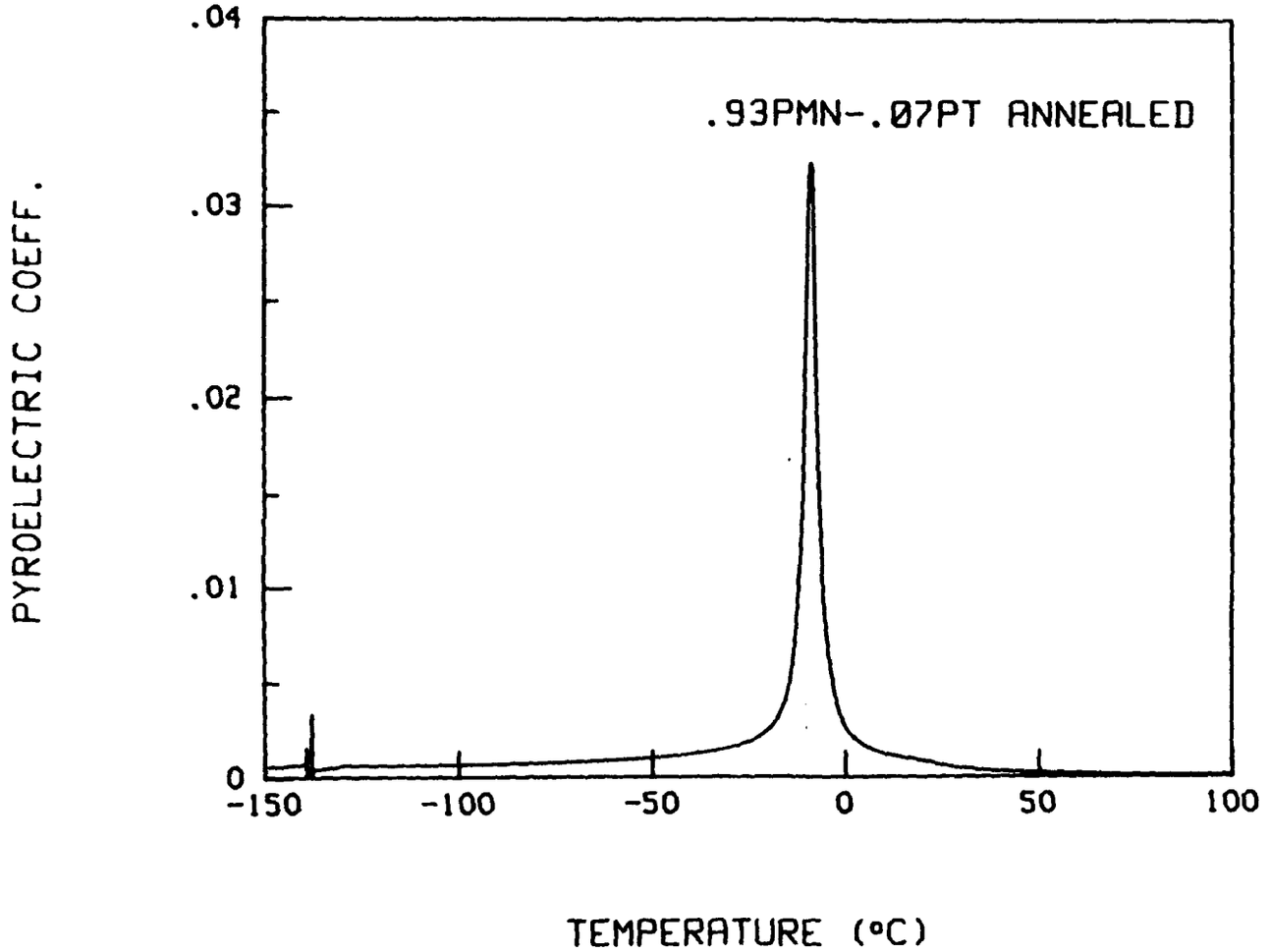
.93PMN-.07PT ANNEALED
PYROELECTRIC COEFF.
.04
.03
.02
.01
0
-150
-100
-50
0
50
100
TEMPERATURE (°C)

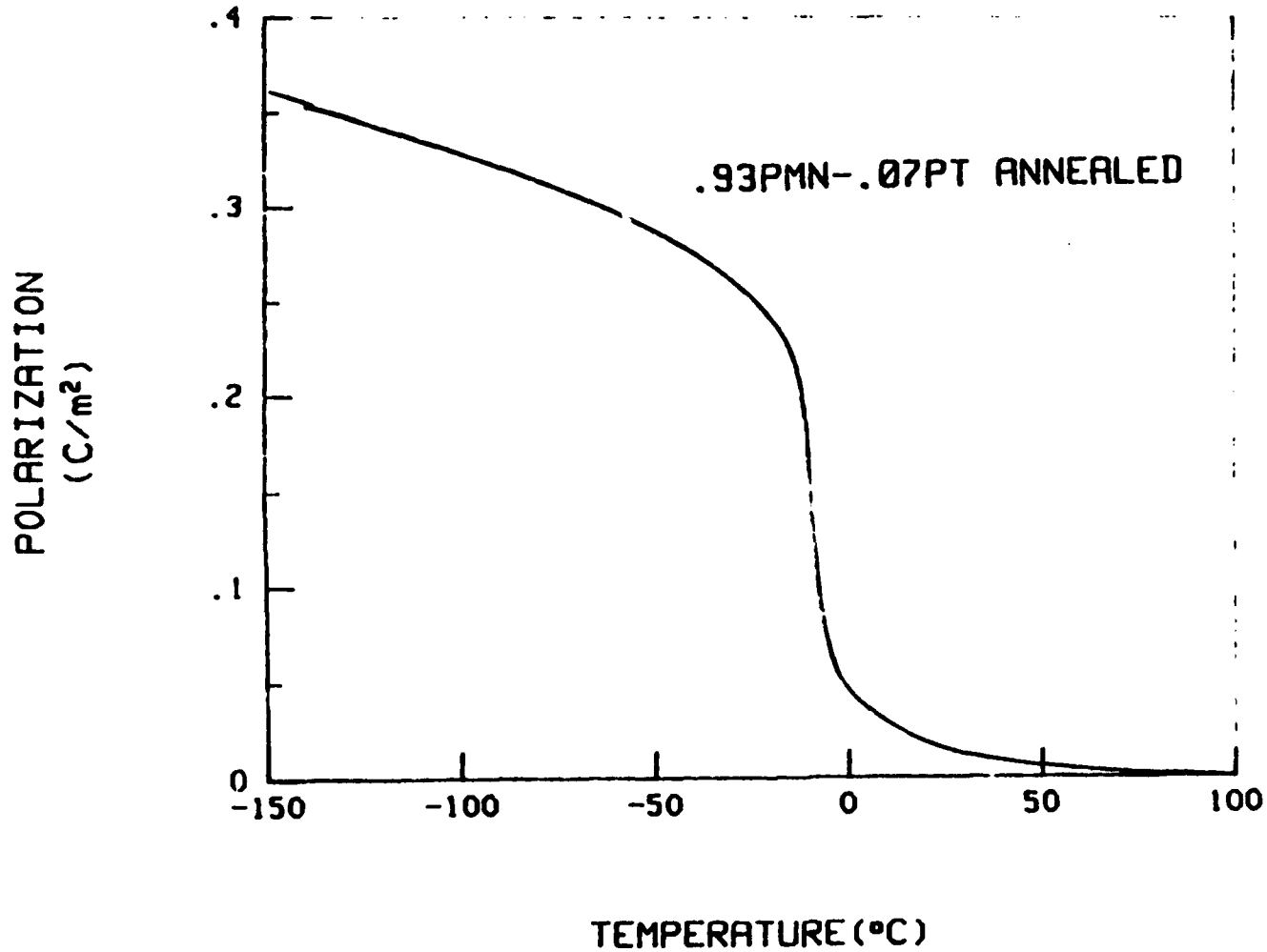
.4
.3
.2
.1
0
-150
-100
-50
0
50
100
.93PMN-.07PT ANNEALED
POLARIZATION
(C/m²)
TEMPERATURE(°C)

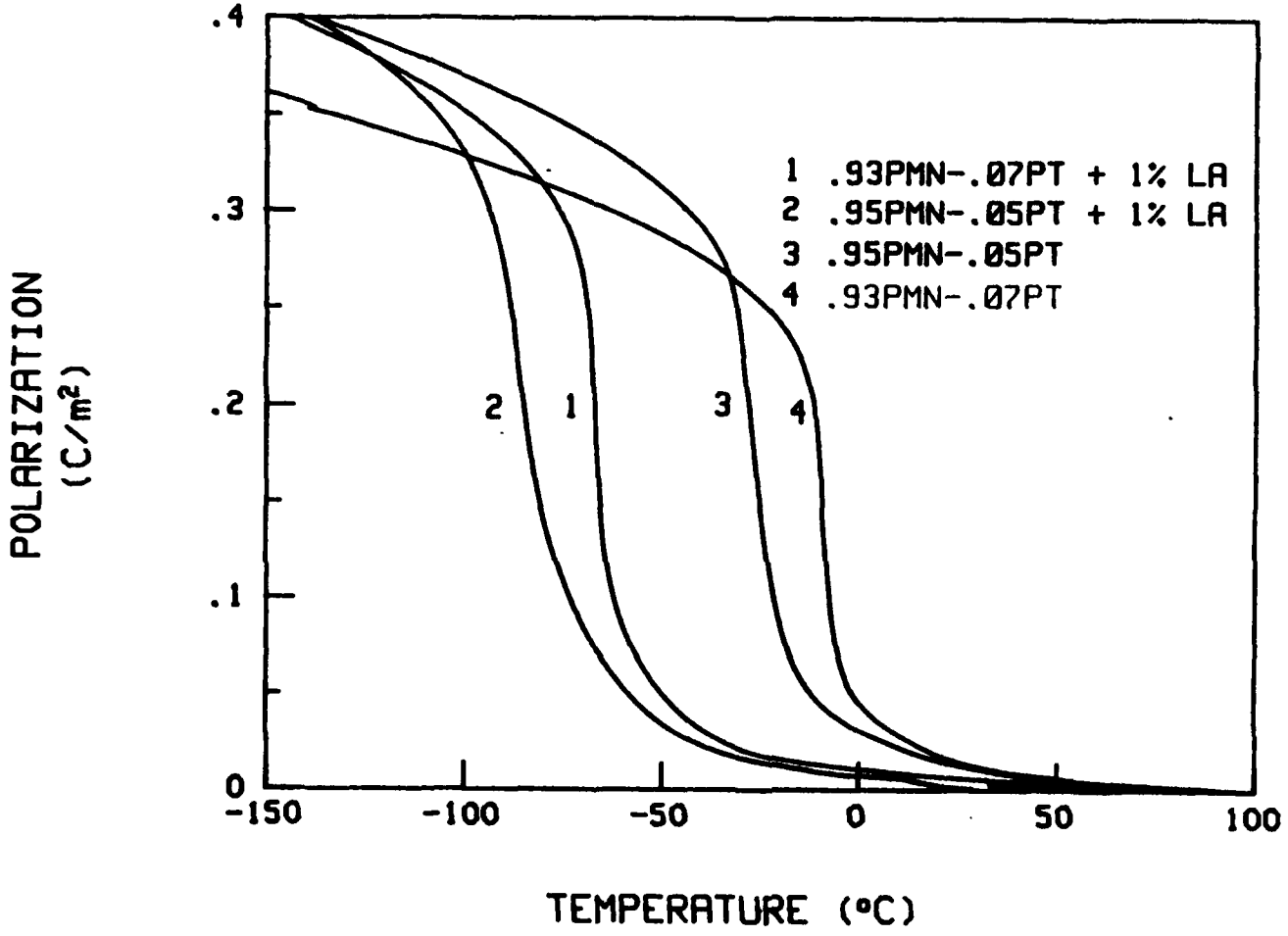
.4
.3
.2
.1
0
-150
-100
-50
0
50
100
POLARIZATION
(C/m²)
TEMPERATURE (°C)
1 .93PMN-.07PT + 1% LA
2 .95PMN-.05PT + 1% LA
3 .95PMN-.05PT
4 .93PMN-.07PT
2
1
3
4

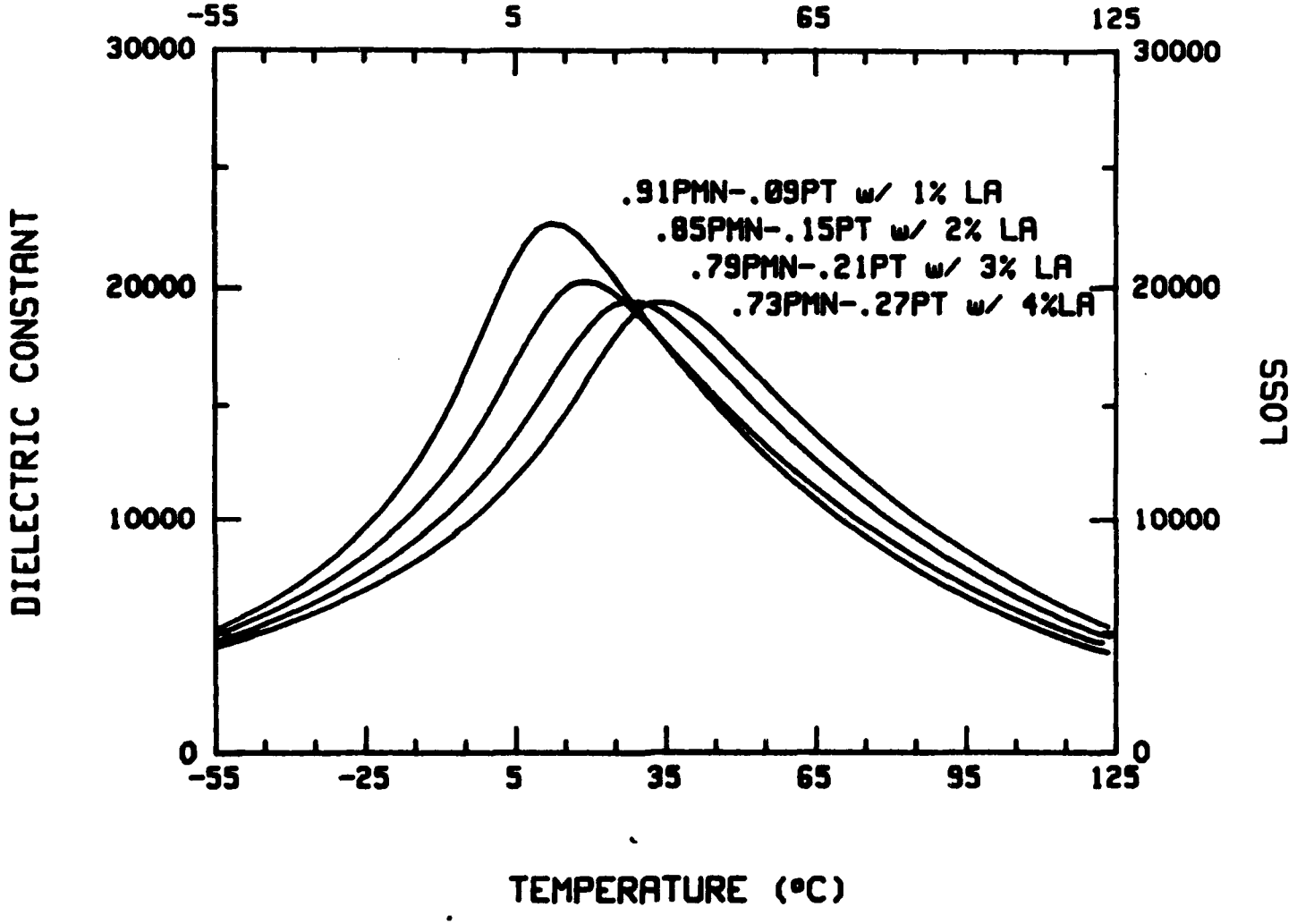
-55
5
65
125
30000
20000
10000
0
.91PMN-.09PT w/ 1% LA
.85PMN-.15PT w/ 2% LA
.79PMN-.21PT w/ 3% LA
.73PMN-.27PT w/ 4%LA
DIELECTRIC CONSTANT
LOSS
-55
-25
5
35
65
95
125
TEMPERATURE (°C)

1KHz DATA

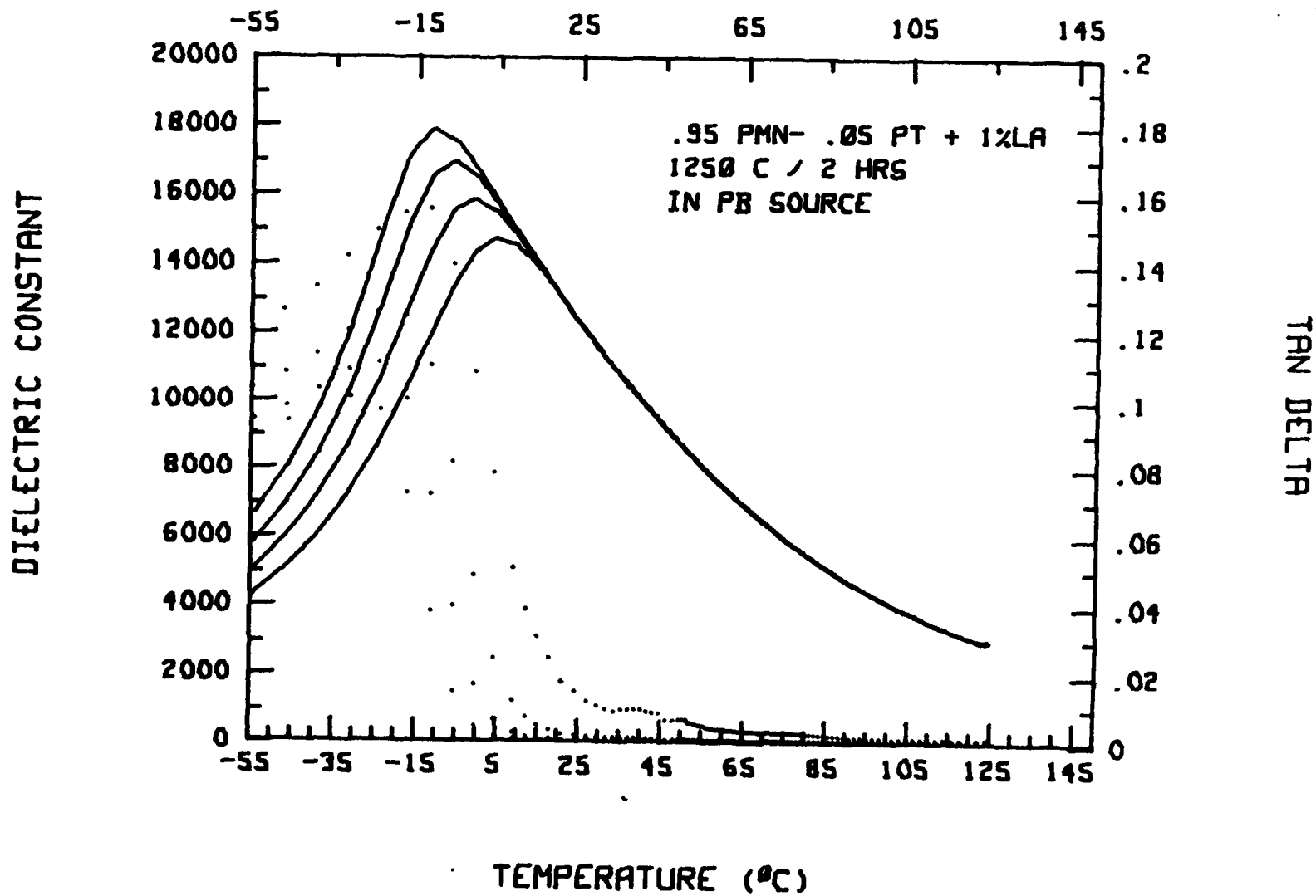
.95 PMN- .05 PT + 1%LA
1250 C / 2 HRS
IN PB SOURCE
DIELECTRIC CONSTANT
TAN DELTA
TEMPERATURE (°C)
-55
-15
25
65
105
145
20000
18000
16000
14000
12000
10000
8000
6000
4000
2000
0
.2
.18
.16
.14
.12
.1
.08
.06
.04
.02
0
-55
-35
-15
5
25
45
65
85
105
125
145

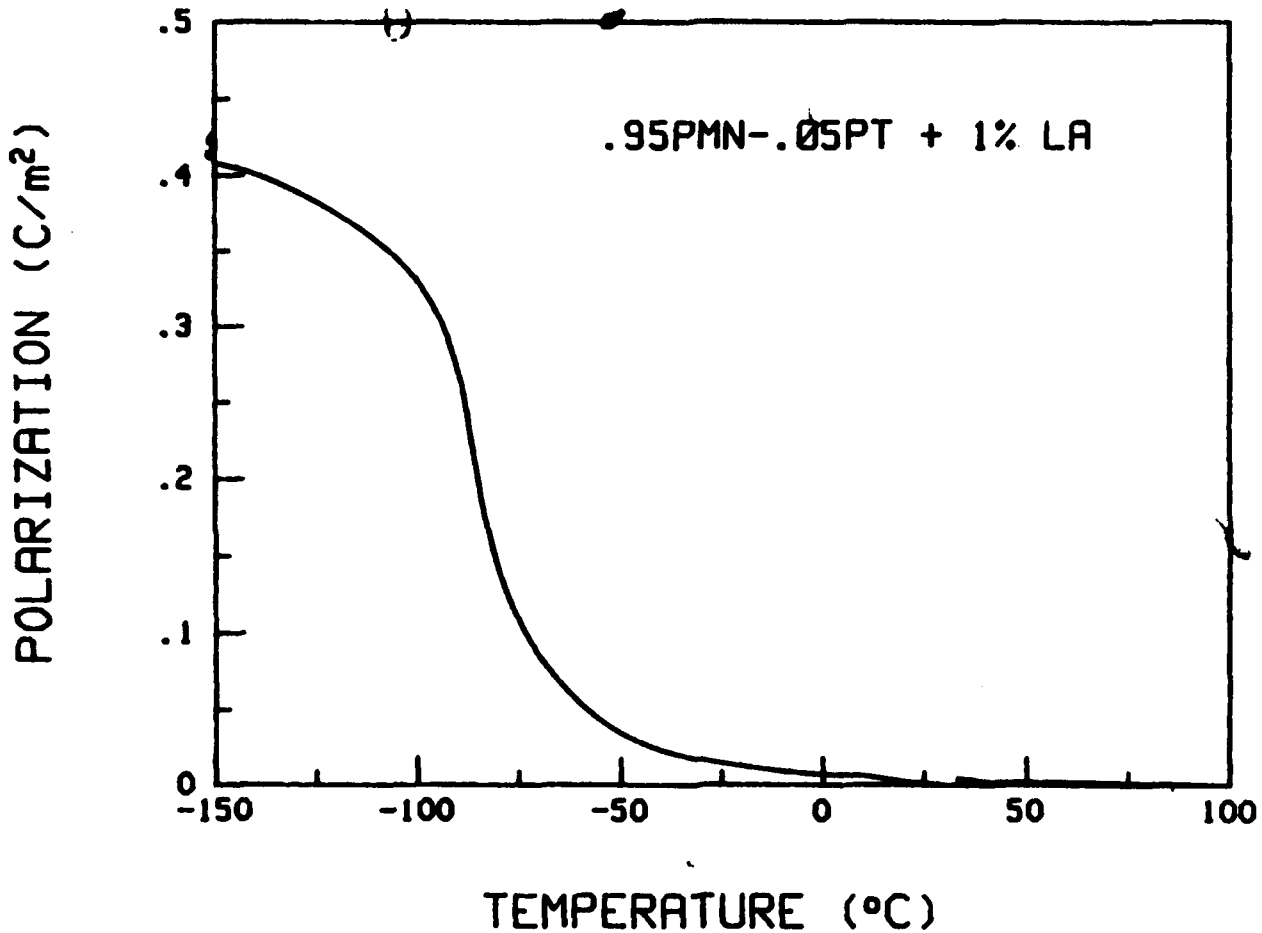
.95PMN-.05PT + 1% LA
POLARIZATION (C/m²)
.5
.4
.3
.2
.1
0
-150
-100
-50
0
50
100
TEMPERATURE (°C)

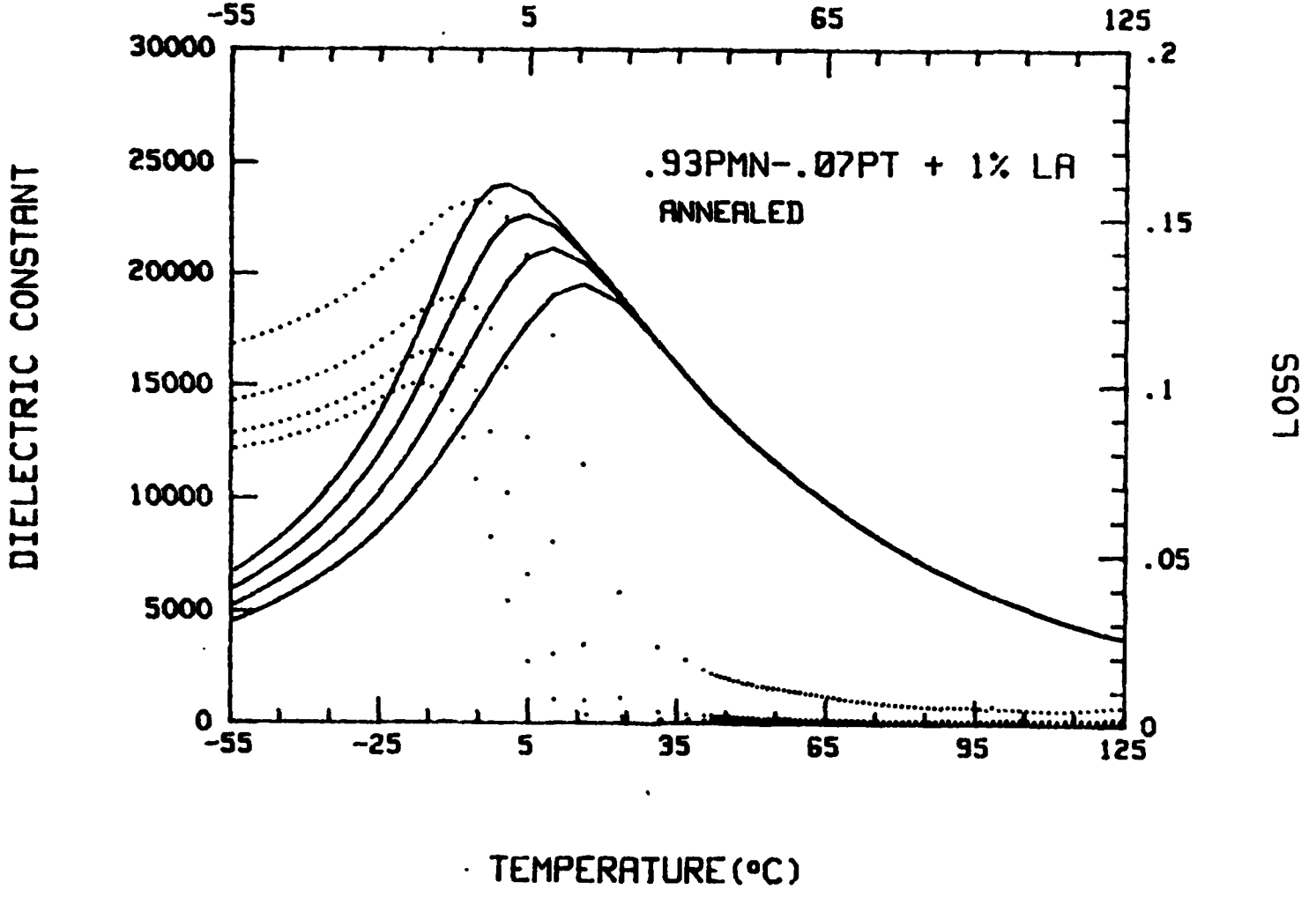
-55
5
65
125
30000
25000
20000
15000
10000
5000
0
.2
.15
.1
.05
0
.93PMN-.07PT + 1% LA
ANNEALED
DIELECTRIC CONSTANT
LOSS
-55
-25
5
35
65
95
125
TEMPERATURE(°C)

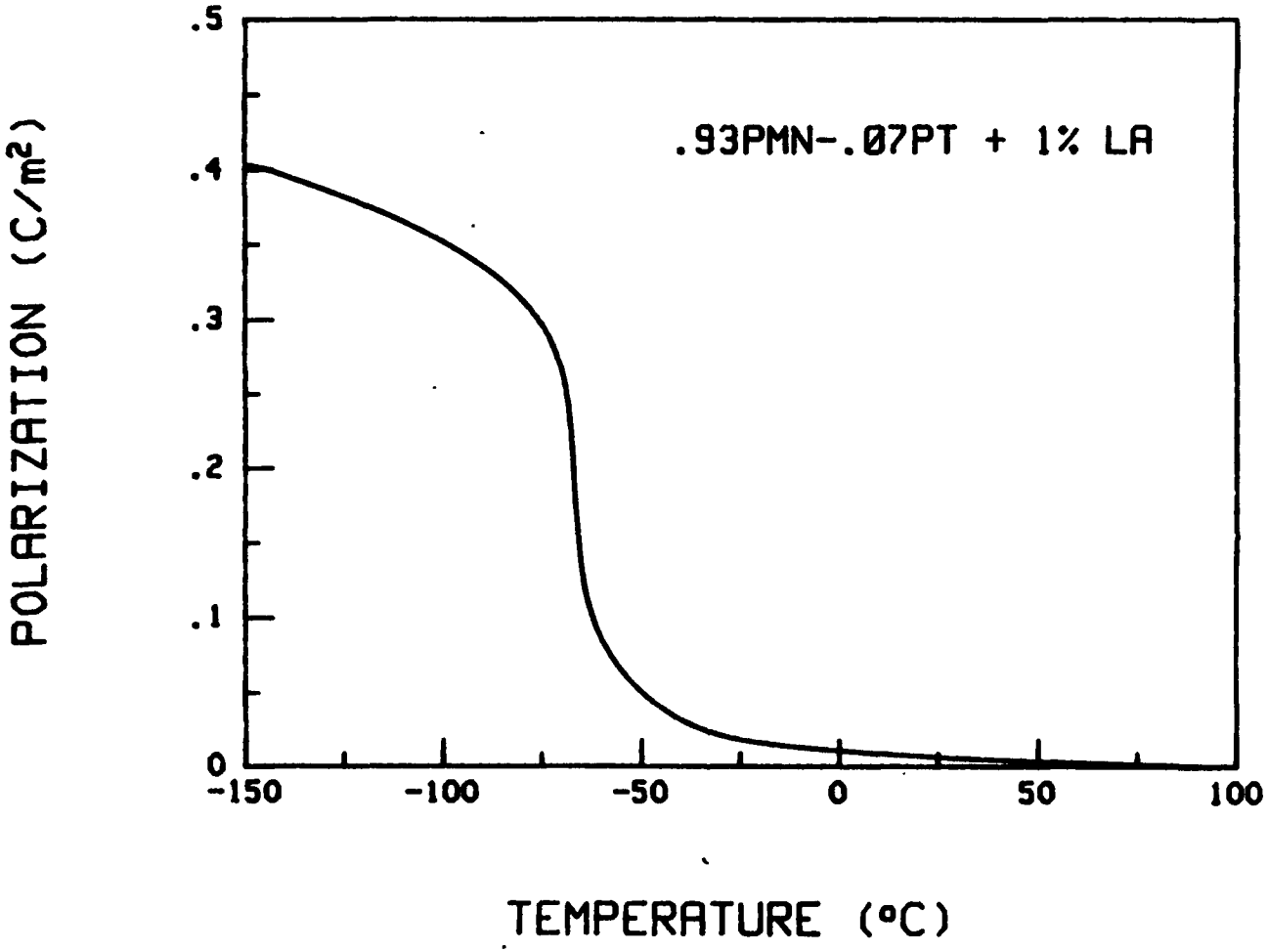
.93PMN-.07PT + 1% LA
POLARIZATION (C/m²)
.5
.4
.3
.2
.1
0
-150
-100
-50
0
50
100
TEMPERATURE (°C)

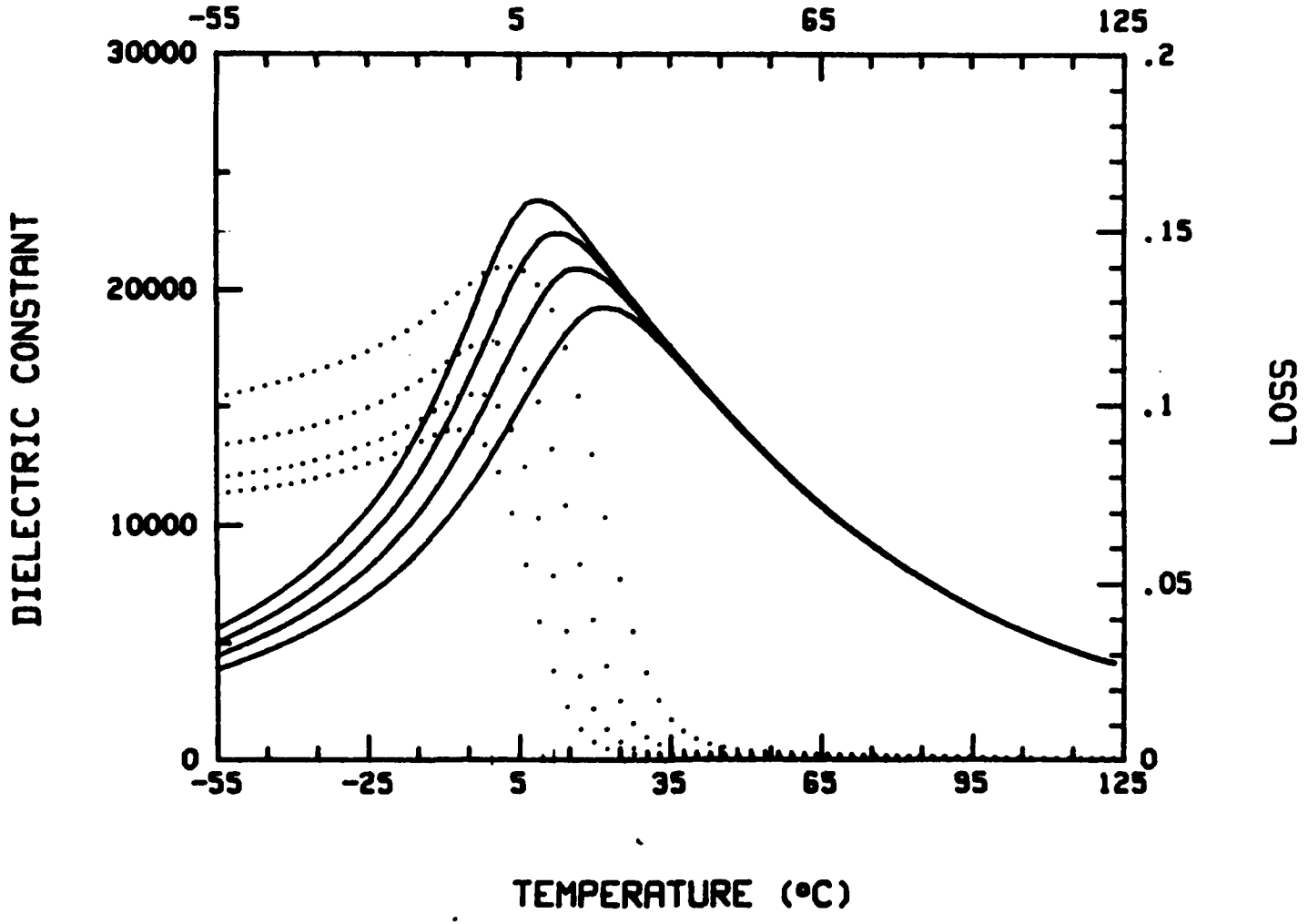
-55
5
65
125
30000
20000
10000
0
.2
.15
.1
.05
0
DIELECTRIC CONSTANT
LOSS
-55
-25
5
35
65
95
125
TEMPERATURE (°C)
.91PMN-.09PT w/ 1% LA

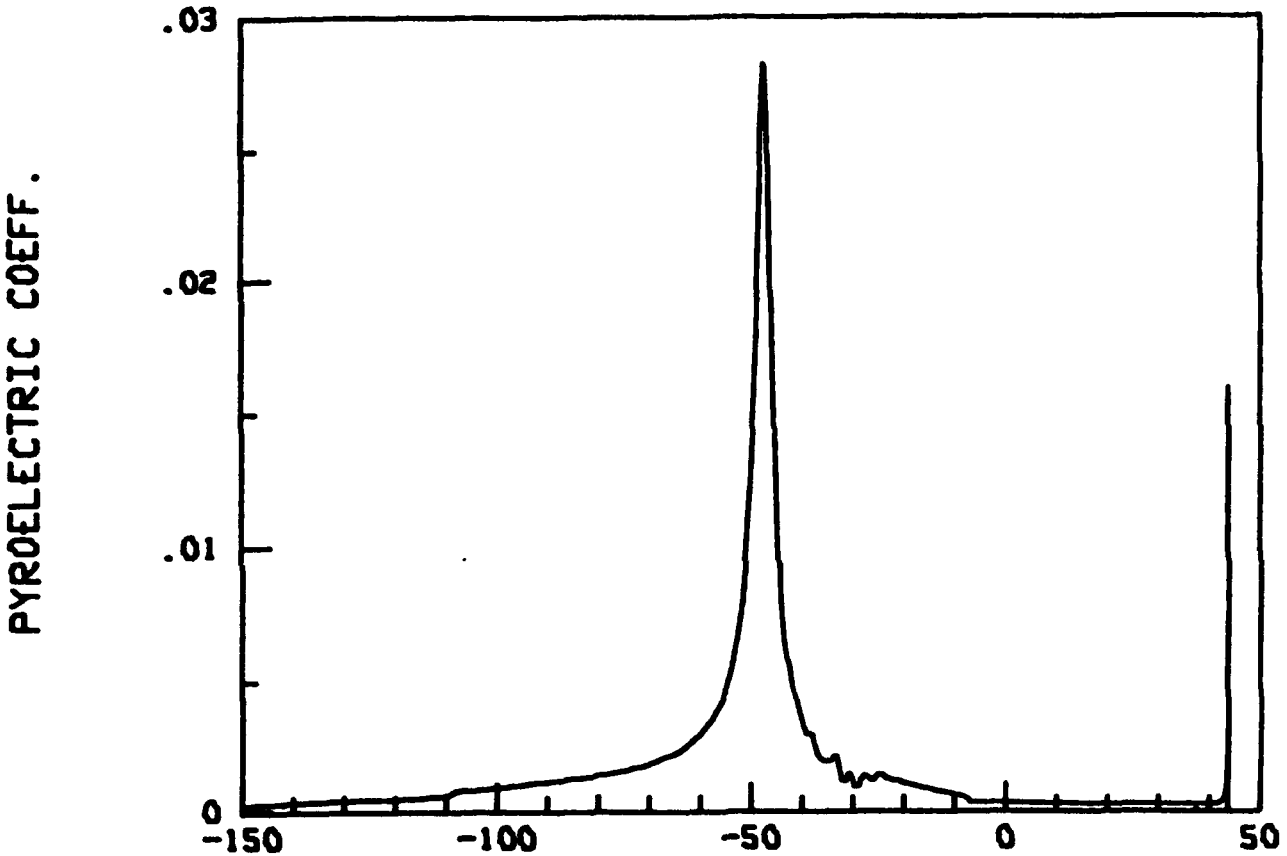

.91PMN-.09PT + 1% LA

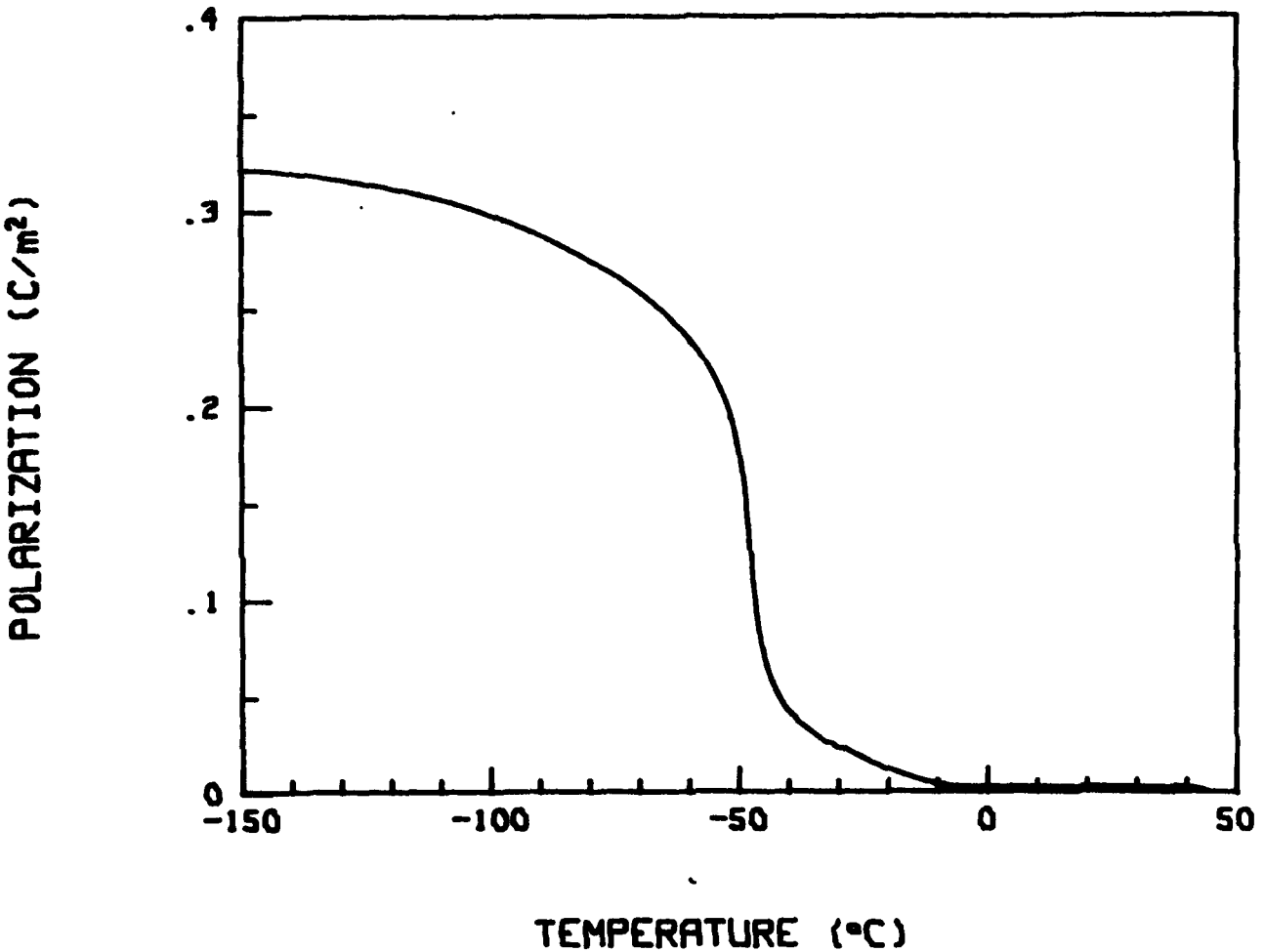

.91PMN-.09PT + 1% LA

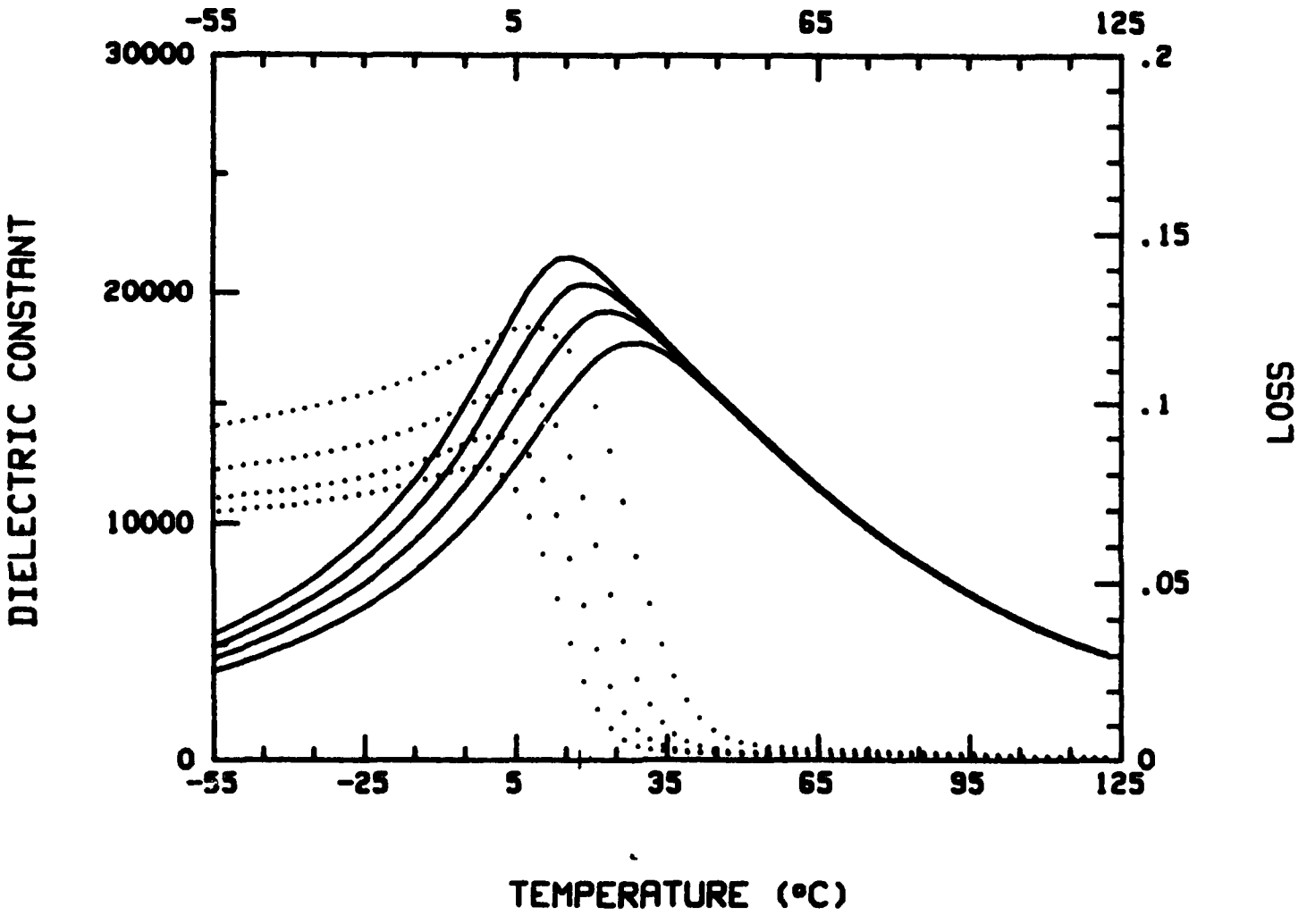

.85PMN-.15PT w/ 2% LA

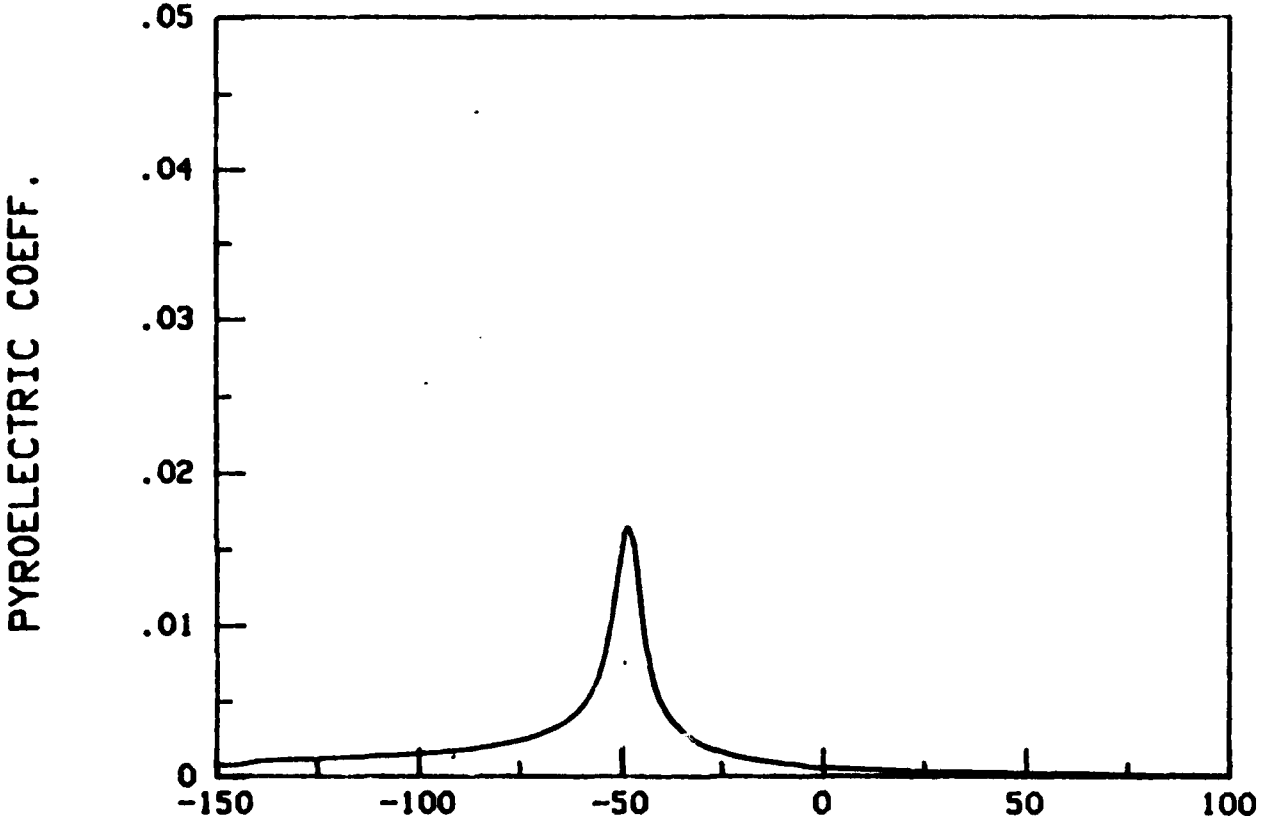

.85PMN-.15PT w/ 2% LA

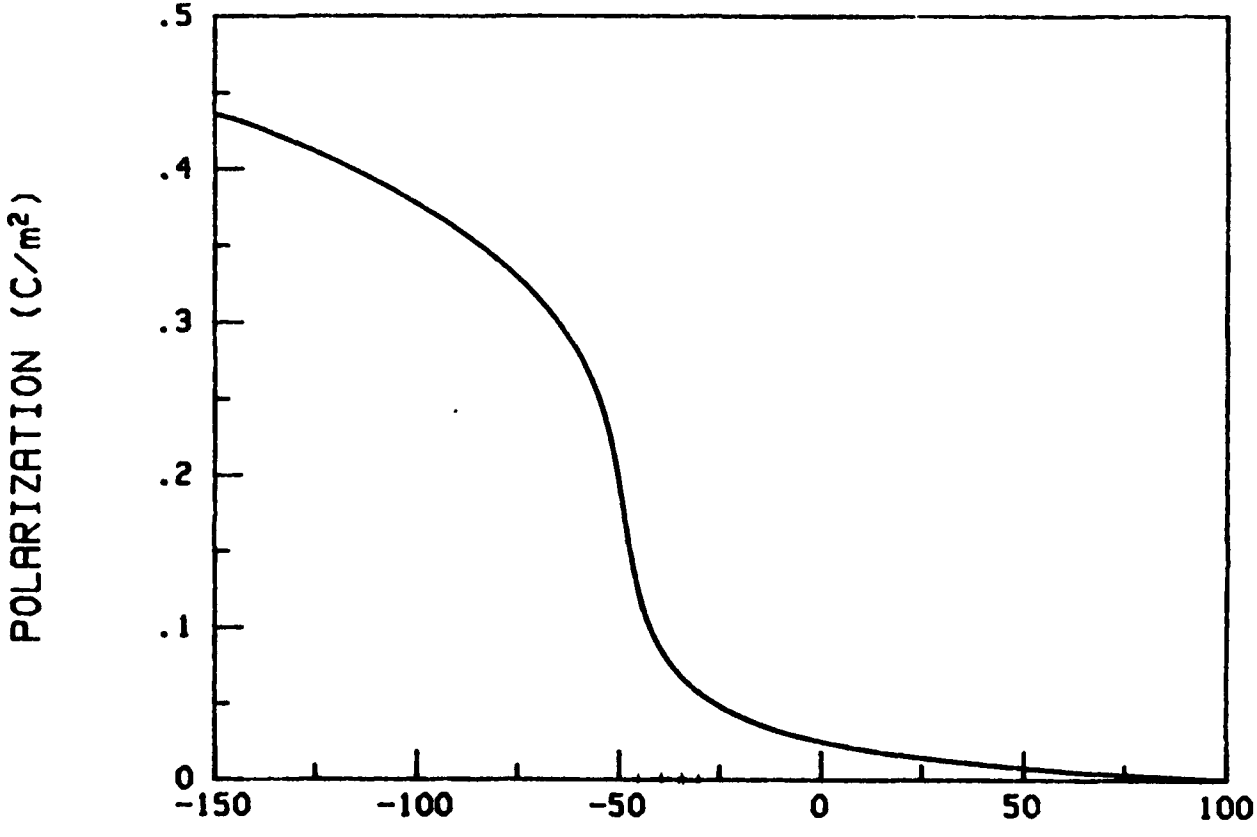

.85PMN-.15PT w/ 2% LA

6/6/92

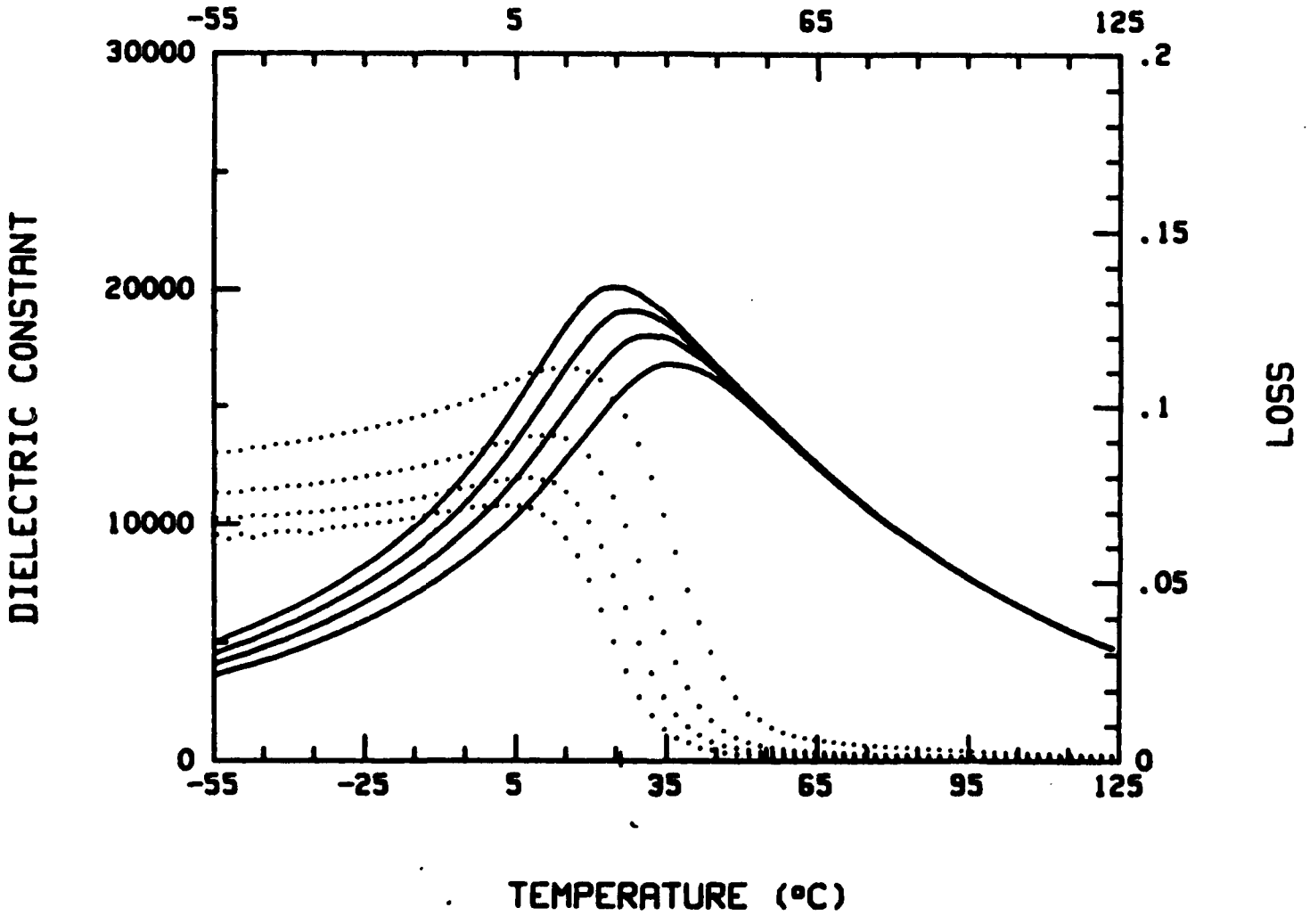

.79PMN-.21PT w/ 3% LA

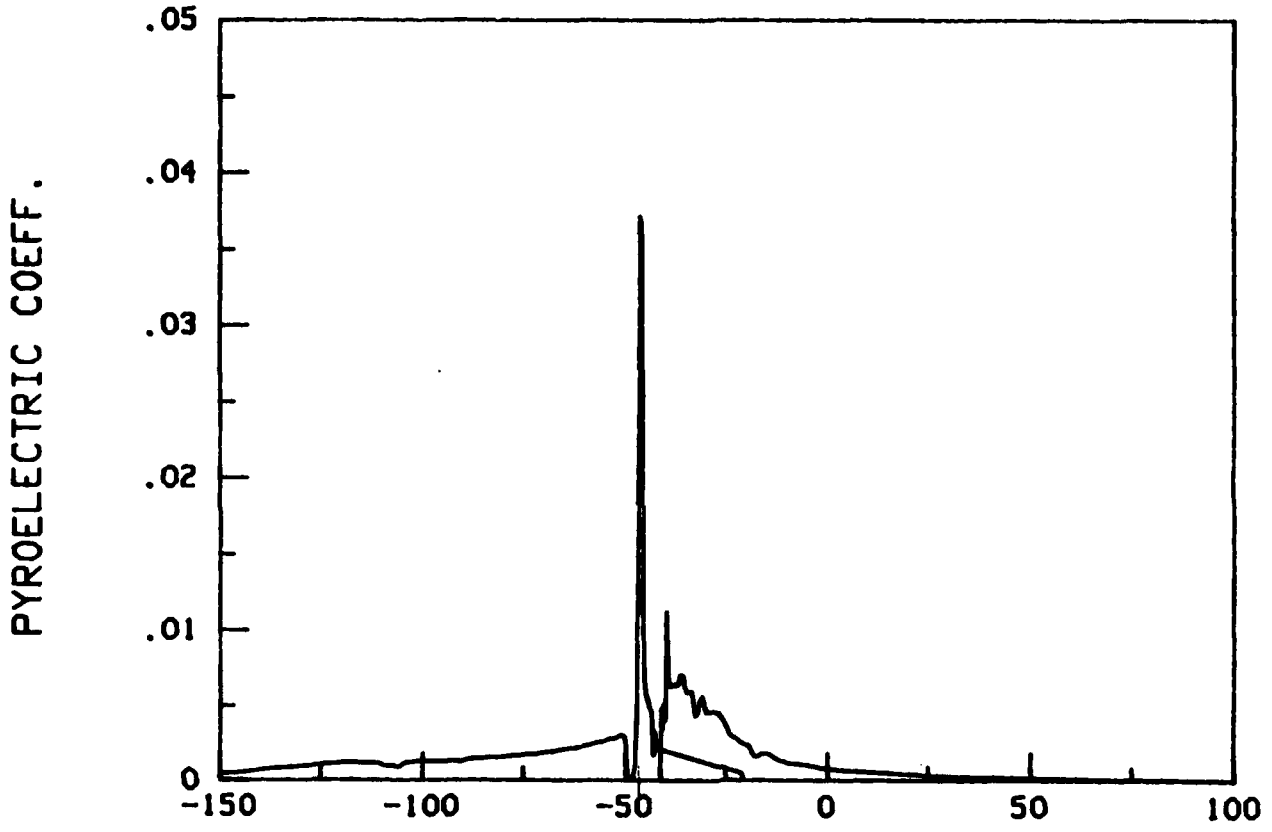

.79PMN-.21PT w/ 3% LA

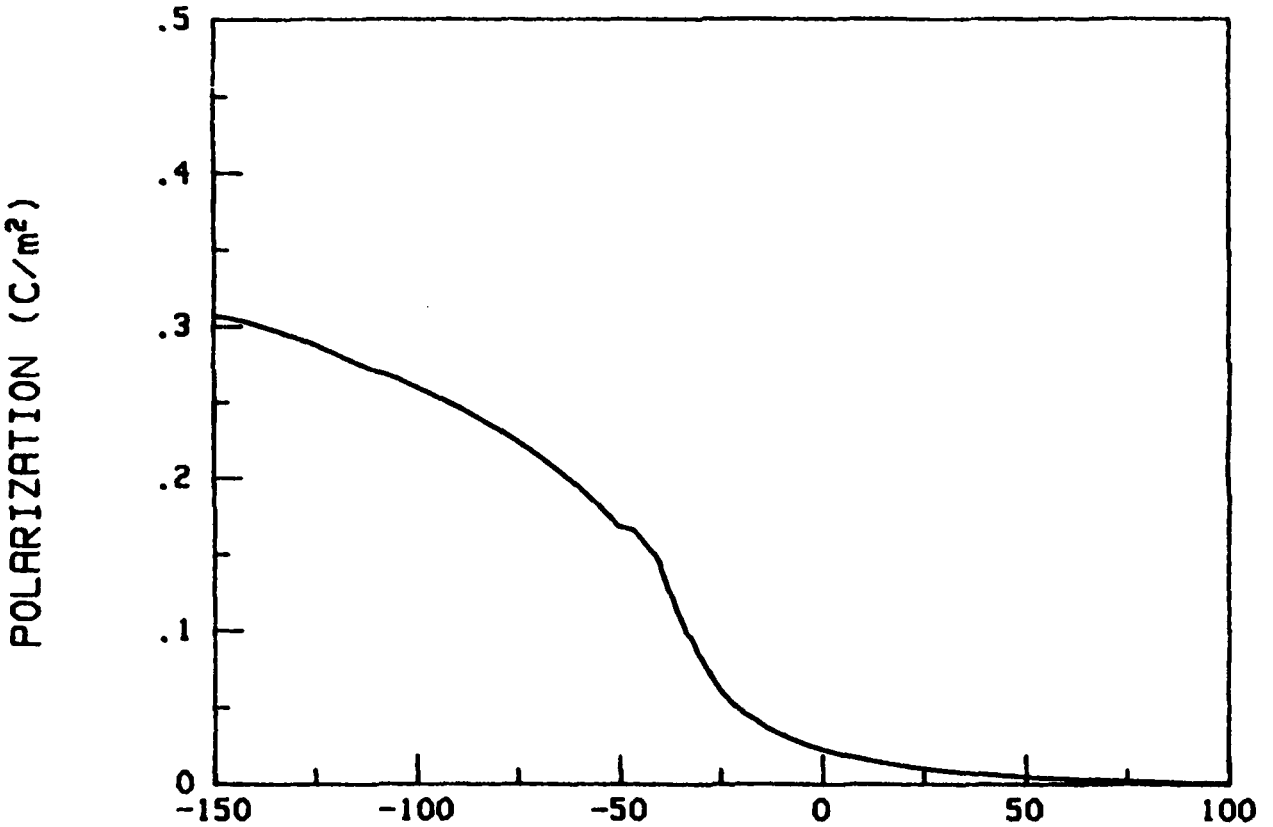

.79PMN-.21PT w/ 3% LA

6/8/92

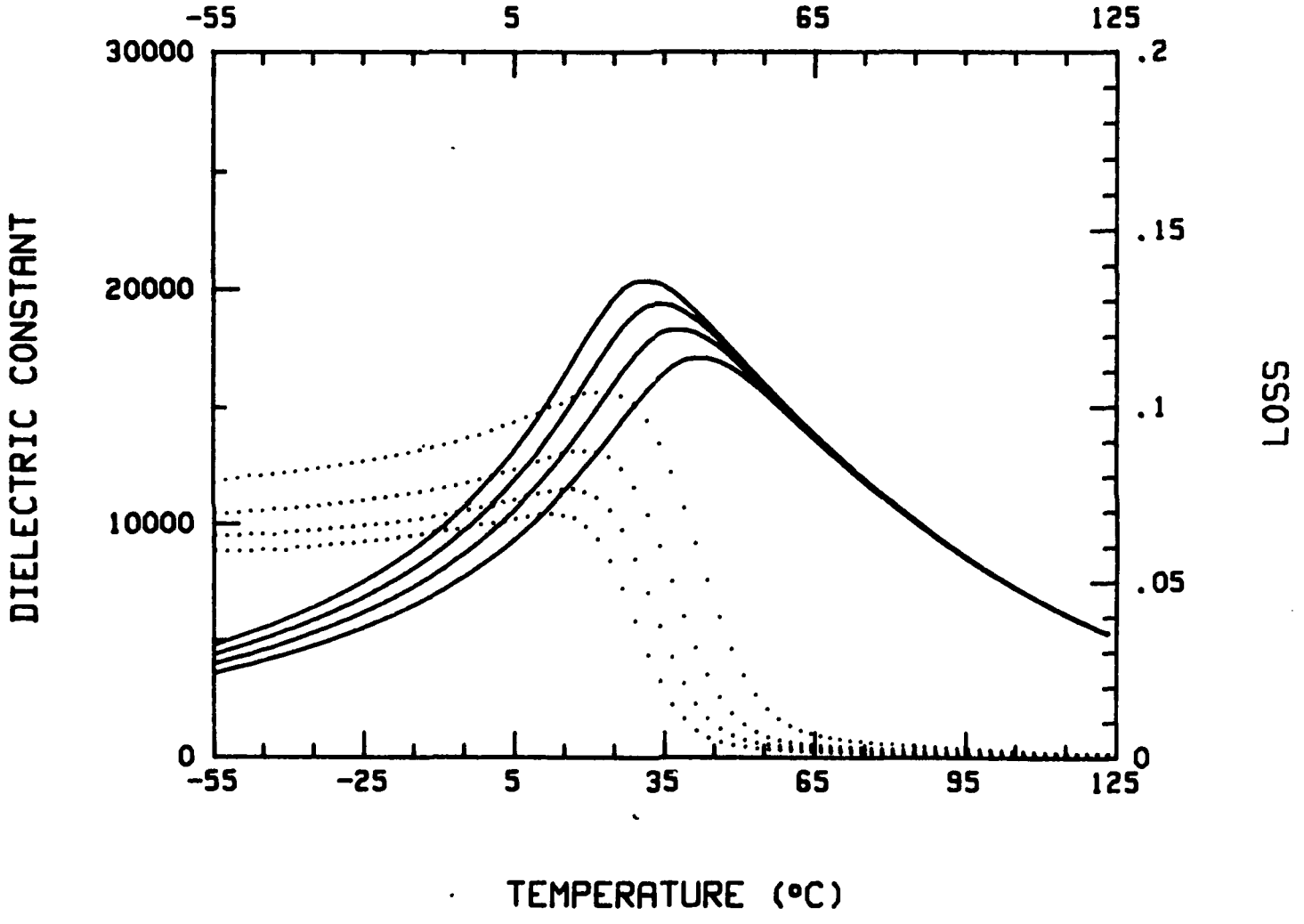

.73PMN-.27PT w/ 4% LA

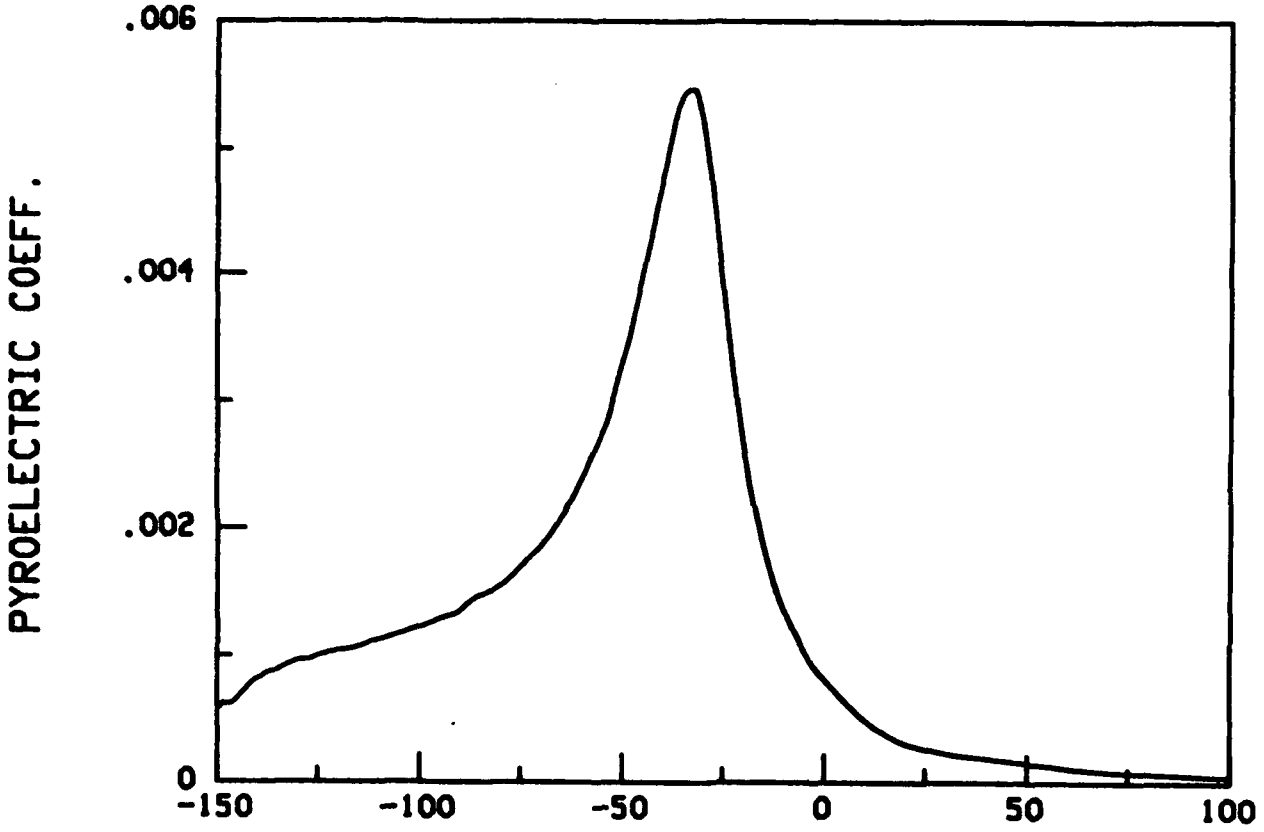

.73PMN-.27PT w/ 4% LA

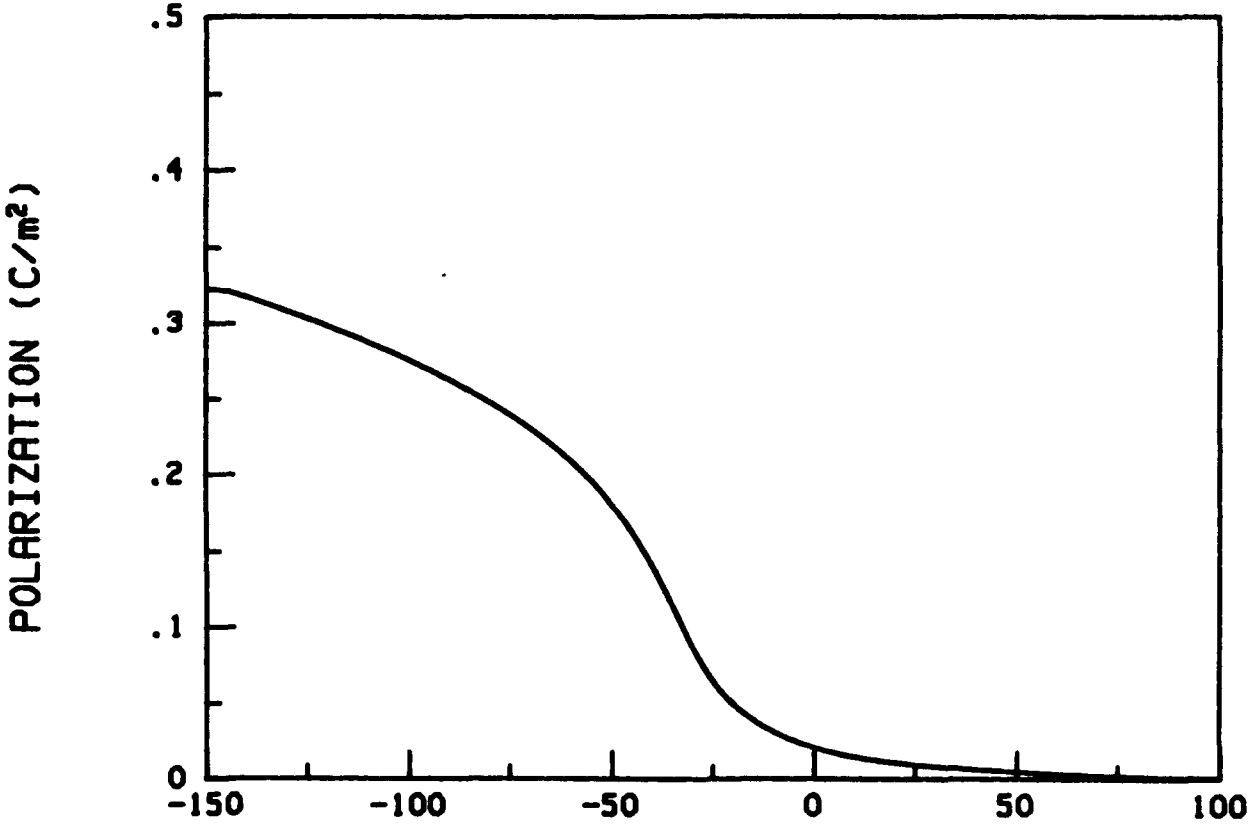

.73PMN-.27PT w/ 4% LA

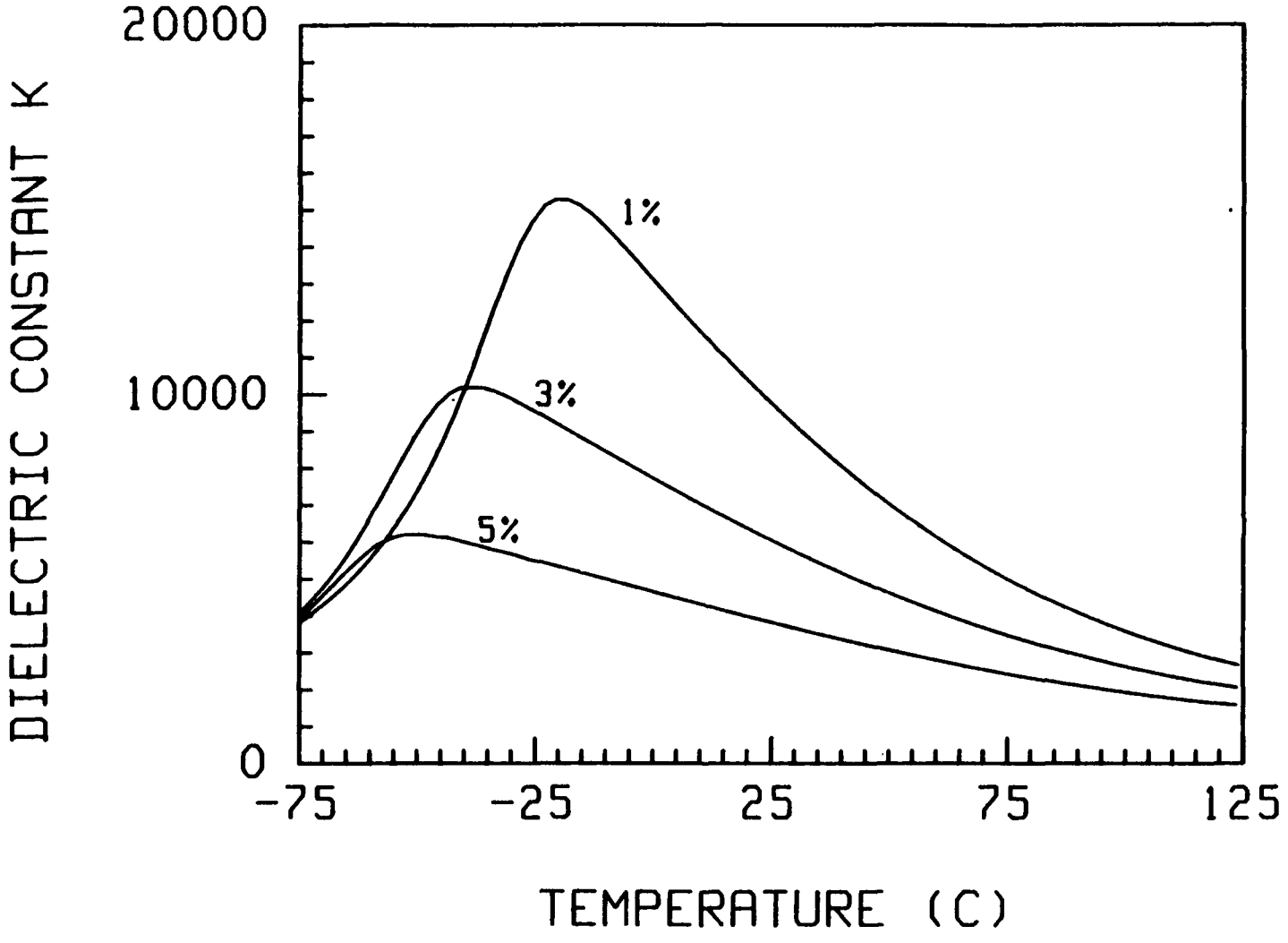

DIELECTRIC LOSS

PMN WITH 1,3 AND 5 MOL% CA SUBSTITUTIONS

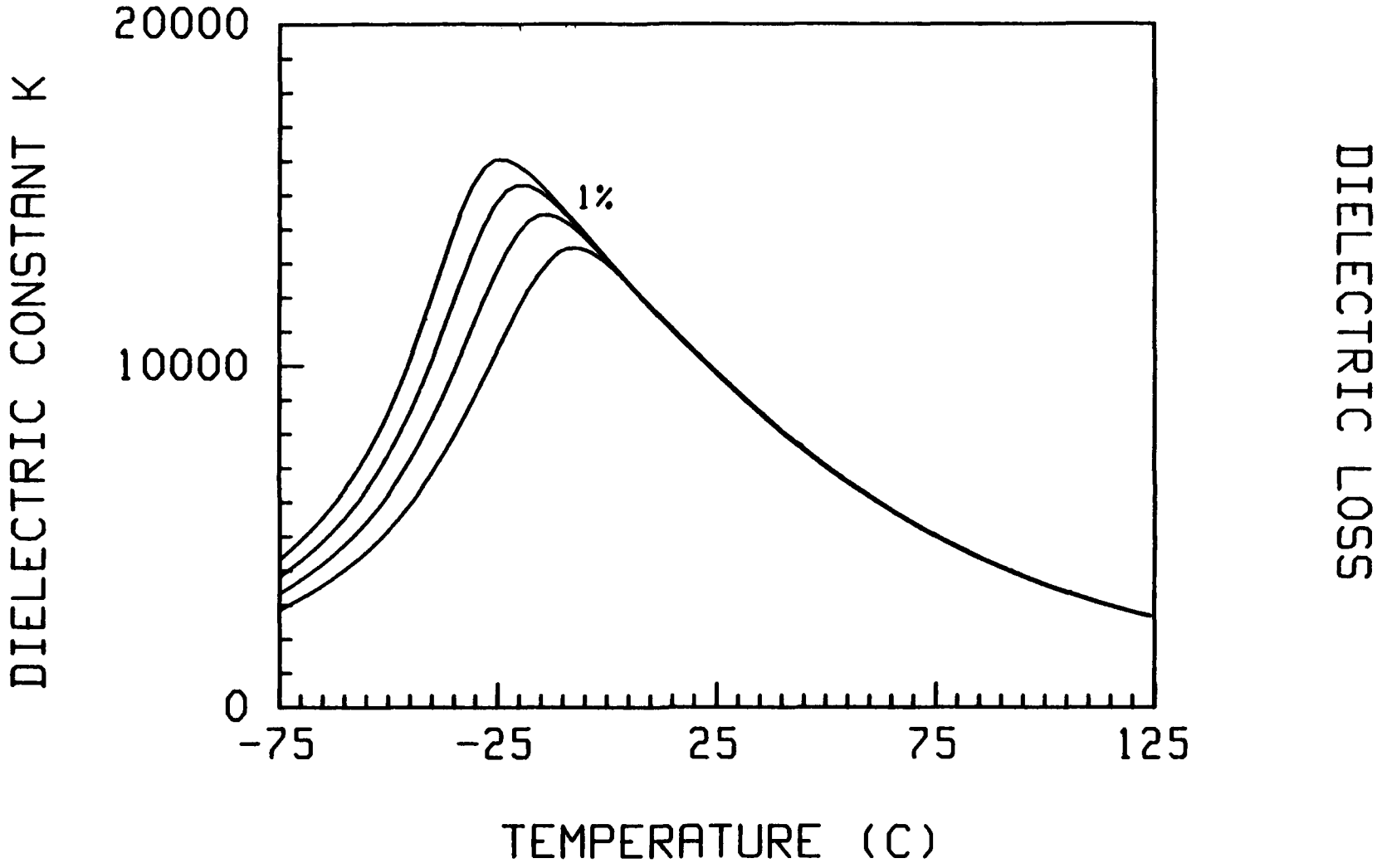

PMN WITH 1,3 AND 5 MOL% CA SUBSTITUTIONS
CVT1106_1 PMN 1% CA J91140

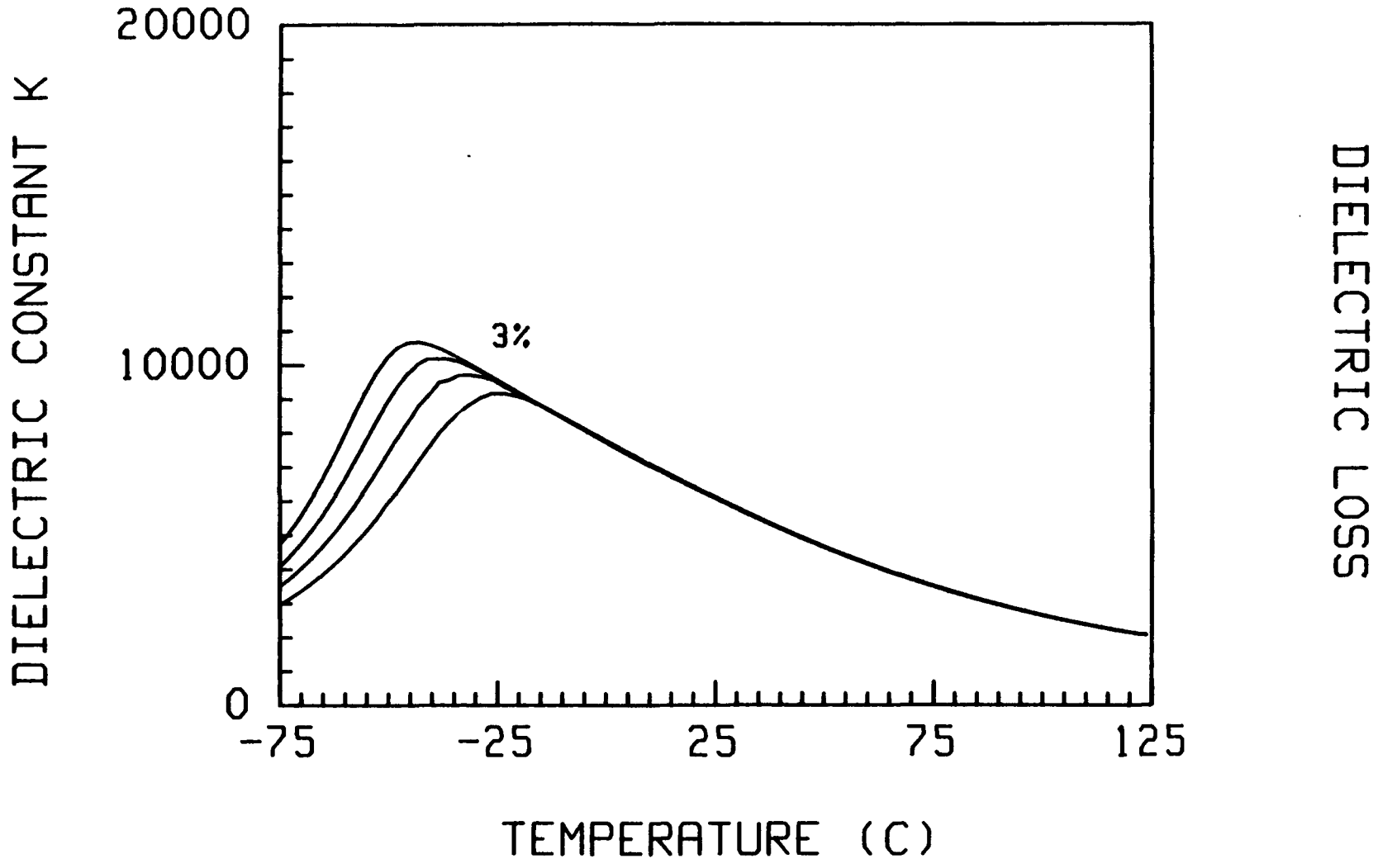

PMN WITH 1,3 AND 5 MOL% CA SUBSTITUTIONS

CVT1106_2 PMN 3% CA J91141

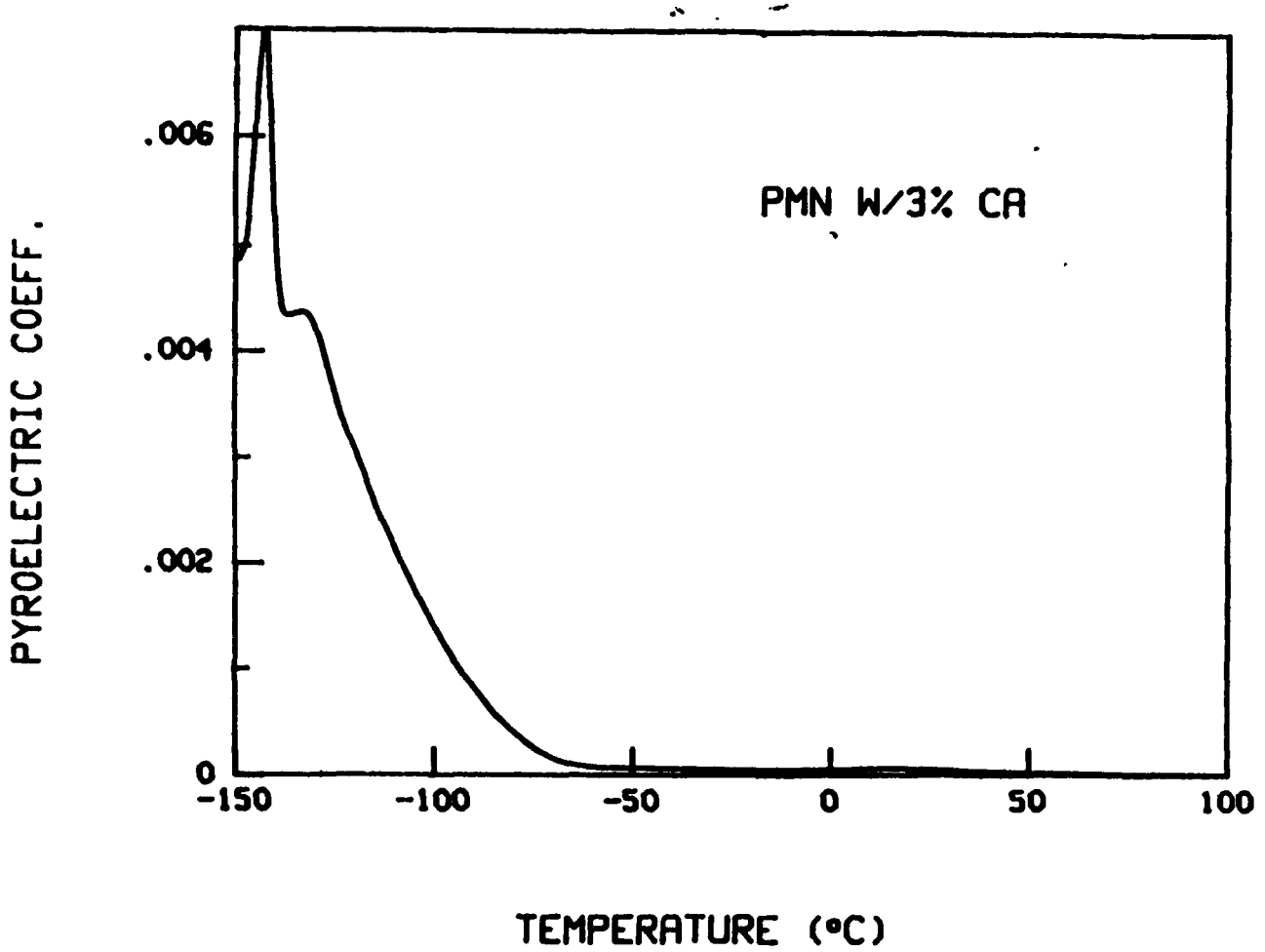
PMN W/3% CA
PYROELECTRIC COEFF.
.006
.004
.002
0
-150
-100
-50
0
50
100
TEMPERATURE (°C)

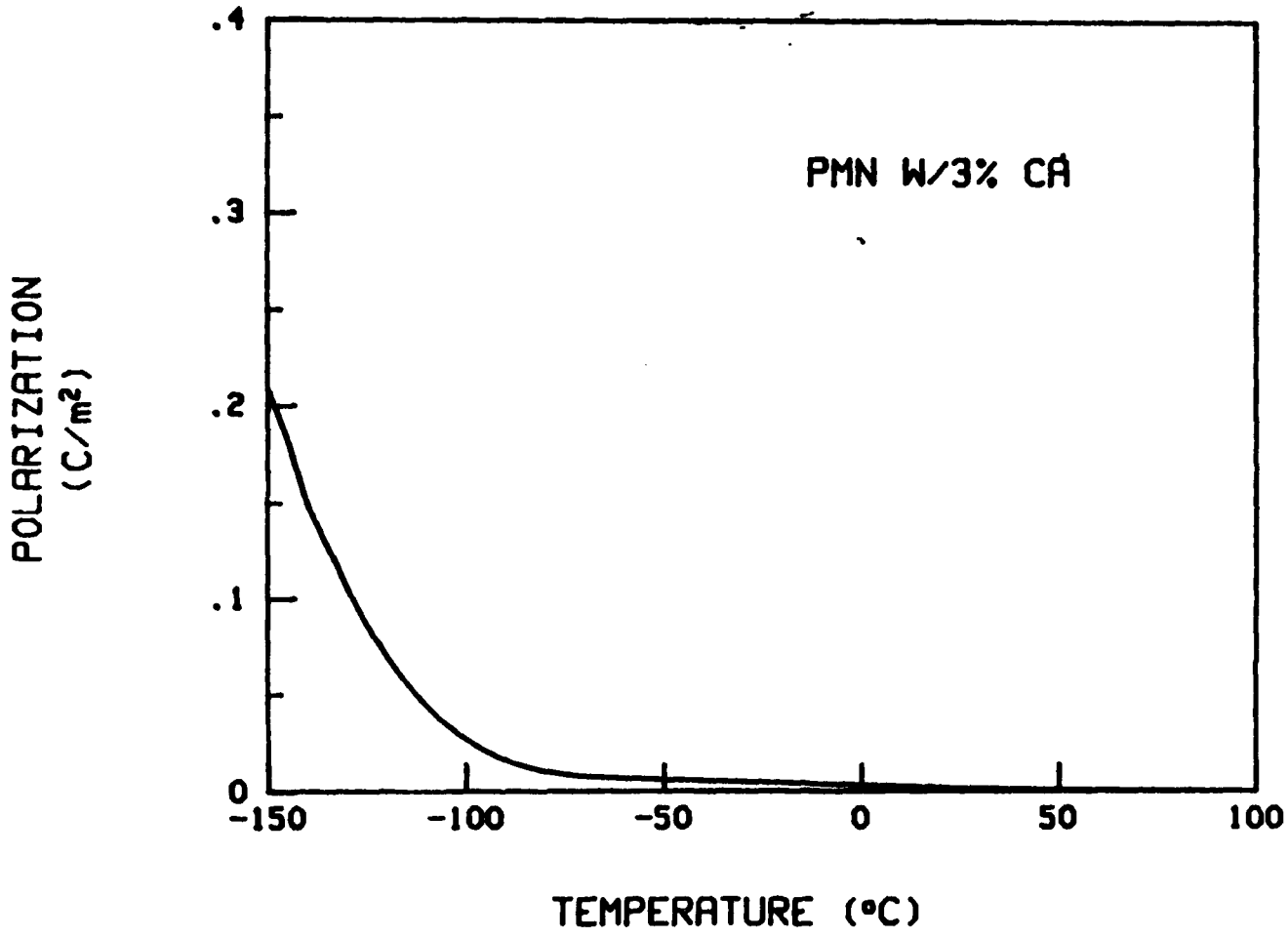
PMN W/3% CA
POLARIZATION (C/m²)
.4
.3
.2
.1
0
-150
-100
-50
0
50
100
TEMPERATURE (°C)

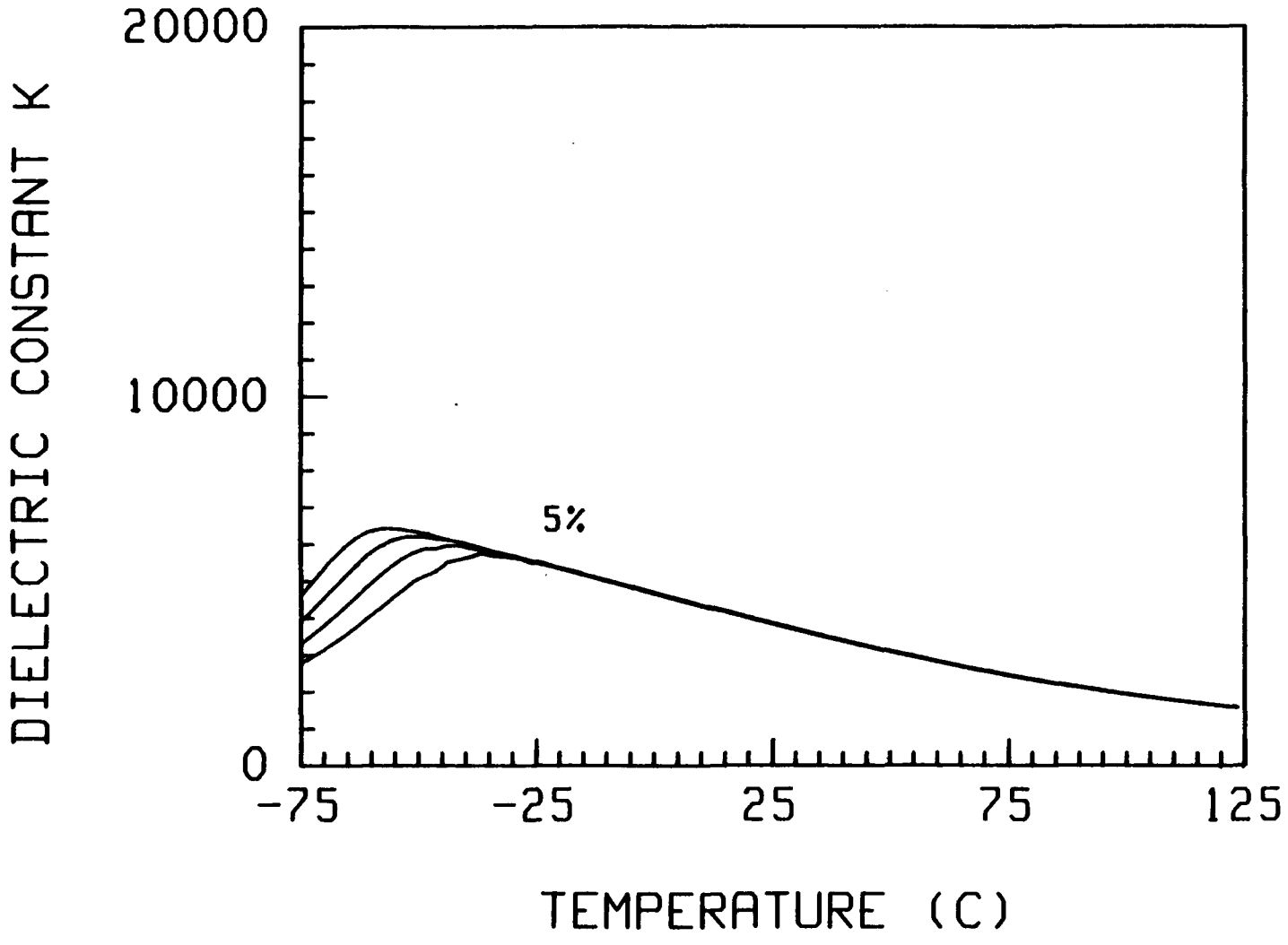

PMN WITH 1,3 AND 5 MOL% CA SUBSTITUTIONS

CVT1106_3 PMN 5%CA J91142

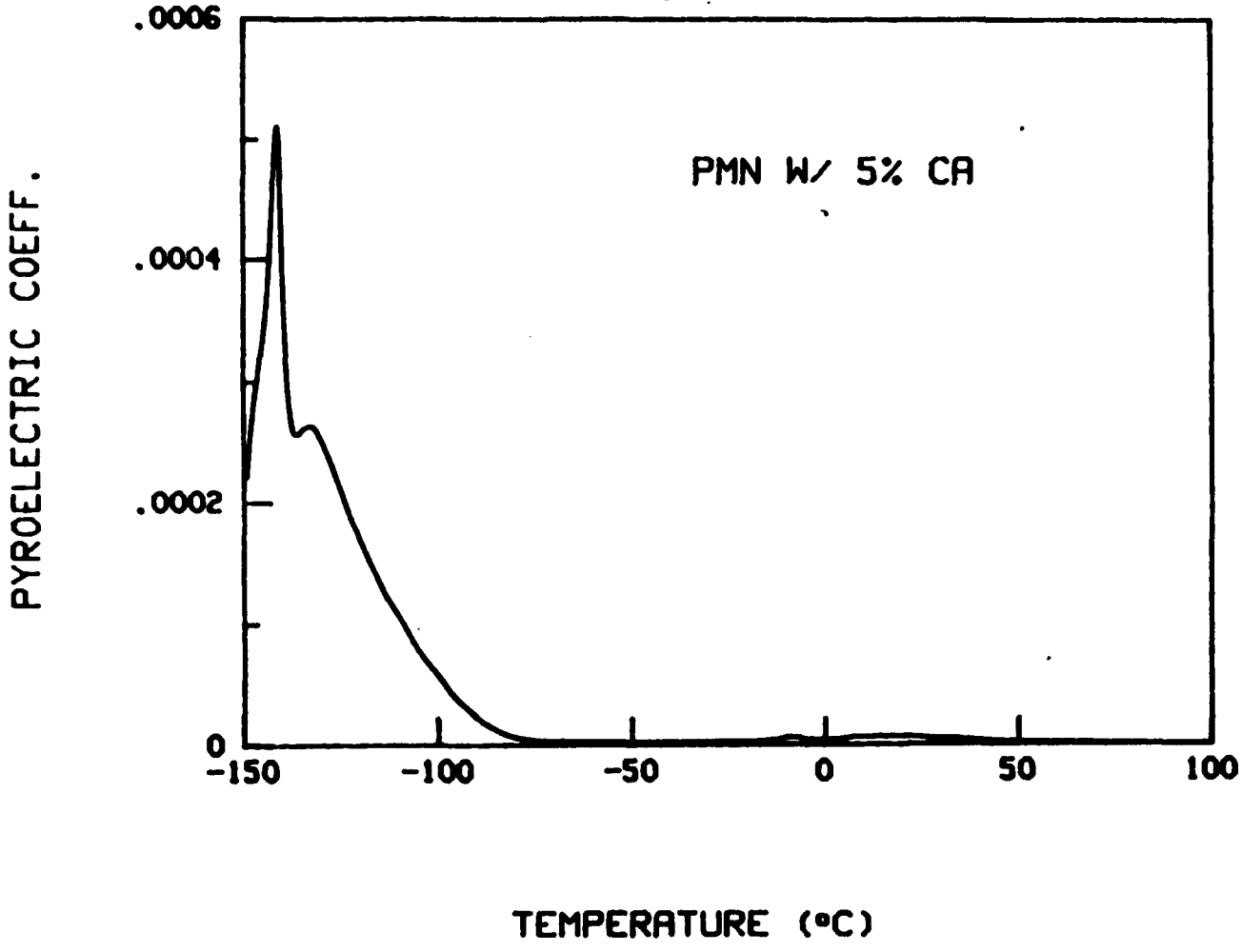
PMN W/ 5% CA
.0006
.0004
.0002
0
-150
-100
-50
0
50
100
PYROELECTRIC COEFF.
TEMPERATURE (°C)

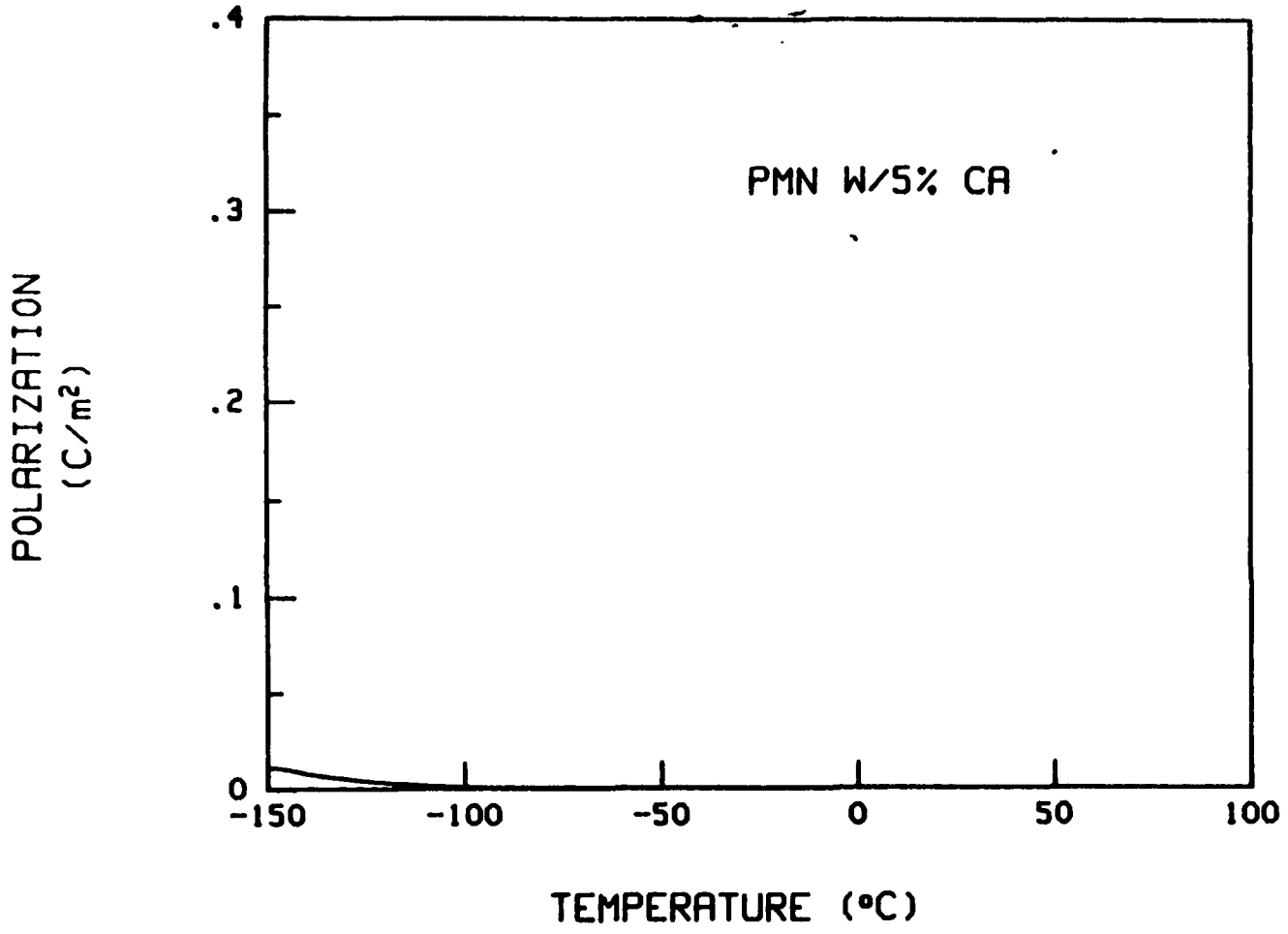
PMN W/5% CA
POLARIZATION
(C/m²)
.4
.3
.2
.1
0
-150
-100
-50
0
50
100
TEMPERATURE (°C)

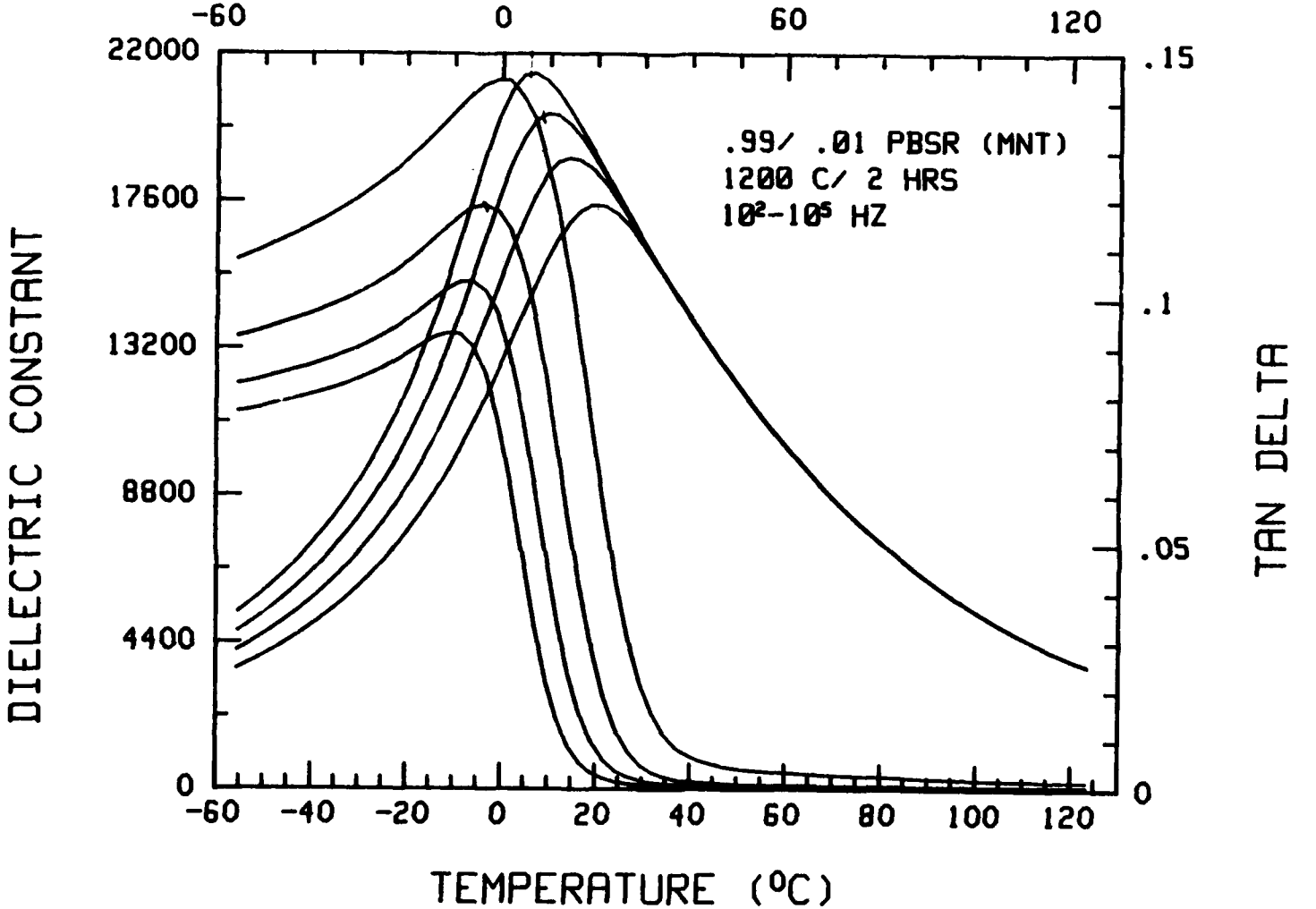
-60
0
60
120
22000
17600
13200
8800
4400
0
.15
.1
.05
0
.99/ .01 PBSR (MNT)
1200 C/ 2 HRS
10²-10⁵ HZ
DIELECTRIC CONSTANT
TAN DELTA
-60 -40 -20 0 20 40 60 80 100 120
TEMPERATURE (°C)

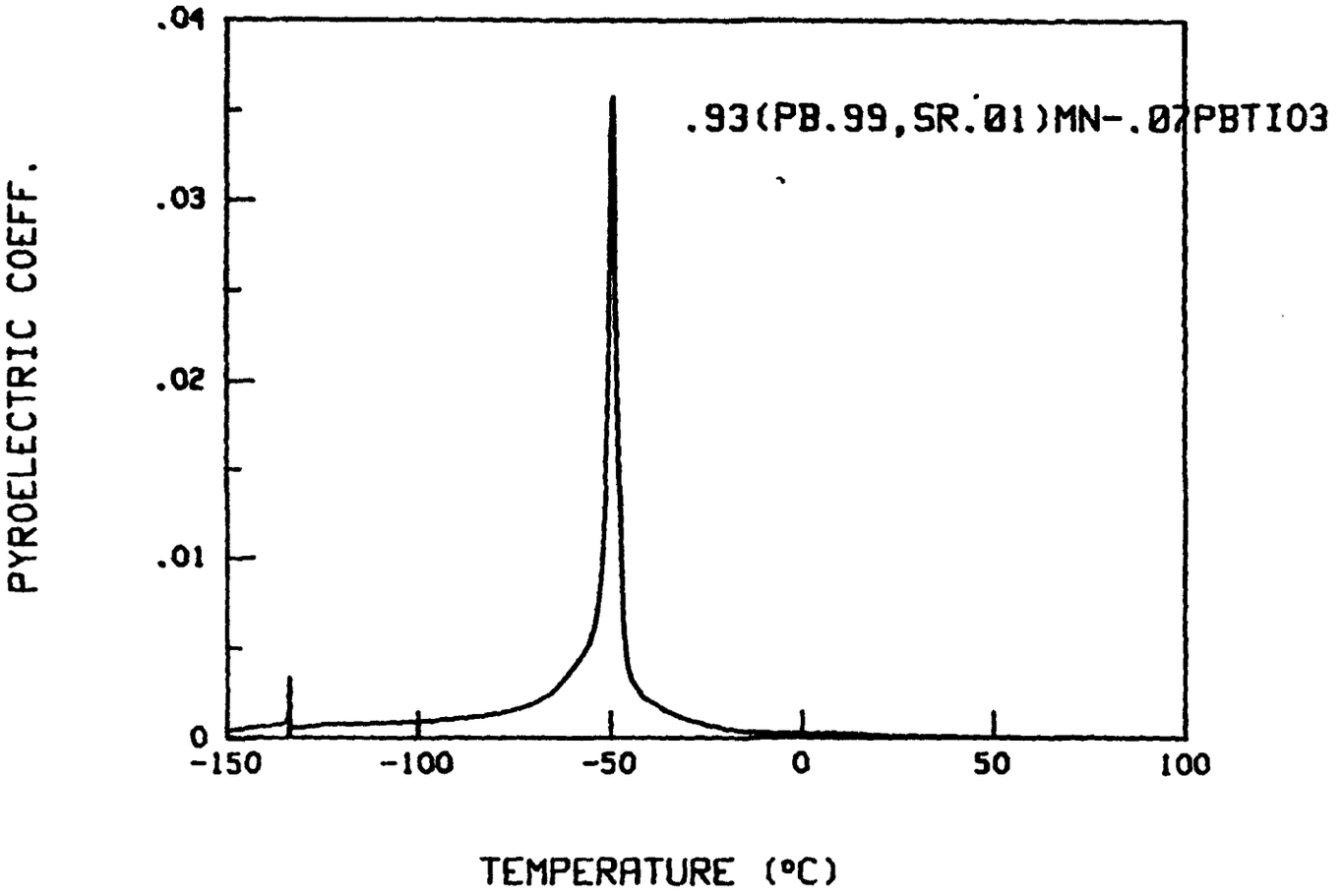
.93(PB.99,SR.01)MN-.07PBTIO3
PYROELECTRIC COEFF.
.04
.03
.02
.01
0
-150
-100
-50
0
50
100
TEMPERATURE (°C)

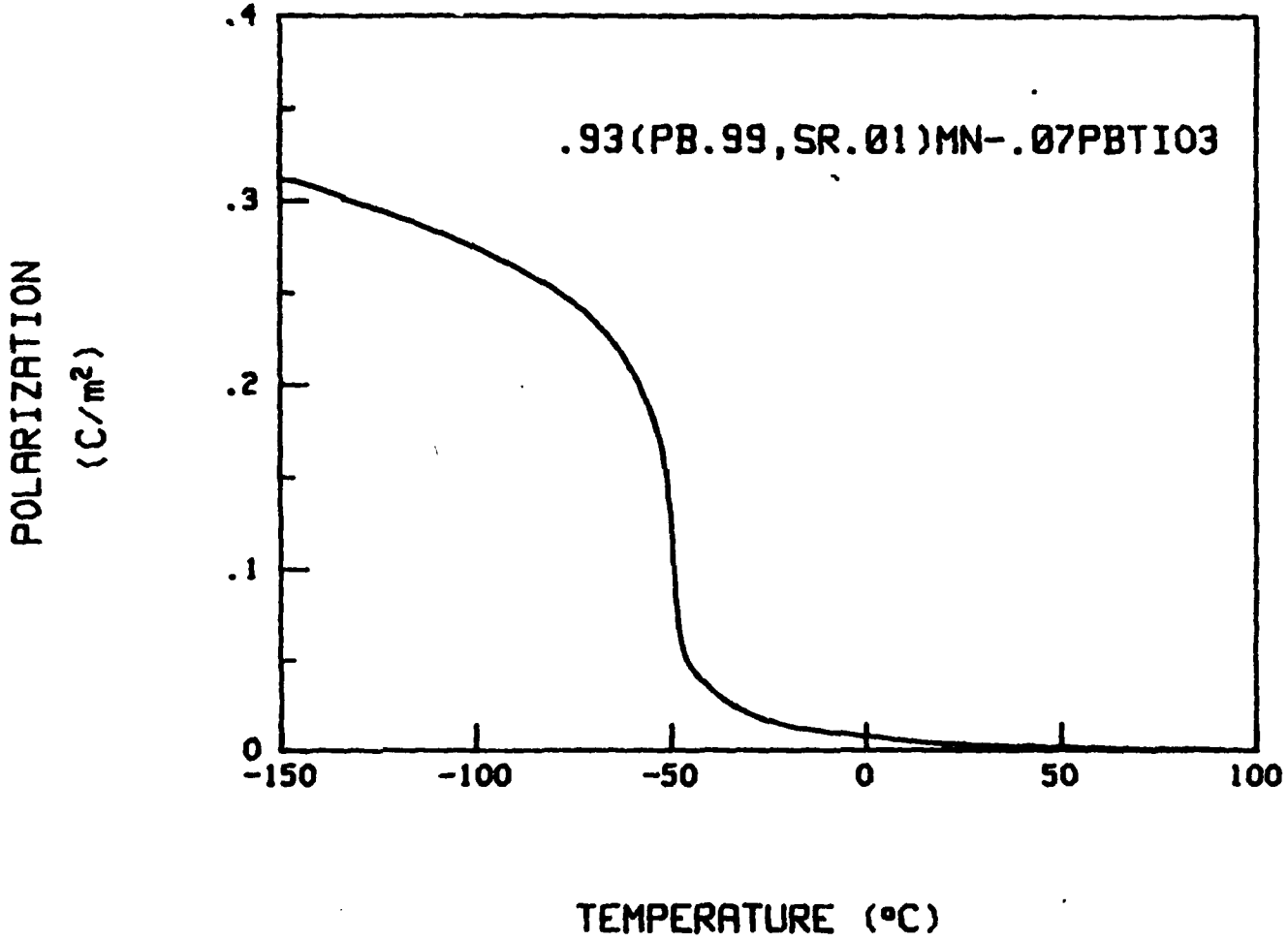
.93(PB.99,SR.01)MN-.07PBTIO3
POLARIZATION
(C/m²)
.4
.3
.2
.1
0
-150
-100
-50
0
50
100
TEMPERATURE (°C)

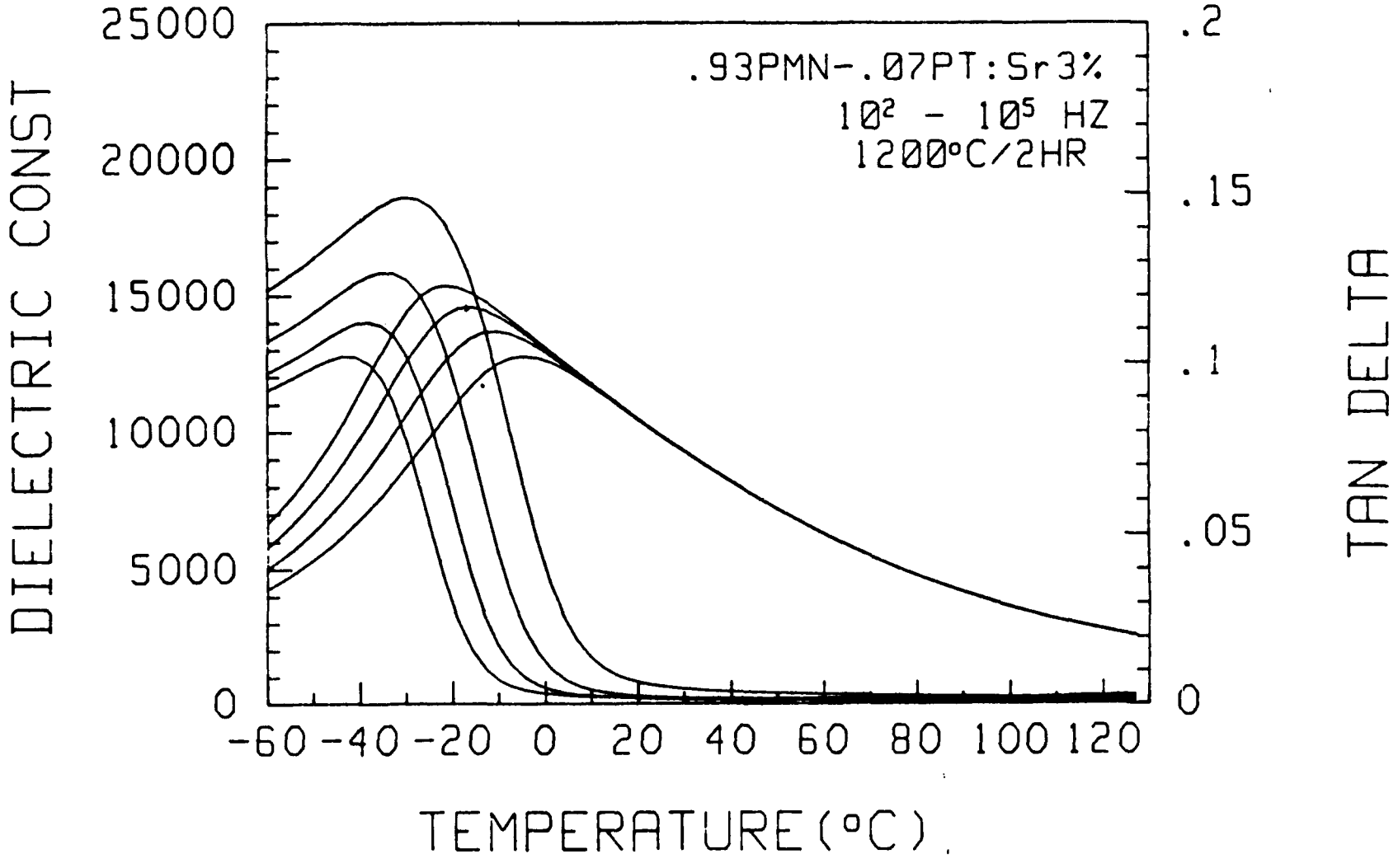
.93PMN-.07PT:Sr3%
10² - 10⁵ HZ
1200°C/2HR
DIELECTRIC CONST
TAN DELTA
TEMPERATURE(°C)
25000
20000
15000
10000
5000
0
.2
.15
.1
.05
0
-60 -40 -20 0 20 40 60 80 100 120

SONAR 5_5

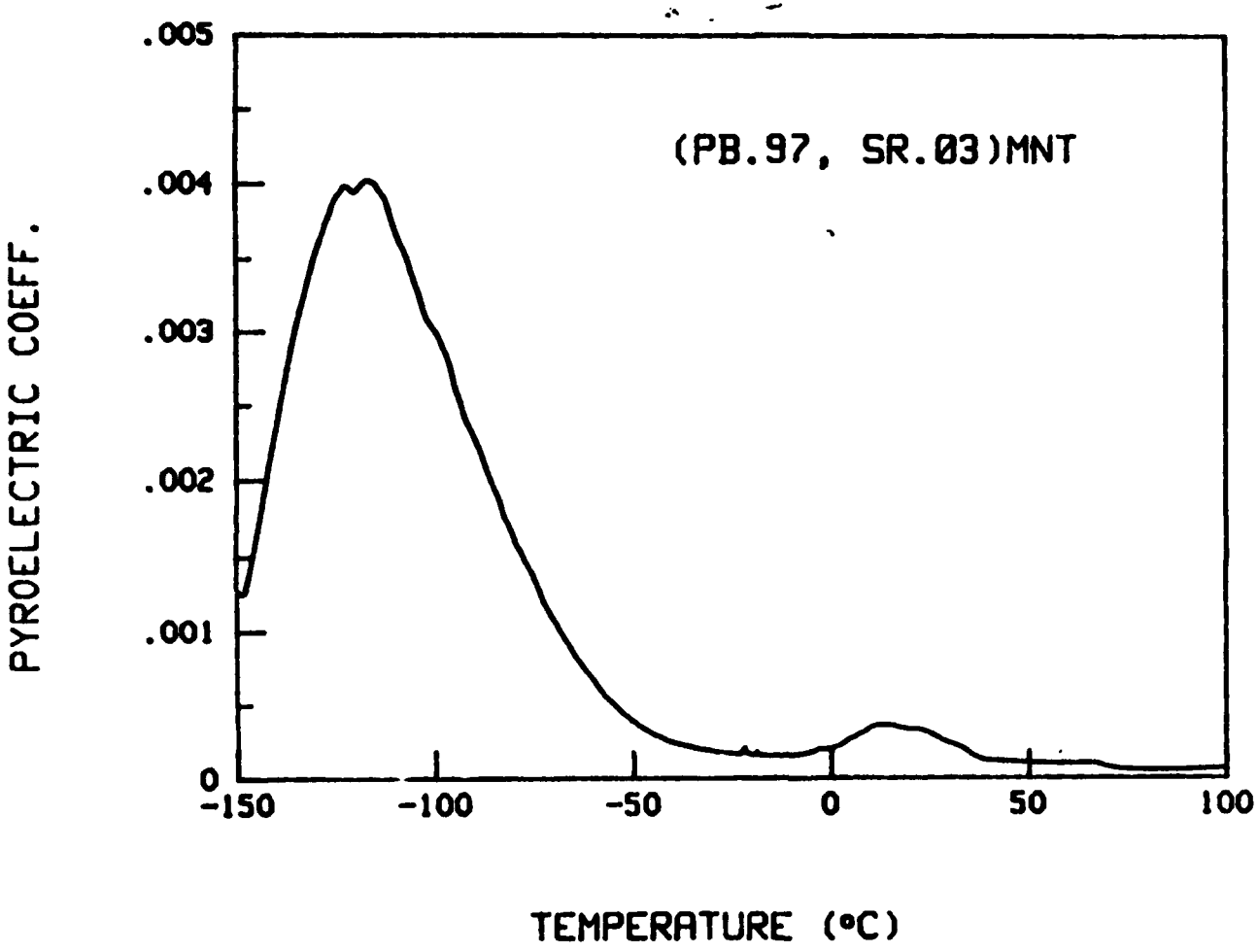
(PB.97, SR.03)MNT
PYROELECTRIC COEFF.
.005
.004
.003
.002
.001
0
-150
-100
-50
0
50
100
TEMPERATURE (°C)

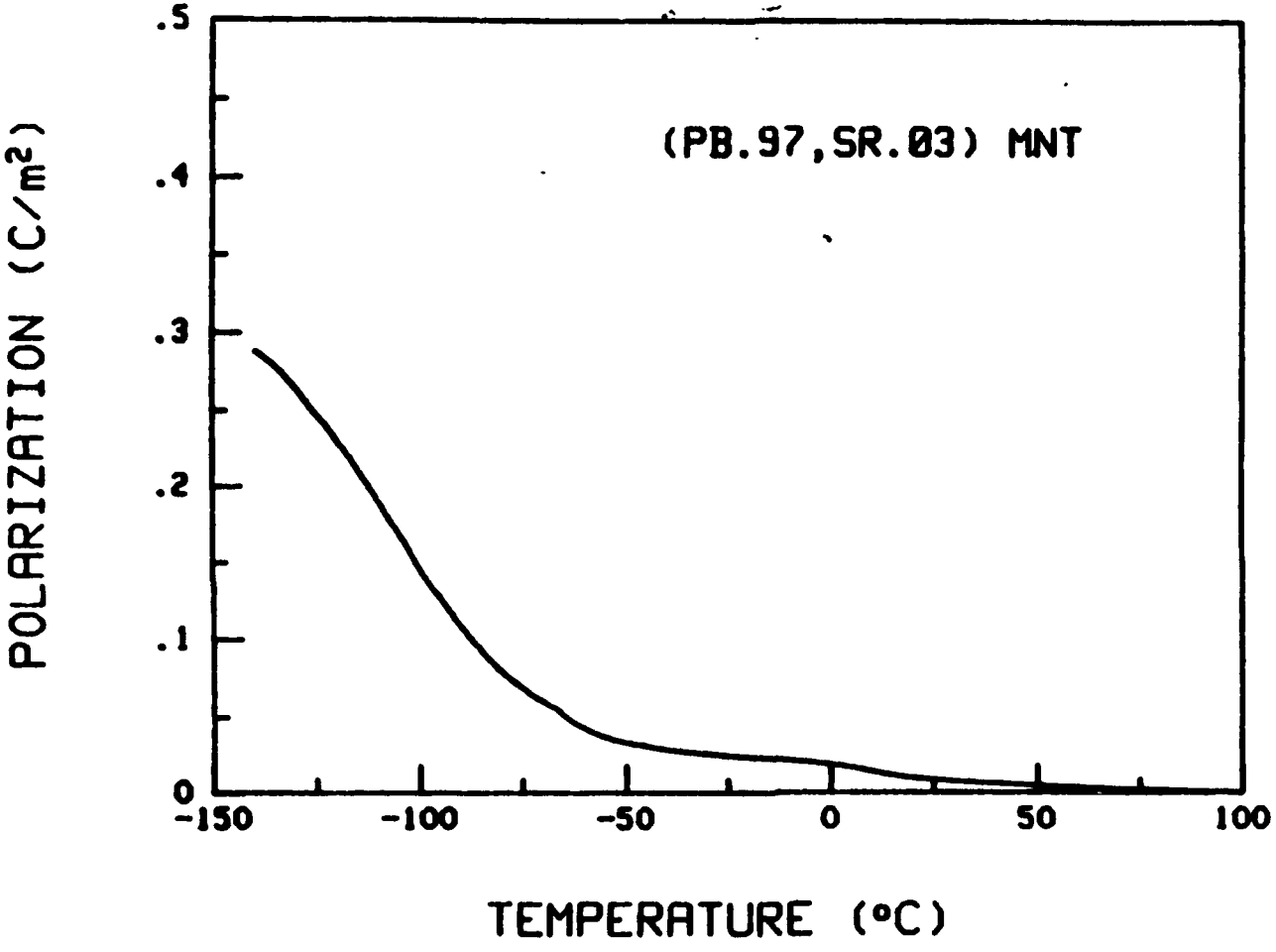
(PB.97,SR.03) MNT
POLARIZATION (C/m²)
.5
.4
.3
.2
.1
0
-150
-100
-50
0
50
100
TEMPERATURE (°C)

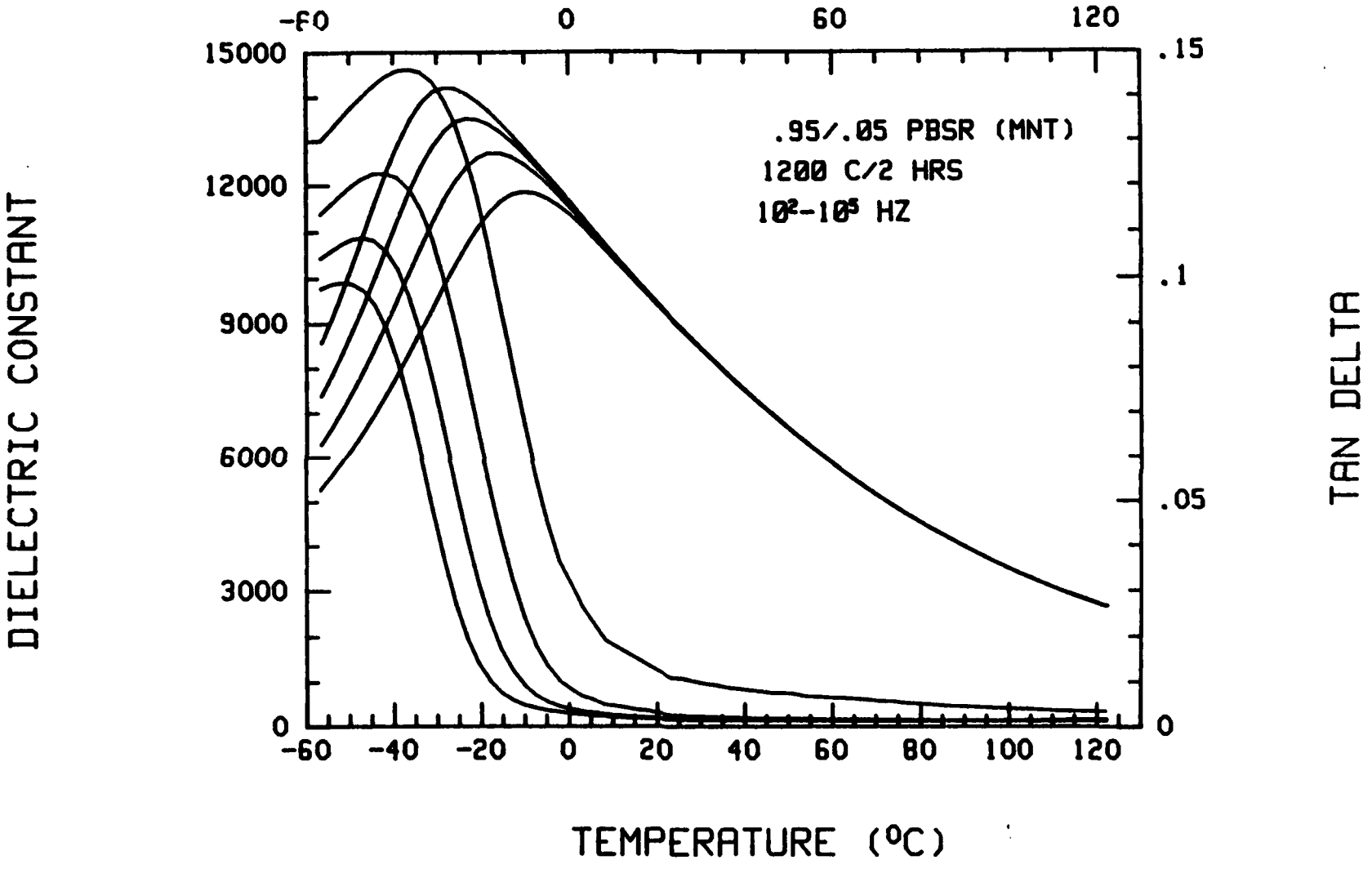
-60
0
60
120
15000
12000
9000
6000
3000
0
.15
.1
.05
0
.95/.05 PBSR (MNT)
1200 C/2 HRS
10²-10⁵ HZ
-60
-40
-20
0
20
40
60
80
100
120
DIELECTRIC CONSTANT
TAN DELTA
TEMPERATURE (°C)

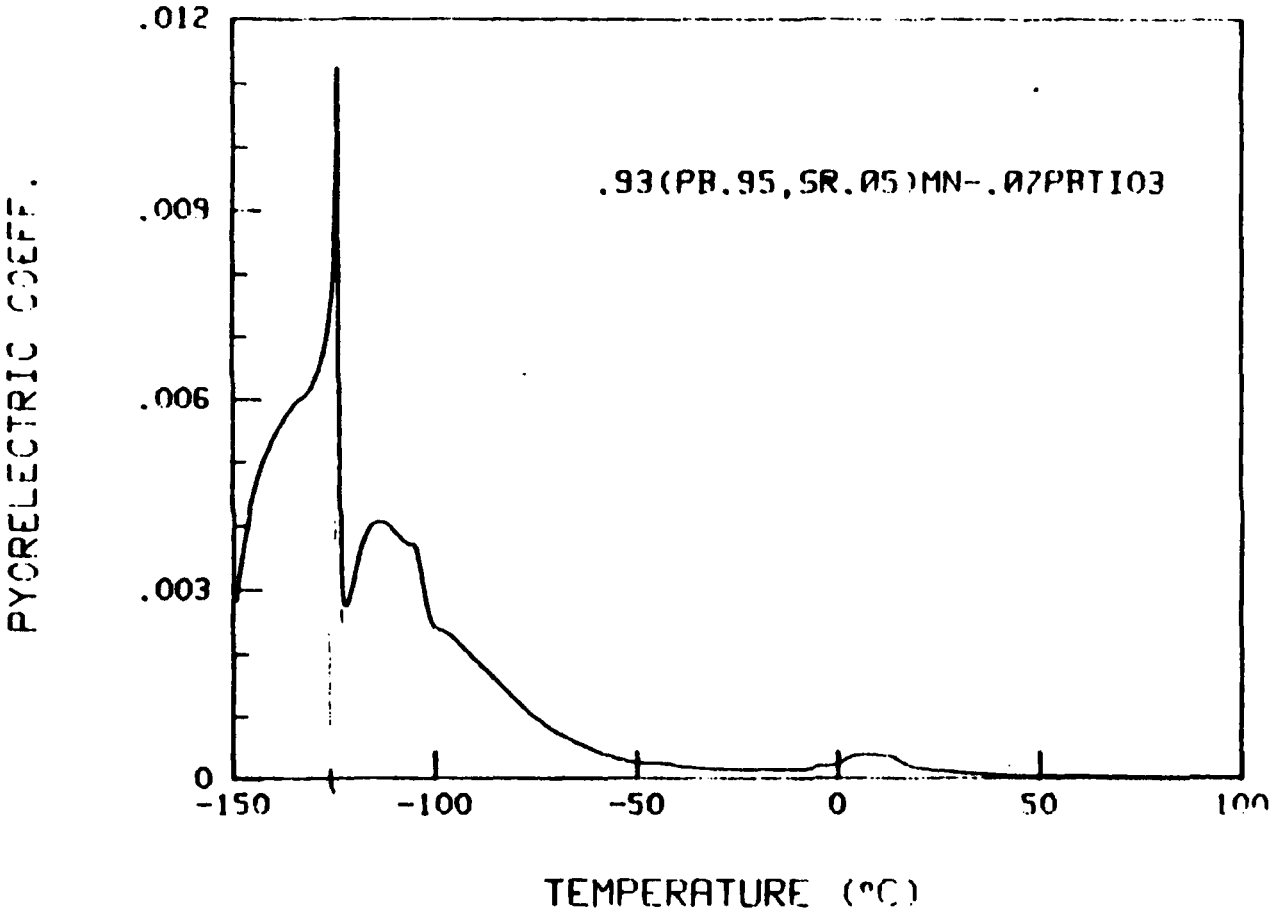
.012
.009
.006
.003
0
PYOELECTRIC COEFF.
.93(PB.95,SR.05)MN-.07PRTI03
-150
-100
-50
0
50
100
TEMPERATURE (°C)

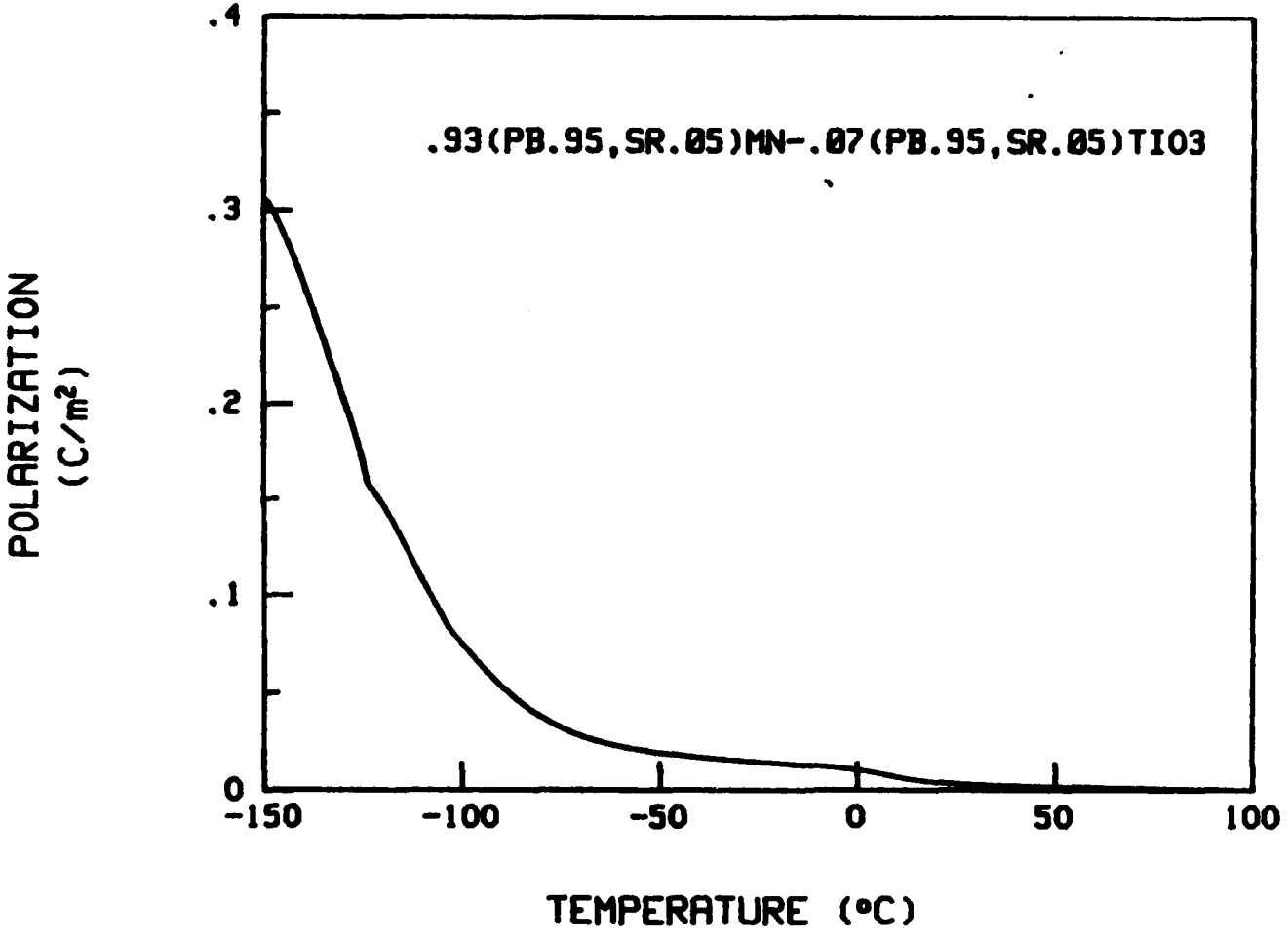
.93(PB.95,SR.05)MN-.07(PB.95,SR.05)TIO3
POLARIZATION
(C/m²)
.4
.3
.2
.1
0
-150
-100
-50
0
50
100
TEMPERATURE (°C)

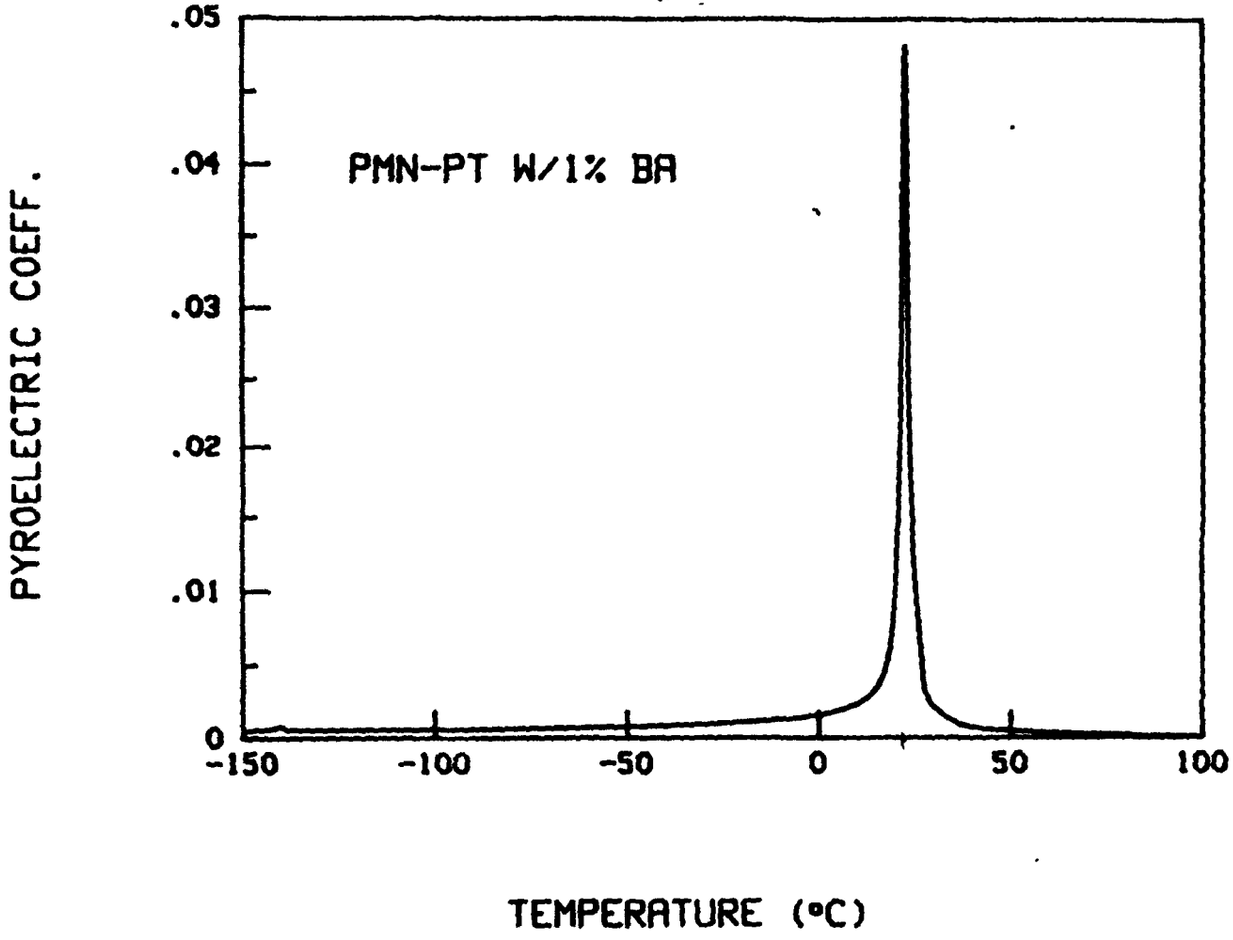
PMN-PT W/1% BA
PYROELECTRIC COEFF.
.05
.04
.03
.02
.01
0
-150
-100
-50
0
50
100
TEMPERATURE (°C)

85/05/1

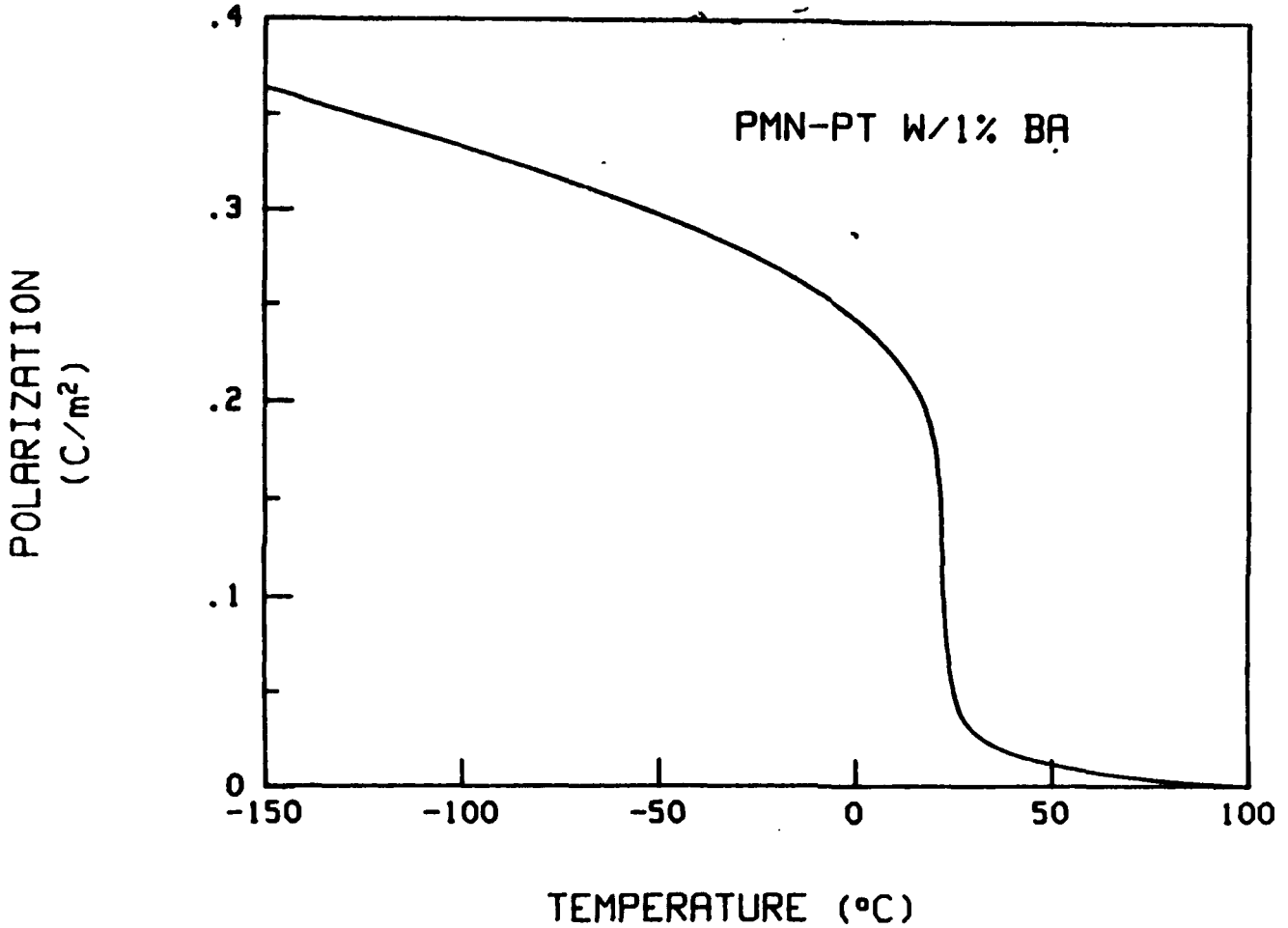
PMN-PT W/1% BA
POLARIZATION
(C/m²)
.4
.3
.2
.1
0
-150
-100
-50
0
50
100
TEMPERATURE (°C)

85/15/1

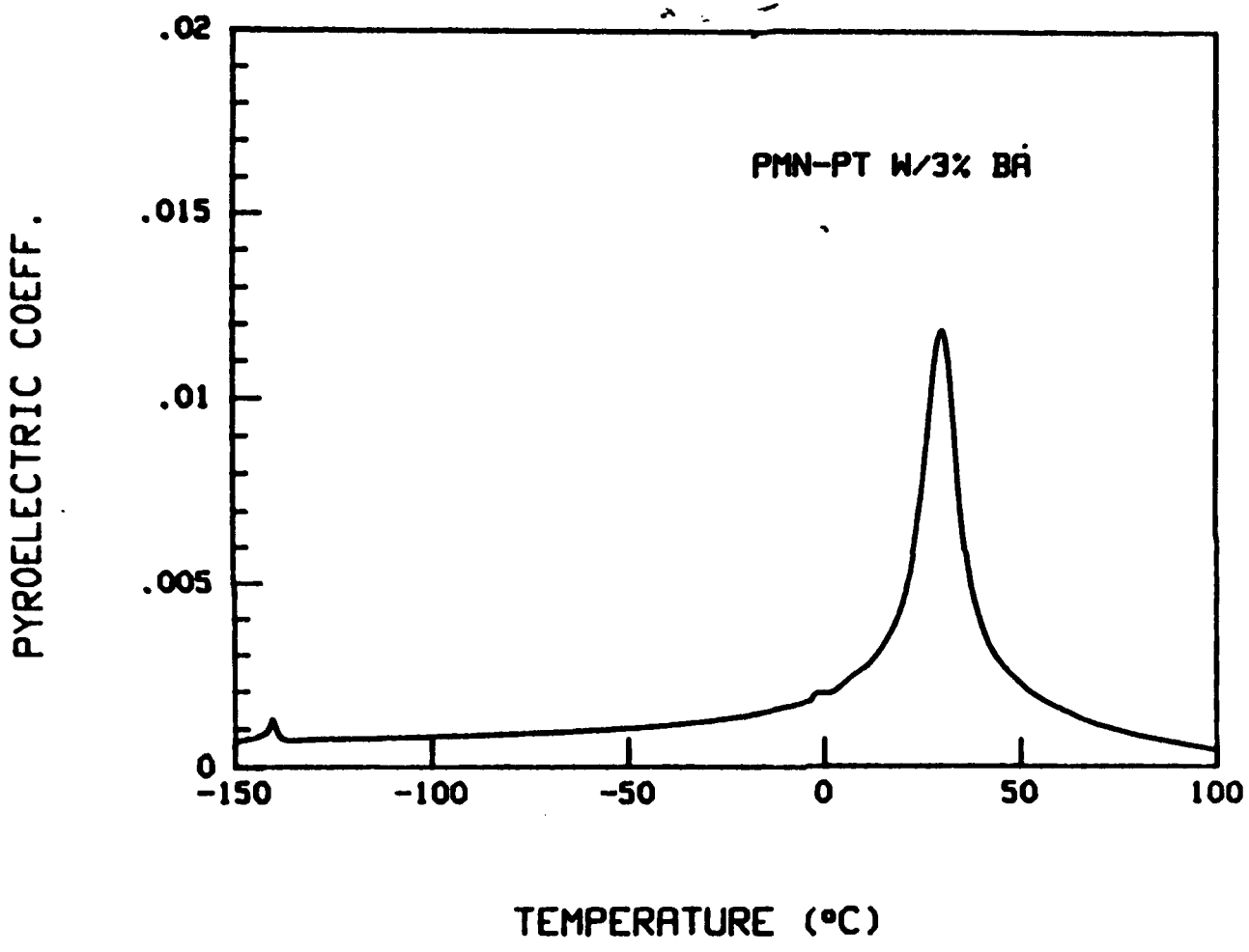
PMN-PT W/3% BA
PYROELECTRIC COEFF.
.02
.015
.01
.005
0
-150
-100
-50
0
50
100
TEMPERATURE (°C)

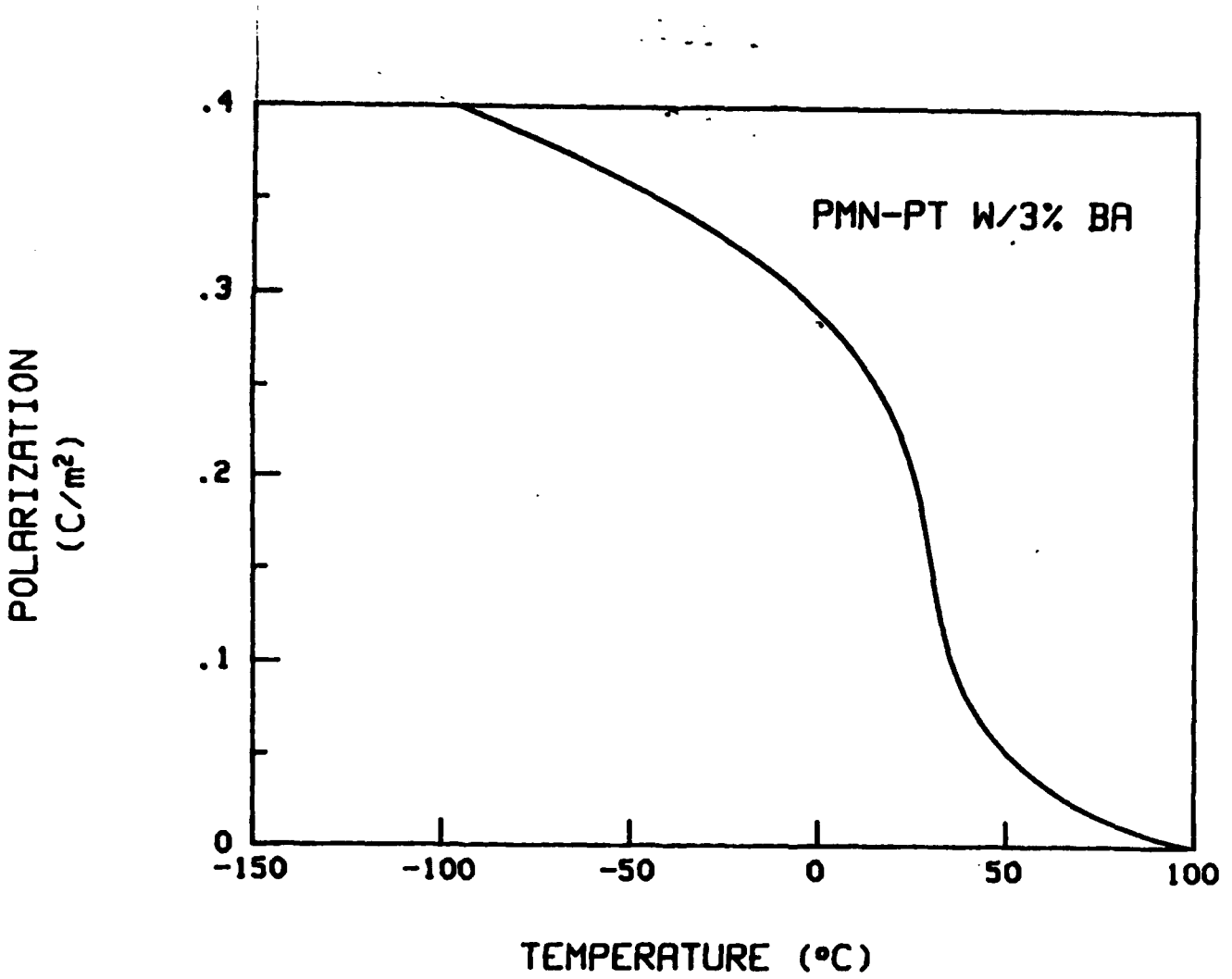
PMN-PT W/3% BA
POLARIZATION (C/m²)
.4
.3
.2
.1
0
-150
-100
-50
0
50
100
TEMPERATURE (°C)

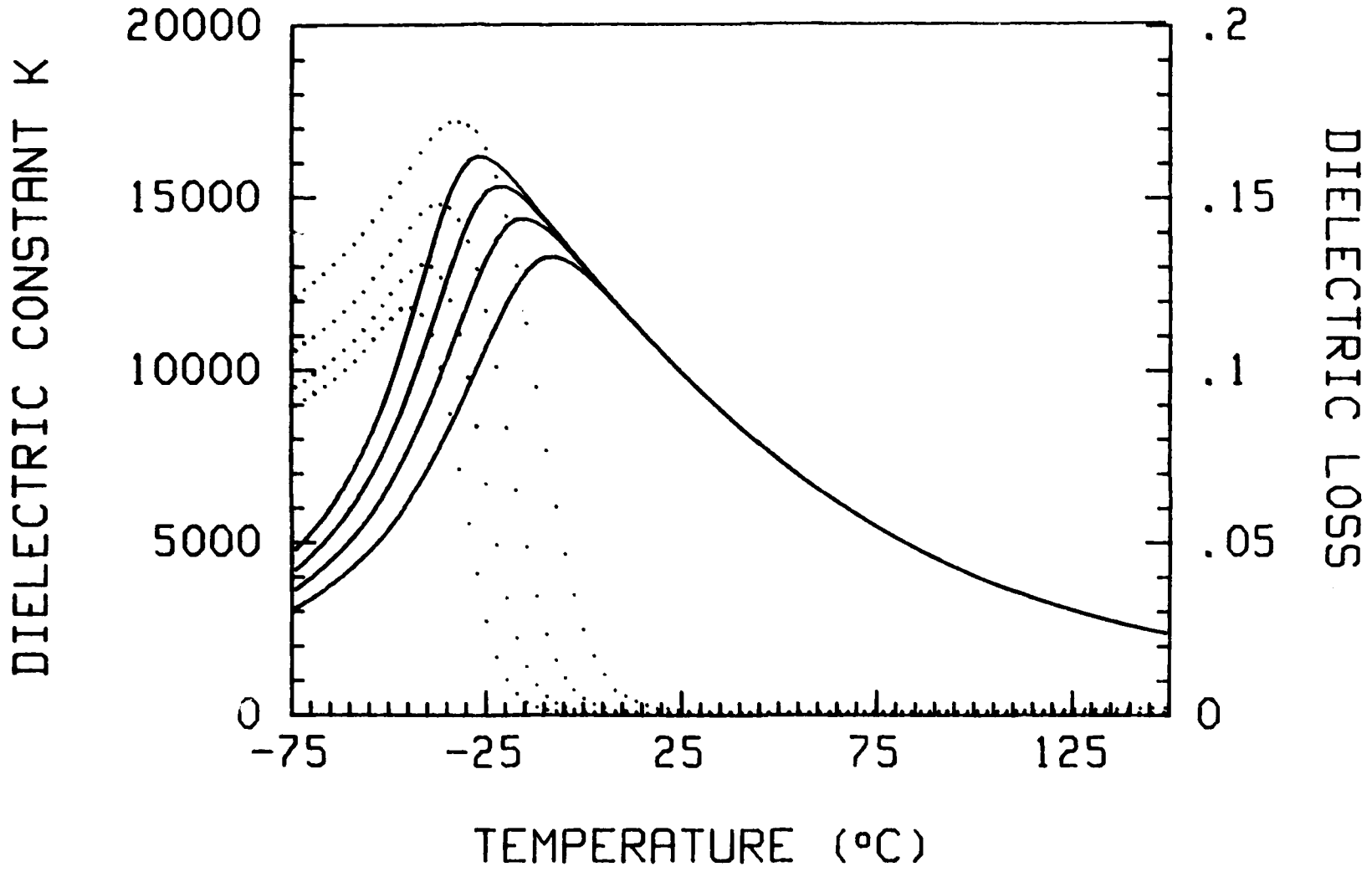

CVT31192_2 PMN+1%BI 1150/2HRS #198-8

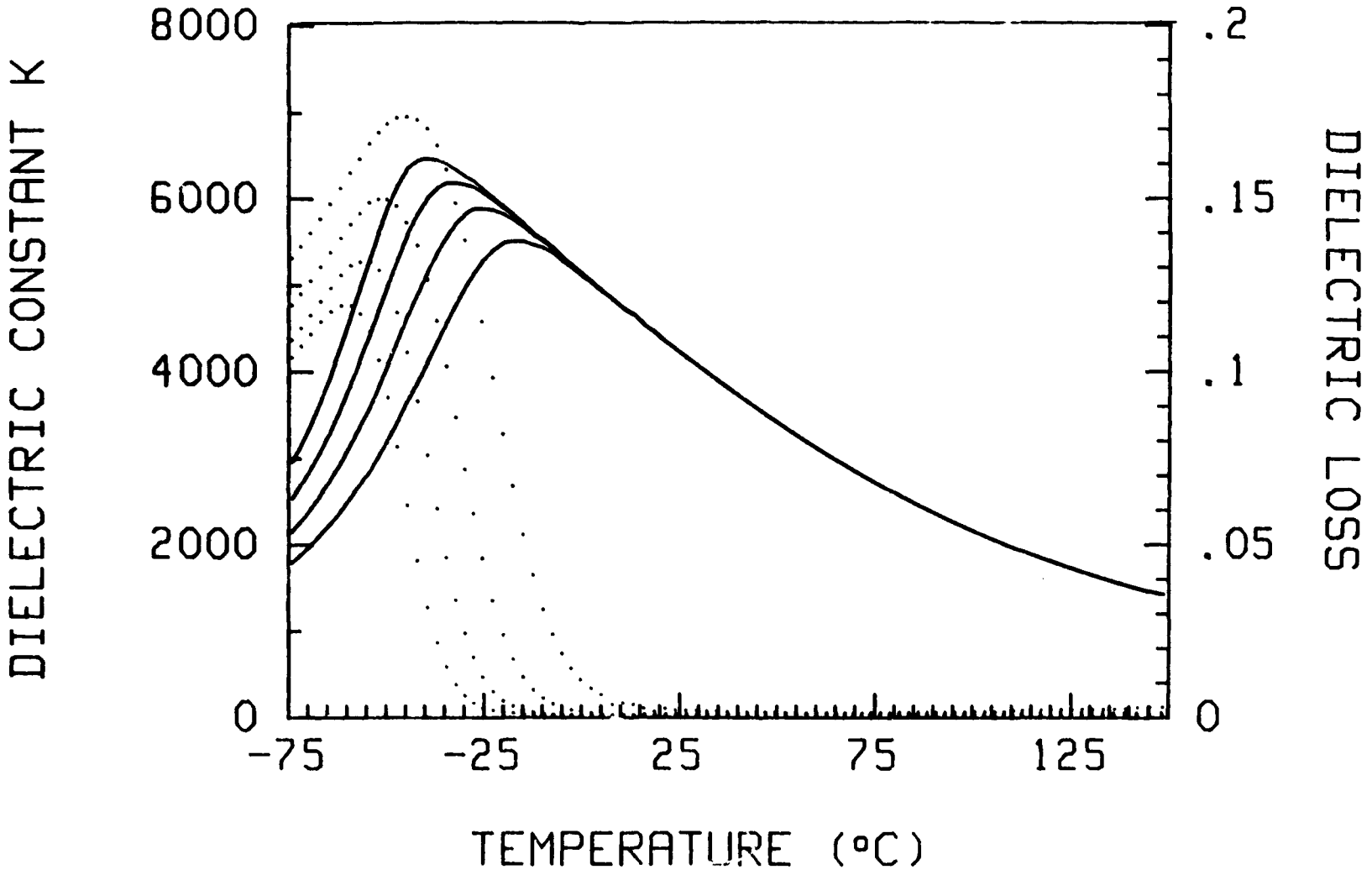

CVT31192_3 PMN+3%BI 1150/2HRS #199-7

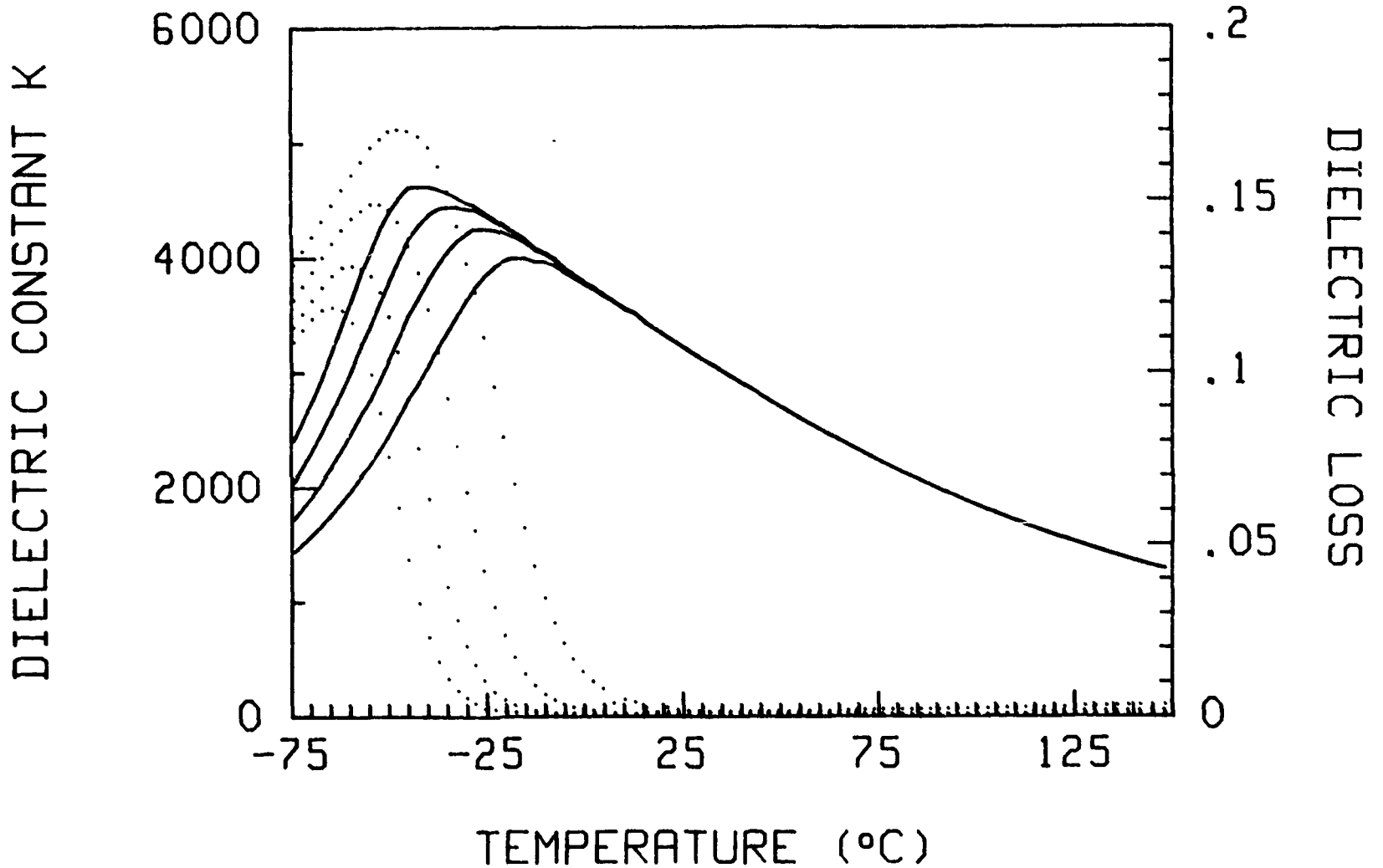

CVT31192_4 PMN+5%BI 1150/2HRS #200-2

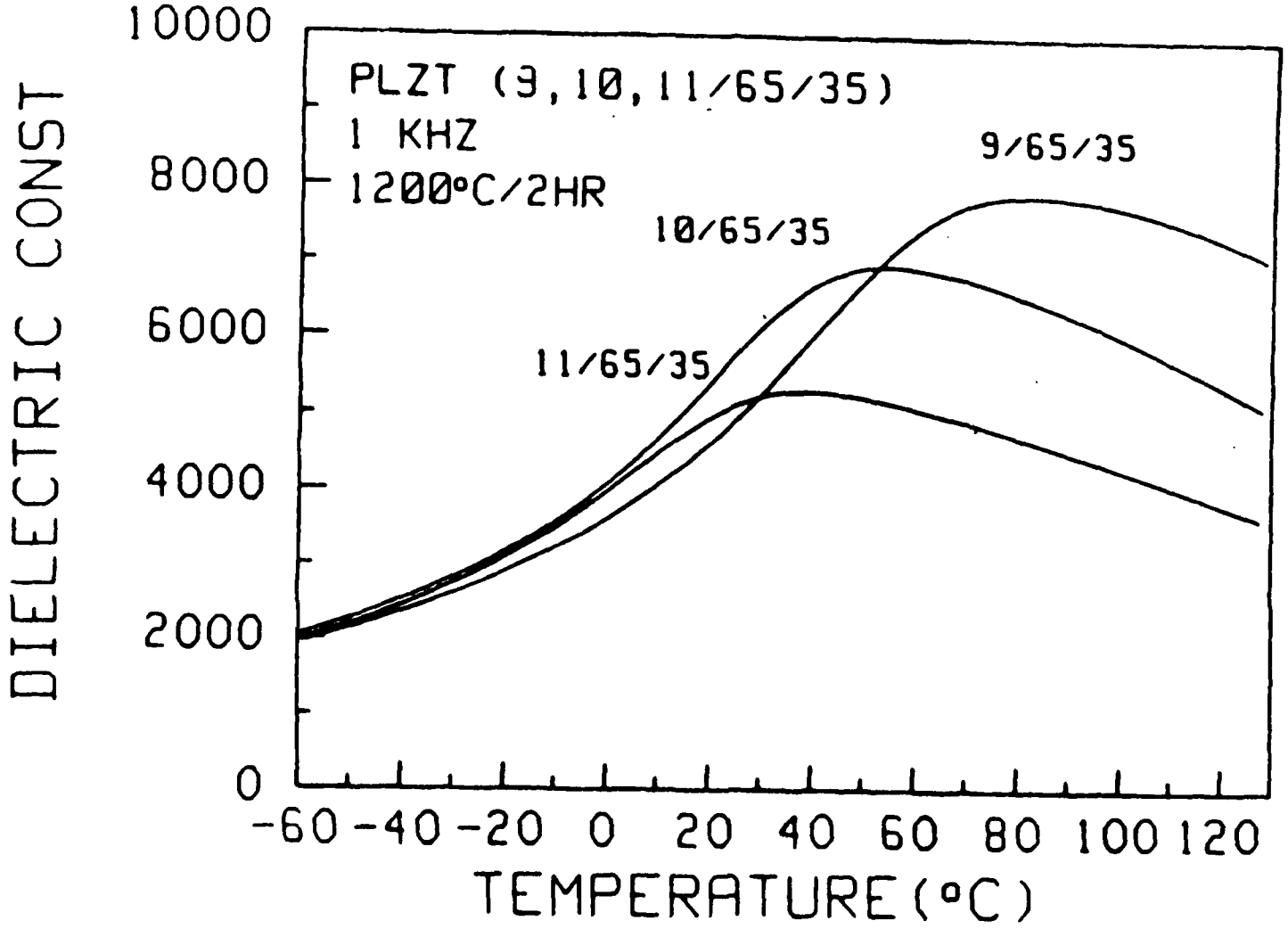
PLZT (9,10,11/65/35)
1 KHZ
1200°C/2HR
9/65/35
10/65/35
11/65/35
DIELECTRIC CONST
10000
8000
6000
4000
2000
0
-60 -40 -20 0 20 40 60 80 100 120
TEMPERATURE (°C)

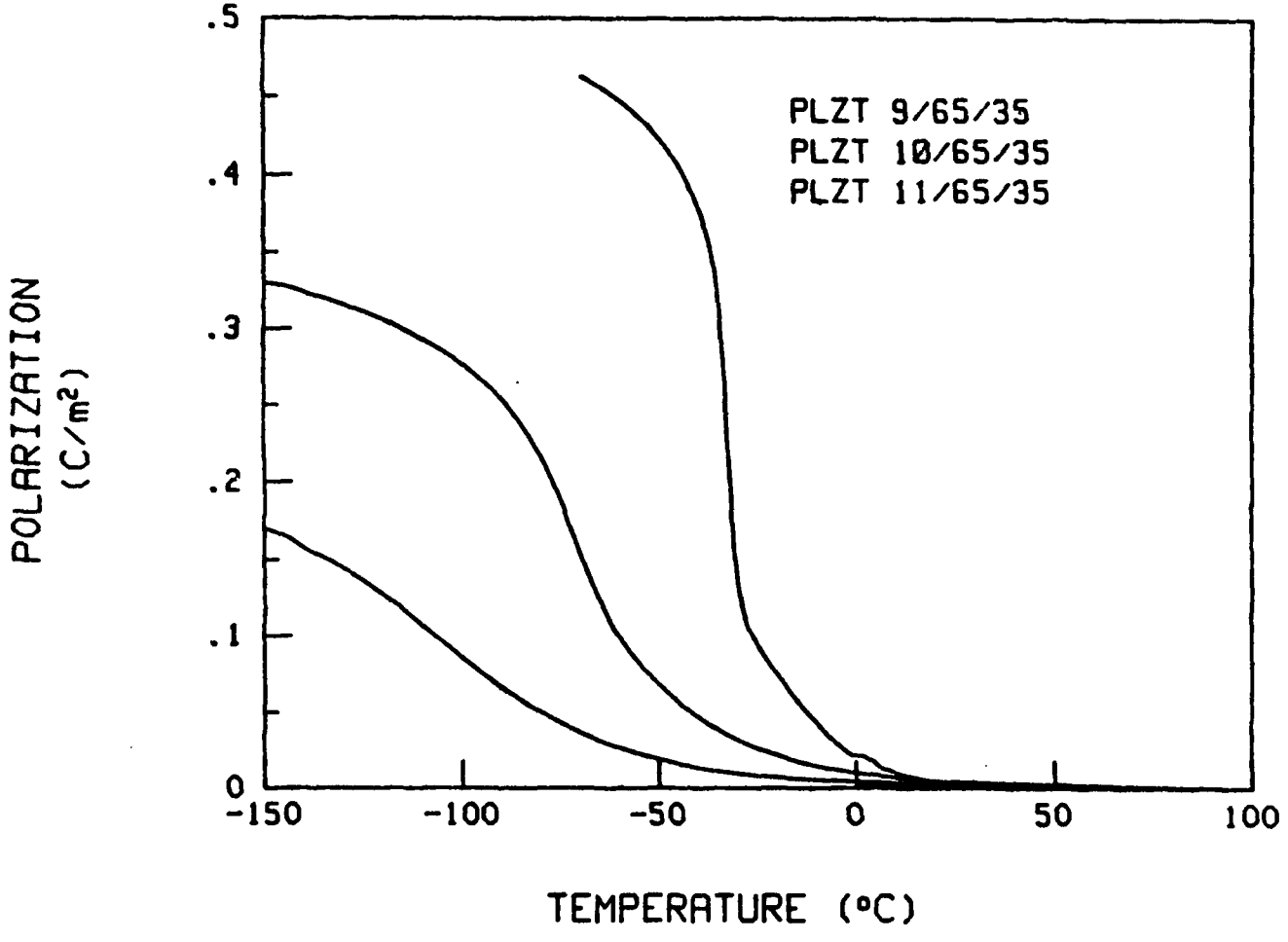
PLZT 9/65/35
PLZT 10/65/35
PLZT 11/65/35
POLARIZATION (C/m²)
.5
.4
.3
.2
.1
0
-150
-100
-50
0
50
100
TEMPERATURE (°C)

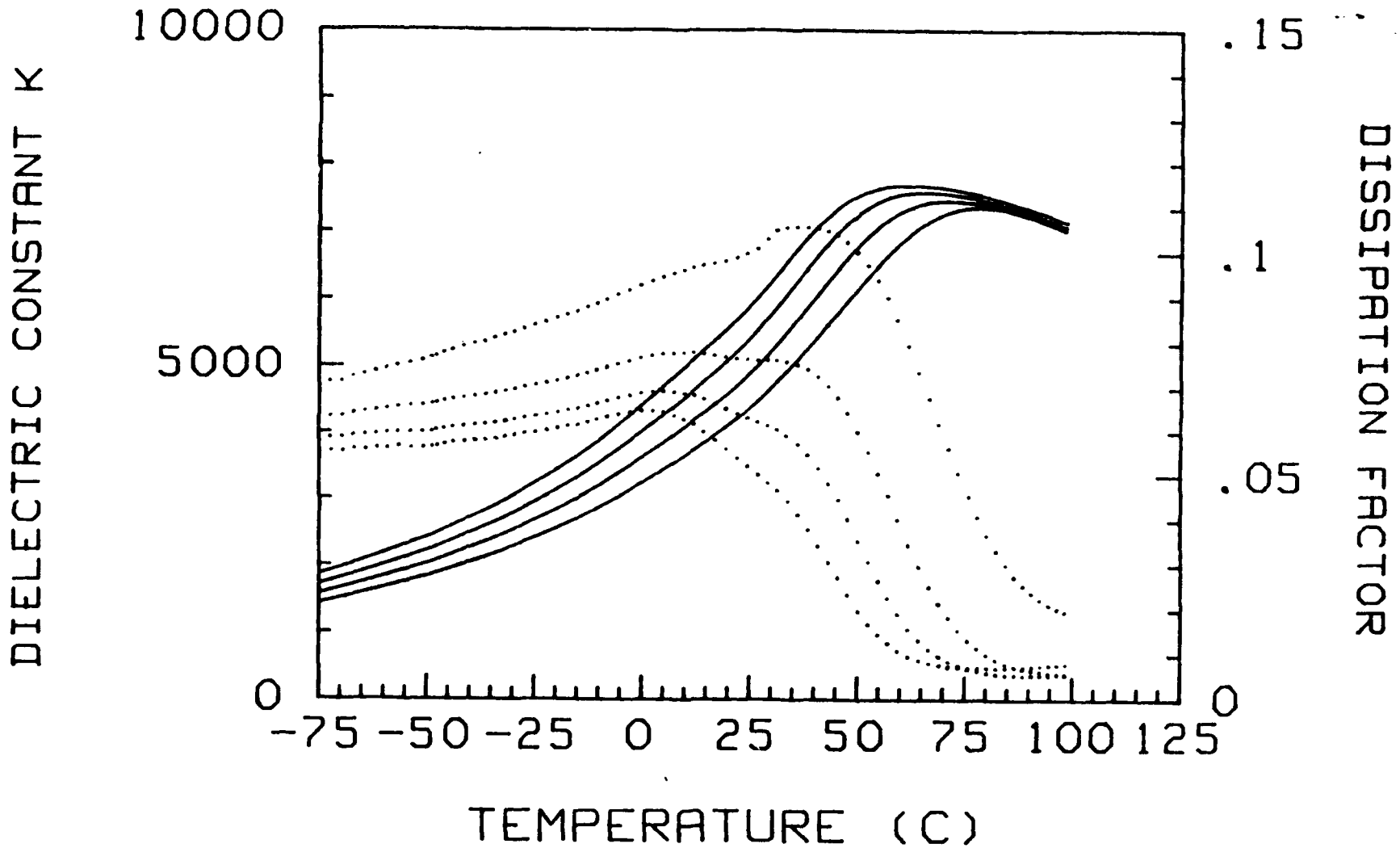

PLZT 9065 SQUARE #A

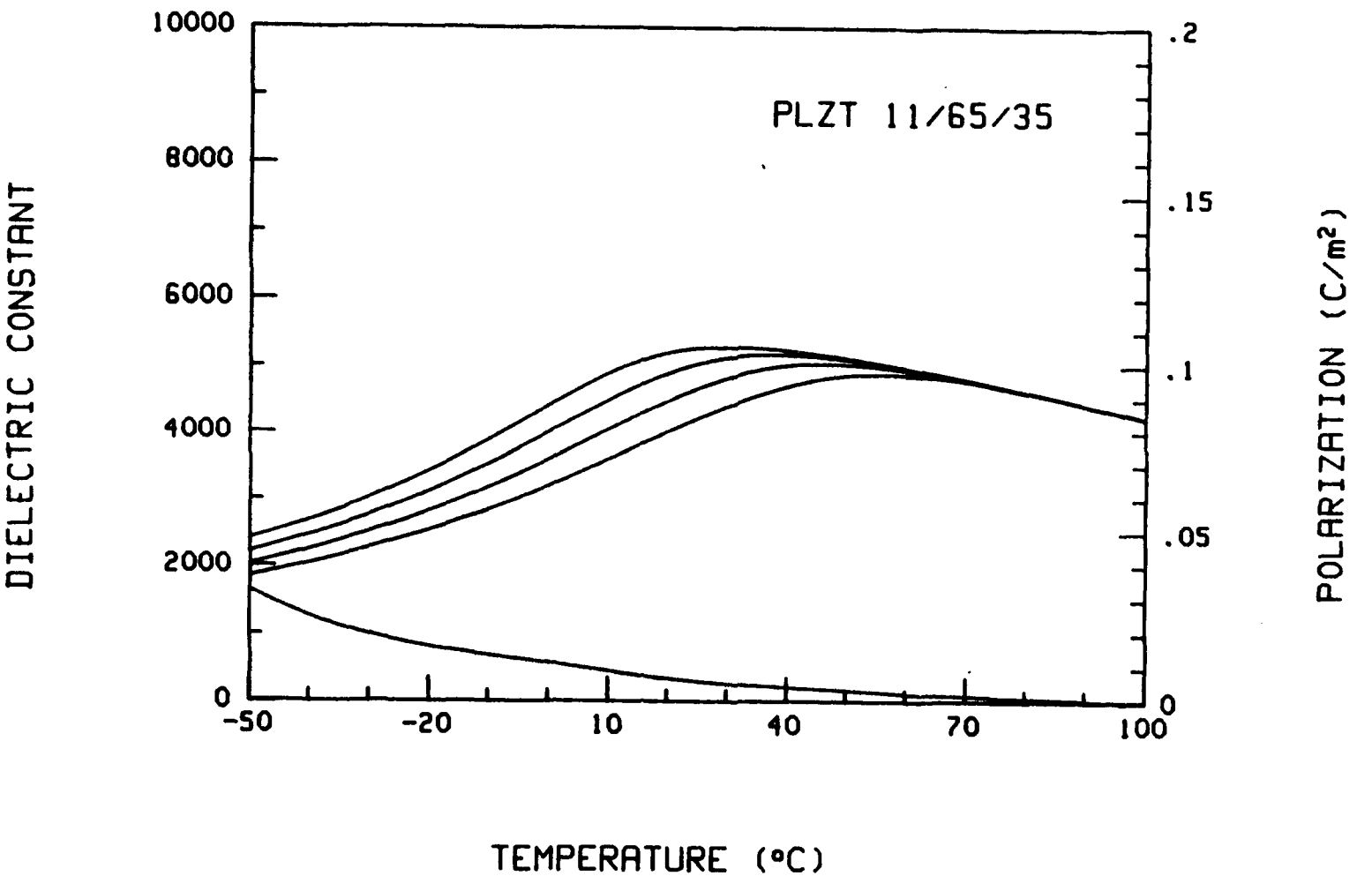
PLZT 11/65/35
DIELECTRIC CONSTANT
POLARIZATION (C/m²)
TEMPERATURE (°C)
10000
8000
6000
4000
2000
0
.2
.15
.1
.05
0
-50
-20
10
40
70
100

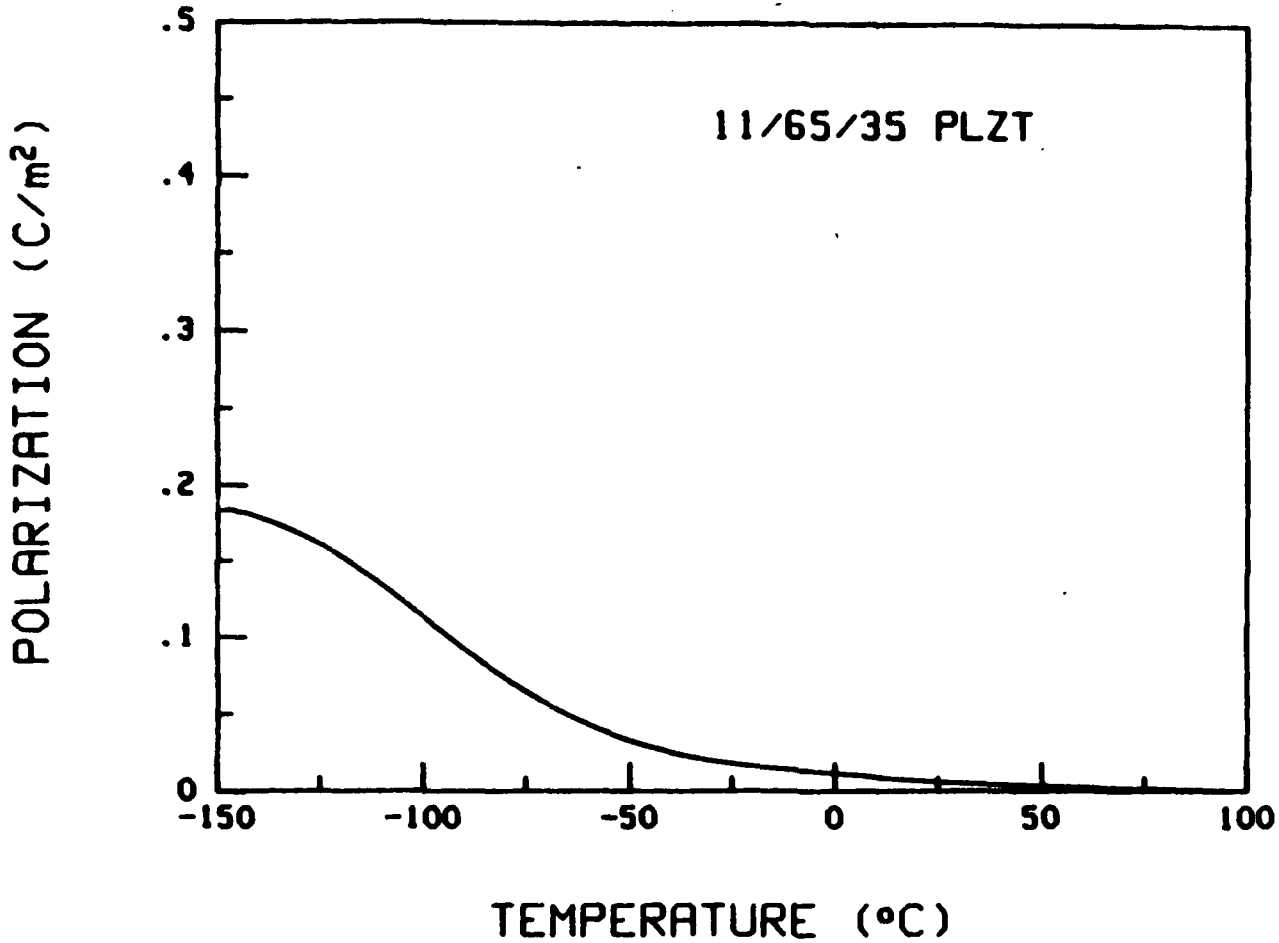
11/65/35 PLZT
POLARIZATION (C/m²)
.5
.4
.3
.2
.1
0
-150
-100
-50
0
50
100
TEMPERATURE (°C)

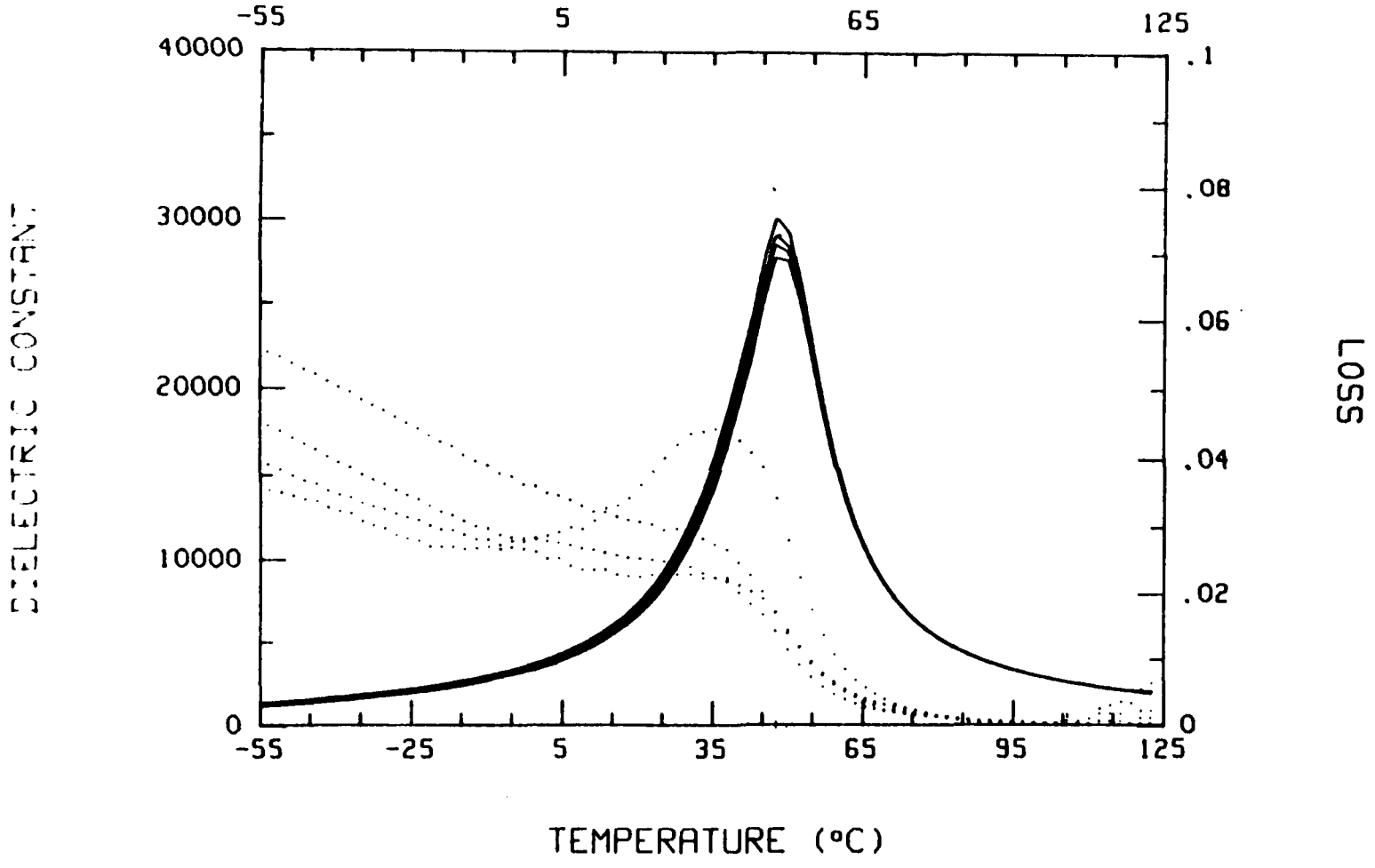
-55
5
65
125
40000
30000
20000
10000
0
.1
.08
.06
.04
.02
0
-55
-25
5
35
65
95
125
DIELECTRIC CONSTANT
LOSS
TEMPERATURE (°C)

Ba(Ti.9, Sn.1)03

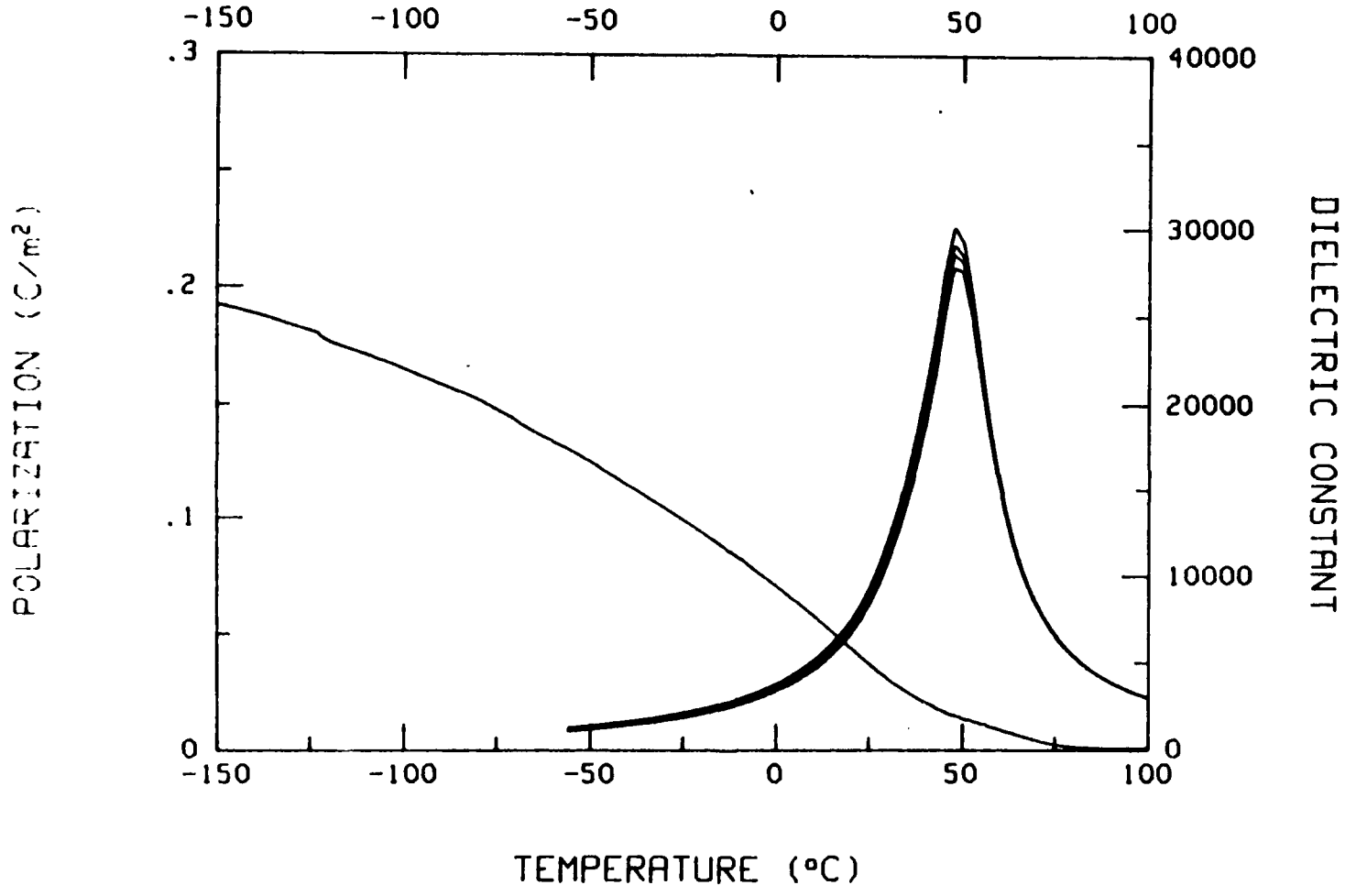
-150
-100
-50
0
50
100
.3
.2
.1
0
40000
30000
20000
10000
0
POLARIZATION (C/m²)
DIELECTRIC CONSTANT
TEMPERATURE (°C)

Ba(Ti.9, Sn.1)03

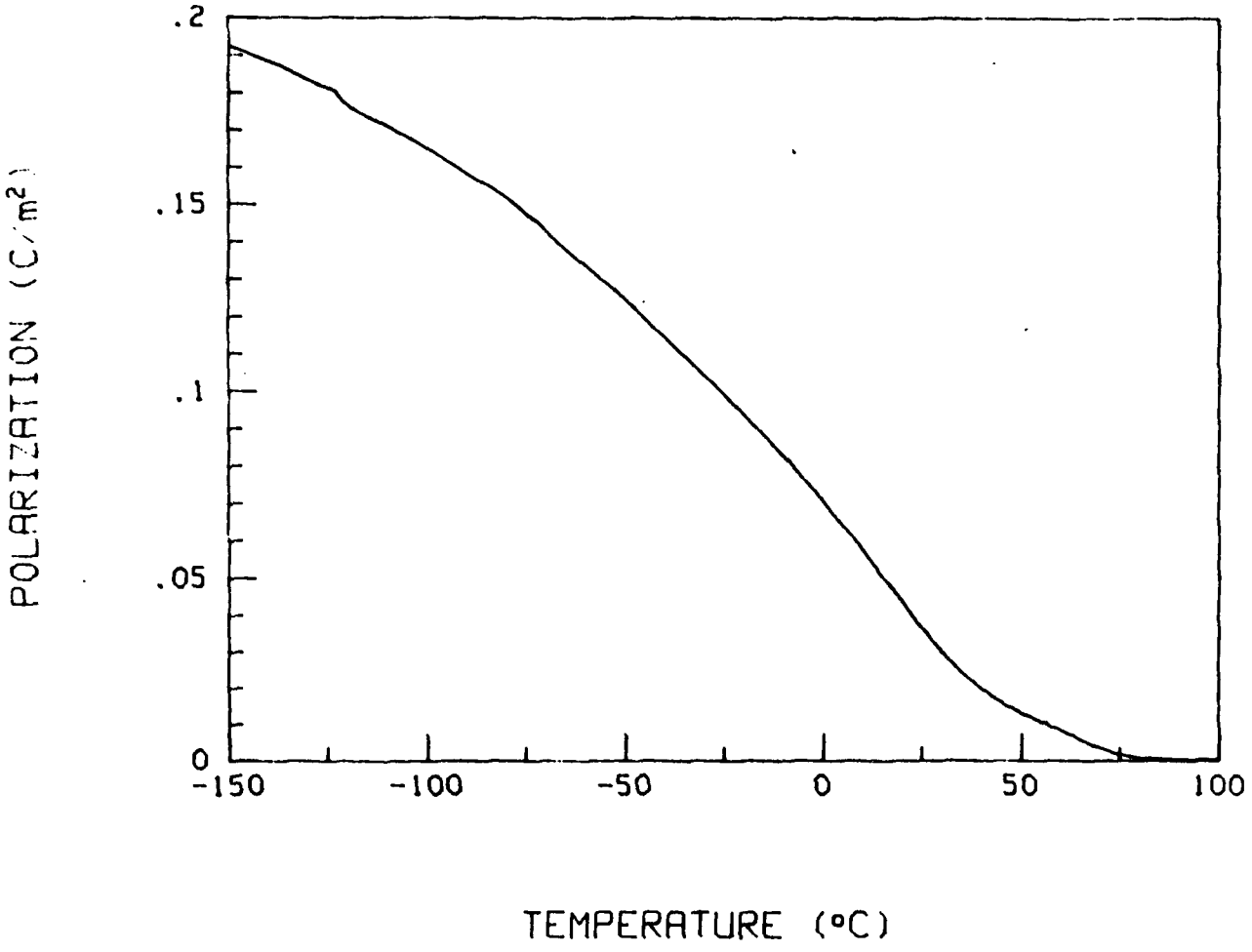

BA(SN.1, TI.9)03

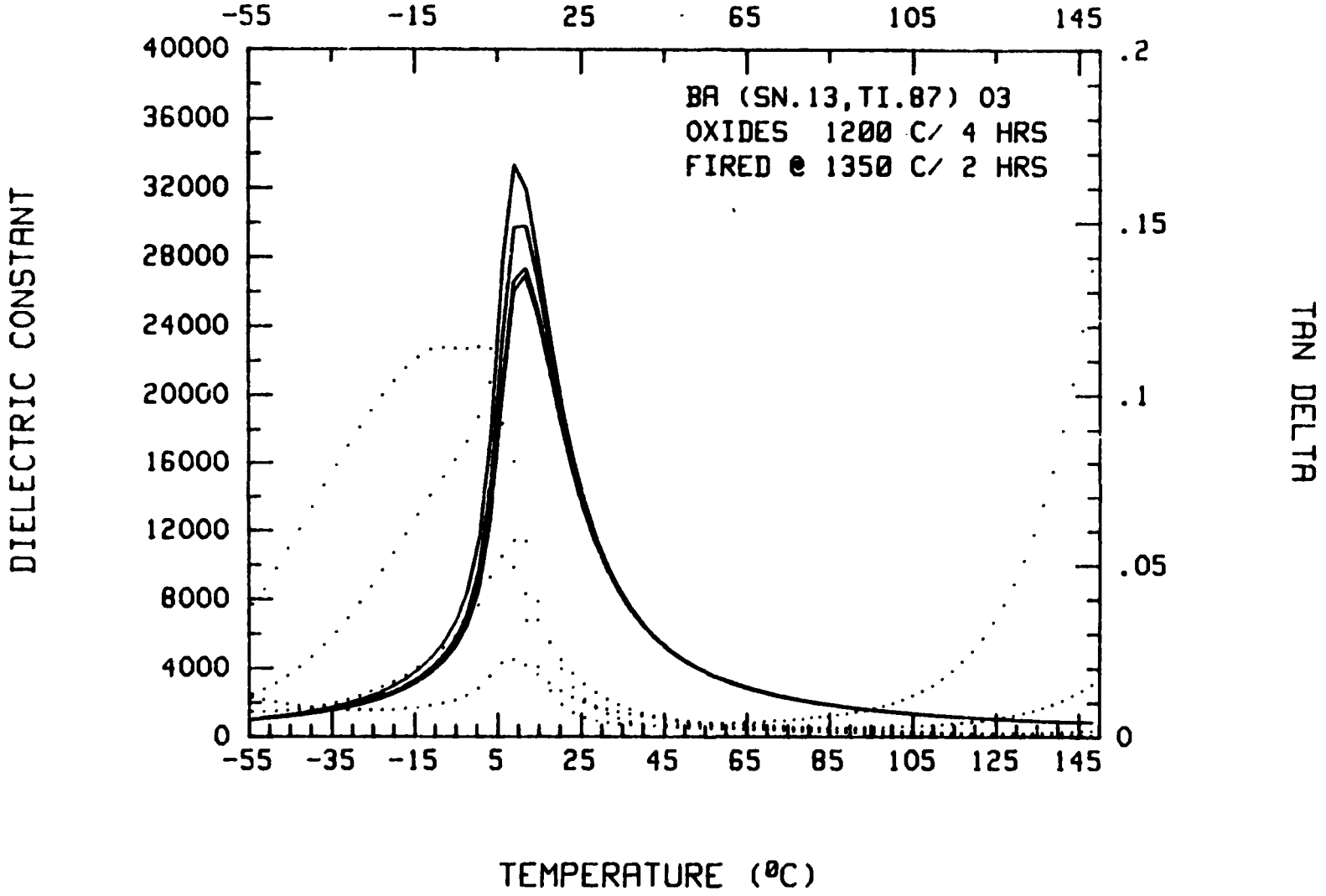
BA (SN.13,TI.87) 03
OXIDES 1200 C/ 4 HRS
FIRED @ 1350 C/ 2 HRS
DIELECTRIC CONSTANT
TAN DELTA
TEMPERATURE (ºC)
-55 -15 25 65 105 145
40000 36000 32000 28000 24000 20000 16000 12000 8000 4000 0
.2 .15 .1 .05 0
-55 -35 -15 5 25 45 65 85 105 125 145

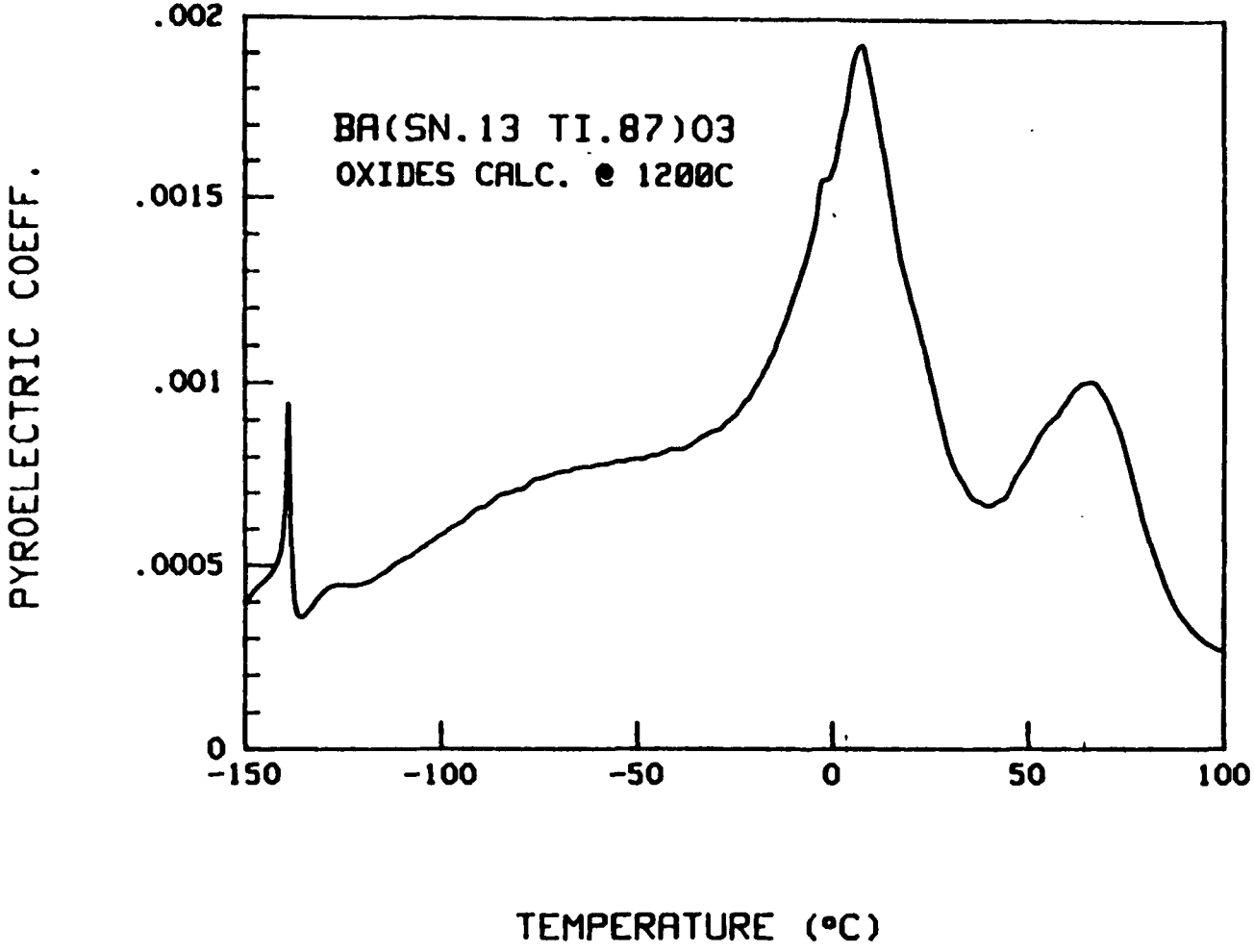
BA(SN.13 TI.87)03
OXIDES CALC. @ 1200C
PYROELECTRIC COEFF.
.002
.0015
.001
.0005
0
-150
-100
-50
0
50
100
TEMPERATURE (°C)

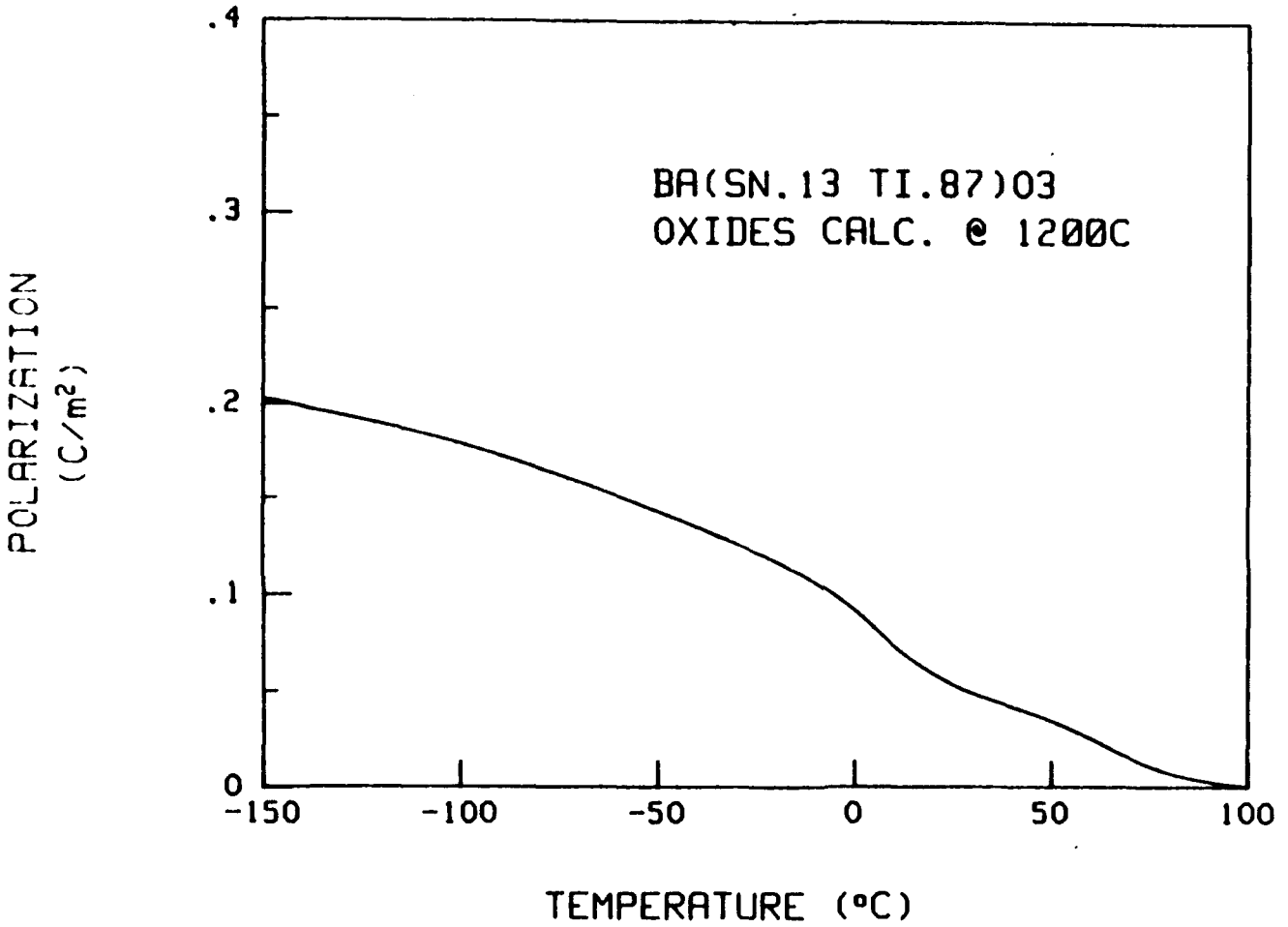
BA(SN.13 TI.87)03
OXIDES CALC. @ 1200C
POLARIZATION
(C/m²)
.4
.3
.2
.1
0
-150
-100
-50
0
50
100
TEMPERATURE (°C)

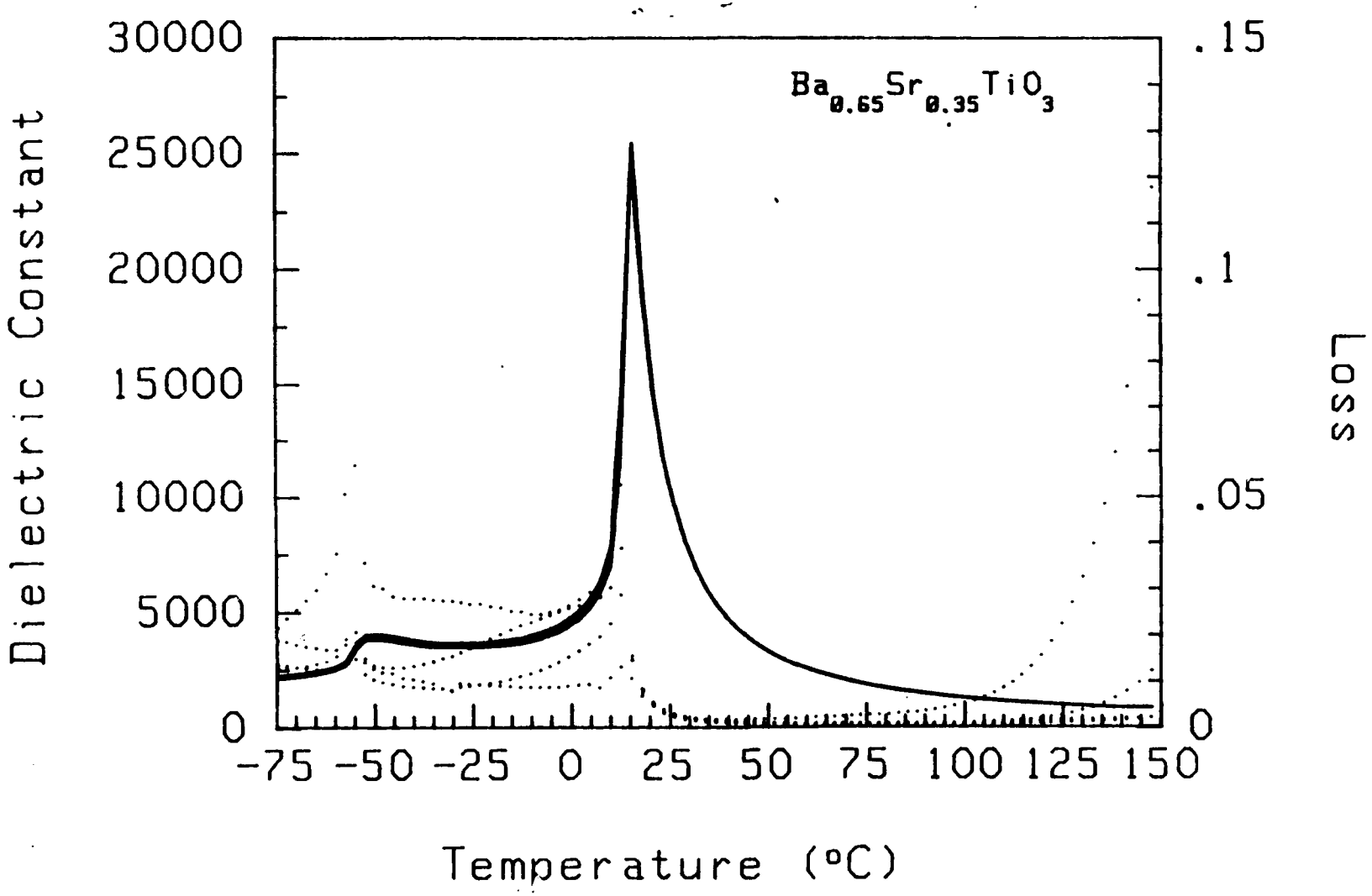
Ba0.65Sr0.35TiO3
Dielectric Constant
Loss
Temperature (°C)
30000
25000
20000
15000
10000
5000
0
.15
.1
.05
0
-75 -50 -25 0 25 50 75 100 125 150

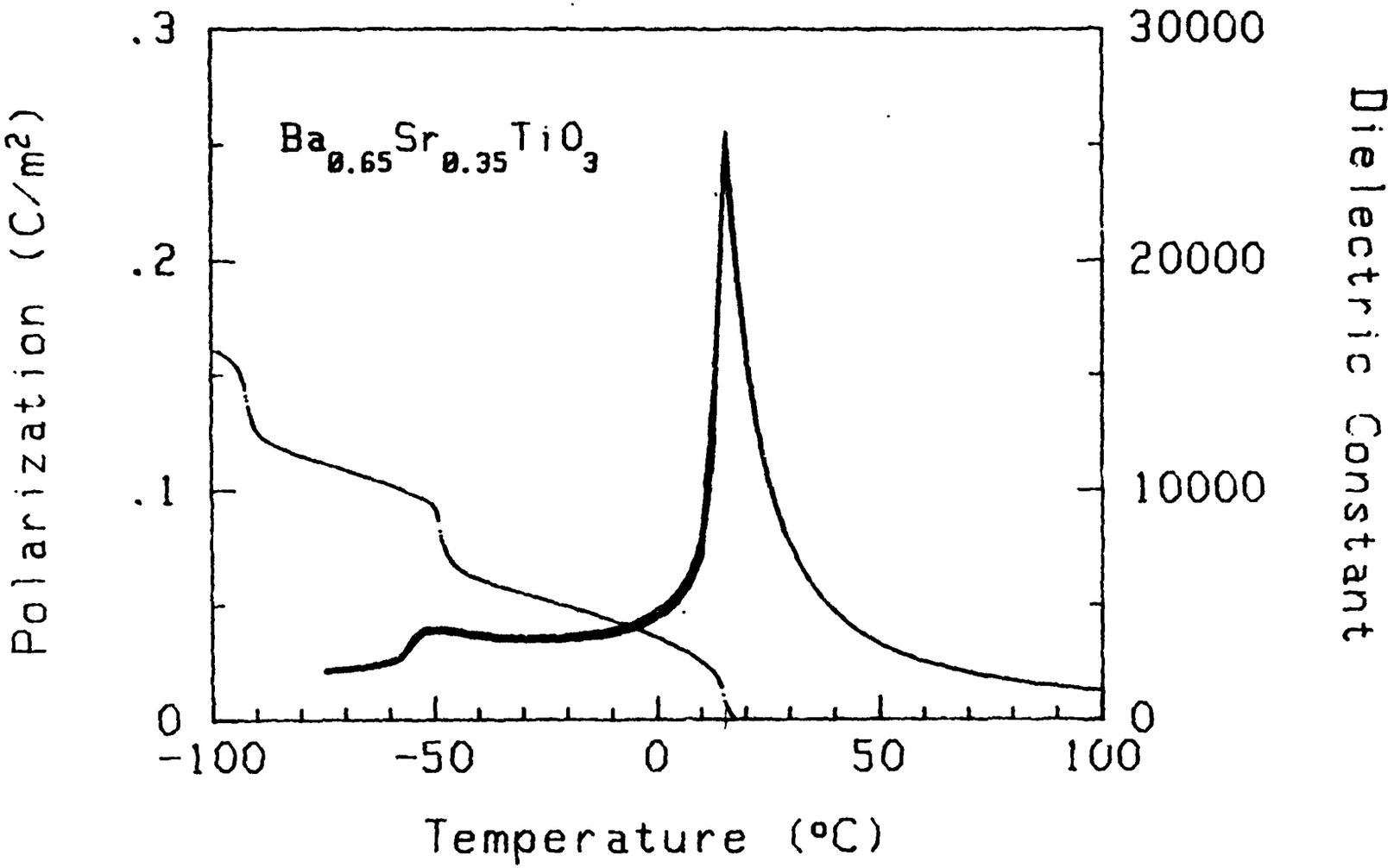
$Ba_{0.65}Sr_{0.35}TiO_3$
Polarization (C/m²)
Dielectric Constant
Temperature (°C)
.3
.2
.1
0
30000
20000
10000
0
-100
-50
0
50
100

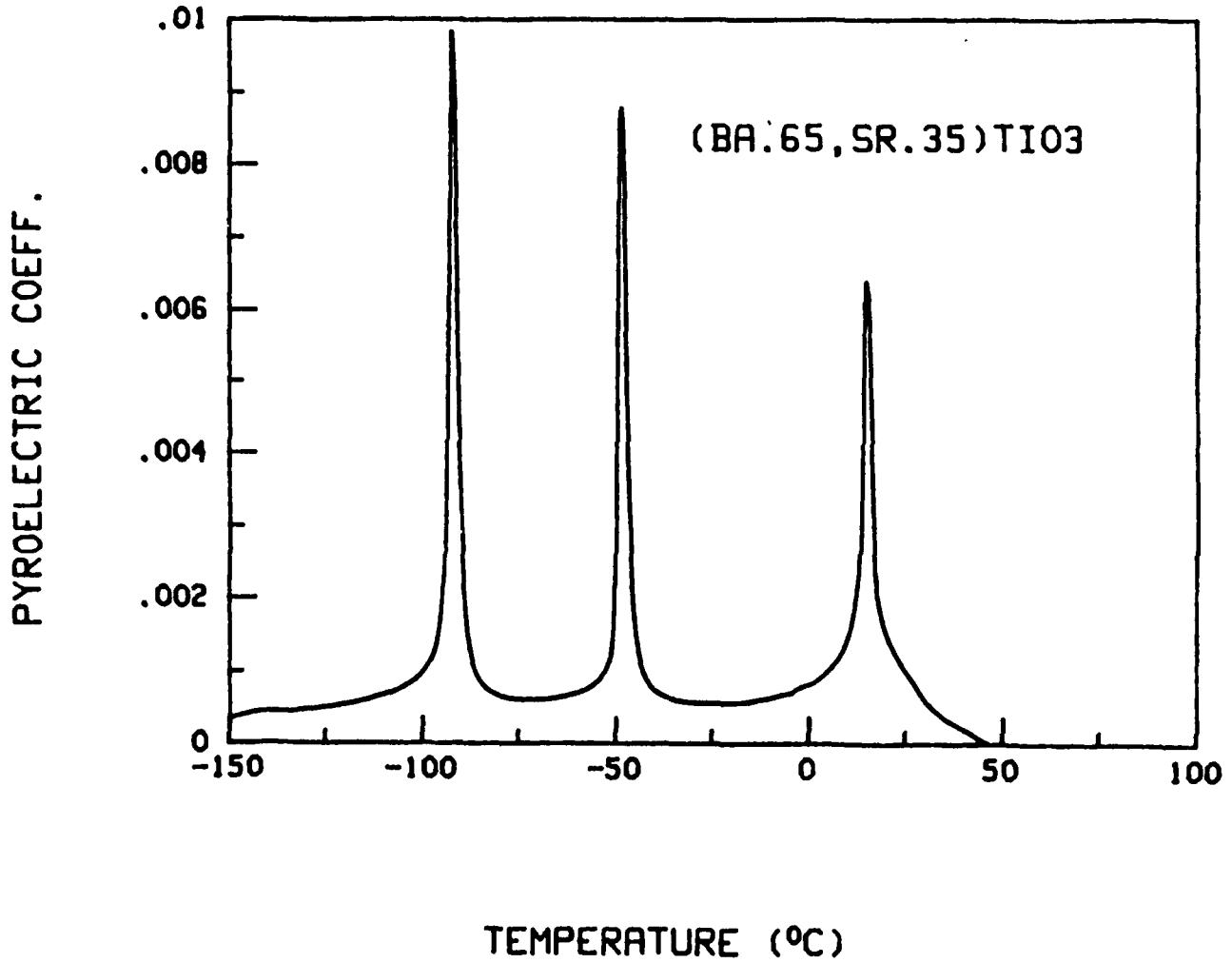
.01
.008
.006
.004
.002
0
PYROELECTRIC COEFF.
(BA.65,SR.35)TIO3
-150
-100
-50
0
50
100
TEMPERATURE (°C)

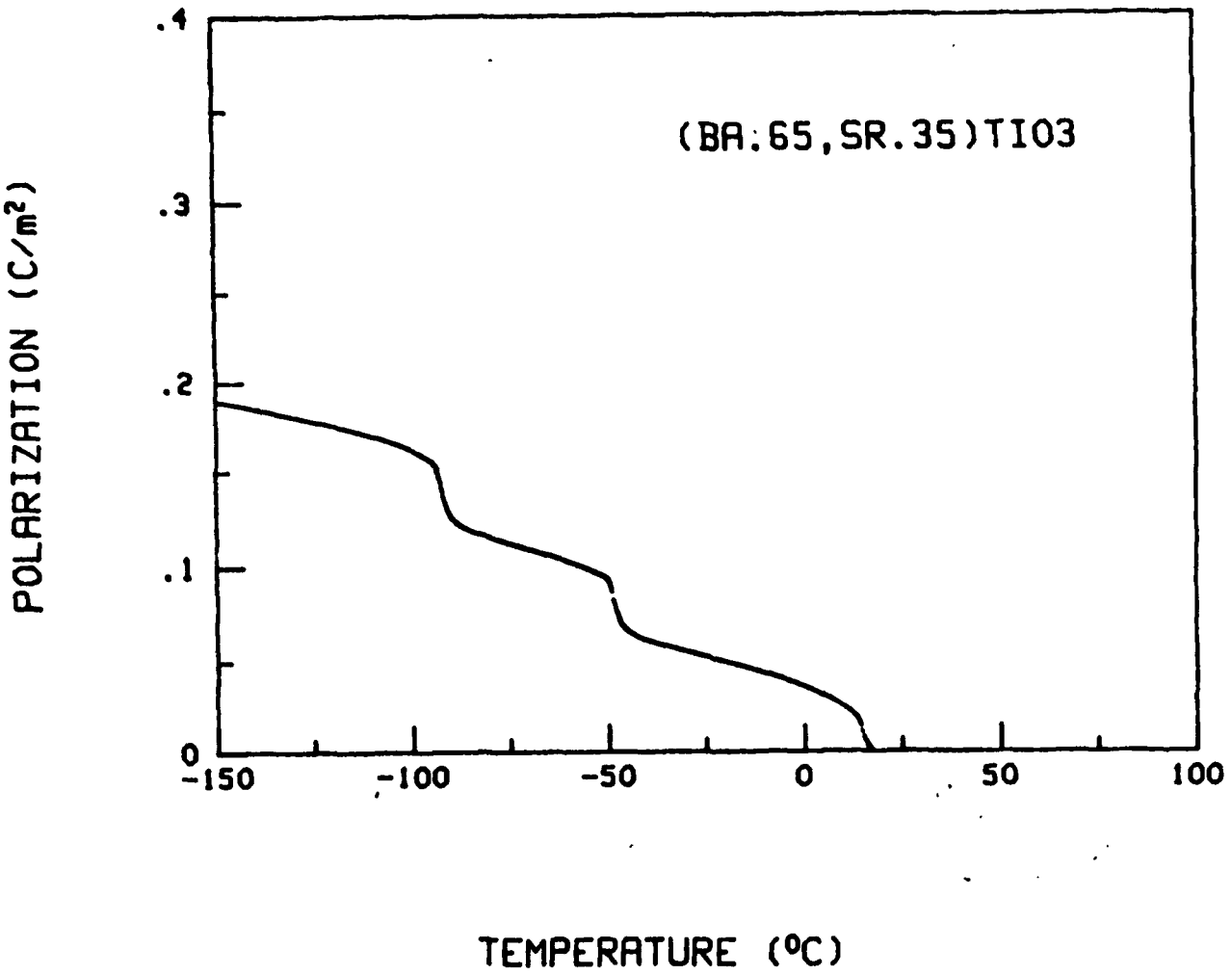
(BA:65,SR.35)TIO3
POLARIZATION (C/m²)
.4
.3
.2
.1
0
-150
-100
-50
0
50
100
TEMPERATURE (°C)

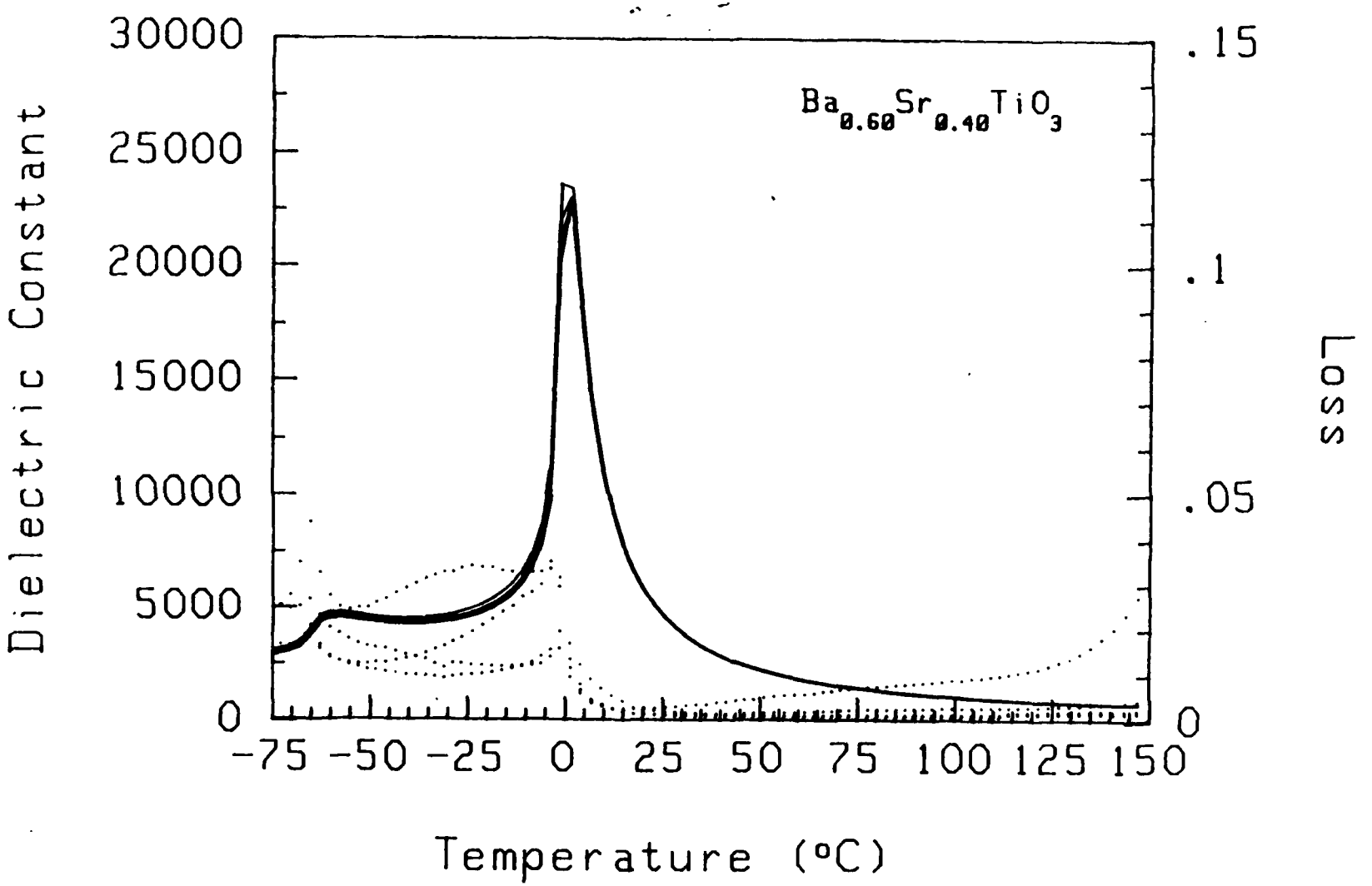
30000
25000
20000
15000
10000
5000
0
Dielectric Constant
.15
.1
.05
0
Loss
$Ba_{0.60}Sr_{0.40}TiO_3$
-75 -50 -25 0 25 50 75 100 125 150
Temperature (°C)

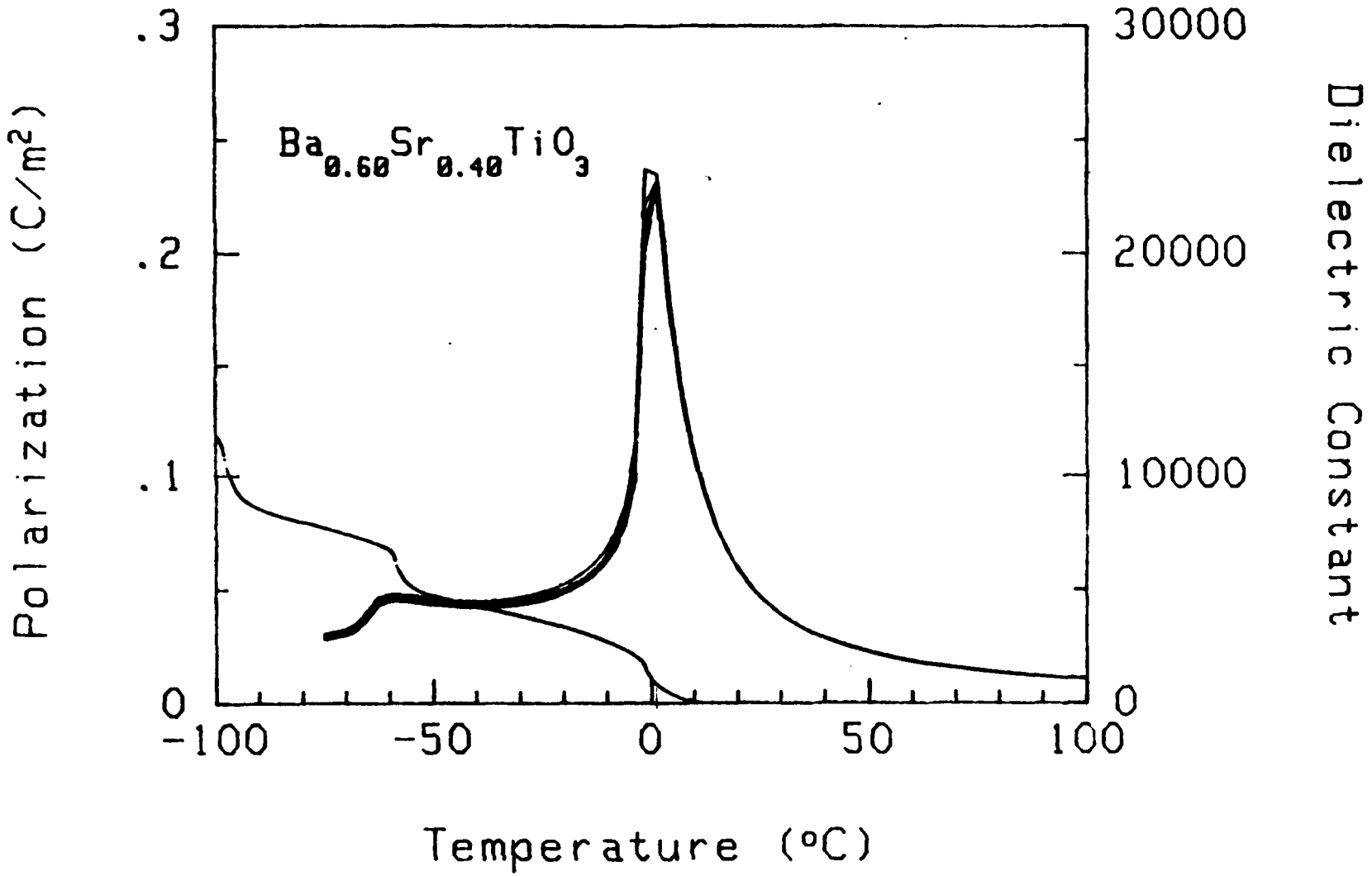
$Ba_{0.60}Sr_{0.40}TiO_3$
Polarization (C/m²)
.3
.2
.1
0
30000
20000
10000
0
Dielectric Constant
-100
-50
0
50
100
Temperature (°C)

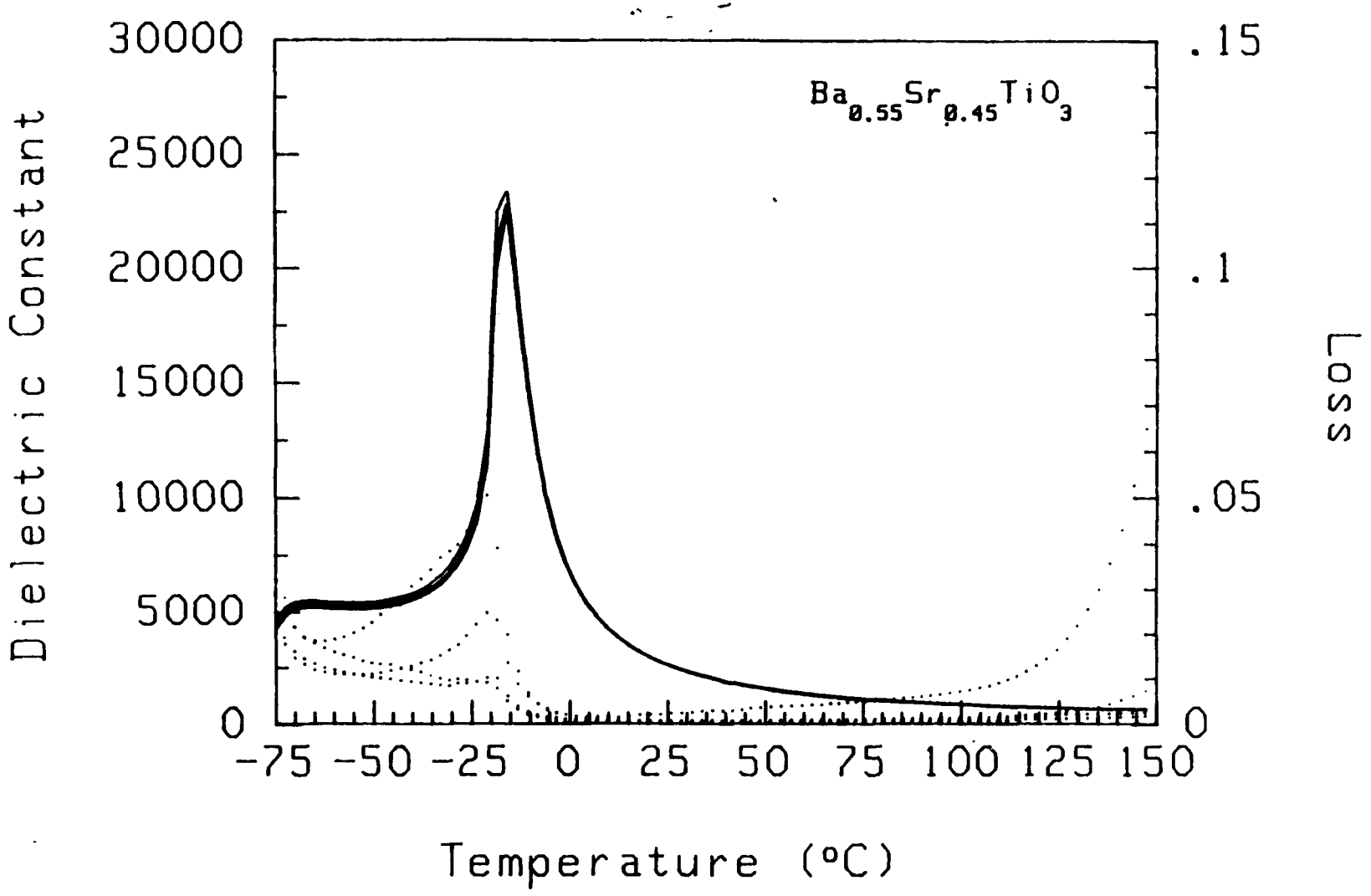
Ba0.55Sr0.45TiO3
Dielectric Constant
Loss
Temperature (°C)
30000
25000
20000
15000
10000
5000
0
.15
.1
.05
0
-75 -50 -25 0 25 50 75 100 125 150

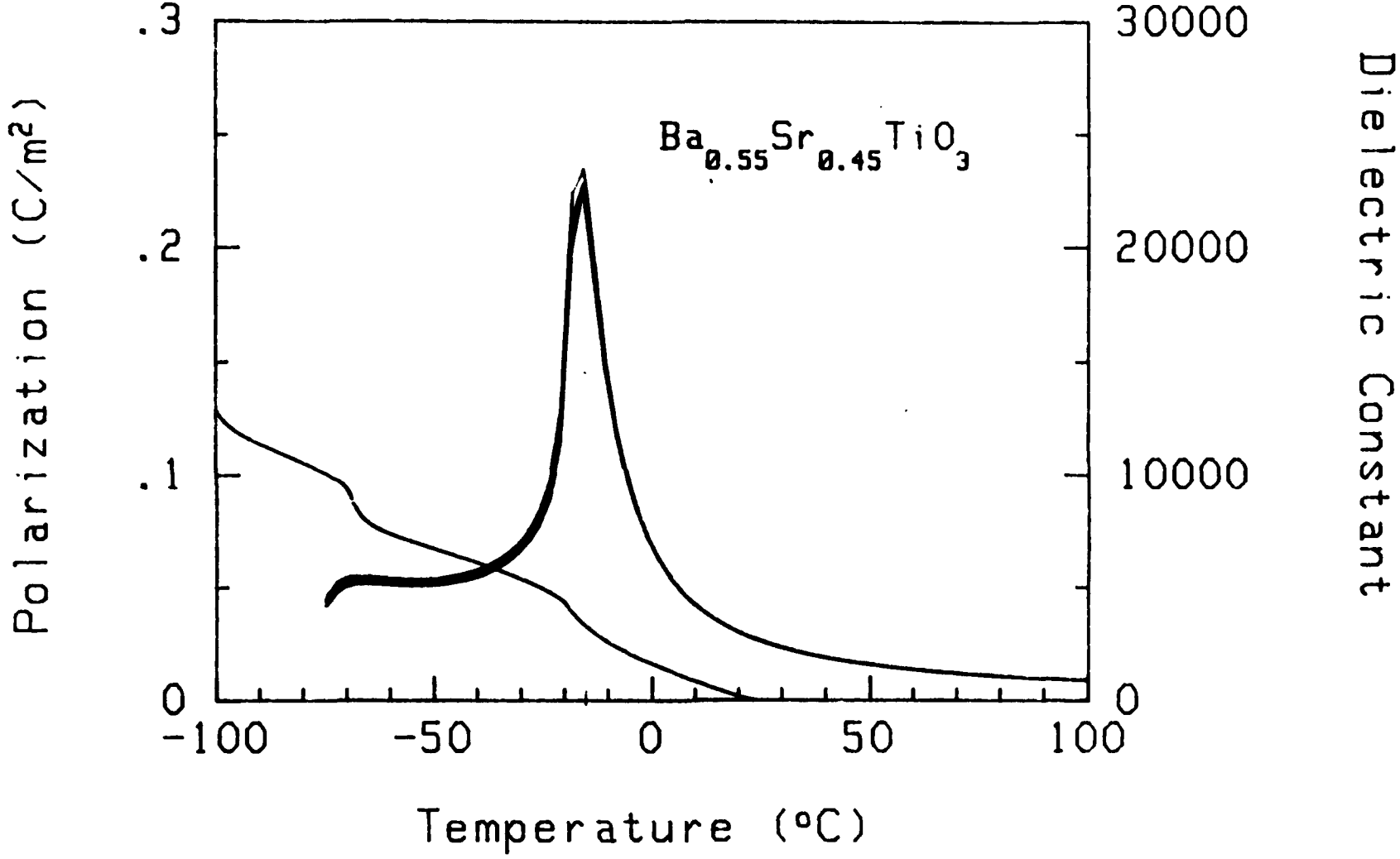
Ba0.55Sr0.45TiO3
Polarization (C/m²)
Dielectric Constant
.3
.2
.1
0
30000
20000
10000
0
-100
-50
0
50
100
Temperature (°C)

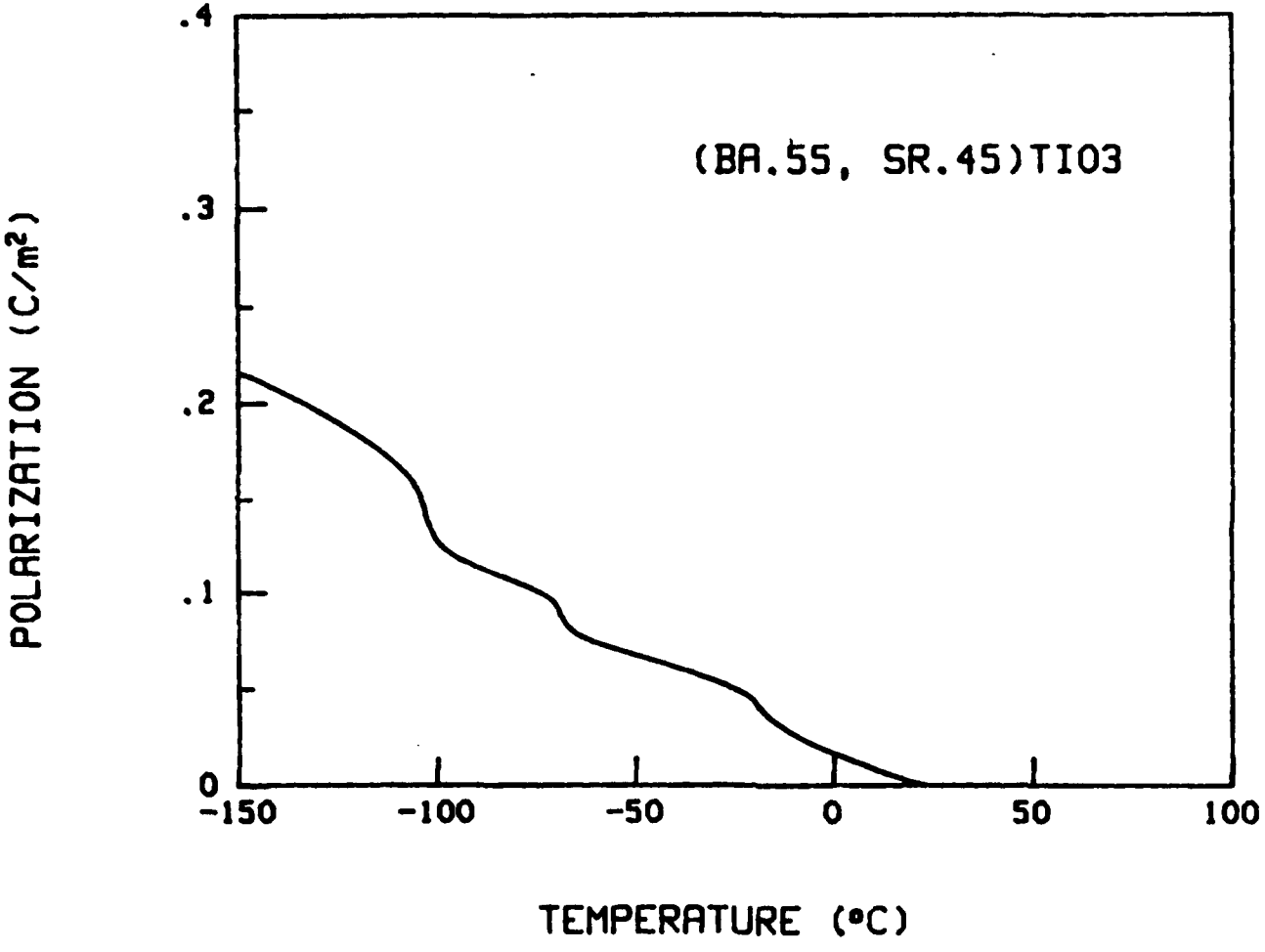
(BA.55, SR.45)TIO3
POLARIZATION (C/m²)
.4
.3
.2
.1
0
-150
-100
-50
0
50
100
TEMPERATURE (°C)

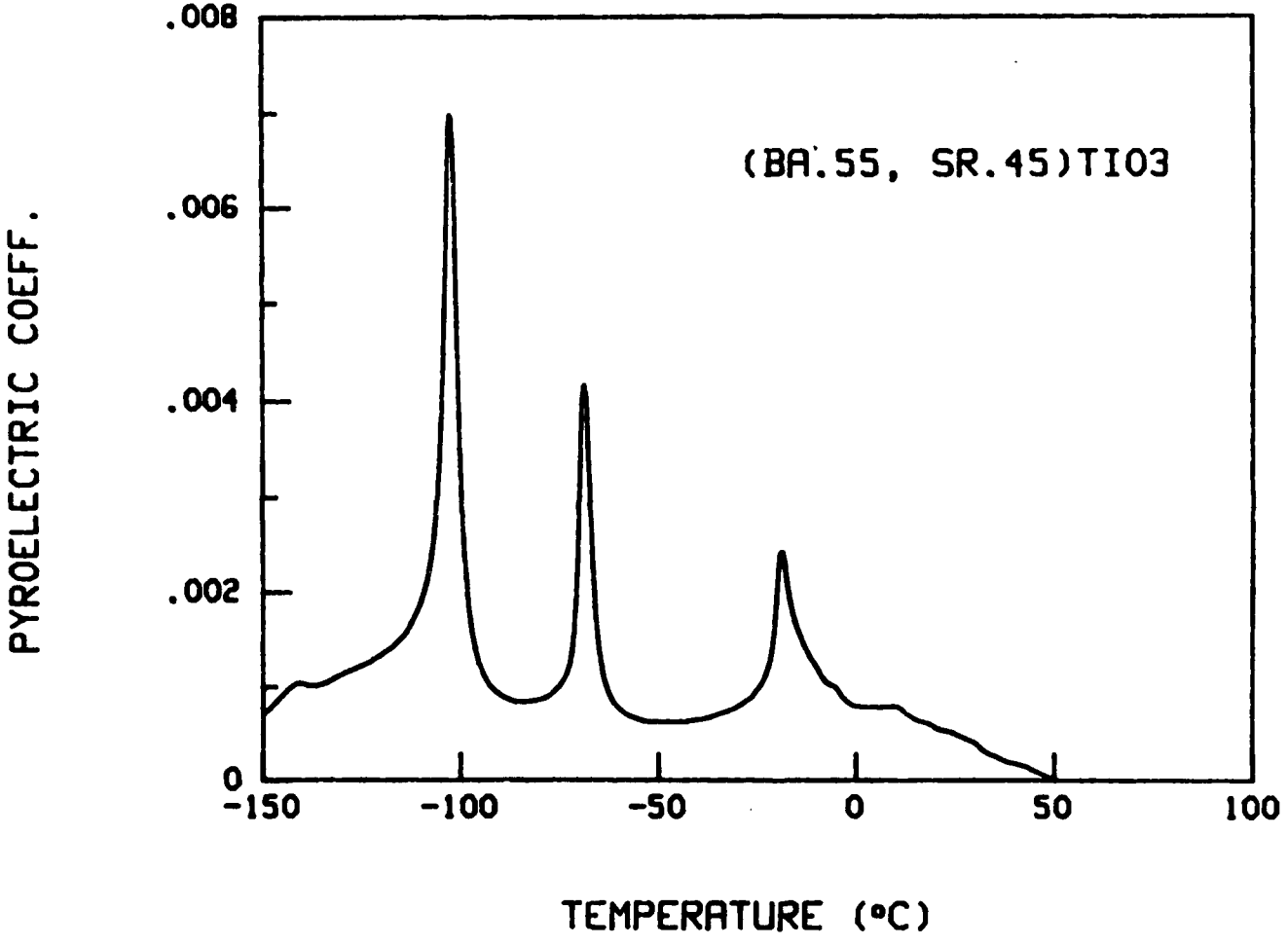
.008
.006
.004
.002
0
PYROELECTRIC COEFF.
(BA.55, SR.45)TIO3
-150
-100
-50
0
50
100
TEMPERATURE (°C)

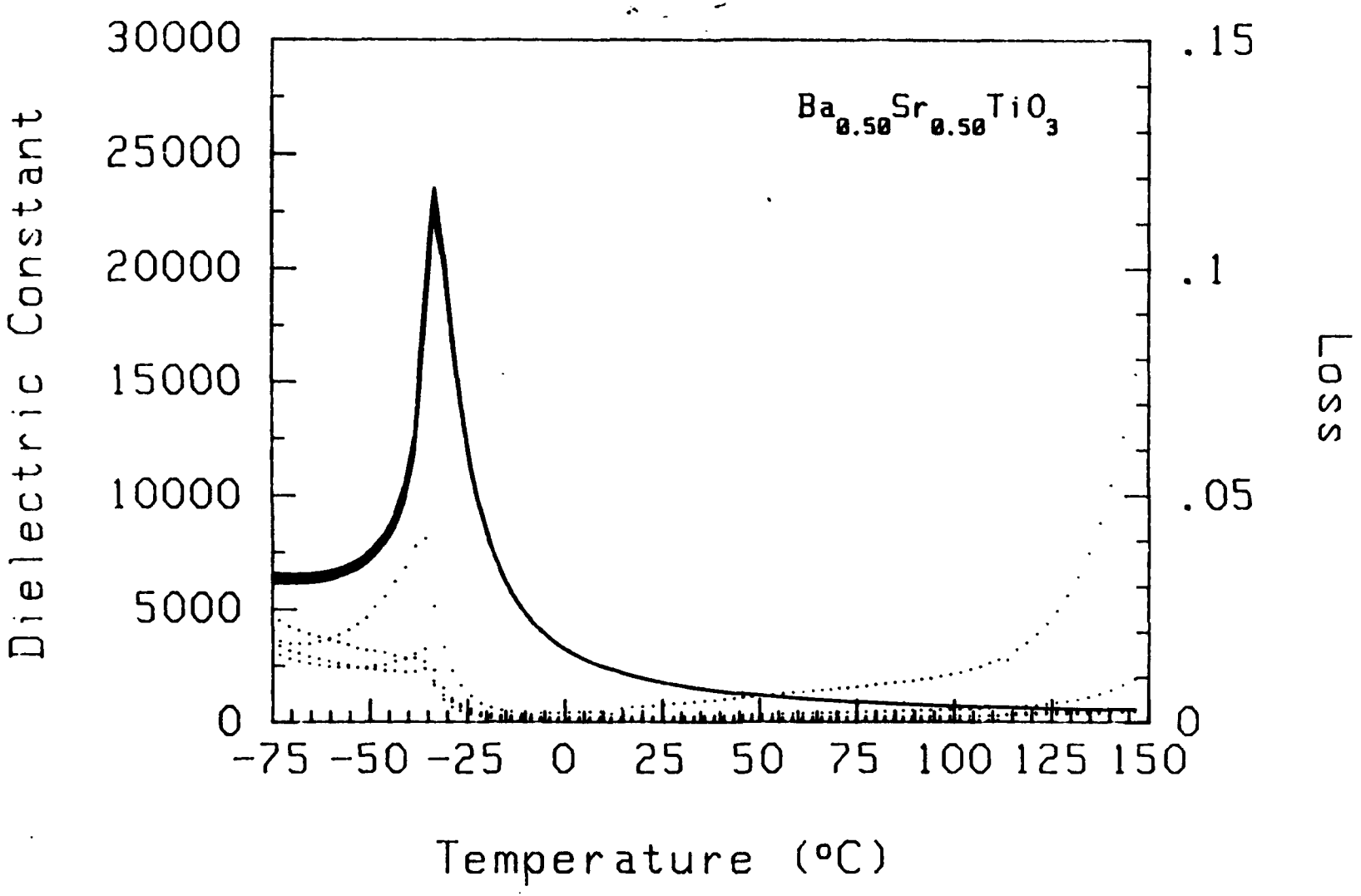
30000
25000
20000
15000
10000
5000
0
Dielectric Constant
.15
.1
.05
0
Loss
$Ba_{0.50}Sr_{0.50}TiO_3$
-75 -50 -25 0 25 50 75 100 125 150
Temperature (°C)

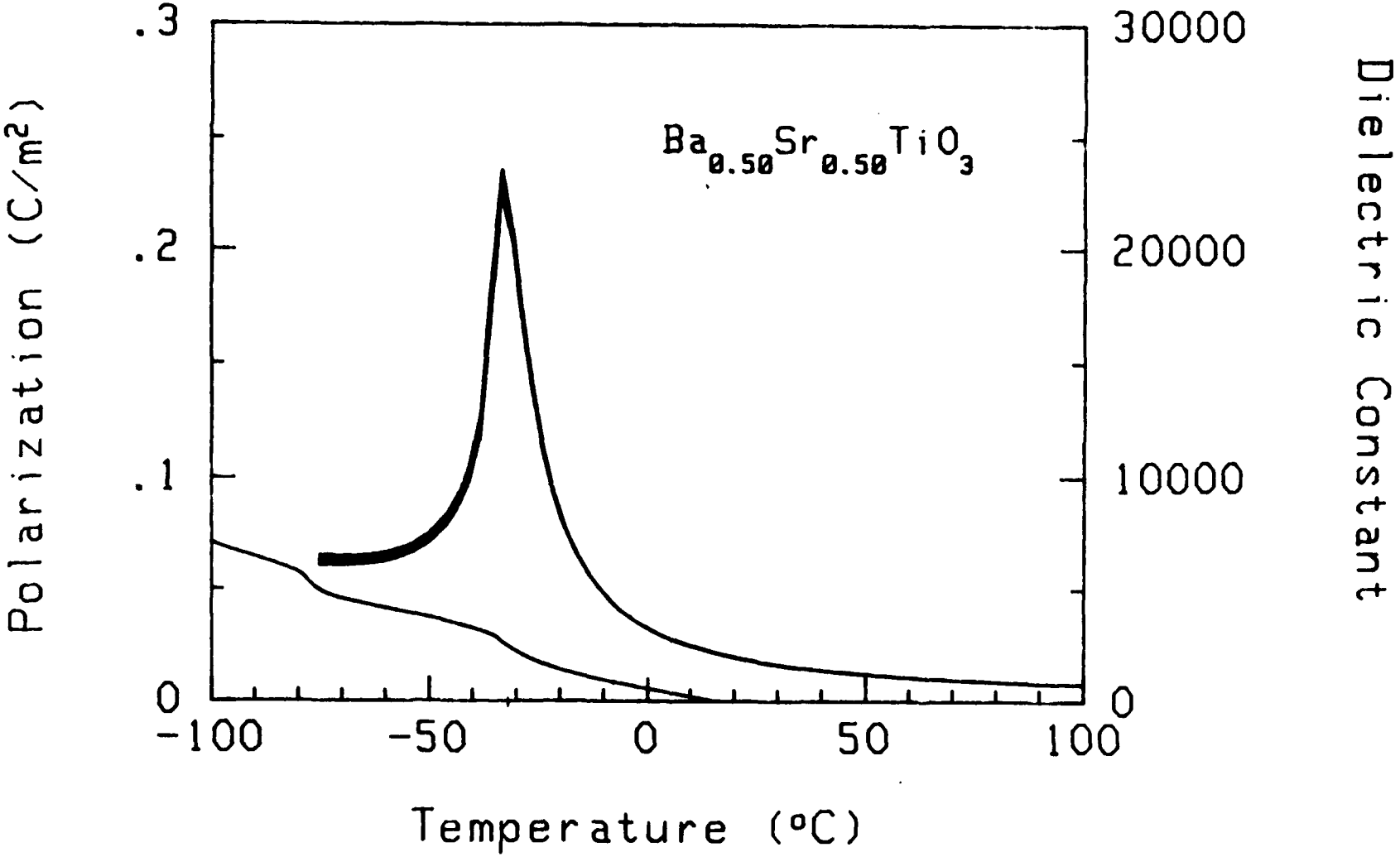
Polarization (C/m²)
.3
.2
.1
0
30000
20000
10000
0
Dielectric Constant
Ba0.50Sr0.50TiO3
-100
-50
0
50
100
Temperature (°C)

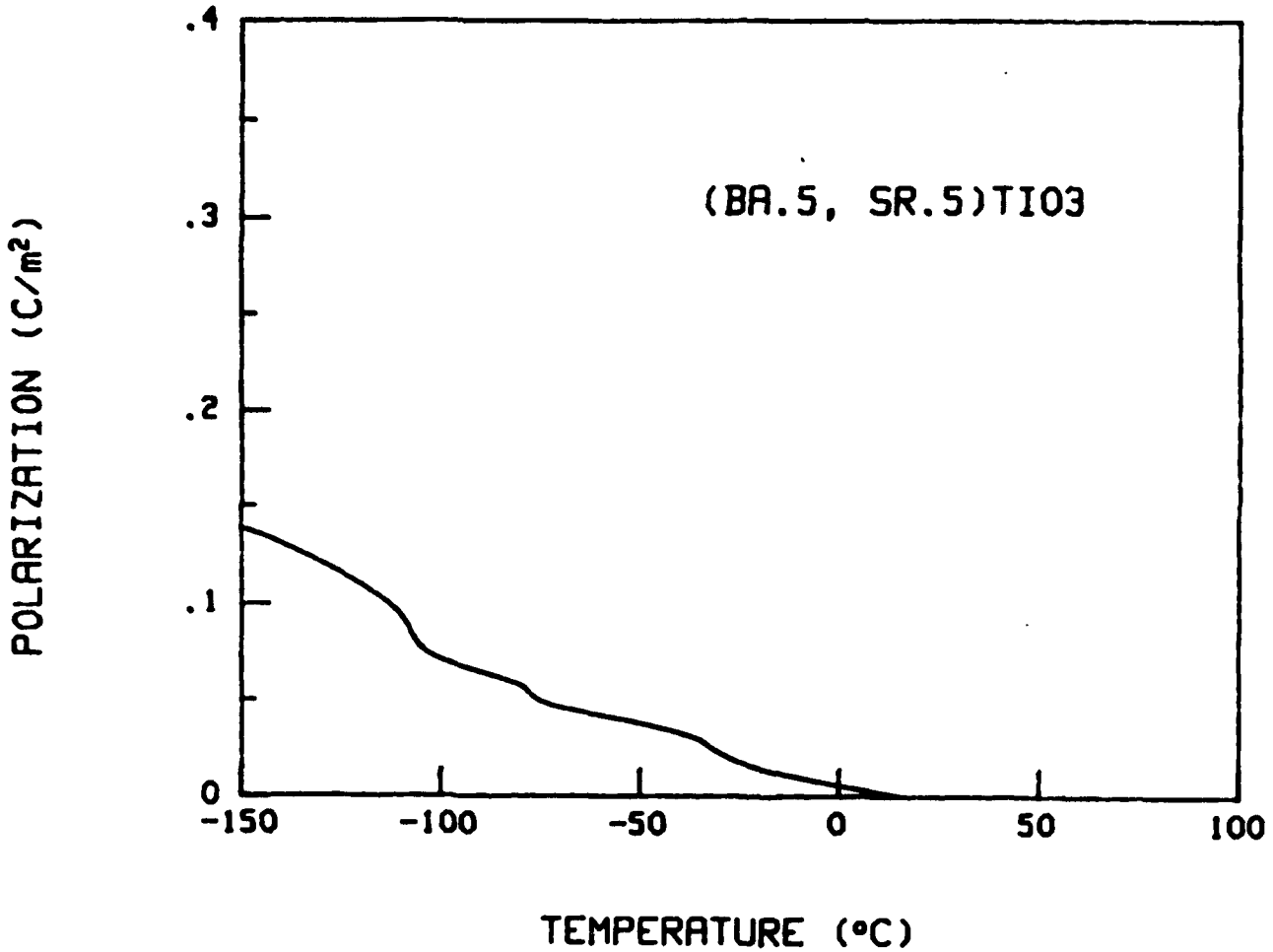
(BA.5, SR.5)TIO3
POLARIZATION (C/m²)
.4
.3
.2
.1
0
-150
-100
-50
0
50
100
TEMPERATURE (°C)

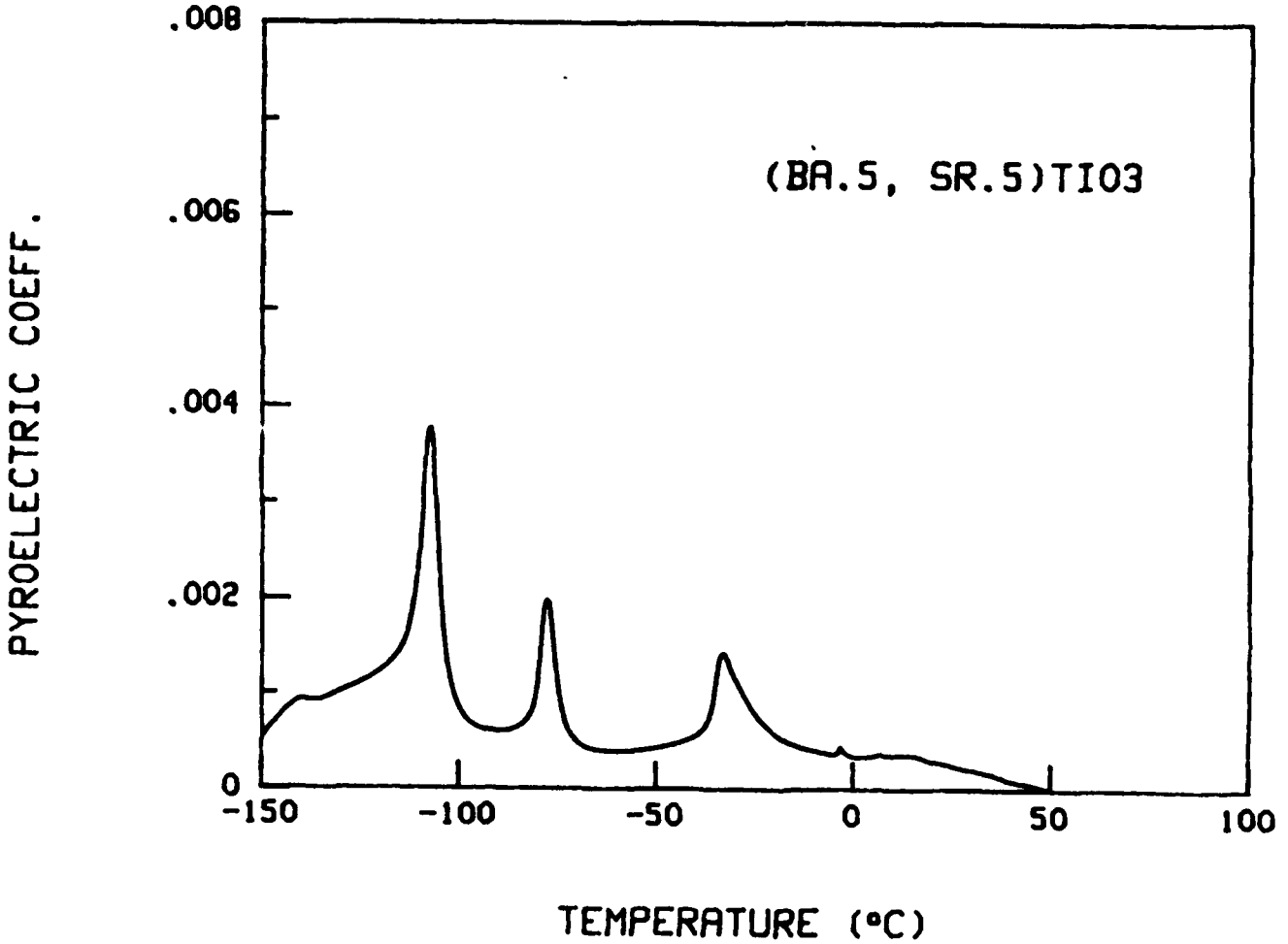
.008
.006
.004
.002
0
PYROELECTRIC COEFF.
(BA.5, SR.5)TIO3
-150
-100
-50
0
50
100
TEMPERATURE (°C)

Appendix B. Polarization/Strain Data.

Table B1. Induced polarization/transverse strain data for modified Type I relaxor PMN compositions.

Composition	Temp. (°C)	Polarization (C/m^2) 10 kV/cm	Polarization (C/m^2) 20 kV/cm	Transverse Strain ($x10^{-6}$) 10 kV/cm	Transverse Strain ($x10^{-6}$) 20 kV/cm	Hysteresis %
PMN-PT						
85/15	-28.5			323	419	11.5
	-10			269	358	9.8
97/3	33	0.11	0.175	55	165	11.4
	30	0.11	0.175	70	180	8.9
	10	0.13	0.198	80	195	14.5
	26			52	130	9.2
	-30			100	235	18.8
	-4	0.149	0.211			
	-8			95	240	17.3
	-9	0.152	0.221			
93/7	-8	0.205	0.234	320	420	10.2
	0	0.215	0.254	280	395	6.4
	35	0.185	0.234	215	345	5.8
	-3	0.238	0.268	315	415	9.2
	18	0.202	0.269	300	415	6.5
	23	0.225	0.269	270	380	6.4
95/5	-50	0.28	0.317			
	25	0.181	0.237			
	-17	0.225	0.293			
	0			184	267	8.1
	3	0.225	0.268	187	295	11.5
	-13			216	273	25.2
	-20.5	0.237	0.286			
	12	0.205	0.258			
	14			170	236	4.1
	26	0.142	0.206	117	201	4.3
	22			170	235	4.2
	21			184	237	4.4

Table B1. (cont'd).

La/PMN/PT 2/85/15	5	0.1797	0.2405	199	371	6.0
	25			152	307	3.4
	0			217	392	9.1
	-26			267	407	27.0
	19			136	282	
4/73/27	1.5	0.205	0.2474			
	26	0.1718	0.2295	223	403	2.6
	10.5	0.188	0.2346	291	470	7.5
	-4	0.2141	0.25			
	-27	0.234	0.2705			
	0			354	522	12.9
	-5			358	549	17.0
1/93/7	21	0.101	0.181	95	210	<1
	-32	0.176	0.243			
	-1	0.137	0.216			
	-10	0.141	0.210			
	-32	0.208	0.275			
	-29	0.208	0.265			
	22	0.134	0.204			
	24			95	215	<2
	-12			212	340	6.0
	1			135	270	3.0
	-27			248	366	8.5
	-19			263	324	34.0
Sr/PMN/PT 1/93/7	-43	0.216	0.26	235	380	15.9
	27	0.142	0.207	95	230	12.0
	4	0.180	0.236	156	325	17.1
	-8	0.190	0.243	190	335	13.5
	8	0.144	0.207	105	235	10.3

Table B2. Induced polarization/strain data for Type II relaxor PLZT (x/65/35).

Composition	Temp. (°C)	Polarization (C/m^2) 10 kV/cm	Polarization (C/m^2) 20 kV/cm	Transverse Strain ($x10^{-6}$) 10 kV/cm	Transverse Strain ($x10^{-6}$) 20 kV/cm	Hysteresis %
PLZT						
9/65/35	22	0.245		580		40.0
	20	0.226				
	17			540		50
	14			590		43.1
	12	0.255		610		53.2
	10	0.24		615		43.6
	6	0.245		690		53.3
	4			655		61.7
	1	0.248		670		67.1
	-36			940		80
	2			700		64.3
	26	0.238	0.297	433	725	23.9
	40	0.212	0.290	383	708	9.4
10/65/35	23	0.046	0.088	85	315	5.7
	4	0.053	0.101	110	380	8.2
	-16	0.056	0.109	130	460	13.6
11/65/35	24	0.171	0.207	190	315	2.3
	18	0.167	0.206	225	320	3.4
	13	0.181	0.208	220	350	4.3
	10	0.187	0.211	230	360	
	0	0.197	0.229	255	275	4.1
	-7			270	395	5.3

Table B3. Induced polarization/strain data for Type III "pinched" ferroelectric $Ba(Ti_{1-x}Sn_x)O_3$.

Composition $Ba(Ti_{1-x}Sn_x)O_3$	Temp. (°C)	Polarization (C/m^2) 10 kV/cm	Polarization (C/m^2) 20 kV/cm	Transverse Strain ($x10^{-6}$) 10 kV/cm	Transverse Strain ($x10^{-6}$) 20 kV/cm	Hysteresis %
x = 0.13	25	0.061	0.089	46.4	90	5.3
	-15	0.099	0.116	113	146	12.2
	-36			97	149	12.3
	-46	0.135	0.141	96	149	13.4
	-110			35	59	13.5
	-31	0.114	0.133			
	-59	0.110	0.137			
	-106	0.075	0.098			
x = 0.10	-40	0.118	0.146			
	-33	0.122	0.150			
	-26	0.124	0.144			
	-20	0.118	0.144			
	-6	0.106	0.134			
	1	0.106	0.132			
	30	0.106	0.128			
	40	0.089	0.115			
	45	0.085	0.111			
	-14	0.111	0.138	166	259	20.2
	5	0.108	0.132			
	24	0.079	0.094			
	-17			157	247	20.5
	-8			166	247	17.1
	1			158	247	17.5
	4			160	255	16.1
	24			159	241	12.5
	36			112	176	8.9
	43			85.3	143	6.1
	50			50	100	<1
	52			61	116	<1
	-36			177	278	39.5
	6			155	243	16.2
	21			133	215	9.5

Table B4. Induced polarization/strain data for Type IV ferroelectric $(Ba_{1-x}Sr_x)TiO_3$..

Composition	Temp. (°C)	Polarization (C/m^2) 10 kV/cm	Polarization (C/m^2) 20 kV/cm	Transverse Strain ($x10^{-6}$) 10 kV/cm	Transverse Strain ($x10^{-6}$) 20 kV/cm	Hysteresis %
$Ba_{1-x}Sr_xTiO_3$						
x = 0.35	26	0.055	0.082	55	115	<1
	23			64	129	<1
	14	0.079	0.1012	106	170	6.7
	10			152	226	9.8
	6			154	280	9.9
	4	0.0859	0.1051			
	-2	0.092	0.1077			
	-43	0.118	0.143	300	484	22.8
	-50			294	495	33.0
	-58			230	350	20.7
	-64	0.125	0.148	198	276	9.9
x = 0.45	22	0.027	0.046	8.5	23	<1
	-8	0.078	0.105			
	-12	0.100	0.118			
	-24	0.107	0.135			
	-29	0.115	0.143			
	-36	0.120	0.150	189	310	13.9
	-78	0.165	0.188	212	344	22.5
	-88	0.172	0.193			
	-74			175	270	14.6
	-32			187	304	11.0
	-3			30	70	2.4
	-18			160	235	12.1
x = 0.50	22	0.016	0.032			
	10	0.021	0.037			
	-12	0.036	0.064			
	-16	0.047	0.071			
	-22	0.049	0.077			
	-46	0.093	0.116			
	-52	0.110	0.137			
	-47			134	226	11.6
	-51			142	235	7.5

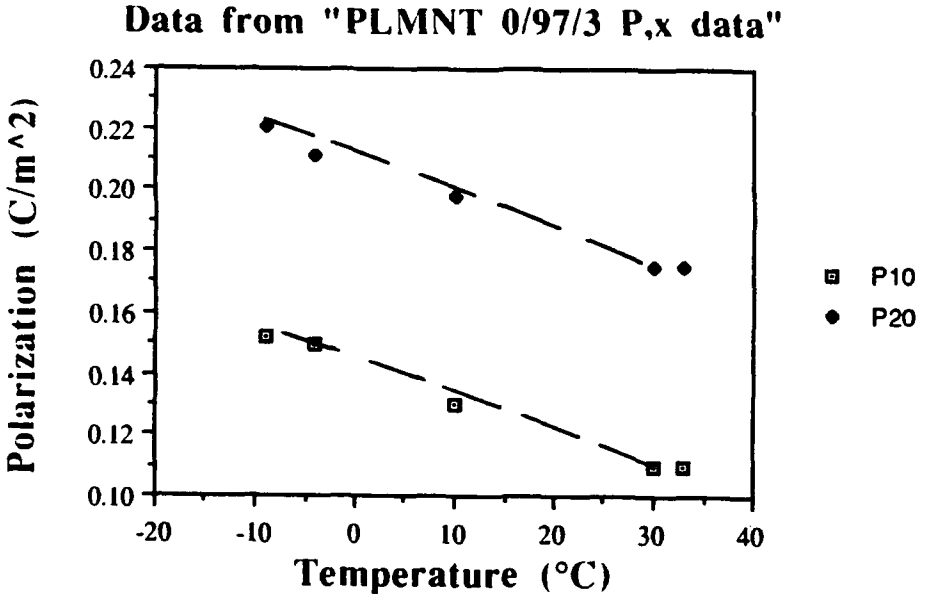
Data from "PLMNT 0/97/3 P,x data"
Polarization (C/m^2)
0.24
0.22
0.20
0.18
0.16
0.14
0.12
0.10
-20
-10
0
10
20
30
40
Temperature (°C)
P10
P20

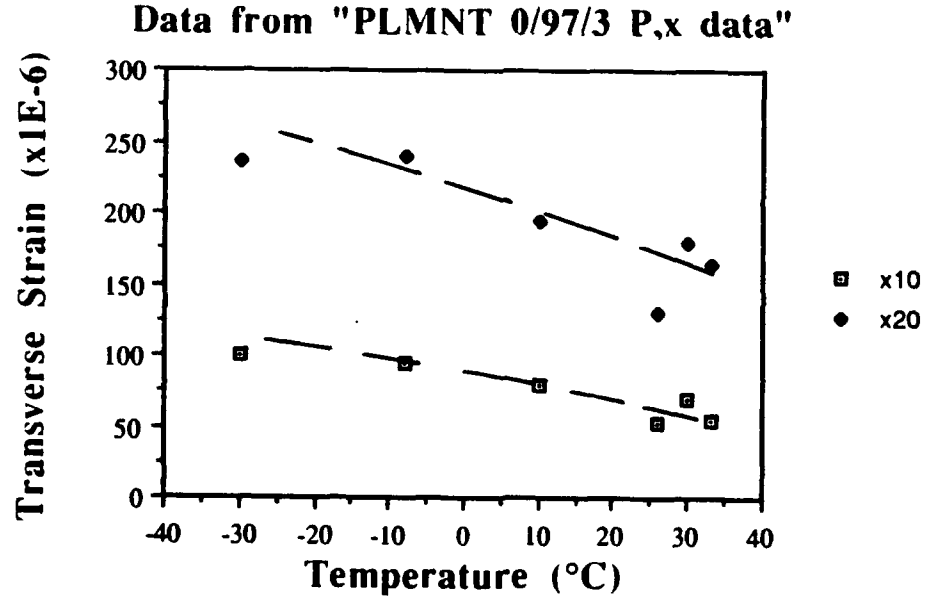
Data from "PLMNT 0/97/3 P,x data"
Transverse Strain (x1E-6)
300
250
200
150
100
50
0
-40
-30
-20
-10
0
10
20
30
40
Temperature (°C)
x10
x20

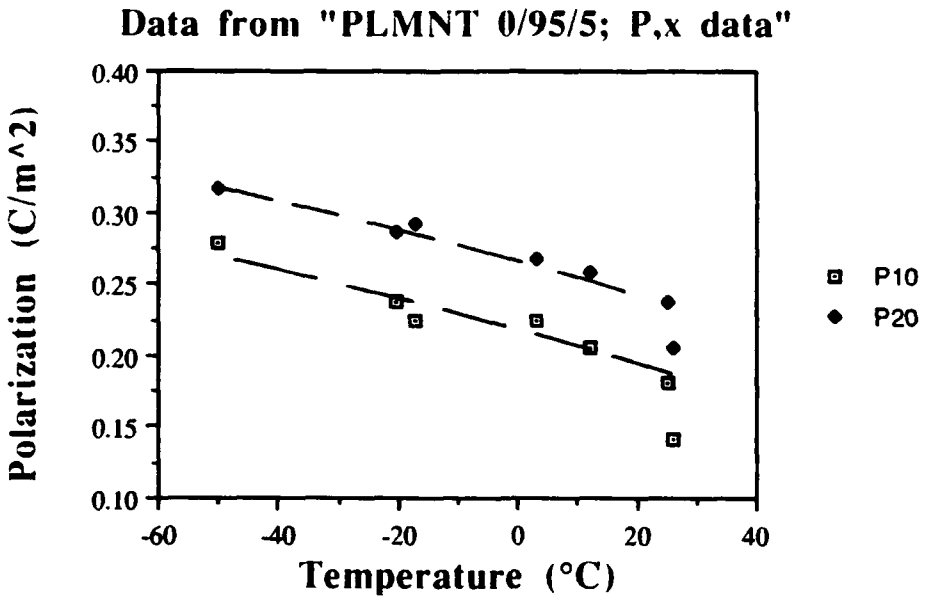
Data from "PLMNT 0/95/5; P,x data"
Polarization (C/m^2)
0.40
0.35
0.30
0.25
0.20
0.15
0.10
-60
-40
-20
0
20
40
Temperature (°C)
P10
P20

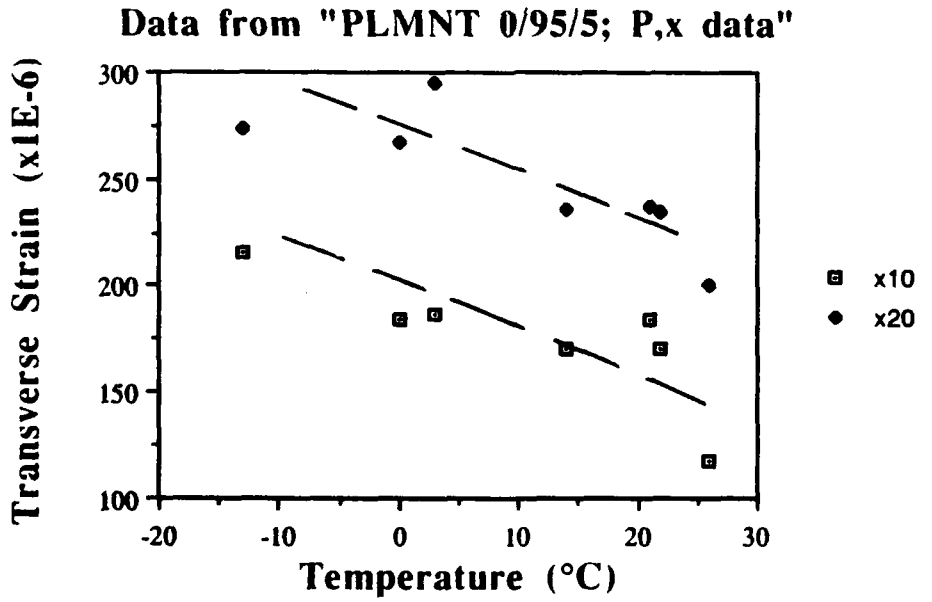
Data from "PLMNT 0/95/5; P,x data"
Transverse Strain (x1E-6)
300
250
200
150
100
-20
-10
0
10
20
30
Temperature (°C)
x10
x20

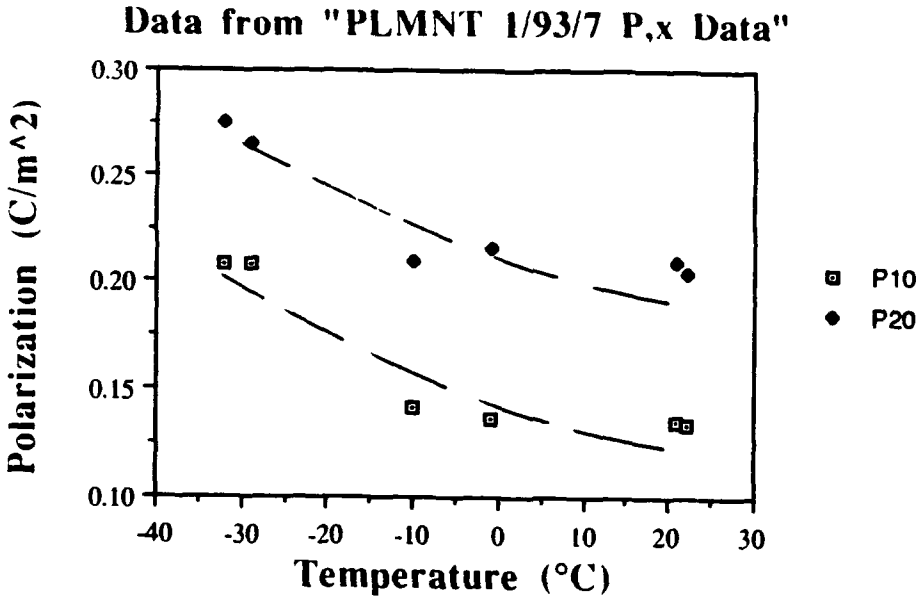
Data from "PLMNT 1/93/7 P,x Data"
Polarization (C/m^2)
0.30
0.25
0.20
0.15
0.10
-40
-30
-20
-10
0
10
20
30
Temperature (°C)
P10
P20

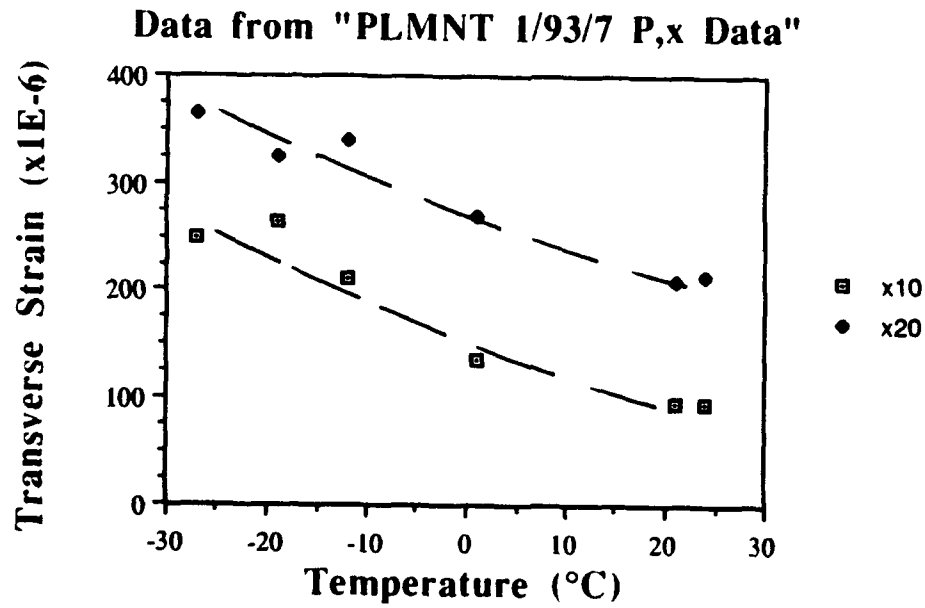
Data from "PLMNT 1/93/7 P,x Data"
Transverse Strain (x1E-6)
400
300
200
100
0
-30
-20
-10
0
10
20
30
Temperature (°C)
x10
x20

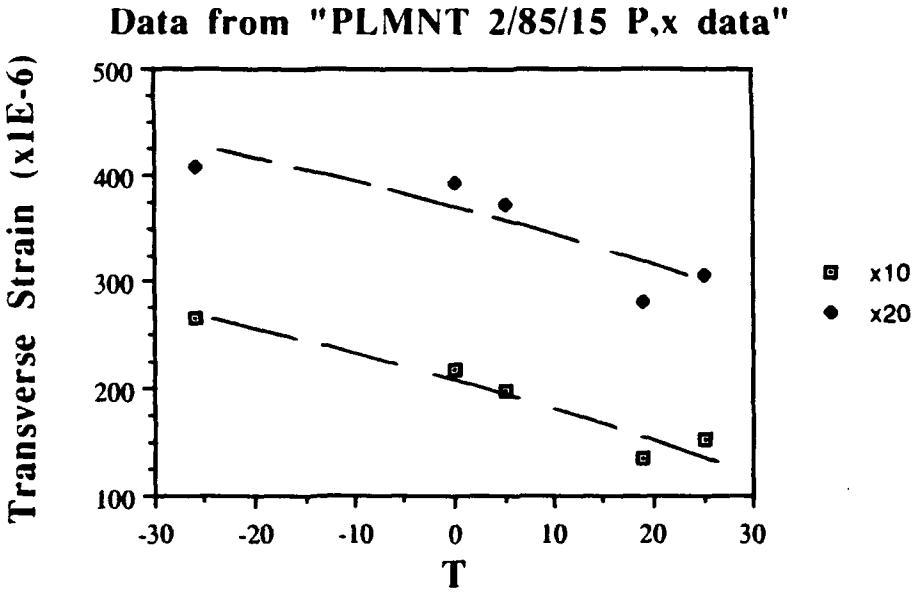
Data from "PLMNT 2/85/15 P,x data"
Transverse Strain (x1E-6)
500
400
300
200
100
-30
-20
-10
0
10
20
30
T
x10
x20

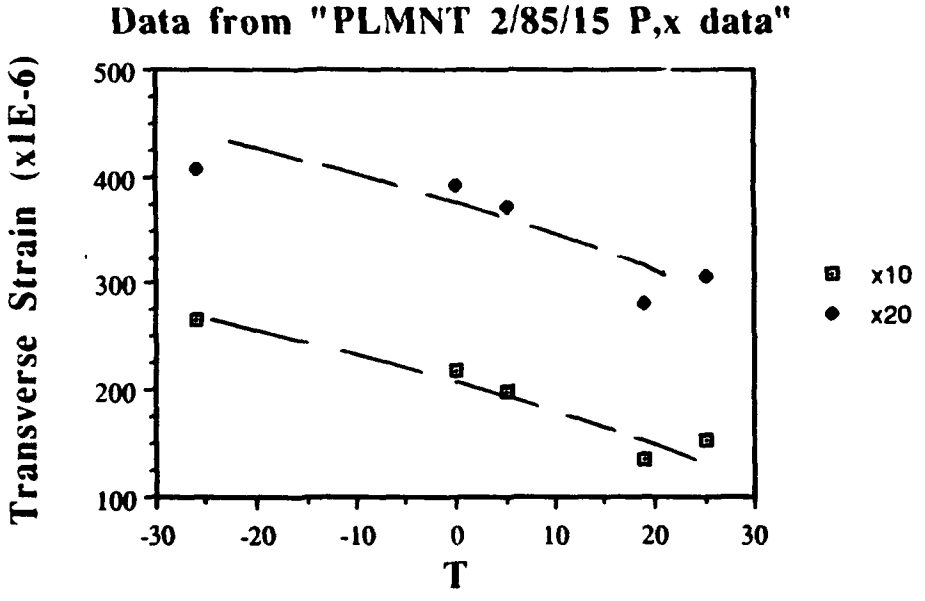
Data from "PLMNT 2/85/15 P,x data"
Transverse Strain (x1E-6)
500
400
300
200
100
-30
-20
-10
0
10
20
30
T
x10
x20

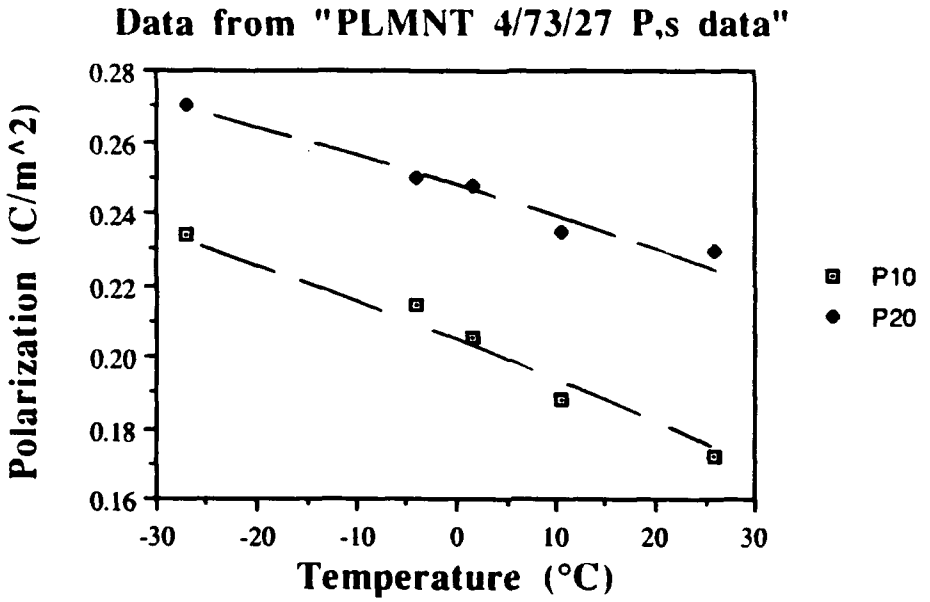
Data from "PLMNT 4/73/27 P,s data"
Polarization (C/m^2)
0.28
0.26
0.24
0.22
0.20
0.18
0.16
-30
-20
-10
0
10
20
30
Temperature (°C)
P10
P20

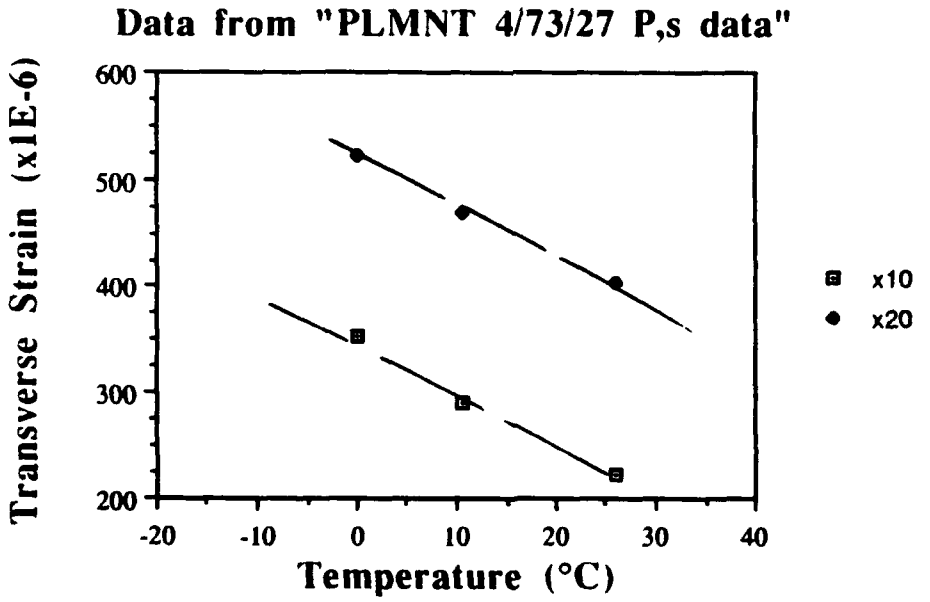
Data from "PLMNT 4/73/27 P,s data"
Transverse Strain (x1E-6)
600
500
400
300
200
-20
-10
0
10
20
30
40
Temperature (°C)
x10
x20

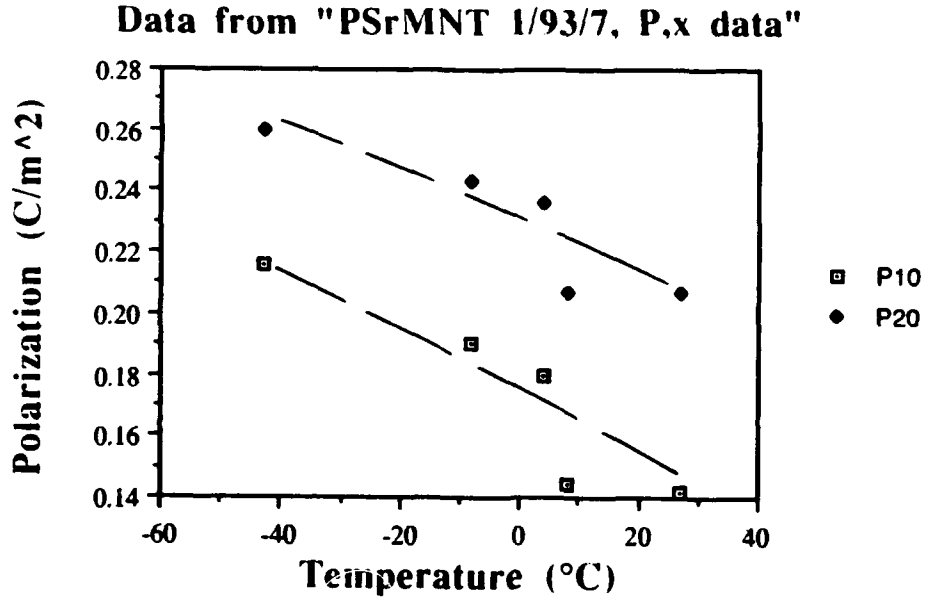
Data from "PSrMNT 1/93/7, P,x data"
Polarization (C/m^2)
0.28
0.26
0.24
0.22
0.20
0.18
0.16
0.14
-60
-40
-20
0
20
40
Temperature (°C)
P10
P20

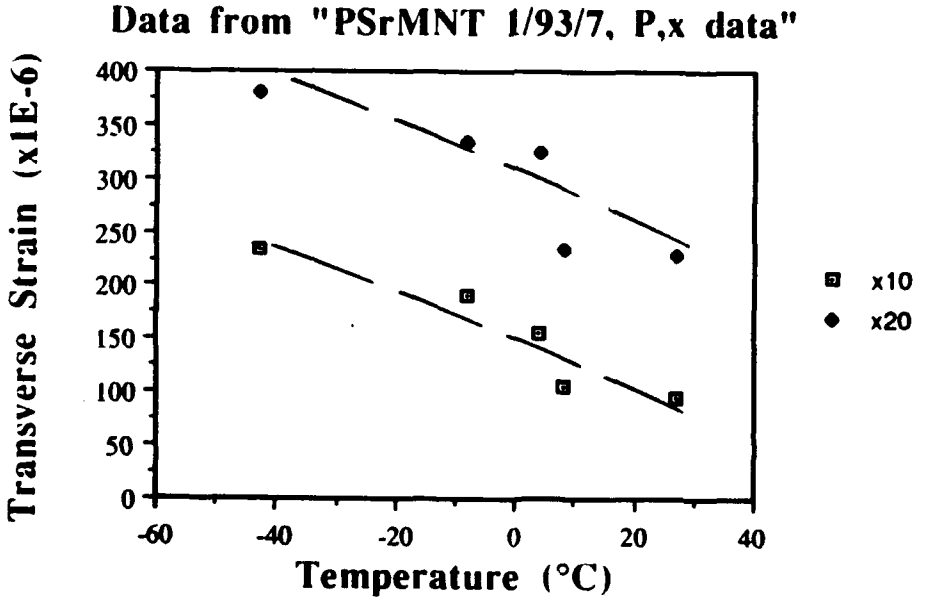
Data from "PSrMNT 1/93/7, P,x data"
Transverse Strain (x1E-6)
400
350
300
250
200
150
100
50
0
-60
-40
-20
0
20
40
Temperature (°C)
x10
x20

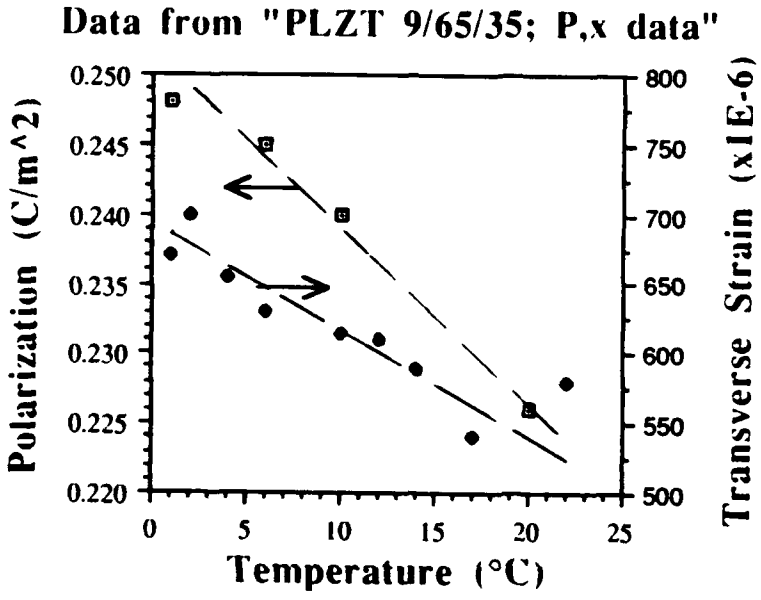
Data from "PLZT 9/65/35; P,x data"
Polarization (C/m^2)
0.250
0.245
0.240
0.235
0.230
0.225
0.220
Transverse Strain (x1E-6)
800
750
700
650
600
550
500
0
5
10
15
20
25
Temperature (°C)

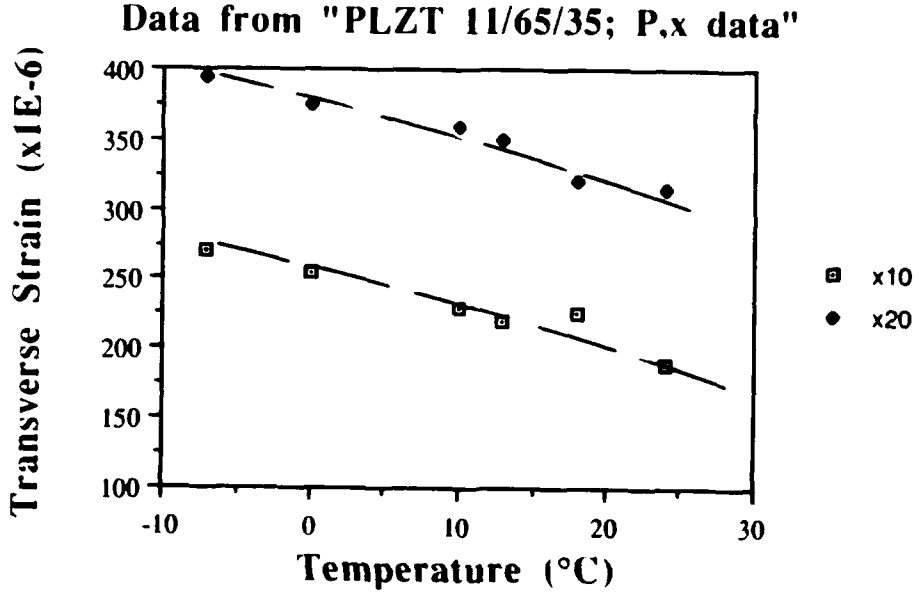
Data from "PLZT 11/65/35; P,x data"
Transverse Strain (x1E-6)
400
350
300
250
200
150
100
-10
0
10
20
30
Temperature (°C)
x10
x20

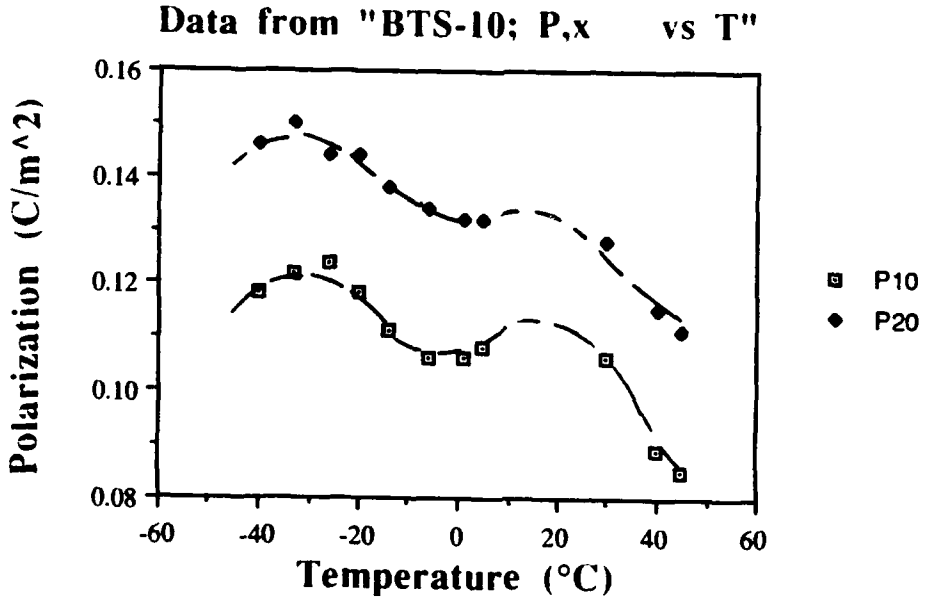
Data from "BTS-10; P,x vs T"
Polarization (C/m^2)
0.16
0.14
0.12
0.10
0.08
-60
-40
-20
0
20
40
60
Temperature (°C)
P10
P20

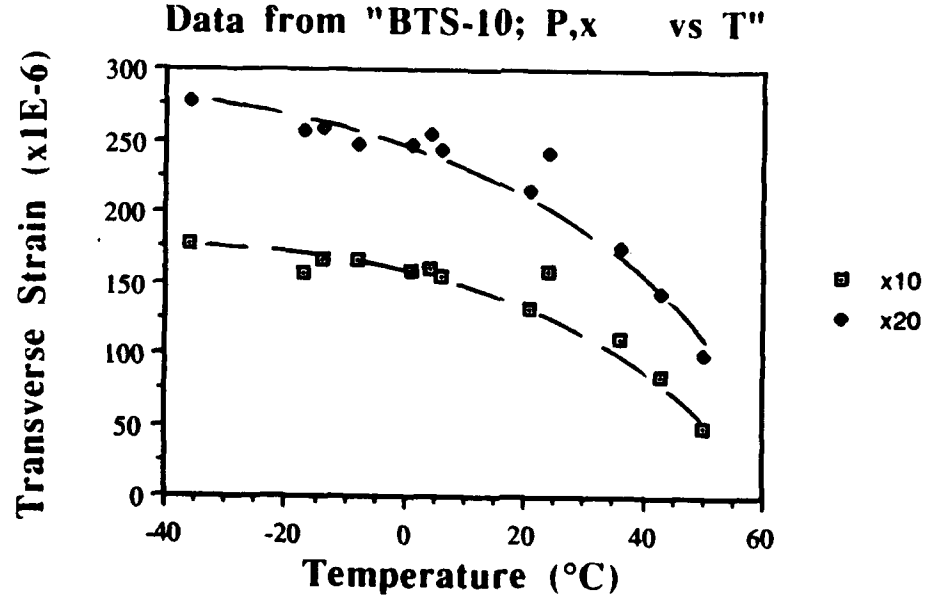
Data from "BTS-10; P,x vs T"
Transverse Strain (x1E-6)
300
250
200
150
100
50
0
-40
-20
0
20
40
60
Temperature (°C)
x10
x20

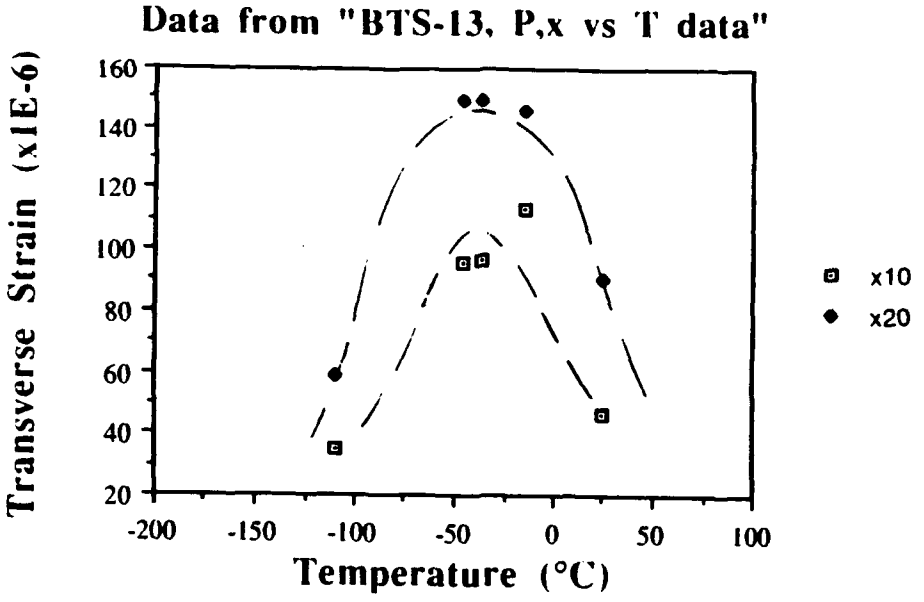
Data from "BTS-13, P,x vs T data"
Transverse Strain (x1E-6)
160
140
120
100
80
60
40
20
-200
-150
-100
-50
0
50
100
Temperature (°C)
x10
x20

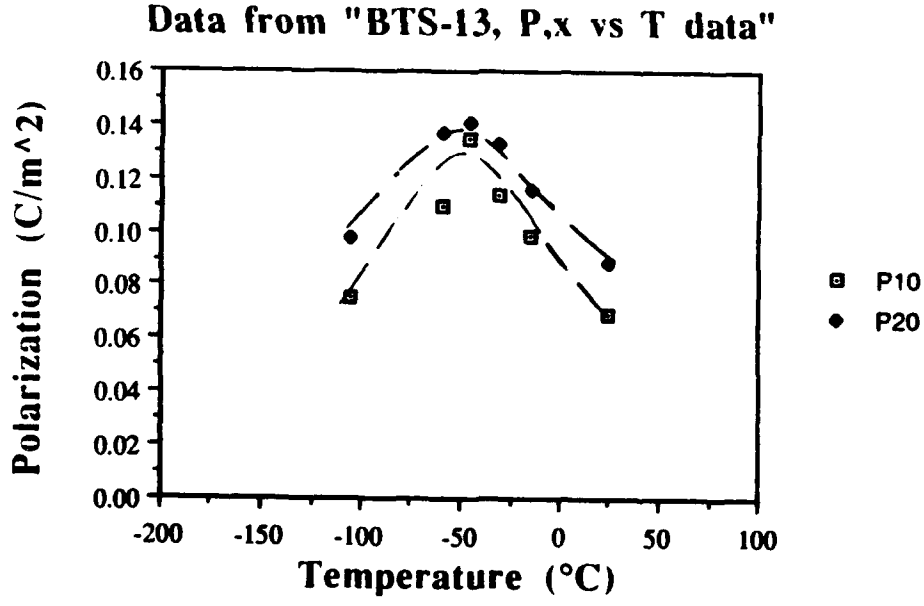
Data from "BTS-13, P,x vs T data"
Polarization (C/m^2)
0.16
0.14
0.12
0.10
0.08
0.06
0.04
0.02
0.00
-200
-150
-100
-50
0
50
100
Temperature (°C)
P10
P20

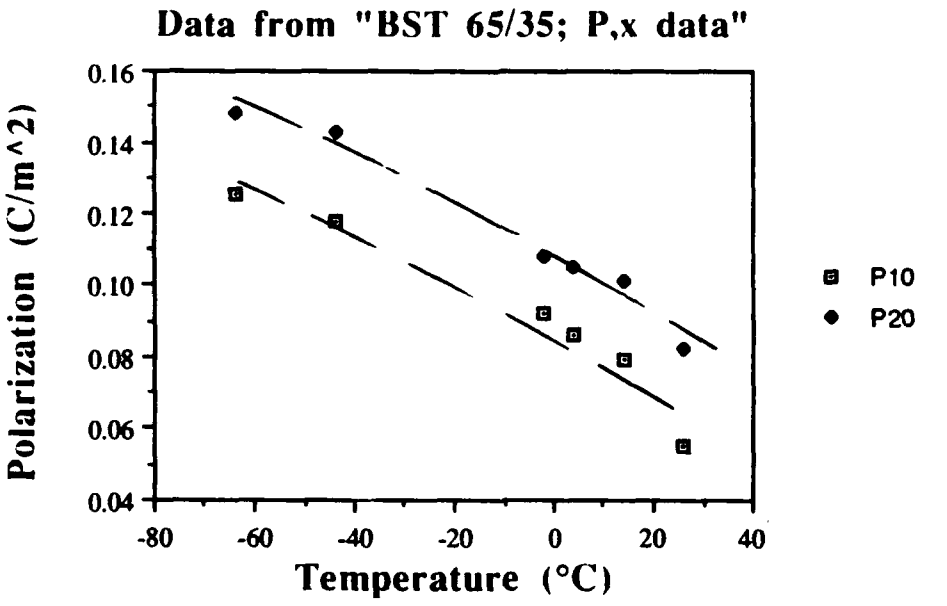
Data from "BST 65/35; P,x data"
Polarization (C/m^2)
0.16
0.14
0.12
0.10
0.08
0.06
0.04
-80
-60
-40
-20
0
20
40
Temperature (°C)
P10
P20

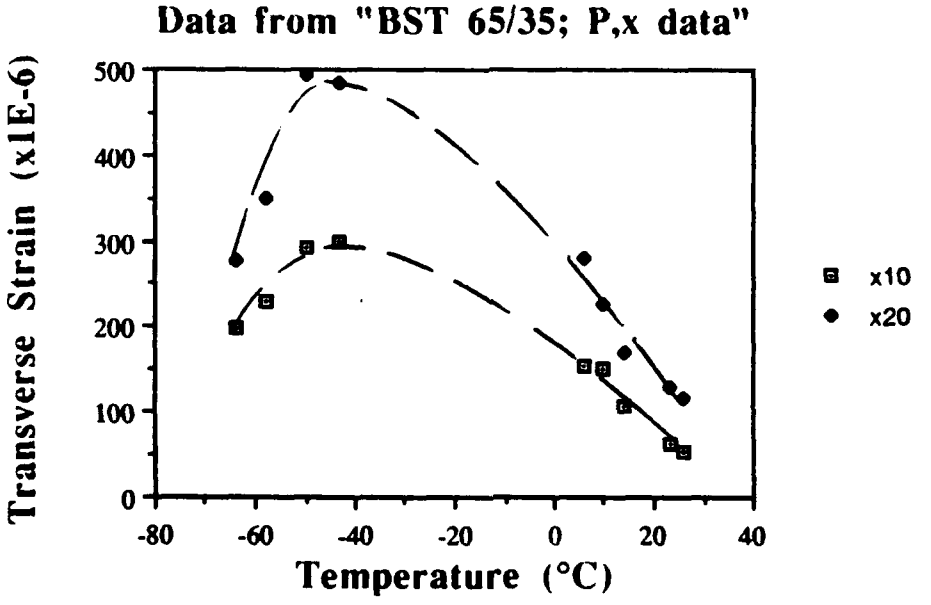
Data from "BST 65/35; P,x data"
Transverse Strain (x1E-6)
500
400
300
200
100
0
-80
-60
-40
-20
0
20
40
Temperature (°C)
x10
x20

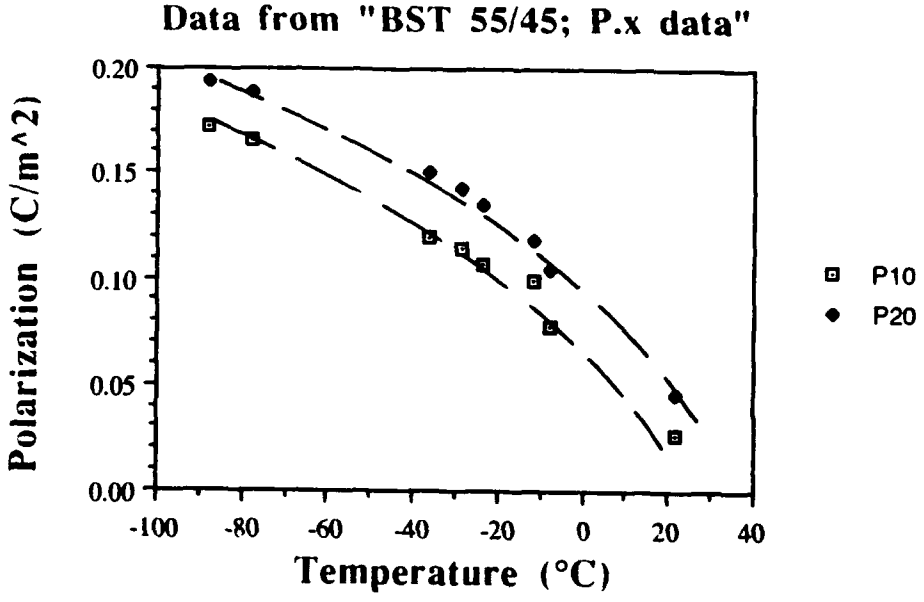
Data from "BST 55/45; P.x data"
Polarization (C/m^2)
0.20
0.15
0.10
0.05
0.00
-100
-80
-60
-40
-20
0
20
40
Temperature (°C)
P10
P20

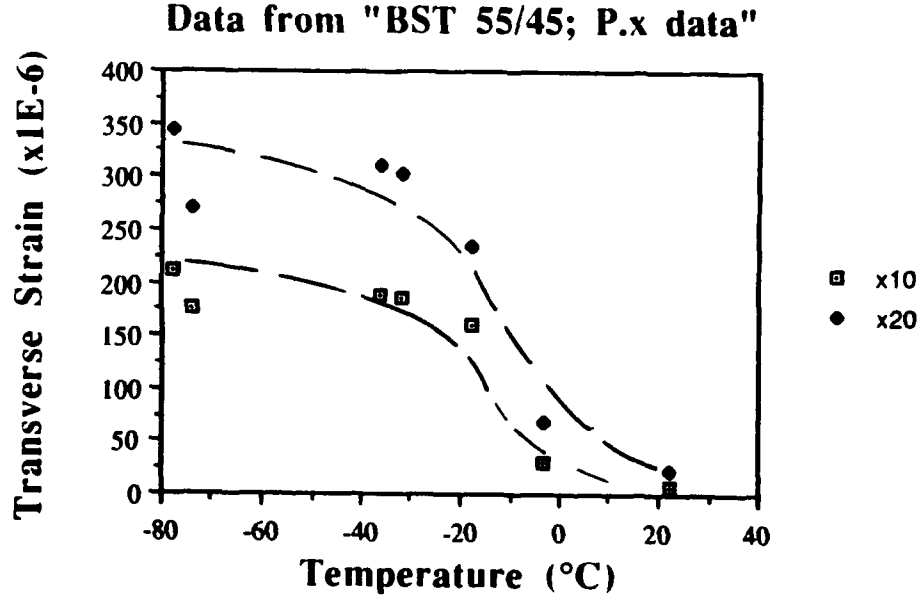
Data from "BST 55/45; P.x data"
Transverse Strain (x1E-6)
400
350
300
250
200
150
100
50
0
-80
-60
-40
-20
0
20
40
Temperature (°C)
x10
x20

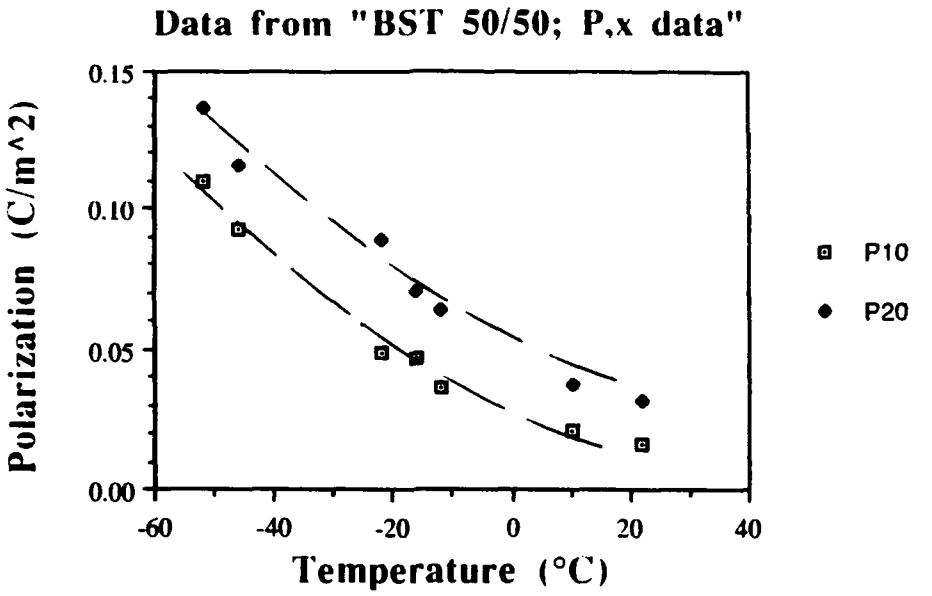
Data from "BST 50/50; P,x data"
Polarization (C/m^2)
0.15
0.10
0.05
0.00
-60
-40
-20
0
20
40
Temperature (°C)
P10
P20

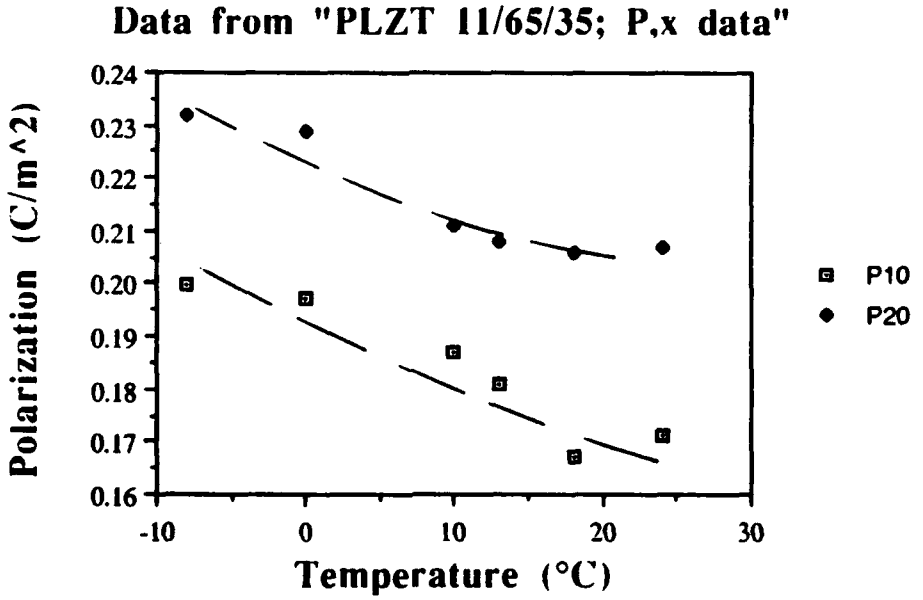
Data from "PLZT 11/65/35; P,x data"
Polarization (C/m^2)
0.24
0.23
0.22
0.21
0.20
0.19
0.18
0.17
0.16
-10
0
10
20
30
Temperature (°C)
P10
P20